Doctoral Dissertation
博士論文

Origin of Big Bang in Mixed Higgs-R^2 Inflation Model

(ヒッグス-R^2 混合インフレーションモデルにおける
ビッグバンの起源)

A Dissertation Submitted for the Degree of Doctor of Philosophy
July 2021
令和 3 年 7 月博士（理学）申請

Department of Physics, Graduate School of Science,
The University of Tokyo
東京大学大学院理学系研究科
物理学専攻

Minxi He
何 敏熙

To my family.

Acknowledgements

I would like to express my sincere gratitude to all the people who supported me in conducting exciting research for the past three years and completing this thesis, especially in the difficult 2020 and 2021 when the pandemic came together with a tense international situation.

The first person I have to mention is my supervisor, Jun'ichi Yokoyama, without whose inspiring education, generous support, patience, and encouragement I could have never finished all the work during my Ph.D. years. Besides, I am also profoundly grateful for his stimulating advice when I was confused in my career and life, which helps me find my own position. In addition, he devotes himself to the development of the physical societies in not only Japan but the whole Asia-Pacific area, which impresses me and reminds me of the responsibility to unite and create a better research environment for researchers from our homeland and from all over the world.

There is a particular group of people who play an essential role in my research experience. They are my collaborators for the past three years, Ryusuke Jinno, Kohei Kamada, Seong Chan Park, Alexei A. Starobinsky, and Teruaki Suyama, whom I greatly appreciate. With the help from them, I have explored various research topics and learned a wide range of knowledge, which is extremely useful for my future career development. In addition, working in an extensive collaboration allows me to interact with researchers of different styles so that I could establish my own.

I am grateful to my secondary supervisor Masahiro Takada, and Misao Sasaki, for their continuous support and valuable suggestion on my research and career. I also genuinely appreciate all the excellent senior researchers for their precious time and helpful discussion, including Fedor Bezrukov, Chengcheng Han, Shi Pi, and Yusuke Yamada.

I would like to thank my colleagues at the University of Tokyo for their great help, beneficial discussion, and organizing exciting activities to make the laboratory life enjoyable, especially Soichiro Hashiba, Ayako Ishii, Jun'ya Kume, Kana Moriwaki, and Hiroaki W. H. Tahara. Besides, I would express my special thanks to our respected secretaries and good friends Sayuri Nagano, Reiko Sugiyama, and Chiyo Ueda at

RESCEU, and Kazuyo Sawabe from the Graduate School Office, for their patient and generous help from the day I accepted the offer from the University of Tokyo.

I shall never forget Yi-Fu Cai, Yi Wang, and Siyi Zhou who took me into the field of cosmology for the first time, showing me a second chance to pursue my academic career after my first failure in PhD application.

The University of Tokyo is an amazing place that provides incredible academic environment for me to study and conduct researches, without which I might have never met and collaborated with all my excellent collaborators. Thanks to the Global Science Graduate Course (GSGC) program, I received funding to support my life in Tokyo, and met many good friends in different laboratories. I am also deeply grateful to the support from Japan Society for the Promotion of Science (JSPS) as a JSPS fellow (DC), because the funding of KAKENHI allowed me to attend international conferences and visit other institutes abroad to establish academic communication and potential collaboration with distinguished researchers, which are valuable experiences for my scientific career.

I would also thank all the friends I met in these years for their beautiful smiles and close connection thanks to which I could always keep healthy and positive to resist the great pressure from research and life. Particularly, I shall mention my roommates Mingjie Jian and Sirui Li, my best friends on the badminton court, Lichen Luo and Guo-Wei Qian, and other puzzle-solving team members, Xiangchong Li, Mengsi Liu, Jue Wang, Yuchen Wu, and Tong Xing.

Special thanks are expressed to my favorite singers Jacky Cheung and Wu Bai, whose songs (especially live versions) had stayed with me through every sleepless night when I was upset or busy. Enjoying their songs makes me focus and feel no existence of time such that I could keep on going.

I shall express many thanks to the Chief of the dissertation defense committee, Koichi Hamaguchi, and other committee members, Shoji Asai, Masahiro Kawasaki, Shigeki Matsumoto, and Tomotake Matsumura, for their precious time and valuable comments to this thesis.

Lastly but most importantly, I can never express enough my love and gratitude towards my mother Xiuqin Liu, my father Linbai He, and my sister Peishan He who are always there reminding me to be a kind person, supporting and encouraging me to seek my dream with endless love, patience, and understanding.

Abstract

This thesis is devoted to investigating the origin of the Big Bang in an observationally favored two-field inflationary model, namely the mixed Higgs-R^2 inflation model.

In inflationary cosmology, reheating is a period connecting the inflationary phase and the radiation-dominated Universe, serving as the origin of the Big Bang by particle production and thermalization. The temperature and duration of reheating can impact various observables and phenomena that can probe physics in the very early Universe. Reheating is a highly model-dependent process during which the energy that drives inflation is transferred to other matter fields through different mechanisms according to concrete models. Generally, reheating is characterized by two sequential stages for models where inflation is followed by inflaton oscillation, preheating that is dominated by non-perturbative particle production, and reheating during which inflaton experiences perturbative decay.

The mixed Higgs-R^2 inflation model, as a theoretically well-motivated and observationally favored inflationary model, possesses rich and interesting phenomena at different stages of reheating. Especially, the multi-field nature plays an essential role in the particle production mechanism throughout the whole reheating process, which distinguishes the model from its two single-field limits. Following a brief review of the mixed Higgs-R^2 inflation, different stages of the reheating process in this model are discussed in the thesis, including the first stage of preheating, the occurrence of tachyonic preheating, and the perturbative reheating. The first stage of preheating, which is involved in the unitarity issue discussion, is not significant enough to reheat the Universe; the occurrence of tachyonic preheating for specific parameter choices can reheat the Universe instantaneously; the perturbative decay of the scalaron field and Higgs field at the late time that can determine the reheating temperature and duration. The discussion is presented in both the Jordan frame and the Einstein frame.

Contents

List of Figures

Chapter 1

Introduction

The conventional Hot Big Bang theory[1] can successfully explain, in a comprehensive manner, the expansion of the Universe, the Cosmic Microwave Background (CMB) radiation, and the primordial abundance of light elements. It describes the Universe in a hot and dense phase dominated by thermalized relativistic particles (usually termed radiation) that expands to cool down to another phase dominated by non-relativistic particles (usually termed matter). However, there are still challenges for the Hot Big Bang theory. For example, the homogeneity, isotropy, and flatness of the observable Universe cannot be naturally predicted within its framework. Also, the origins of the anisotropy on CMB and seed fluctuations of large scale structure (LSS) are not answered in this theory. To overcome these difficulties, the inflationary cosmology [3–7][2] provides an elegant picture for the very early Universe which naturally solves the previously mentioned problems and sets the initial conditions for the Big Bang[3]. The essence of this scenario is to extend the physical time beyond the Big Bang by a quasi-de Sitter phase when the Universe experiences (almost) exponential growth in space for a sufficiently long time. Inflation stretches the space and dilutes the spatial curvature, which solves the flatness problem, while the large-scale homogeneity and isotropy are naturally explained because the observed Universe is originally from a single particle horizon at the early time. The quantum fluctuations generated during inflation, on the other hand, seed the CMB anisotropy and the formation of large-scale structure.

Instead of replacement, inflation serves as a powerful complement to the Hot Big Bang at the earliest period to make the cosmology model more complete. However,

[1] See e.g. the classic textbooks [1, 2] for details.

[2] See e.g. [8] for a review.

[3] Here the terminology follows from Ref. [9] that the Big Bang refers loosely to a gaseous era well before the Big Bang nucleosynthesis where the Universe is not necessarily thermalized or dominated by radiation.

inflation does not last forever because the standard evolution in the Hot Big Bang theory should take place in time as it successfully describes the thermal history of the Universe from the radiation-dominated epoch to the present. Furthermore, the observed properties of the Universe, such as the baryon asymmetry, should also be generated between inflation and the Big Bang nucleosynthesis (BBN). Nonetheless, the realization of inflation is still unclear. The standard inflationary models usually contain one or more scalar field(s) called inflaton(s) whose vacuum-like energy density dominates the Universe and drives inflation until a graceful exit. After the end of inflation, the inflaton fields oscillate around the bottom of the potential, triggering the particle production process. Depending on the concrete interaction between inflaton and other matter fields, the inflaton energy is transferred into relativistic particles through different mechanisms that can be either perturbative or non-perturbative. This process is called reheating of the Universe [6], which is highly model-dependent due to the unknown physics at inflation scale. At the end of reheating, all the inflaton energy goes into relativistic particles that interact with each other and eventually reach thermal equilibrium. The Universe is then dominated by radiation, and its temperature at this stage is dubbed reheating temperature. Subsequently, the evolution of the Universe is along the storyline of the Hot Big Bang theory.

Reheating is an essential ingredient for a successful inflationary model as a transition from an "empty" space after inflation to a radiation-dominated Universe [6]. The reheating temperature and duration are two of the most crucial quantities characterizing this period which tightly connect with other important observables, for example, the duration of inflation, possibly baryogenesis, high-frequency gravitational waves, and the production of dark matter. Proper analysis of the cosmic history during reheating regime is required to express the pivot scale of curvature perturbation in terms of the number of e-folds of inflation, in order to confront the prediction of inflation with observational data [10, 11], because the thermal history between inflation and BBN directly affects how we map the curvature perturbation mode at the moments when they exit and reenter the horizon. Therefore, investigation of the uncertainties during reheating can improve the observational constraint on inflation models. Unfortunately, reheating is challenging to probe[4] because the corresponding scale is small such that the late-time non-linear dynamics will strongly wash out the information left by reheating. The thermal equilibrium state during the radiation-dominated era also diminishes the possible trace of reheating. Finding the potential observables

[4]One possibility is the future space gravitational wave detector DECIGO [12, 13].

that can survive the non-linear dynamics and thermalization for current and future experiments becomes crucial for a better understanding of the early Universe.

For standard inflationary models with inflaton oscillations after inflation, reheating can sequentially occur in two characteristic regimes in general. The first is preheating, which usually involves short but rapid and non-perturbative processes transferring a significant fraction of the energy from inflaton to other matter fields through broad parametric resonance [14–17] or tachyonic instability [18–20]. The second is perturbative reheating, where the inflaton field decays perturbatively into other species of matter and losses all its energy [3, 21, 22]. The most significant complication of reheating comes from the non-perturbative and non-linear preheating regime. The particle production during preheating is non-adiabatic and often explosive. As a result, the backreaction from such a violent process to the background dynamics may soon become significant when the energy of the produced particles becomes comparable with that of the background, which is a non-linear process. An elaborate numerical method such as lattice simulation is often adopted to take into account the backreaction. However, these simulations are classical, so quantum effects are neglected, while some of those effects could be potentially important for the rescattering process of relativistic particles. Another essential ambiguity of reheating is that the validity of the Standard Model (SM) of particle physics around the inflation scale is unclear since the existing colliders on earth cannot probe such a high energy scale. But conversely, reheating provides a free but powerful "collider" in the sky because any discovery or observation from the reheating epoch can shed light on the possible new physics at that scale. Therefore, a thorough investigation of the reheating process is eagerly desired to comprehend the high energy physics and the early Universe.

Particular interest should lie in the observationally favored models because extra constraints are needed to decrease the number of models allowed by current observation. The simplest viable version of inflation models is the so-called single-field slow-roll inflation where only one scalar field is responsible for the inflationary dynamics. Two of these models stand out as the best-fit candidates according to the CMB observation [23], namely the Starobinsky model [3, 24] (or R^2-inflation) and the original Higgs inflation with a non-minimal coupling between the SM Higgs and gravity [25–27][5]. The former is the simplest inflation model extending the General Relativity (GR) by a new geometric term R^2 with only one parameter, equivalent

[5]See Ref. [28] for all the variants.

to a scalar-tensor theory with one scalar degree of freedom called scalaron [3] in addition to the two tensor modes in GR. The latter identifies the inflaton with the only scalar field in SM, i.e. the Higgs field which has been discovered at the Large Hadron Collider (LHC). Making use of a large non-minimal coupling between Higgs and gravity, it fits the observation as well as the Starobinsky model. The reheating processes in the Starobinsky model [3, 29, 30] and the Higgs inflation [31–35] have also been intensively studied in the literature. However, a sensible UV theory for both models is still missing, which motivates us to consider the UV extension beyond them. More detail about single-field slow-roll inflation and the inflation dynamics of these two models are reviewed in Chapter 2. The theory of particle production in a time-dependent background as well as the reheating processes in the R^2-inflation and the Higgs inflation is reviewed in Chapter 3.

This thesis focuses on a two-field inflationary model, namely the mixed Higgs-R^2 inflation model [36–40]. Increasing the number of inflaton fields is one way to go beyond the standard single-field slow-roll inflation but also significantly increases the complication of the system. Nevertheless, this model is well-motivated in both phenomenological and theoretical perspectives. Phenomenologically, it combines the two observationally most favored inflationary models mentioned above, i.e. the R^2-inflation and the Higgs inflation. In the regime where isocurvature mode is heavy and Higgs self-coupling is non-critical during inflation, this model always inherits the predictions on the scalar spectral index n_s and tensor-to-scalar ratio r at CMB scale from its two single-field limits which well match the observation by WMAP and Planck [23]. This is naturally explained by the attractor behavior during inflation that enables us to describe this model as an effective R^2-inflation or effective Higgs inflation [38,41]. Theoretically, the mixed Higgs-R^2 inflation model can be a candidate of UV-extension of the Higgs inflation [37, 42] as the cutoff scale of the model is lifted up to the Planck scale. Due to the presence of R^2 term, the strong coupling issue during preheating in the Higgs inflation [34] is also resolved [41], which is discussed exhaustively in Chapter 4. The origin of the R^2 term is discussed from the viewpoint of the renormalization group running [43–47], and of scattering amplitude and the non-linear sigma model [48, 49]. The detailed motivation and inflation dynamics of this model are reviewed in Chapter 2.

The interplay of the multi-field nature of the system and various couplings between inflaton fields and SM particles generates the rich phenomena during reheating in the mixed Higgs-R^2 inflation model. Depending on the model parameters,

different mechanisms dominate the reheating process [41, 50–53], which leads to different reheating temperatures connecting its two single-field limits. As the Higgs- and R^2-inflation can be distinguished by different reheating temperatures [54], it is also applicable to break the degeneracy among different model parameters in the mixed Higgs-R^2 inflation model. Conversely, future experiments that determine the reheating temperature can settle down the mixing ratio between the Higgs- and R^2-inflation. Based on the original works [41, 51] in collaboration with Ryusuke Jinno, Kohei Kamada, Seong Chan Park, Alexei A. Starobinsky, and Jun'ichi Yokoyama, and the independent one [53], the reheating process for different parameter choices in the mixed Higgs-R^2 inflation model is discussed in Chapter 4, which constitutes the main part of this thesis, including the generic first stage of preheating, tachyonic preheating at an early stage, and the perturbative reheating at late time.

A brief summary of the structure of this thesis is as follows.

- Chapter 2 is devoted to the review of inflation. In Sec. 2.1, the basic idea of inflationary cosmology is briefly reviewed. In Sec. 2.2, the simplest class of models, single-field slow-roll inflation, is introduced, together with the inflation dynamics of two typical examples, the Starobinsky model and the Higgs inflation. A review of the general formalism for multi-field inflation is presented in Sec. 2.3, followed by the analysis of the mixed Higgs-R^2 inflation.

- Chapter 3 mainly reviews the theory of reheating after inflation. A general discussion of the particle production in a time-dependent background is presented in Sec. 3.1, including perturbative and non-perturbative processes. The application to the Starobinsky model and the Higgs inflation is given in Sec. 3.2.

- Chapter 4 is the most important part of this thesis where the reheating process is comprehensively discussed. The analysis of the first stage of preheating is presented in Sec. 4.1. The occurrence of tachyonic instability and the necessary degree of fine-tuning for realization is discussed in detail in Sec. 4.2. For the cases where tachyonic preheating is insufficient, perturbative decay of the inflaton fields dominates the late-time reheating process, which is investigated in Sec. 4.3.

- The last Chapter serves as the summary and conclusion of this thesis.

This thesis adopts the Planck units, i.e. $c = k_B = \hbar = 1$ and uses the reduced Planck mass $M_{\rm pl} = (8\pi G)^{-1/2}$ explicitly.

Chapter 2

Inflation

As an indispensable part of modern cosmology, inflation refers to a quasi-de Sitter phase at the beginning of the Universe. The existence of such a period overcomes various difficulties encountered in the conventional Hot Big Bang cosmology, such as the horizon problem, flatness problem, and monopole problem [4]. In addition, the initial conditions for the temperature fluctuations on CMB and the formation of LSS can be naturally generated during inflation. Therefore, the inflation scenario provides an elegant description of the early Universe, although much ambiguity remains about the concrete realization of inflation and the connection between inflation and other observed facts such as baryon asymmetry and dark matter production. Testing inflation by direct observational evidence and constructing a viable inflation model become two of the main tasks in modern cosmology, which will fill the blank history of the early Universe and lead to a deeper understanding of physics at a currently unreachable high energy scale. One of the most important predictions of inflation is the primordial gravitational waves generated in the early quasi-de Sitter phase [55] which are only constrained by the null observation [23]. The primary target of many ongoing and future experiments is to probe the primordial tensor mode fluctuations whose discovery will be the smoking gun of inflation.

This chapter is a review of inflation, including the basic idea of inflationary scenario (Sec. 2.1), the realization of inflation in single-field models for an illustrative purpose (Sec. 2.2), and more realistic model construction, multi-field inflation (Sec. 2.3). In the last section, after a review of the general formalism of multi-field inflation, special attention is drawn to a specific two-field model, namely the mixed Higgs-R^2 inflation model. The motivation and inflationary dynamics of this model are discussed in detail.

2.1 Inflation Scenario

The observed Universe which is homogeneous and isotropic at large scale can be well described by the four-dimensional flat Friedmann-Lemaître-Robertson-Walker (FLRW) metric, a solution of the Einstein field equations in GR. The FLRW metric for general spatial curvature in a comoving coordinate system is given by

$$ds^2 = -dt^2 + a^2(t)\gamma_{ij}dx^i dx^j = -dt^2 + a^2(t)\left[\frac{dr^2}{1-Kr^2} + r^2 d\Omega_2^2\right] , \tag{2.1}$$

where γ_{ij} is the spatial metric; $d\Omega_2^2$ is the metric of the 2-dimensional Euclidean sphere; K is the spatial curvature parameter which takes -1, 0, $+1$ for hyperbolic, flat, and spherical space with constant curvature respectively; and $a(t)$ is the scale factor whose absolute size is related to the radius of curvature of the spatial geometry in curved space but has no physical meaning in flat space because one can always absorb it into the redefined coordinate. A more meaningful quantity is the Hubble parameter defined as

$$H \equiv \dot{a}/a , \tag{2.2}$$

that measures the spatial expansion rate of the Universe. The over-dot $\dot{(\,)}$ represents the derivative with respect to t. The Hubble parameter characterizes the typical length scale and time scale of the expanding Universe. Specifically, H^{-1} roughly estimates the size of observable Universe or "Hubble horizon" as well as the time with which the scale factor $a(t)$ becomes double in size. A comoving version is called comoving Hubble horizon $(aH)^{-1}$ which represents the comoving distance light can travel within one Hubble time beyond which *current* causal contact is forbidden. Another convenient and important quantity is the conformal time

$$\eta \equiv \int a^{-1} dt = \int (aH)^{-1} d\ln a , \tag{2.3}$$

with which Eq. (2.1) can be rewritten in a conformal form that is convenient for calculation

$$ds^2 = a^2(\eta)\left[-d\eta^2 + \frac{dr^2}{1-Kr^2} + r^2 d\Omega_2^2\right] . \tag{2.4}$$

The conformal time also measures the comoving distance that light could have traveled since the beginning of time, roughly the accumulation of the comoving Hubble horizon as seen in the second equality in Eq. (2.3). Therefore, this distance represents a "comoving particle horizon" beyond which, by definition, no causal connection could have been made before the present moment.

Considering a perfect fluid with energy density ρ and isotropic pressure p in the comoving frame, its energy-momentum tensor is written as

$$T_{\mu\nu} = (\rho + p)u_\mu u_\nu + p g_{\mu\nu} \ , \tag{2.5}$$

where u^μ is the 4-velocity of the fluid. The equation of state of the perfect fluid is parameterized by the equation of state parameter $w = p/\rho$ which takes the value of 0 for (pressureless) matter, 1/3 for radiation, and -1 for cosmological constant. If the Universe is dominated by this fluid and described by the geometry in Eq. (2.1), the Einstein field equations turn out to be the famous Friedmann equations

$$\begin{aligned} H^2 &= \frac{1}{3M_{\rm pl}^2}\rho - \frac{K}{a^2} \ , \\ \dot{H} + H^2 &= -\frac{1}{6M_{\rm pl}^2}(\rho + 3p) \ , \end{aligned} \tag{2.6}$$

and a continuity equation follows from them as

$$\dot{\rho} + 3H(\rho + p) = 0 \ , \tag{2.7}$$

which is independent of K. From Eq. (2.7), the relation between ρ and a can be derived

$$\rho \propto a^{-3(1+w)} \ , \tag{2.8}$$

which shows the evolution of different components as the Universe expands, for example, radiation $\rho_{\rm rad} \propto a^{-4}$ and matter $\rho_{\rm m} \propto a^{-3}$. An important quantity called critical density ρ_c is defined as the energy density that makes $K = 0$, i.e. $\rho_c \equiv 3M_{\rm pl}^2 H^2$. For the case with multiple components with different ρ_i where the subscription i denotes different species, ρ in Eqs. (2.6) should be replaced by $\sum_i \rho_i$.

From the lower of Eqs. (2.6), it can be found that $\ddot{a} < 0$ as long as $w > -1/3$, which means that the cosmic expansion is decelerating. Therefore, during a radiation-dominated or matter-dominated epoch, the Universe experiences decelerated expansion. For $w < -1/3$, the accelerated expansion is realized, in particular, $w = -1$ corresponding to exact de Sitter spacetime.

The Hot Big Bang cosmology assumes that the Universe is initially dominated by radiation. As the cosmic expansion dilutes radiation much faster than matter, the Universe becomes matter-dominated later. In this framework, the cosmic expansion, CMB, and BBN are comprehensively explained. However, this theory suffers from some shortcomings which are summarized as follows.

- **Horizon Problem** The observable Universe is homogeneous and isotropic at large scales as can be seen on CMB where the amplitude of curvature fluctuation is tiny $\sim 10^{-5}$ [23], which cannot be naturally explained by the standard Hot Big Bang cosmology. This problem can be seen easily by considering the comoving Hubble horizon and comoving particle horizon. According to the discussion above, for $w \geq 0$ case[6], it is easy to find that

$$\frac{d}{dt}(aH)^{-1} = -\frac{\ddot{a}}{\dot{a}^2} > 0 \ , \tag{2.9}$$

$$\Delta\eta = \int_0^t a^{-1} dt = \int_0^t (aH)^{-1} d\ln a \ , \tag{2.10}$$

  which means that both horizons increase monotonically with time. This implies that the causally connected region at early time is much smaller than that observed today, so it is not natural that all the regions from outside the horizon look so similar to the one inside without any previous causal contact.

- **Flatness Problem** The flatness of the observed Universe is also mysterious in the standard Hot Big Bang cosmology. If the quantities evaluated at present time are denoted with a subscript "0", observation tells that the Universe is extremely flat, $\rho_0 \simeq \rho_{c0}$. However, from the upper of Eqs. (2.6),

$$|1 - \Omega(t)| = K(aH)^{-2} \ , \tag{2.11}$$

  where $\Omega \equiv \rho/\rho_c$ is the density parameter. As long as $w > -1/3$, $|1 - \Omega(t)|$ is increasing with time, which means that $K(aH)^{-2} = 0$ is not a stable point during radiation- and matter-dominated Universe. Normalizing $a_0 = 1$, the observation gives $|1 - \Omega(t_0)| \lesssim 0.01$, which means that $|1 - \Omega(t_{\rm BBN})| \lesssim \mathcal{O}(10^{-16})$ and even smaller at earlier time. There is no explanation in the conventional Hot Big Bang theory why the density parameter of the Universe is extremely close to unity at the early stage.

- **Monopole Problem** If the Universe has a very high temperature at the very early stage, the symmetry of Grand Unified Theory (GUT) may be restored so topological defects, e.g. magnetic monopoles, may be produced when the symmetry is spontaneously broken. These monopoles are stable and can survive until the present, with abundance typically higher than that allowed by observation. The absence of such topological defects casts another doubt on the validity of the standard Hot Big Bang cosmology at the very early time.

[6] This is always true for radiation- and matter-dominated Universe.

The observation of large-scale homogeneity, isotropy, and flatness may be achieved by setting some unnatural initial conditions for the early Universe, which, however, are not physically motivated and make the theory less predictive. In order to overcome these difficulties, the concept of inflation is introduced [4]. Furthermore, as shown in the next section, the initial perturbations for CMB anisotropy and LSS are also naturally generated by inflation.

The basic idea of inflation is to insert a period of accelerated expansion ($\ddot{a} > 0$) before the Big Bang. This scenario can be intuitively understood, on the one hand, as the expansion dilutes all the unwanted features or initial conditions, including the spatial curvature and the abundance of GUT relics, which solves the flatness problem and monopole problem. On the other hand, the size of comoving Hubble horizon shrinks during the accelerated expansion, which means that the comoving particle horizon could cover a large region at the early time because of the significant contribution from $(aH)^{-1}$. If the duration of accelerated expansion is long enough, the originally covered region can be as large as the Hubble horizon observed today, which solves the horizon problem because all the observed regions today would be causally connected in the past. A brief quantitative discussion is as follows.

- **Solving Horizon Problem** The natural consequence from inflation ($\ddot{a} > 0$) is that the comoving Hubble horizon decreases with time

$$\frac{d}{dt}(aH)^{-1} = -\frac{\ddot{a}}{\dot{a}^2} < 0 \ , \tag{2.12}$$

  which means that a large comoving volume could be in causal contact before inflation and some part of it exited the horizon during inflation. It is the causal connection before inflation that establishes the large-scale homogeneity and isotropy, which solves the horizon problem.

- **Solving Flatness Problem** If the comoving Hubble horizon decreases during inflation, $K(aH)^{-2}$ in Eq. (2.11) also decreases with time. As a result, $\Omega(t) = 1$ is no longer an unstable point but an attractor during inflation. In other words, inflation inevitably generates an initial condition $\Omega \simeq 1$ for the Big Bang, which solves the flatness problem.

- **Solving Monopole Problem** Even if the unwanted relics could be generated during a GUT phase transition at early Universe, the long period of accelerated expansion could dilute the abundance of such relics exponentially to a level allowed by present observation, which solves the monopole problem. Of course,

it is necessary to keep the temperature of the Universe low enough during and after reheating to prevent the production of these relics after inflation.

From Eqs. (2.6) and $\ddot{a} > 0$, an immediate result is that $\rho + 3p < 0$ which means a negative pressure $w < -1/3$ that pushes the Universe to expand with acceleration. The way to realize negative pressure is discussed in the next section. In addition, the primordial quantum fluctuations generated during inflation play an essential role in providing the origin of density fluctuations which is absent in the Hot Big Bang cosmology. Since the comoving Hubble horizon shrinks during inflation, the quantum fluctuations with comoving wavelengths comparable to the horizon size immediately exit the horizon and freeze at the superhorizon scale. These fluctuations re-enter the Hubble horizon at late time (for example, the fluctuation with a comoving wavelength equal to $(a_0 H_0)^{-1}$ enters the horizon today) and seed the CMB anisotropy and LSS formation. Since the statistical properties of such perturbations can be observed by current and future experiments (e.g. [23]), contrasting the theoretical predictions of these fluctuations to observation can constrain inflation models.

Based on the brief discussion above, inflation solves the problems in the conventional Hot Big Bang theory elegantly and explains the origin of the perturbations for late-time structure formation.

2.2 Single-Field Inflation

To realize inflation, the generation of negative pressure is necessary, as mentioned in the previous section. The simplest way to do that is by introducing a positive cosmological constant $\Lambda > 0$ which creates an exact de Sitter spacetime where the Universe grows exponentially forever. However, such expansion does not have a graceful exit to connect with a subsequent Big Bang, which cannot lead to the existence of the observed Universe. Another choice is to introduce one or more scalar fields called inflatons which drive inflation for a finite duration and smoothly connect with the Hot Big Bang after the end of inflation. The simplest class of inflation models constructed in this way is called single-field slow-roll inflation[7], on which this section focuses. These models make use of one scalar field (inflaton) whose potential energy dominates over the kinetic one during inflation so that the inflaton slowly rolls down its potential,

[7]There are other classes of models, for instance, k-inflation [56] which is also single-field but not slow-roll. The most general framework of single-field inflation is called generalized G-inflation [57, 58] which includes all single-field inflationary models with second-order equations of motion in a covariant form. The Generalized Galileon theory is also found to be equivalent to Horndeski theory [59].

which plays a role similar to a cosmological constant to drive inflation. The specific shape of the potential largely determines the properties (e.g. scale-dependence) of the quantum fluctuations which are testable by observation[8]. Among all of them, there are two models that are exceptionally favored by observation, namely the Starobinsky model [3, 24] and the Higgs inflation [25–27], which will be introduced later.

2.2.1 Conformal Transformation

Before considering the dynamics in concrete inflation models, it is necessary to discuss the "frame issue" in scalar-tensor theories because the inflation models discussed in this thesis belong to this class of gravitational theories. There are two types of frames in scalar-tensor theories, the Jordan frame (JF) and the Einstein frame (EF). In the former, the Ricci scalar appears not only in the Einstein-Hilbert (E-H) term but also in some direct coupling terms with the scalar fields. On the contrary, if the Ricci scalar only appears in the E-H term without being multiplied by any function of the scalar fields, it is in EF. There are advantages to consider systems in EF because it is more intuitive to see the dynamics of the scalar fields simply by their potentials in such a frame, and the Einstein field equations take a simpler form than that in JF, which simplifies the calculation. Therefore, it would be convenient to study general scalar-tensor theories if there is equivalence or any relation between the two frames.

In Refs. [62,63], the equivalence between these two frames is beautifully presented. Consider a general scalar-tensor theory with only one scalar field ϕ given as (this is sufficient for the purpose of this thesis)

$$S_{\mathrm{J}} = \int d^D x \sqrt{-g_{\mathrm{J}}} \left[F\left(R_{\mathrm{J}}, \phi\right) - \frac{1}{2} \nabla_{\mathrm{J}\mu} \phi \nabla_{\mathrm{J}}^{\mu} \phi \right] \ , \tag{2.13}$$

where $F\left(R_{\mathrm{J}}, \phi\right)$ is an arbitrary function of ϕ and the Ricci scalar R_{J}, and D is the dimension of spacetime. Generally speaking, this action is in JF because the arbitrary function $F(R_{\mathrm{J}}, \phi)$ can contain direct coupling between R_{J} and ϕ. Therefore, the subscript "J" here is to denote the quantities in JF and $\nabla_{\mathrm{J}\mu}$ is the covariant derivative with respect to $g_{\mathrm{J}\mu\nu}$. Through a conformal transformation (see Appendix A and Ref. [64] for details)

$$g_{\mathrm{E}\mu\nu}(x) = e^{2\omega(x)} g_{\mathrm{J}\mu\nu}(x) \ , \tag{2.14}$$

[8] In α-attractor models [60, 61], the original inflaton potential can be arbitrary because its non-trivial kinetic term plays a crucial role in generating the observationally favored slow-roll inflation.

where $\omega(x)$ is set to be

$$\omega = \frac{1}{D-2} \ln \left(\frac{2}{M_{\rm pl}^2} \left| \frac{\partial F}{\partial R_{\rm J}} \right| \right) \ , \tag{2.15}$$

to make the terms of higher order derivatives cancel each other in the Einstein equations, it is possible to transform Eq. (2.13) to EF. As can be seen in Eq. (2.15), the definition of ω contains $\partial F/\partial R_{\rm J}$ which may contain new degrees of freedom other than the two tensor modes in GR and the scalar field ϕ, depending on the form of $F(R_{\rm J}, \phi)$.

In the case that $F(R_{\rm J}, \phi) = f(\phi) R_{\rm J} - U_{\rm J}(\phi)$ where $f(\phi)$ and $U_{\rm J}(\phi)$ are arbitrary functions of ϕ, it is obvious that ω is only a function of ϕ so it is not a new degree of freedom, which is consistent with the observation in the original JF that there is no higher order derivative to induce any new degrees of freedom. Redefining a new scalar field $\tilde{\phi}$ as

$$\frac{\tilde{\phi}}{M_{\rm pl}} \equiv \int d\phi \left[\frac{(D-2)f + 2(D-1)(df/d\phi)^2}{2(D-2)f^2} \right]^{1/2} \ , \tag{2.16}$$

the action (2.13) is rewritten as

$$S_{\rm E} = ({\rm sign}) \int d^D x \sqrt{-g_{\rm E}} \left[\frac{M_{\rm pl}^2}{2} R_{\rm E} - \frac{1}{2} \nabla_{{\rm E}\mu} \tilde{\phi} \nabla_{\rm E}^{\mu} \tilde{\phi} - U_{\rm E}(\tilde{\phi}) \right] \ , \tag{2.17}$$

where

$$U_{\rm E}(\tilde{\phi}) \equiv ({\rm sign}) \left[\frac{2}{M_{\rm pl}^2} |f(\phi)| \right]^{-\frac{D}{D-2}} U_{\rm J}(\phi) \ , \tag{2.18}$$

and $({\rm sign}) \equiv f/|f|$. It is assumed that the integral in Eq. (2.16) is real and (sign) is positive to ensure that the kinetic term has the right sign. As can be seen here, theories with $F(R_{\rm J}, \phi) = f(\phi) R_{\rm J} - U_{\rm J}(\phi)$ still describes a system of GR plus a canonical scalar field with the original potential rescaled.

In the case that $\partial F/\partial R_{\rm J}$ is still a non-trivial function of $R_{\rm J}$, the theory possesses a new scalar degree of freedom which is simply given as ω (or a function of ω). This is also consistent with the observation of JF because $F(R_{\rm J}, \phi)$ contains higher-order derivatives which should lead to new degrees of freedom when rewriting the theory back to one with second-order derivatives only. Defining a new scalar field to represent the new degree of freedom in ω

$$\psi/M_{\rm pl} \equiv \sqrt{(D-1)(D-2)}\ \omega \ , \tag{2.19}$$

the action (2.13) is rewritten as an E-H term plus two scalar fields

$$S_{\rm E}=({\rm sign})\int d^Dx\sqrt{-g_{\rm E}}\left[\frac{M_{\rm pl}^2}{2}R_{\rm E}-\frac{1}{2}\nabla_{{\rm E}\mu}\phi\nabla_{\rm E}^{\mu}\phi-\frac{({\rm sign})}{2}e^{-\sqrt{\frac{D-2}{D-1}}\frac{\psi}{M_{\rm pl}}}\nabla_{{\rm E}\mu}\psi\nabla_{\rm E}^{\mu}\psi-U_{\rm E}(\phi,\psi)\right], \quad (2.20)$$

where

$$U_{\rm E}(\phi,\psi)\equiv({\rm sign})\left(\frac{2}{M_{\rm pl}^2}\left|\frac{\partial F}{\partial R_{\rm J}}\right|\right)^{-\frac{D}{D-2}}\left[R_{\rm J}(\phi,\psi)\frac{\partial F}{\partial R_{\rm J}}-F(\phi,\psi)\right] . \quad (2.21)$$

and $({\rm sign})\equiv(\partial F/\partial R_{\rm J})/|\partial F/\partial R_{\rm J}|$ which is assumed to be positive. Here, $R_{\rm J}$ should be written in terms of ϕ and ψ by Eq. (2.15). As a result, such a system describes GR plus two scalar fields one of which is non-canonical. The non-canonical kinetic term of ψ means the field space spanned by ϕ and ψ is non-trivial and may play an important role during (multi-field) inflation if its curvature is large (see e.g. Ref. [65]).

To summarize, the scalar-tensor theory given in Eq. (2.13) can always be written in terms of the E-H system with one or two scalar fields by the conformal transformation (2.14), which is extremely useful when analyzing such a system, as will be seen in the rest of this thesis.

2.2.2 Classical Background

Consider a general single-field slow-roll inflation model in four-dimensional spacetime whose action is written as

$$S=\int d^4x\sqrt{-g}\left[\frac{M_{\rm pl}^2}{2}R-\frac{1}{2}\partial_\mu\phi\partial^\mu\phi-V(\phi)\right] , \quad (2.22)$$

where R is Ricci scalar and ϕ is the scalar field that acts as inflaton with a potential $V(\phi)$. Since conformal transformation can always transform the JF action into EF [62, 63] as shown previously, it is sufficient to study the system in EF from the beginning. In this model, the energy density of the Universe is dominated by inflaton ϕ which drives inflation. Focusing on a flat FLRW metric (corresponds to $K=0$ in Eq. (2.1)) and a homogeneous $\phi=\phi(t)$, the Friedmann equation and equation of motion for ϕ are then

$$3M_{\rm pl}^2H^2=\dot\phi^2/2+V(\phi) , \quad (2.23)$$

$$\ddot\phi+3H\dot\phi+V_{,\phi}=0 , \quad (2.24)$$

where the comma in subscript denotes partial derivatives, e.g. $V_{,\phi}\equiv\partial V/\partial\phi$. The inflaton field acts as a perfect fluid whose equation of state parameter is given by

$$w_\phi=\frac{p_\phi}{\rho_\phi}=\frac{\dot\phi^2/2-V(\phi)}{\dot\phi^2/2+V(\phi)} . \quad (2.25)$$

According to the "definition" of inflation $\ddot{a} > 0$, it is easy to derive that

$$0 < \frac{\ddot{a}}{a} = \dot{H} + H^2 = \frac{1}{3M_{\rm pl}^2}\left(V - \dot{\phi}^2\right) \ , \tag{2.26}$$

which leads to $w_\phi < -1/3$ from Eq. (2.25). Therefore, to realize inflation, the potential energy of ϕ must dominate over the kinetic one, which is the reason why the name "slow-roll inflation" is given to this class of models. It is convenient to introduce the so-called slow-roll parameter

$$\epsilon_1 \equiv -\dot{H}/H^2 \ , \tag{2.27}$$

to quantify the inflation dynamics. Since $\dot{H}$ is basically the kinetic energy of ϕ while H^2 is dominated by the potential, ϵ_1 is describing the ratio between them. Therefore, this model requires $\epsilon_1 \ll 1$ all the time during inflation and $\epsilon_1 = 1$ characterizes the end of inflation. In this sense, Eq. (2.25) gives $w_\phi \approx -1$ during inflation, which corresponds to (almost) exponential expansion, i.e. $a(t) \propto t^{Ht}$ with $H \approx$ constant. Another important point is that inflation should last long enough to explain the size of the homogeneous and isotropic Universe observed today, which leads to the introduction of the second slow-roll parameter ϵ_2 to describe the growth rate of ϵ_1. There are several ways to define ϵ_2 among which the following is adopted in this thesis

$$\epsilon_2 \equiv \epsilon_1 - \frac{\dot{\epsilon}_1}{2H\epsilon_1} = -\frac{\ddot{H}}{2H\dot{H}} = -\frac{\ddot{\phi}}{H\dot{\phi}} \ , \tag{2.28}$$

where Eqs. (2.23) and (2.24) are used in the last equality which holds for canonical scalar fields. Long duration of inflation means small $\epsilon_2 \ll 1$ so that ϵ_1 can remain small for a long time. In Eq. (2.24), small ϵ_2 indicates that $\ddot{\phi}$ can be neglected and the friction term dominates the evolution of ϕ. In other words, the Hubble friction always prevents ϕ from accelerating so that $V(\phi)$ can always be larger than the kinetic energy of ϕ. According to this argument, Eqs. (2.23) and (2.24) are approximated by

$$3M_{\rm pl}^2 H^2 \approx V \approx \text{const.} \ , \tag{2.29}$$

$$3H\dot{\phi} + V_{,\phi} \approx 0 \ , \tag{2.30}$$

during inflation, which results in expressing the slow-roll parameters in terms of $V(\phi)$ and its derivatives

$$\epsilon_1 \approx \frac{M_{\rm pl}^2}{2}\left(\frac{V_{,\phi}}{V}\right)^2 \equiv \epsilon_{V1} \ , \tag{2.31}$$

$$\epsilon_2 \approx -\epsilon_1 + M_{\rm pl}^2 \frac{V_{,\phi\phi}}{V} \equiv -\epsilon_1 + \epsilon_{V2} \ . \tag{2.32}$$

Therefore, for single-field slow-roll inflation with a canonical kinetic term, the inflationary dynamics is completely determined by the potential shape of the inflaton. With a given concrete scalar potential, it is possible to examine the conditions for inflation to occur, such as $\epsilon_{V1} \ll 1$ and $\epsilon_{V2} \ll 1$, and calculate the duration of inflation. Using subscripts "ini" and "end" to denote the quantities evaluated at the beginning and the end of inflation, the condition $\epsilon_{V1}(t_{\rm end}) = 1$ determines the inflaton field value at the last moment of inflation $\phi_{\rm end}(t_{\rm end})$. After fixing $\phi_{\rm end}$, it is easy to calculate the duration of inflation which is usually expressed in terms of the number of e-folds

$$N_{\rm inf} \equiv \ln \frac{a(t_{\rm end})}{a(t_{\rm ini})} \ , \tag{2.33}$$

where $t_{\rm end}$ represents the initial moment of inflation as explained. As a result, the e-fold number is calculated as a function of the initial field value of inflaton

$$N_{\rm inf}(\phi_{\rm ini}) = -\int_{t_{\rm ini}}^{t_{\rm end}} d \ln \frac{a(t_{\rm end})}{a(t)} = \int_{t_{\rm ini}}^{t_{\rm end}} H dt = \int_{\phi_{\rm ini}}^{\phi_{\rm end}} \frac{H}{\dot{\phi}} d\phi \approx \int_{\phi_{\rm end}}^{\phi_{\rm ini}} \frac{d\phi}{M_{\rm pl}\sqrt{2\epsilon_{V1}}} \ . \tag{2.34}$$

Usually, the number of e-folds of inflation is required to be around $50 \sim 60$, which constrains the initial field values in inflation models.

So far, the quantitative discussion has focused on the classical homogeneous background evolution of the single-field slow-roll inflation models. Using a homogeneous scalar field ϕ whose potential energy dominates the Universe during inflation playing a role similar to a cosmological constant, it is possible to realize a long enough quasi de Sitter phase that solves three critical issues problems in the standard Hot Big Bang theory as desired. Next, a brief review of the cosmological perturbation theory is given, showing how to calculate the power spectrum of the quantum fluctuations generated during inflation which is directly related to the observed CMB anisotropy and LSS formation.

2.2.3 Quantum Fluctuation

With homogeneous classical background fields, only an unperturbed Universe is generated after inflation, which is inconsistent with current observation. In order to seed the observed CMB anisotropy and LSS formation, quantum fluctuations generated during inflation must be taken into account to provide the initial conditions for the subsequent evolution of the perturbed Universe. These quantum fluctuations are usually called primordial perturbations, which will be treated within the framework of

cosmological perturbation theory in the following[9]. The primordial perturbations are assumed to be small and superimposed upon a homogeneous and isotropic background (or, more specifically, a flat FLRW metric), which allows order-by-order calculation in the perturbative expansion. In this thesis, only linear perturbations are considered[10].

Quantum fluctuations inevitably exist in the metric and the inflaton field(s). According to the helicities of different components, they can be decomposed into three types, scalar-, vector-, and tensor-perturbations. The scalar and tensor perturbations have an important property that allows the comparison between theoretical predictions from inflation and observables, i.e. such perturbations behaving classically and remaining frozen at the superhorizon scale. During inflation, perturbations with physical wavelengths around the horizon size initially are stretched outside the Hubble radius soon after their generation, which leads to the fact that the quantum nature (or non-commutativity) of these primordial perturbations becomes negligible [72, 73] and their amplitudes become constant as soon as they are created. When these modes gradually re-enter the horizon as the Hubble radius grows after inflation, they leave imprints on CMB and LSS that can be observed by current and future observation, which allows us to learn about the past. On the other hand, vector modes are always diluted by Hubble expansion, so they are naturally considered subdominant and negligible. Therefore, in the following, the discussion focuses on the scalar and tensor perturbations which are responsible for the observed density perturbations and future experimental target, primordial gravitational waves, respectively.

2.2.3.1 Decomposition

As mentioned previously, the quantum fluctuations in the metric and matter can be decomposed into scalar-, vector-, and tensor-type, according to their behavior under coordinate transformations. At the linear order, they evolve independently. This important result can be proved by rewriting the covariant linear differential equation of second-order for the perturbations into decoupled equations, each of which contains only one type of perturbations [66][11]. A brief discussion of this proof is presented here.

Consider an $(n+1)$-dimensional FLRW spacetime generalized from Eq. (2.1), with γ_{ij} as the n-dimensional spatial metric which raises and lowers the spatial indices in this discussion. Denote the covariant derivative with respect to γ_{ij} as $\tilde{\nabla}_i$, and $_{|i} = \tilde{\nabla}_i$.

[9] See e.g. Ref. [66] for an excellent review.

[10] Higher order perturbations such as primordial non-Gaussianity are also intensively studied in e.g. Refs. [67–71].

[11] See Ref. [74] for another approach by making use of the symmetry of the flat FLRW background.

General scalar, vector, and tensor perturbations are denoted, respectively, as,

$$
\begin{aligned}
&a^{\rm S}\ ,\\
&b_i = b^{\rm S}_{|i} + b^{\rm V}_i\ ,\ b^{{\rm V}|i}_i = 0\ ,\\
&c_{ij} = c^{\rm TT}_{ij} + 2c^{\rm V}_{(i|j)} + \left(c^{\rm S}_{|ij} - \frac{1}{n}\gamma_{ij}\tilde{\Delta}\, c^{\rm S}\right) + \frac{1}{n}\gamma_{ij}\tilde{c}\ ,\ c^{{\rm TT}i}_i = c^{{\rm TT}|i}_{ij} = c^{{\rm V}|i}_i = 0\ ,
\end{aligned}
\tag{2.35}
$$

where $\tilde{\Delta} = \gamma^{ij}\tilde{\nabla}_i\tilde{\nabla}_j$ and $\tilde{c} = c^i_i$. From the definition of the Riemann tensor

$$
\left(\tilde{\nabla}_i\tilde{\nabla}_j - \tilde{\nabla}_j\tilde{\nabla}_i\right) v_k = R_{ijk}{}^m v_m\ ,
\tag{2.36}
$$

it can be shown that all the scalar quantities (up to second-order differentiation) appear in the following forms

$$
a^{\rm S}\ ,\ b^i_{|i} = \tilde{\Delta}b^{\rm S}\ ,\ \tilde{c}\ ,\ \tilde{\Delta}\tilde{c}\ ,\ \left(c^{ij} - \frac{1}{n}\gamma^{ij}\tilde{c}\right)_{|ij} = \frac{n-1}{n}\left(\tilde{\Delta} + nK\right)\tilde{\Delta}\, c^{\rm S}\ ,
\tag{2.37}
$$

where only the original scalar parts in $a^{\rm S}$, b_i, and c_{ij} show up. Similarly, the vector quantities only appear in the following forms

$$
\begin{aligned}
&a^{\rm S}_{|i}\ ,\ b_i\ ,\ \tilde{\Delta}b_i = \tilde{\Delta}b^{\rm V}_i + \left[\tilde{\Delta}b^{\rm S} + (n-1)Kb^{\rm S}\right]_{|i}\ ,\ \tilde{c}_{|i}\ ,\ \tilde{\nabla}_i\tilde{\Delta}\,\tilde{c}\ ,\\
&\left(c^{ij} - \frac{1}{n}\gamma^{ij}\tilde{c}\right)_{|j} = \left[\tilde{\Delta} + (n-1)K\right]b^{{\rm V}i} + \frac{n-1}{n}\tilde{\nabla}^i\left(\tilde{\Delta} + nK\right)c^{\rm S}\ ,
\end{aligned}
\tag{2.38}
$$

where, due to the transverse property of $b^{\rm V}_i$, $c^{\rm V}_i$, and $c^{\rm TT}_{ij}$, the scalar parts of these quantities only consist of the scalar modes appear in Eqs. (2.35), and the vector parts only consist of vector modes. As for the tensor quantities, the only combinations are as follows

$$
\begin{aligned}
&\gamma_{ij}a^{\rm S}\ ,\ \left(\tilde{\nabla}_i\tilde{\nabla}_j - \frac{1}{n}\gamma_{ij}\tilde{\Delta}\right)a^{\rm S}\ ,\ \gamma_{ij}\tilde{\Delta}a^{\rm S}\ ,\ \gamma_{ij}\tilde{\nabla}_k b^k = \gamma_{ij}\tilde{\nabla}b^{\rm S}\ ,\\
&2b_{(i|j)} = 2b^{\rm V}_{(i|j)} + 2\left(\tilde{\nabla}_i\tilde{\nabla}_j - \frac{1}{n}\gamma_{ij}\tilde{\Delta}\right)b^{\rm S} + \frac{2}{n}\gamma_{ij}\tilde{\Delta}b^{\rm S}\ ,\\
&c_{ij}\ ,\ \gamma_{ij}\tilde{c}\ ,\ \gamma_{ij}\tilde{\Delta}\,\tilde{c}\ ,\ \tilde{c}_{|ij} = \left(\tilde{\nabla}_i\tilde{\nabla}_j - \frac{1}{n}\gamma_{ij}\tilde{\Delta}\right)\tilde{c} + \frac{1}{n}\gamma_{ij}\tilde{\Delta}\,\tilde{c}\ ,\\
&2\tilde{\nabla}_{(i}\tilde{\nabla}^k c_{j)k} - \frac{2}{n}\tilde{c}_{|ij} = 2\tilde{\nabla}_{(i}\left[\tilde{\Delta} + (n-1)K\right]b^{\rm V}_{j)} + \frac{2(n-1)}{n}\left[\left(\tilde{\Delta} + nK\right)c^{\rm S}\right]_{|ij}\ ,\\
&\tilde{\Delta}\, c_{ij} = \tilde{\Delta}\, c^{\rm TT}_{ij} + 2\tilde{\nabla}_{(i}\left[\tilde{\Delta} - (n-1)\right]c^{\rm V}_{j)} + \left(\tilde{\nabla}_i\tilde{\nabla}_j - \frac{1}{n}\gamma_{ij}\right)\left[\tilde{\Delta} + (2n-1)K\right]c^{\rm S}\\
&+ \frac{1}{n}\gamma_{ij}\tilde{\Delta}\left[(n-1)Kc^{\rm S} + \tilde{c}\right]\ ,\\
&\gamma_{ij}c^{km}{}_{|km} = \frac{2(n-2)}{n}\tilde{\Delta}(\tilde{\Delta} + nK)\gamma_{ij}c^{\rm S} + \frac{2}{n}\gamma_{ij}\tilde{\Delta}\tilde{c}\ ,
\end{aligned}
\tag{2.39}
$$

where the transverse and traceless properties of $c_{ij}^{\rm TT}$ as well as the transverse properties of the vector modes ensure that the tensor, vector, and scalar parts are also well separated as in the previously situations. As a result, the equations of motion for different types of perturbations are decoupled with each other at linear level, which greatly simplifies the study of first-order perturbation.

2.2.3.2 Gauge Invariance

In GR, there are different ways to foliate the spacetime allowed by the diffeomorphism invariance, which corresponds to slicing the spacetime by a family of spacelike hypersurfaces $(\Sigma_t)|_{t\in\mathbb{R}}$ threaded by a smooth regular scale field t. This scalar field is usually regarded as the time coordinate, and spatial coordinates can also be attached to the spacelike hypersurfaces of constant time[12]. A choice of foliation is usually called a choice of gauge, and the diffeomorphism invariance is also correspondingly called gauge invariance. The gauge choice is important for studying cosmological perturbations because, generally speaking, the definition of perturbations is gauge-dependent. However, the physical quantities or observables should not depend on the choice of gauge. Therefore, before the calculation of power spectra of cosmological perturbations, it is necessary to remove the confusion caused by gauge choices by finding out the gauge-invariant physical quantities [80, 81].

The metric perturbations (neglecting the vector modes) on a flat FLRW metric are usually written in the following form

$$ds^2=-(1+2\Phi)dt^2+2a(t)B^{\rm S}_{,i}dx^i dt+a^2(t)\left[(1-2\Psi)\delta_{ij}+2E^{\rm S}_{,ij}+h^{\rm TT}_{ij}\right]dx^i dx^j \ , \quad (2.40)$$

where $\delta^{ij}E^{\rm S}_{,ij}=\delta^{ij}h^{\rm TT}_{ij}=\delta^{jk}h^{\rm TT}_{ij,k}=0$, and the relevant perturbations in inflaton are

$$\rho(t,\mathbf{x})=\bar{\rho}(t)+\delta\rho(t,\mathbf{x}) \ , \ p(t,\mathbf{x})=\bar{p}(t)+\delta p(t,\mathbf{x}) \ , \ \phi(t,\mathbf{x})=\bar{\phi}(t)+\delta\phi(t,\mathbf{x}) \ , \quad (2.41)$$

where the over-line $\bar{(\ )}$ denotes the homogeneous background. For simplicity, the notation $(\ )_{,i}\equiv\partial_i(\ )$ is adopted for the spatial partial derivatives. According to the gauge transformation rules shown in Appendix B, it is straightforward to construct as many gauge-invariant quantities as possible among which, however, only a few unique combinations are physically meaningful. In the context of inflation, one of the most essential quantities is the gauge-invariant curvature perturbation that seeds

[12] This picture can be seen more clearly in ADM formalism [75] where all the perturbations on the metric are encoded in the lapse of time, shift on the spacelike hypersurfaces, and the spatial metric. More details about ADM can be found in textbooks and reviews, e.g. [76–79].

the CMB anisotropy and LSS formation. Specifically, the definition of the gauge-invariant variable which coincides with the curvature perturbation on the comoving slicing ($\delta\phi = 0$) is given as

$$\mathcal{R} \equiv \Psi + \frac{H}{\dot{\phi}}\delta\phi \ . \tag{2.42}$$

This variable will be used later to calculate the scalar power spectrum and the scalar spectral index. A closely related quantity is the curvature perturbation defined on uniform-density slicing ($\delta\rho = 0$) [81]

$$-\zeta \equiv \Psi + \frac{H}{\dot{\bar{\rho}}}\delta\rho \ . \tag{2.43}$$

At superhorizon scale, these two curvature perturbations on different slicings coincide $\mathcal{R} \approx -\zeta$ [81]. One crucial property of $\mathcal{R}$ (or ζ) is its conservation after horizon exit under the circumstances where there are no external sources, for instance, during single-field inflation, which ensures that the subhorizon physics does not affect the modes outside the horizon until their re-entry. This is the reason why the observed power spectrum of the curvature perturbation generated during inflation can be computed simply at the horizon exit regardless of its superhorizon evolution. In the case of multi-field inflation where this is not only curvature perturbation but isocurvature ones, possible mixing among them can spoil the conservation of curvature perturbation at superhorizon scale, which will be discussed shortly. Another useful gauge-invariant quantity is the so-called Mukhanov-Sasaki variable [82, 83] which represents the perturbation of inflaton field on a spatially flat slicing ($\Psi = E^{\mathrm{S}} = 0$)

$$Q \equiv \delta\phi + \frac{\dot{\bar{\phi}}}{H}\Psi \ . \tag{2.44}$$

These gauge-invariant quantities are, by definition, unchanged under the gauge transformation. In particular, $\mathcal{R}$ and ζ represent the physical or observable curvature perturbation in corresponding gauges that can be chosen for convenience according to different situations[13]. Choosing Q, on the other hand, can greatly simplify the equation of motion for first-order scalar perturbations, leading to the well-known Mukhanov-Sasaki equation [82, 83]. Transforming from one to another is just through some simple gauge transformation (see Appendix B).

In a multi-component system, there is not only adiabatic (or curvature) perturbation mentioned above but also entropy (or isocurvature) perturbations. Intuitively

[13]There are generally no preferred gauges, but some of them do have their own advantages on the "good" behavior of the perturbations. See e.g. Refs. [66, 74, 79, 84] for details of different gauges.

speaking, the former describes how each component fluctuates according to the total energy density fluctuation with their relative ratios unchanged while the latter describe the relative fluctuations among all the components without changing the total energy density. More specifically, assuming that there are two components in the fluid with total energy density $\rho_{\rm tot}$, the adiabatic perturbation is given by the part where the pressure is a unique function of the (smoothed) total energy density at a relevant scale such that (see e.g. Ref. [85])

$$\delta p_{\rm ad} \equiv \frac{\dot{\bar{p}}_{\rm tot}}{\dot{\bar{\rho}}_{\rm tot}} \delta\rho \ , \tag{2.45}$$

while the isocurvature perturbation is defined as the deviation from the adiabatic one

$$\delta p_{\rm en} \equiv \delta p - \delta p_{\rm ad} \ , \tag{2.46}$$

or alternatively a dimensionless gauge-invariant entropy perturbation can be defined as [86]

$$\mathcal{S} \equiv H \left(\frac{\delta p}{\dot{\bar{p}}} - \frac{\delta\rho}{\dot{\bar{\rho}}} \right) \ . \tag{2.47}$$

There are more than one scalar modes in multi-field inflation models, among which only one linear combination is the curvature perturbation while others are of isocurvature type. In this case, the curvature perturbation corresponds to the perturbations along the classical inflaton trajectory, while the isocurvature perturbations represent the perturbations orthogonal to it. If the orthogonal direction possesses a mass much heavier than the Hubble parameter, the heavy isocurvature mode is hardly excited and can be integrated out. Generally speaking, the isocurvature modes can serve as a source term to the adiabatic one through the turning rate of the inflaton, so if the inflaton trajectory is curved, the curvature perturbation is no longer conserved at superhorizon scale [86]. Usually, the isocurvature mode cannot survive until today because the thermalization process after inflation washes out such type of perturbations[14].In the cases considered in this thesis, isocurvature modes are always negligible, so further discussion is omitted.

2.2.3.3 Power Spectrum

One of the most important observable in cosmology is the power spectrum of the curvature perturbation $\Delta^2_{\mathcal{R}}$ about which most data come from CMB anisotropy and

[14]See discussion in e.g. Refs. [87–90].

LSS. Currently, the observation determines its amplitude to be $\sim \mathcal{O}(10^{-9})$ [23]. In order to confront the theory with observation, it is essential to calculate $\Delta^2_{\mathcal{R}}$ in given inflation models, through which the model parameters are constrained.

To solve the dynamics for the first-order perturbation, it is necessary to expand the action up to the second order. On the comoving slicing, it is known from Eq. (2.42) that $\mathcal{R} = \Psi$ holds, and so the action in second order of curvature perturbation is given as[15]

$$S = \frac{1}{2}\int d^3x d\eta \left[(v')^2 - (v_{,i})^2 + \frac{z''}{z}v^2\right] \ , \tag{2.48}$$

where $v \equiv z\mathcal{R}$, $z \equiv a\dot{\phi}/H$, and ($'$) denotes the derivative with respect to the conformal time η [82, 83]. Quantizing the scalar field v with proper normalization, the equation of motion for its mode function is easily derived as

$$v_k'' + (k^2 - z''/z)v_k = 0 \ , \tag{2.49}$$

which is known as the Mukhanov-Sasaki equation [82,83]. As can be seen, the Hubble expansion induces a time-dependent effective mass $-z''/z$ for the scalar field which encodes the interaction between background spacetime and perturbation.

In single-field slow-roll inflation models which are of interest here, the Universe is in a quasi-de Sitter phase during inflation so the effective mass can be expressed in terms of the slow-roll parameters (up to second order) [91] as

$$z''/z = a^2H^2(2 + 2\epsilon_1 - 3\epsilon_2 + \epsilon_2^2 - \epsilon_1\epsilon_2) + a^2H\dot{\epsilon}_1 - a^2H\dot{\epsilon}_2 \ , \tag{2.50}$$

with which Eq. (2.49) can be solved to yield

$$v_k = \frac{\sqrt{\pi}}{2}e^{i(\nu+1/2)\pi/2}\sqrt{-\eta}H_\nu^{(1)}(-k\eta) \ . \tag{2.51}$$

Here, $H_\nu^{(1)}(x)$ is the Hankel function of the first kind, and

$$\nu = \frac{1 + \epsilon_1 - \epsilon_2}{1 - \epsilon_1} + \frac{1}{2} \ . \tag{2.52}$$

In de Sitter limit where $\epsilon_1 = \epsilon_2 = 0$ and $H = $ const., Eq. (2.51) coincides with the mode function for the Bunch-Davies vacuum [92]

$$v_k = \frac{e^{-ik\eta}}{\sqrt{2k}}(1 - \frac{i}{k\eta}) \ . \tag{2.53}$$

[15]Here, the sound speed of the perturbation is $c_s^2 = 1$. Later in the discussion of multi-field inflation, more discussion on the non-trivial sound speed is presented.

Soon after generation, perturbations exit the horizon and freeze until they re-enter the Hubble horizon after inflation. At superhorizon scale $|k\eta| \to 0$, Eq. (2.51) behaves as

$$\lim_{|k\eta|\to 0} v_k \to e^{i(\nu-1/2)\pi/2}\frac{\Gamma(\nu)}{\Gamma(3/2)}\frac{2^{\nu-3/2}}{\sqrt{2k}}(-k\eta)^{1/2-\nu} \ . \tag{2.54}$$

which is of interest in cosmology. The dimensionless power spectrum of curvature perturbation $\Delta^2_{\mathcal{R}}(k)$ is defined as

$$\langle \mathcal{R}_{\mathbf{k}}\mathcal{R}_{\mathbf{p}}\rangle = (2\pi)^3\,\delta^{(3)}\left(\mathbf{k}+\mathbf{p}\right)\frac{2\pi^2}{k^3}\Delta^2_{\mathcal{R}}(k) \ , \tag{2.55}$$

which should be evaluated at the horizon crossing moment, $a_*H_* = k_*$. As a result,

$$\Delta^2_{\mathcal{R}}(k_*) = \frac{k}{4\pi^2}\frac{H^2}{M^2_{\rm pl}\epsilon_1}\left|v_k\right|^2\Big|_{a_*H_*=k_*} \simeq \frac{H^2}{8\pi^2 M^2_{\rm pl}\epsilon_1}\Big|_{a_*H_*=k_*} \simeq \frac{1}{24\pi^2 M^4_{\rm pl}}\frac{V}{\epsilon_1}\Big|_{a_*H_*=k_*} \ , \tag{2.56}$$

from which the scalar spectral index can be obtained [93]

$$n_s - 1 \equiv \frac{d\ln\Delta^2_{\mathcal{R}}}{d\ln k} \simeq -4\epsilon_1 + 2\epsilon_2\big|_{a_*H_*=k_*} \ , \tag{2.57}$$

which is slow-roll suppressed. In other words, single-field slow-roll inflation results in a nearly scale-invariant scalar spectrum.

As for the primordial tensor mode, the procedure is similar [55, 94–97]. Specifically, the equation of motion for the tensor mode function is simply, in Eq. (2.49), substituting z with a, and v_k with $v^r_{\mathbf{k}} \equiv a h^r_{\mathbf{k}}$ which is given by

$$\begin{aligned} h^{\rm TT}_{ij}(\eta,\mathbf{x}) =& \frac{\sqrt{2}}{M_{\rm pl}}\int\frac{d^3k}{(2\pi)^3}e^{i\mathbf{k}\cdot\mathbf{x}}\sum_{r=+,\times}\epsilon^r_{ij}(\mathbf{k})h^r_{\mathbf{k}}(\eta) \ , \\ h^r_{\mathbf{k}}(\eta) =& h_k(\eta)a^r_{\mathbf{k}} + h^*_k(\eta)a^{r\dagger}_{-\mathbf{k}} \ , \end{aligned} \tag{2.58}$$

where ϵ^r_{ij} with $r = +, \times$ are the symmetric unit polarization vectors satisfying $\epsilon^r_{ii} = \delta^{ij}k_i\epsilon^r_{jk} = 0$ and normalized as $\delta^{ij}\delta^{kl}\epsilon^r_{ik}\left(\epsilon^s_{jl}\right)^* = 2\delta^{rs}$. Consequently, the dimensionless tensor power spectrum is calculated as

$$\Delta^2_h(k_*) \equiv \frac{d}{d\ln k}\langle\left(h^{\rm TT}_{ij}\right)^2\rangle\Big|_{a_*H_*=k_*} = \frac{8}{M^2_{\rm pl}}\frac{k^3}{2\pi^2}\left|h_k\right|^2\Big|_{a_*H_*=k_*} = 8\left(\frac{H}{2\pi M_{\rm pl}}\right)^2\Big|_{a_*H_*=k_*} \ , \tag{2.59}$$

with which the tensor spectral tilt is obtained

$$n_t \equiv \frac{d\ln\Delta^2_h}{d\ln k} \approx -2\epsilon_1 \ , \tag{2.60}$$

which is also slow-roll suppressed. Another useful quantity is the tensor-to-scalar ratio r

$$r(k) \equiv \frac{\Delta_h^2(k)}{\Delta_{\mathcal{R}}^2(k)} = 16\epsilon_1 \ . \tag{2.61}$$

As can be seen, the single-field slow-roll inflation predicts a suppressed r, which indicates that the primordial tensor perturbation is much smaller than the scalar. From Eqs. (2.60) and (2.61), a consistency relation of single-field inflation is obtained

$$r = -8n_t \ , \tag{2.62}$$

which can be one of the ways to falsify single-field slow-roll class of models if a deviation from it is observed in the future.

The amplitude of scalar power spectrum, the scalar spectral index and the tensor-to-scalar ratio are three very important observables to constrain inflation models [23]. The current observed value of scalar power spectrum amplitude at pivot scale $k_* = 0.05\text{Mpc}^{-1}$ is [23]

$$\Delta_{\mathcal{R}}^2 \simeq 2.1 \times 10^{-9} \ , \tag{2.63}$$

the spectral tilt n_s at pivot scale $k_* = 0.05\text{Mpc}^{-1}$ is [23]

$$n_s = 0.9649 \pm 0.0042 \text{ at } 68\% \text{ CL} \ , \tag{2.64}$$

while only a upper bound is put on r as no tensor mode has ever been detected yet [23]

$$r_{0.002} \lesssim 0.056 \text{ at } 95\% \text{ CL} \ , \tag{2.65}$$

where the subscript means that it is measured at the pivot scale $k_* = 0.002\text{Mpc}^{-1}$. Focusing on a larger scale for r is because primordial gravitational waves basically has no contribution to CMB anisotropy at $\ell \gtrsim 100$ where ℓ is the multipole moment. An important point is that these values depend on the pivot scale considered which is determined by the duration of inflation and the thermal history of the Universe after inflation. The period after BBN has already been well probed while the physics before that is still of large ambiguity. Therefore, knowing the inflation period and the post-inflationary reheating process in given models is essential to improve the constraints from observation.

2.2.4 Typical Examples

Single-field slow-roll inflation is simple but powerful because different primordial perturbation spectra can be achieved simply by altering the shape of the inflaton potential, as shown previously. Given that the desired values are shown in Eqs. (2.63)-(2.65), models satisfying these constraints can be constructed by manipulating the potential shape almost arbitrarily, which, however, is too ambiguous and lacks motivation. Instead, inflationary models with fewer parameters and natural origins from particle physics or quantum gravity are much more attractive. Among all the single-field inflation models, two stay inside the best-fit regime of the observationally allowed region, the Starobinsky model with only one model parameter and the Higgs inflation constructed from the only known scalar field in SM. The review of the inflationary dynamics in these two models is presented in the following, which will help to understand this thesis's main topic, the mixed Higgs-R^2 inflation model.

2.2.4.1 Starobinsky Model

The Starobinsky model (or R^2-inflation) was originally proposed in Ref. [3] when considering the one-loop quantum correction to the E-H action. As will be shown below, however, to fit the observational data, the coefficient in front of the "correction" term R^2 has to be extremely large, which makes the original point of view break down. So far, there is no satisfying explanation of the origin of the R^2 term, but the Starobinsky model is still one of the most attractive inflation models because of its simpleness and best-fit observational predictions[16].

The action of R^2-inflation consists of only two geometric terms in JF without introducing any additional scalar fields

$$S_{\rm J} = \int d^4x\sqrt{-g_{\rm J}}\left[\frac{M_{\rm pl}^2}{2}R_{\rm J} + \frac{M_{\rm pl}^2}{12M^2}R_{\rm J}^2\right] \ , \tag{2.66}$$

where M is a new mass scale and the only one parameter in this model. As is known from Sec. 2.2.1, the quadratic term in Eq. (2.66) induces a new scalar degree of freedom in EF because of the higher derivatives. This scalar field plays the role of inflaton and is dubbed "scalaron" in the literature. Consequently, M is usually called the scalaron mass. The inflation dynamics in this model is clear and simple, which will be shown here in both JF and EF for completeness.

• **Jordan frame** Here, all the quantities are defined in JF so the subscripts "J" will be dropped for convenience. Assuming the background spacetime to be the flat

[16] See e.g. Ref. [98] for an excellent review for $f(R)$ theory. See also Ref. [99].

FLRW metric, the Ricci scalar can be expressed in terms of Hubble parameter and its derivatives

$$R = 12H^2 + 6\dot{H} \ , \tag{2.67}$$

and the Einstein equations are given by

$$2H\ddot{H} - \dot{H}^2 + 6H^2\dot{H} + M^2H^2 = 0 \ , \tag{2.68}$$

$$\ddot{R} + 3H\dot{R} + M^2R = 0 \ , \tag{2.69}$$

where R is treated as an independent scalar degree of freedom (scalaron) so that the equations of motion for both R and H are kept to be of second order in time derivatives. During inflation, the slow-roll approximations $\epsilon_1 \ll 1$ and $\epsilon_2 \ll 1$ are valid (which indicates $R \simeq 12H^2 > 0$), so the first two terms in Eq. (2.68) and the first term in Eq. (2.69) are negligible. The former leads to a simple result

$$\dot{H} \simeq -M^2/6 \ , \tag{2.70}$$

which gives the solution of H as

$$H \simeq H_{\rm ini} - \frac{M^2}{6}(t - t_{\rm ini}) \ , \tag{2.71}$$

where the Hubble parameter takes the initial value $H_{\rm ini} \gg M$ at $t = t_{\rm ini}$, while the latter can be solved with the help of the solution above and gives

$$R \simeq 12H^2 - M^2 \ . \tag{2.72}$$

For duration of inflation $N_{\rm inf} = 60$, the initial Hubble parameter is $H_{\rm ini} \simeq 2\sqrt{5}M$, while the end of inflation is set by $\epsilon_1 = 1$ which gives $H_{\rm end} \simeq M/\sqrt{6}$. The scalaron mass can be fixed to be $M = M_c \sim 10^{-5}M_{\rm pl}$ by using Eqs. (2.56) and the observed amplitude of scalar power spectrum. This value makes the R^2 term coefficient unusually large, which still remains unexplained. Hereafter, the specific value of M_c will be adopted for calculation [24, 38, 41, 100]

$$M_c \equiv \sqrt{\frac{24\pi^2\Delta^2_{\mathcal{R}}}{N^2_{\rm inf}}}M_{\rm pl} \simeq 1.3 \times 10^{-5}\left(\frac{54}{N_{\rm inf}}\right)M_{\rm pl} \ , \tag{2.73}$$

where $\Delta^2_{\mathcal{R}}$ is given in Eq. (2.63).

• **Einstein frame** Here, all the quantities without subscript "J" are defined in EF. Using the technique in Sec. 2.2.1, the scalaron field is defined as

$$\alpha\varphi \equiv \sqrt{\frac{2}{3}}\frac{\varphi}{M_{\rm pl}} \equiv \ln\left[1 + \frac{R_{\rm J}}{3M^2}\right] \ , \tag{2.74}$$

which enters the conformal transformation as follows

$$g_{\mu\nu} = e^{\alpha\varphi} g_{\mathrm{J}\mu\nu} \ . \tag{2.75}$$

As a result, the action is rewritten in EF as

$$\begin{aligned} S =& \int d^4x\sqrt{-g}\left[\frac{M_{\rm pl}^2}{2}R - \frac{1}{2}g^{\mu\nu}\partial_\mu\varphi\partial_\nu\varphi - U(\varphi)\right] \ , \\ U(\varphi) =& \frac{3}{4}M_{\rm pl}^2M^2\left(1-e^{-\alpha\varphi}\right)^2 \ . \end{aligned} \tag{2.76}$$

This potential is asymptotically flat for large φ regime where inflation occurs. During inflation, $\alpha\varphi \gg 1$ so the inflaton potential is nearly constant $U_{\rm inf} \simeq 3M_{\rm pl}^2M^2/4$. With slow-roll approximation, the Hubble parameter is determined as $H_{\rm ini} \simeq M/2$. Given the potential in Eq. (2.76), the slow-roll parameters defined in Eqs. (2.31) and (2.32) can be easily calculated, which fixes the field value of scalaron at the end of inflation $\varphi_{\rm end} \simeq 0.94M_{\rm pl}$ and the initial value $\varphi_{\rm ini} \simeq 5.45M_{\rm pl}$ for $N_{\rm inf} \simeq 3e^{\alpha\varphi_{\rm ini}}/4 = 60$. The scalar spectral index and tensor-to-scalar ratio are also calculated as

$$n_s - 1 \simeq -6\epsilon_{V1} + 2\epsilon_{V2} \simeq -2/N_{\rm inf} \ , \ r \simeq 16\epsilon_{V1} \simeq 12/N_{\rm inf}^2 \ , \tag{2.77}$$

which, for $N_{\rm inf} = 60$, are

$$n_s \simeq 0.967 \ , \ r \simeq 0.003 \ . \tag{2.78}$$

These predictions are automatically located in the best-fit region of the current experimental results [23] with only one model parameter M fixed by $\Delta_{\mathcal{R}}^2$, which is one of the most important reasons to consider the Starobinsky model.

2.2.4.2 Higgs Inflation

To construct an inflation model usually requires the introduction of a new scalar field from some extension of SM, such as GUT and supersymmetry (SUSY), to serve as the inflaton. However, there is an interesting possibility that the inflaton field comes from SM, specifically, the Higgs field that has already been discovered at LHC. In this case, no additional scalar fields from new physics are needed to realize inflation in the very early Universe.

To achieve this, a large non-minimal coupling between Higgs and gravity is required to render the Higgs potential to be flat enough [25–27]. The action of the Higgs inflation is written as

$$S_{\rm J} = \int d^4x\sqrt{-g_{\rm J}}\left[\left(\frac{M_{\rm pl}^2}{2} + \xi\left|\mathcal{H}_{\rm SM}\right|^2\right)R_{\rm J} - g_{\rm J}^{\mu\nu}\partial_\mu\mathcal{H}_{\rm SM}^\dagger\partial_\nu\mathcal{H}_{\rm SM} - \lambda\left|\mathcal{H}_{\rm SM}\right|^4\right] \ , \tag{2.79}$$

where $\mathcal{H}_{\rm SM}$ is the SM Higgs complex doublet, λ is the Higgs self-coupling, $\xi > 0$ is the non-minimal coupling between Higgs and Ricci scalar[17]. The mass and electroweak (EW) vacuum expectation value (vev) of Higgs are neglected because the inflation scale is much higher than EW scale. When studying inflation and reheating, it is sufficient to work in the unitary gauge where $\mathcal{H}_{\rm SM} = h/\sqrt{2}$ with the real scalar field h as the physical degree of freedom. As a result, Eq. (2.79) is simplified as

$$S_{\rm J} = \int d^4x\sqrt{-g_{\rm J}}\left[\left(\frac{M_{\rm pl}^2}{2} + \frac{\xi}{2}h^2\right)R_{\rm J} - \frac{1}{2}g_{\rm J}^{\mu\nu}\partial_\mu h\partial_\nu h - \frac{\lambda}{4}h^4\right] . \tag{2.80}$$

It will be shown in the following that the inflationary dynamics in this model with $\xi \gg 1$ is the same as the Starobinsky model.

• **Jordan frame** Here, all the quantities are defined in JF so the subscripts "J" will be dropped for convenience. Since the Ricci scalar R contains second-order time derivatives of the metric $g_{\mu\nu}$, the non-minimal coupling in Eq. (2.80) induces an extra kinetic term for the Higgs field which is proportional to $\xi \gg 1$. Therefore, the original kinetic term for Higgs is negligible compared with $\xi h^2 R/2$, which yields a constraint equation from the equation of motion for Higgs as [101]

$$\lambda h^2 = \xi R . \tag{2.81}$$

Inserting this constraint back to Eq. (2.80) without the canonical kinetic term for Higgs, the resulting action is nothing but the Starobinsky model except for the scalaron mass now replaced by the combination of ξ and λ in the following form

$$M^2 \to \frac{\lambda}{3\xi^2}M_{\rm pl}^2 . \tag{2.82}$$

Knowing that $M = M_c$ for observationally favored inflation, the constraint on the model parameters in the Higgs inflation is

$$\xi/\sqrt{\lambda} \simeq 4 \times 10^4 . \tag{2.83}$$

If the self-coupling is $\lambda \sim 10^{-2}$ (non-critical)[18], then $\xi \sim \mathcal{O}(10^3)$. A specific value ξ_c will be adopted in this thesis [41]

$$\xi_c \equiv \sqrt{\frac{\lambda N_{\rm inf}^2}{72\pi^2\Delta_{\mathcal{R}}^2}} \simeq 4.4 \times 10^3 \left(\frac{\lambda}{0.01}\right)^{1/2}\left(\frac{N_{\rm inf}}{54}\right) , \tag{2.84}$$

[17] Conformal coupling corresponds to $\xi = -1/6$. See Appendix A for more detail.

[18] Here, criticality means that the Higgs potential becomes flat around Planck scale, i.e. $\lambda \to 0$, which is used to construct the critical Higgs inflation [102–104]. In this thesis, only non-critical Higgs inflation is considered.

where $\Delta^2_{\mathcal{R}}$ is the dimensionless scalar power spectrum in Eq. (2.63).

• **Einstein frame** Here, omit the subscripts "E" for the quantities defined in EF. Again, making use of the technique in Sec. 2.2.1, the non-minimal coupling can be moved to the potential and non-canonical kinetic term by the conformal transformation, leaving the Ricci scalar only exists in the E-H term. The corresponding EF action is written as

$$g_{\mu\nu} = \Omega^2 g_{\mathrm{J}\mu\nu} \equiv \left(1 + \frac{\xi h^2}{M_{\mathrm{pl}}^2}\right) g_{\mathrm{J}\mu\nu} \ , \tag{2.85}$$

$$\frac{d\phi}{dh} = \sqrt{\frac{\Omega^2 + 6\xi^2 h^2/M_{\mathrm{pl}}^2}{\Omega^4}} \ , \tag{2.86}$$

which results in an EF action as

$$\begin{aligned} S =& \int d^4x\sqrt{-g}\left[\frac{M_{\mathrm{pl}}^2}{2}R - \frac{1}{2}g^{\mu\nu}\partial_\mu\phi\partial_\nu\phi - V(\phi)\right] \ , \\ V(\phi) =& \frac{\lambda}{4\Omega^4(\phi)}h^4(\phi) \ . \end{aligned} \tag{2.87}$$

During inflation $h \gg M_{\mathrm{pl}}/\sqrt{\xi}$, Eq. (2.86) gives the relation $h \approx \exp\left[\phi/\left(\sqrt{6}M_{\mathrm{pl}}\right)\right]$ such that the potential in Eq. (2.87) becomes the same as that in Eq. (2.76) in large ϕ regime with M replaced by $\sqrt{\lambda/3}M_{\mathrm{pl}}/\xi$ which is consistent with Eqs. (2.82).

In conclusion, the inflationary dynamics in the Higgs inflation is equivalent to that in the Starobinsky model. One way to break the degeneracy of these two models is to consider the reheating process which determines the pivot scale and, as a result, the scalar spectral index and tensor-to-scalar ratio. As will be shown later, the reheating processes after inflation are very different in these two models, which leads to different reheating temperatures and N_{inf}.

Although the Higgs inflation is a very attractive model, several important issues need to be taken care of, mostly caused by the large non-minimal coupling $\xi \sim 10^4\sqrt{\lambda}$. Such a large non-minimal coupling is shown to reduce the tree-level cutoff scale of the theory in the vacuum to a scale much lower than the inflation scale $\Lambda_{\mathrm{Higgs}} \sim M_{\mathrm{pl}}/\xi \ll M_{\mathrm{pl}}/\sqrt{\xi}$ [105–108] which casts doubts on the inflationary prediction in this model. This issue was later resolved by recognizing the background-dependent cutoff scale that is higher than the dynamical scale throughout the whole inflationary period in this model [109, 110][19]. However, due to the nonrenormalizability of GR, there is still considerable ambiguity when reconstructing the Higgs potential at inflation

[19] Another point of view is discussed in Ref. [101].

scale from the low-energy observables [111, 112], which requires a sensible UV theory for comprehensive understanding. A more severe issue appears during preheating in the Higgs inflation. It has been shown that the effective mass of the Nambu-Goldstone mode, which constitutes the longitudinal mode of gauge bosons, exhibits spiky behavior [34, 100, 113], which is absent in the traditional analysis of reheating process [14, 15, 21, 22] in the Higgs inflation model [31–33]. This large spike can induce violent particle production [34, 35] which can transfer all the inflaton energy into gauge fields within one inflaton oscillation. However, the amplitude of the spike is shown to be even larger than the cutoff scale of the theory during preheating, meaning that the theory enters the strongly-coupled regime, so the usual treatment is not reliable any more[20]. To understand whether the production of gauge bosons occurs and the subsequent evolution during reheating, an appropriate UV-extension for the Higgs inflation is required, which is one of the main topics in this thesis and will be discussed in more detail later.

Higgs instability is also intensively discussed by many authors. If the SM renormalization group running is valid up to the inflation scale (or Planck scale), the Higgs self-coupling λ might run into a negative value if the top quark mass m_t is too large. Once λ becomes negative, the Higgs potential is unbounded from below so Higgs becomes unstable during inflation. As a result, the analysis of inflation dynamics shown above is invalid. Nevertheless, there are still many attempts to save the Higgs inflation. For example, it is shown in Ref. [112] that the radiative correction to the Higgs effective potential can rescue the Higgs inflation with large non-minimal coupling. The EW vacuum becomes metastable due to the presence of a new vacuum, but the reheating temperature is believed to be high in this model so that the symmetry will be restored temporarily and the Higgs field will end up in the EW vev. However, ambiguity is still inevitable because of the coupling between SM and gravity.

2.3 Multi-Field Inflation

Despite the simpleness and power of the single-field slow-roll inflation, single-field models seem not to be the final answer to the realistic Universe. For example, one of the most promising single-field models considered in the previous section, the Higgs inflation, suffers from the strong coupling preheating problem, which will be discussed later. This problem is unlikely to be solved unless the UV completion (or extension) of this model is found. On the other hand, the candidates of UV physics beyond

[20] See Ref. [114] for the study of this phenomenon with higher dimensional operators.

SM generally contain a number of scalar degrees of freedom that could be relevant to inflation dynamics, such as superpartners in SUSY and moduli fields in string theory (see e.g. Refs. [115, 116]). Therefore, the generalization to a multi-field approach seems to be more realistic and might improve the UV properties of the single-field models.

By definition, multi-field inflation models contain more than one degrees of freedom responsible for the inflation dynamics, such as Brans-Dicke inflation [117], quasi-single field inflation [118], hybrid inflation [119], and multiple inflation [87, 120], etc. Usually, in multi-field cases, both curvature and isocurvature perturbations should be taken into account, and multi-dimensional field dynamics generically leads to rich phenomena that are absent in single-field case, as well as much more complicated situation (see e.g. Ref. [121] for a review). Scalar fields can interact not only through potential but non-canonical kinetic terms (or non-trivial phase space spanned by these fields), which can alter the sound speed of perturbations and the inflaton trajectory, or generate a non-trivial vacuum structure. By searching for the observables such as features on the power spectrum of curvature perturbation, non-Gaussianity, and isocurvature mode with more precise experiments, the information of multi-field inflation could be extracted.

Although multi-field models are of significant complication in a general sense, the situation might be simplified in some special cases, for instance, if an effective field theory approach is applicable during inflation. In models with a large mass hierarchy between different scalar fields, heavy ones[21] may not be dominant components during inflation, and perturbations in these fields are hardly excited. As a result, a possible separation of heavy and light degrees of freedom is available such that a low-energy effective theory can be obtained by integrating out the heavy modes, which significantly reduces the complexity of the system.

In the rest of this section, a general multi-field formalism [122] is reviewed briefly as well as the effective field theory in models with mass hierarchy based on Refs. [123–125], followed by the introduction of an observationally favored and theoretically motivated two-field model, the mixed Higgs-R^2 inflation model [36–40].

[21] During inflation, "heavy" and "light" is defined by the comparison with Hubble parameter.

2.3.1 Formalism

Consider a general action for an N-field inflation model in EF where all the scalar fields responsible for inflation are minimally coupled with gravity

$$S = \int d^4x\sqrt{-g}\left[\frac{M_{\rm pl}^2}{2}R - \frac{1}{2}\gamma_{ab}(\phi)g^{\mu\nu}\nabla_\mu\phi^a\nabla_\nu\phi^b - U(\phi)\right] , \tag{2.88}$$

where $U(\phi)$ is a general potential for all the scalar fields, $g_{\mu\nu}$ is the metric for spacetime while $\gamma_{ab}(\phi)$ is the field space metric with $a, b = 1, 2, \cdots, N$, denoting different scalar fields ϕ^a. Assuming a flat FLRW background, the Friedmann equation and Klein-Gordon equation are given by [122]

$$3M_{\rm pl}^2H^2 = \dot{\bar{\phi}}^2/2 + U(\bar{\phi}) , \tag{2.89}$$

$$D\dot{\bar{\phi}}^a/dt + 3H\dot{\bar{\phi}}^a + \gamma^{ab}U_{,b} = 0 , \tag{2.90}$$

where $\bar{\phi}^a(t)$ are homogeneous background fields, $\dot{\bar{\phi}} \equiv \left(\gamma_{ab}\dot{\bar{\phi}}^a\dot{\bar{\phi}}^b\right)^{1/2}$, notation $U_{,a} \equiv \partial U/\partial\phi^a$ is similar to the single-field case, and a "directional derivative" is defined $DX^a \equiv dX^a + \Gamma^a_{bc}X^b d\bar{\phi}^c$ with $\Gamma^a_{bc} = \frac{1}{2}\gamma^{ad}(\gamma_{cd,b} + \gamma_{db,c} - \gamma_{bc,d})$ the Christoffel symbol for the curved field space. Correspondingly, a covariant derivative ∇_a defined with respect to γ_{ab} is related to the directional derivative in the following way $D/dt = \dot{\bar{\phi}}^a\nabla_a$.

In a multi-dimensional system, it is useful to define the normalized "gradient" vector T^a as well as the orthogonal ones N^a respectively to clarify the evolution [86, 123]

$$T^a \equiv \dot{\bar{\phi}}^a/\dot{\bar{\phi}} , \tag{2.91}$$

$$\dot{\theta}_t N^a \equiv -DT^a/dt , \tag{2.92}$$

where normalization factor $\dot{\theta}_t$ can be understood as the angular velocity (or turning rate) of the inflation trajectory. Obviously, the direction T^a tangent to inflation trajectory is usually some linear combination of all the scalar fields that gives the lightest direction under the influence of both scalar potential and curved field space. Quantum fluctuations along this direction generate the curvature perturbation observed on CMB while those on N^a directions are of isocurvature type. As can be seen later, the two kinds of perturbations are coupled through a bending trajectory, i.e. a non-vanishing $\dot{\theta}_t$ which is one of the essential differences from the single-field case.

As in the single-field case, the time-dependence of the Hubble parameter characterizes the dynamics of inflation through the slow-roll parameters [123]

$$\epsilon_1 \equiv -\frac{\dot{H}}{H^2} = \frac{\dot{\bar{\phi}}^2}{2M_{\rm pl}^2 H^2} \ , \tag{2.93}$$

$$\epsilon_2^a \equiv -\frac{1}{H\dot{\bar{\phi}}}\frac{D\dot{\bar{\phi}}^a}{dt} \ , \tag{2.94}$$

where, in particular, the second slow-roll parameter is no longer a scalar but a vector that measures the acceleration of $\bar{\phi}^a$ in different directions. For the purpose of long enough slow-roll inflation, only small ϵ_2^a in direction T^a is necessary. To be specific, the decomposition of ϵ_2^a can be written as

$$\epsilon_2^a = \epsilon_2^{\parallel} T^a + \epsilon_2^{\perp} N^a \equiv -\frac{\ddot{\bar{\phi}}}{H\dot{\bar{\phi}}} T^a + \frac{U_N}{\dot{\bar{\phi}} H} N^a \ , \tag{2.95}$$

where $U_N \equiv N^a U_{,a}$ is used. Consequently, slow-roll inflation corresponds to the case $\epsilon_1 \ll 1$ and $\epsilon_2^{\parallel} \ll 1$. Given the decomposition of ϵ_2^a, the turning rate of the trajectory can be expressed in terms of the slow-roll parameter $\dot{\theta}_t = H\epsilon_2^{\perp}$ which can be large while keep the slow-roll inflation uninterrupted. In analogy to the single-field case, Eqs. (2.93) and (2.94) can be approximately expressed in terms of the potential (and its derivatives) and, in addition, the field space structure as

$$\epsilon_1 \approx \epsilon_{V1} \equiv \frac{M_{\rm pl}^2}{2}\left(\frac{U_\phi}{U}\right)^2 \ , \tag{2.96}$$

$$\epsilon_1 + \epsilon_2^{\parallel} \approx \epsilon_{V1} + \epsilon_{V2}^{\parallel} \equiv M_{\rm pl}^2 \frac{\nabla_\phi U_\phi}{U} \ , \tag{2.97}$$

where $\nabla_\phi \equiv T^a \nabla_a$ and $U_\phi \equiv T^a U_{,a}$.

Upon the slow-roll background, perturbations in metric and scalar fields are generated. As in the single-field case, the scalar fields and the metric are decomposed into background and perturbations in a similar manner. The equation of motion for the Mukhanov-Sasaki variable $Q^a \equiv \delta\phi^a + \dot{\bar{\phi}}^a \Psi/H$ with $\delta\phi^a(t,\mathbf{x}) = \phi^a(t,\mathbf{x}) - \bar{\phi}^a(t)$ is given by [122]

$$\begin{aligned} &\frac{D^2 Q^a}{dt^2} + 3H\frac{DQ^a}{dt} - \frac{\nabla^2}{a^2}Q^a + C^a_{\ b} Q^b = 0 \ , \\ &C^a_{\ b} \equiv \nabla_b U^{,a} - \dot{\bar{\phi}}^2 R^a_{\ bcd} T^c T^d + 2\epsilon_1 \frac{H}{\dot{\bar{\phi}}}\left(T^a U_{,b} + T_b U^{,a}\right) + 2\epsilon_1(3-\epsilon_1)H^2 T^a T_b \ , \end{aligned} \tag{2.98}$$

where $R^a_{\ bcd} = \Gamma^a_{bd,c} - \Gamma^a_{bc,d} + \Gamma^a_{ce}\Gamma^e_{bd} - \Gamma^a_{de}\Gamma^e_{bc}$ is the Riemann tensor for the field space and the spatial Laplacian operator $\nabla^2 \equiv \delta^{ij}\partial_i\partial_j$ is used to avoid confusion of indices.

Actually, Eq. (2.98) is analogous to the geodesic deviation equation in GR. As can been seen above, not only the potential but the curvature of the field space enters $C^a_{\ b}$ so the inflaton is rolling along neither the local minimum of the potential nor the geodesics in field space. After quantizing the perturbations, the power spectrum is calculated as [122]

$$\Delta^2_{\mathcal{R}} = \left(\frac{H}{2\pi}\right)^2 \gamma^{ab} \frac{\partial N_{\rm inf}}{\partial \phi^a} \frac{\partial N_{\rm inf}}{\partial \phi^b} \ , \tag{2.99}$$

and consequently the scalar spectral index

$$n_s - 1 = -2\epsilon_1 - 2\left[1 + \frac{\partial N_{\rm inf}}{\partial \phi^a} \frac{\partial N_{\rm inf}}{\partial \phi^d} \left(\frac{1}{3} R^{abcd} \frac{U_{;b} U_{;c}}{U^2} - \frac{U^{;ab}}{U}\right)\right] \left(\gamma^{mn} \frac{\partial N_{\rm inf}}{\partial \phi^m} \frac{\partial N_{\rm inf}}{\partial \phi^n}\right)^{-1} , \tag{2.100}$$

where $N_{\rm inf}$ is the e-fold number of expansion, and $U_{;a} \equiv \nabla_a U$ is adopted for the covariant derivative in the field space.

A closed-form, analytical expression for the long-wavelength density perturbations in general multi-field models has been found in Ref. [126] with slow-roll approximation, known as the Mukhanov-Steinhardt functional, which provides a powerful tool to calculate the power spectrum of density perturbation. Moreover, the situation can be further simplified if there is a mass hierarchy among the scalar fields because fields with different masses play distinct roles during inflation, allowing clearer separation of high- and low-frequency modes. Light fields usually drive the expansion of the Universe during the slow rolling along the inflation trajectory where the perturbations correspond to adiabatic modes while the heavy ones oscillate around it and generate isocurvature perturbations. Under the adiabaticity conditions, the high- and low-frequency modes decouple with each other [125] so that integrating out the unexcited heavy degrees of freedom is allowed. As a result, a low-energy effective field theory can be obtained where the calculation becomes much simpler.

Consider a two-field case in the following, i.e. $a, b = 1, 2$ in Eq. (2.88), where there are only two scalar modes which can be projected onto the directions tangent and orthogonal to the inflation trajectory as [86, 123]

$$\mathcal{R} \equiv -\frac{H}{\dot{\phi}} T_a \delta\phi^a \ , \tag{2.101}$$

$$\mathcal{F} \equiv N_a \delta\phi^a \ , \tag{2.102}$$

where spatially flat gauge is adopted. $\mathcal{R}$ corresponds to the curvature perturbation in the light direction while $\mathcal{F}$ the heavy isocurvature perturbation. The second-order

action is given as [125]

$$S_2 = \frac{1}{2}\int d^4x a^3 \left[\frac{\dot{\bar{\phi}}^2}{H^2}\dot{\mathcal{R}}^2 - \frac{\dot{\bar{\phi}}^2}{H^2}\frac{(\mathcal{R}_{,i})^2}{a^2} + \dot{\mathcal{F}}^2 - \frac{(\mathcal{F}_{,i})^2}{a^2} - M_{\rm eff}^2\mathcal{F}^2 - 4\dot{\theta}_t\frac{\dot{\bar{\phi}}}{H}\dot{\mathcal{R}}\mathcal{F}\right] , \tag{2.103}$$

and the resulting equations of motion for the Fourier modes of these two dynamical quantities are as follows [125]

$$\ddot{\mathcal{R}} + (3 + 2\epsilon_1 - 2\epsilon_2^{\parallel})H\dot{\mathcal{R}} + k_p^2\mathcal{R} = 2\dot{\theta}_t\frac{H}{\dot{\bar{\phi}}}\left[\dot{\mathcal{F}} + \left(3 - \epsilon_1 - \epsilon_2^{\parallel} + \frac{\ddot{\theta}_t}{H\dot{\theta}_t}\right)H\mathcal{F}\right] , \tag{2.104}$$

$$\ddot{\mathcal{F}} + 3H\dot{\mathcal{F}} + k_p^2\mathcal{F} + M_{\rm eff}^2\mathcal{F} = -2\dot{\theta}_t\frac{\dot{\bar{\phi}}}{H}\dot{\mathcal{R}} , \tag{2.105}$$

where the subscript $\mathbf{k}$ for Fourier modes is omitted for simplicity, $k_p = k/a$ is the physical momentum, and $M_{\rm eff}^2 = U_{NN} + M_{\rm pl}^2\epsilon_1 H^2 R_{ab}\gamma^{ab} - \dot{\theta}_t^2$ is the effective mass for $\mathcal{F}$ with $U_{NN} \equiv N^a N^b U_{;ab}$. It is obvious that $\dot{\theta}_t$ couples $\mathcal{R}$ and $\mathcal{F}$ on the right hand side so they affect each other as source terms. Therefore in principle, if $\mathcal{F} \neq 0$ and $\dot{\theta}_t \neq 0$, the conservation of $\mathcal{R}$ at superhorizon scale is not valid any more[22], which is an essential different from the single-field case.

In order to write down the effective action in the presence of mass hierarchy $M_{\rm eff} \gg H$ and non-vanishing turning rate $\dot{\theta}_t \neq 0$, the adiabaticity condition [125]

$$\left|\ddot{\theta}_t/\dot{\theta}_t\right| \ll M_{\rm eff} , \tag{2.106}$$

should be satisfied so that the high-frequency mode is not excited and can be integrated out (even for $|\dot{\theta}_t| \gg M_{\rm eff}$). More specifically, $\mathcal{R}$ and $\mathcal{F}$ can be decomposed into high- and low-frequency modes [125]

$$\mathcal{R}_c = \mathcal{R}_+ e^{i\omega_+ t} + \mathcal{R}_- e^{i\omega_- t} , \tag{2.107}$$

$$\mathcal{F} = \mathcal{F}_+ e^{i\omega_+ t} + \mathcal{F}_- e^{i\omega_- t} , \tag{2.108}$$

where $\mathcal{R}_c \equiv \dot{\bar{\phi}}\mathcal{R}/H$ while ω_+ and ω_- represent the high- and low-frequency, respectively. In subhorizon limit and with slow-roll approximation, the solutions of

[22] This is recently utilized to generate large curvature perturbation for primordial black hole (PBH) production, e.g. Refs. [127, 128].

Eqs. (2.104) and (2.105) can be found as [125]

$$\omega_{\pm}^2 = k_p^2 + \frac{M_{\rm eff}^2}{2c_s^2} \pm \frac{M_{\rm eff}^2}{2c_s^2}\sqrt{1+(1-c_s^2)\,c_s^2\frac{4k_p^2}{M_{\rm eff}^2}}\ , \tag{2.109}$$

$$\mathcal{R}_+ = \frac{-2i\dot{\theta}_t\omega_+}{\omega_+^2 - k_p^2}\mathcal{F}_+\ , \tag{2.110}$$

$$\mathcal{F}_- = \frac{2i\dot{\theta}_t\omega_-}{\omega_-^2 - k_p^2 - M_{\rm eff}^2}\mathcal{R}_-\ , \tag{2.111}$$

where the modified sound speed is defined as

$$c_s^{-2} = 1 + 4\dot{\theta}_t^2/M_{\rm eff}^2\ . \tag{2.112}$$

As can be seen here, the exchange of energy between light and heavy modes reduces the sound speed, which may lead to an enhancement of non-Gaussianities (see e.g. Refs. [69, 71]). Large mass hierarchy $M_{\rm eff}^2 \gg k_p^2 c_s^2$ is required to make significant distinction between ω_+ and ω_-

$$\omega_+^2 \approx \frac{M_{\rm eff}^2}{c_s^2} \gg \omega_-^2 \approx k_p^2 c_s^2 + (1-c_s^2)^2\frac{k_p^4 c_s^2}{M_{\rm eff}^2}\ , \tag{2.113}$$

such that high-frequency modes effectively do not participate in the dynamics of low-frequency ones and can be integrated out safely. Consequently, Eq. (2.105) gives

$$\mathcal{F} \approx \frac{-2\dot{\theta}_t}{M_{\rm eff}^2 + k_p^2}\dot{\mathcal{R}}_c\ , \tag{2.114}$$

which means that the low-frequency mode of the heavy field is controlled by the light field. In superhorizon limit, the treatment is still similar so Eq. (2.105) results in

$$\mathcal{F} \approx -\frac{\dot{\bar{\phi}}}{H}\frac{2\dot{\theta}_t}{M_{\rm eff}^2 + k_p^2}\dot{\mathcal{R}}\ . \tag{2.115}$$

Again, the heavy mode is still determined by $\mathcal{R}$. In conclusion, as long as the adiabatic condition (2.106) (or consequently $|\dot{\omega}_+/\omega_+^2| \ll 1$) and mass hierarchy are satisfied, a low-energy effective field theory can be obtained by integrating out the heavy degree of freedom so that the system is significantly simplified. Inserting Eq. (2.115) into action (2.103), the effective single-field action is obtained [125]

$$S_{\rm eff} = \frac{1}{2}\int d^4x a^3 \frac{\dot{\bar{\phi}}^2}{H^2}\left[\frac{\dot{\mathcal{R}}^2}{c_s^2(k)} - k_p^2\mathcal{R}^2\right]\ , \tag{2.116}$$

where the sound speed is written as

$$c_s^{-2}(k) = 1 + \frac{4\dot{\theta}_t^2}{k_p^2 + M_{\rm eff}^2} \ , \tag{2.117}$$

which is consistent with Eq. (2.112) in the limit $M_{\rm eff}^2 \gg k_p^2$. Therefore, such a system is equivalent to a single-field model with a modified sound speed. One way to distinguish a single-field slow-roll model with $c_s = 1$ and an effective single-field model with c_s given in Eq. (2.117) is to look at the consistency relation of single-field models in Eq. (2.62) which will be modified if $c_s \neq 1$. Non-Gaussianity of primordial curvature perturbation [67] and the shape of power spectrum [123] are also affected by the non-trivial sound speed.

The low-energy effective field theory is a useful approach that makes the analytical calculation of the power spectrum in a particular class of two-field inflation models possible. This approach will be adopted below to investigate the inflation dynamics in the mixed Higgs-R^2 inflation model [38].

2.3.2 Mixed Higgs-R^2 Inflation

As is shown previously, the Starobinsky model and the Higgs inflation are the most promising single-field inflation models that give predictions on n_s and r well matching the WMAP and Planck observations [23]. However, there are still unanswered questions within these models that are not likely to be explained within the original frameworks. Therefore, a UV-extended model is desired to understand their behaviors and connections further. Among many proposals for UV-extension[23], considering the combination of the Starobinsky model and the Higgs inflation is one natural and straightforward way to construct a possible UV candidate, i.e. the mixed Higgs-R^2 inflation model [36–40][24]. This two-field model always inherits the observationally favored n_s and r from its two single-field limits when the isocurvature mode is heavy and the Higgs self-coupling is non-critical during inflation, as will be shown later. Moreover, the multi-field nature inevitably leads to rich post-inflationary phenomena, for instance, different preheating and reheating processes depending on model parameters, which can provide a possible way to distinguish itself from the single-field limits.

[23] See Refs. [129–131] for other proposals of the UV-extensions of the Higgs inflation.
[24] See other relevant studies of this model, e.g. [132, 133].

The mixed Higgs-R^2 inflation model is not only phenomenologically well motivated as explained previously, but supported by the consideration from theoretical side which will be discussed in the following. As a starting point, the action is given by

$$\begin{aligned} S_{\rm J} &= \int d^4x\sqrt{-g_{\rm J}}\mathcal{L}_{\rm J} \\ &= \int d^4x\sqrt{-g_{\rm J}}\left[\left(\frac{M_{\rm pl}^2}{2}+\xi|\mathcal{H}_{\rm SM}|^2\right)R_{\rm J}+\frac{M_{\rm pl}^2}{12M^2}R_{\rm J}^2-g_{\rm J}^{\mu\nu}\partial_\mu\mathcal{H}_{\rm SM}\partial_\nu\mathcal{H}_{\rm SM}^\dagger-\lambda|\mathcal{H}_{\rm SM}|^4\right], \end{aligned} \tag{2.118}$$

where there are three model parameters ξ, M, and λ whose convention and physical meaning just follow directly from Eqs. (2.66) and (2.79)[25]. Again, the mass term for Higgs and the EW vev have been neglected[26]. Also, the Higgs self-coupling $\lambda \sim \mathcal{O}(10^{-2})$ is considered to be non-critical up to inflation scale. For the investigation of inflationary dynamics, it is sufficient to focus on the unitary gauge $\mathcal{H}_{\rm SM} = h/\sqrt{2}$. As can be easily seen from Eq. (2.118), the two single-field limits are achieved as

- R^2-limit: $\xi \to 0$ and $M \to M_c$,
- Higgs-limit: $\xi \to \xi_c$ and $M \to \infty$,

where M_c and ξ_c are given in Eqs. (2.73) and (2.84), respectively. To see this model is indeed a UV-extension of the Higgs inflation, it is shown in Refs. [37, 42] that the cutoff scale of this theory is up to Planck scale $M_{\rm pl}$ which is much higher than that of the Higgs inflation whose cutoff around the vacuum is $\sim M_{\rm pl}/\xi$. In order to understand the cutoff scale of the system (2.118), it is convenient to introduce an auxiliary field χ such that

$$\mathcal{L}_{\rm J} \to \frac{M_{\rm pl}^2}{2}R_{\rm J}+\frac{1}{2}\chi^2 R_{\rm J}-\frac{3}{4}\frac{M^2}{M_{\rm pl}^2}\left(\chi^2-\xi h^2\right)^2-\frac{1}{2}g_{\rm J}^{\mu\nu}\partial_\mu h\partial_\nu h-\frac{\lambda}{4}h^4 , \tag{2.119}$$

where, unlike the Higgs field h with a canonical kinetic term, χ is non-dynamical so it can be integrated out to recover the original Lagrangian in Eq. (2.118). The E-H term and the canonical kinetic term for Higgs have a cutoff at $M_{\rm pl}$ automatically. Since χ is just an auxiliary field absorbing all the large non-minimal couplings, the cutoff of the second term is also Planck scale. The essential non-minimal coupling ξ now enters the potential, especially giving a contribution to the effective Higgs self-coupling

$$\lambda_{\rm eff} = \lambda + 3\xi^2 M^2/M_{\rm pl}^2 . \tag{2.120}$$

[25] Similar model is studied in e.g. Ref. [134].

[26] The two-loop renormalization group equations in this model [135] show that the Higgs mass $m_{\mathcal{H}_{\rm SM}}$ can be as large as $\sim M_{\rm pl}/\xi$ at inflation scale, but it does not spoil the predictions of CMB observation calculated with $m_{\mathcal{H}_{\rm SM}} = 0$ as well as the preheating process. It is easy to generalize the analysis to the case $m_{\mathcal{H}_{\rm SM}} \neq 0$.

To ensure the system is under control quantum mechanically, it is required that the effective coupling is sufficiently small $\lambda_{\text{eff}} \ll 1$, which, under the assumption of $\lambda \sim \mathcal{O}(10^{-2})$, indicates that

$$3\xi^2 M^2/M_{\text{pl}}^2 \lesssim 4\pi \ . \tag{2.121}$$

Perturbativity of the system is guaranteed and the cutoff is up to Planck scale as long as Eq. (2.121) is satisfied, beyond which the system enters the strongly-coupled regime. Therefore, the mixed Higgs-R^2 inflation model is healthy up to M_{pl} if the inequality (2.121) holds, which means that it can serve as a UV-extension of the Higgs inflation. Note, however, that the Higgs-limit with $M \to \infty$ and $\xi \to \xi_c$ actually violates the perturbativity condition in Eq. (2.121), which can be understood as the reason why the preheating process of the Higgs inflation mentioned in Sec. 2.2 suffers from the strong coupling issue [34]. Naively speaking, it can be expected that this issue no longer exists if the unitary bound is satisfied. Examining whether the preheating process in this two-field model with Eq. (2.121) fulfilled still encounters the same problem or not is one of the main original works shown in this thesis and will be discussed thoroughly later. The unitary bound shown above can also be derived in EF. Performing a conformal transformation to eliminate the quadratic curvature term and the non-minimal coupling between Higgs and gravity

$$g_{\text{E}\mu\nu}(x) = e^{\alpha\varphi(x)} g_{\text{J}\mu\nu}(x) \ , \tag{2.122}$$

where the new "scalaron" field φ is defined as

$$\alpha\varphi \equiv \sqrt{\frac{2}{3}}\frac{\varphi}{M_{\text{pl}}} \equiv \ln\left(\frac{2}{M_{\text{pl}}^2}\left|\frac{\partial\mathcal{L}_{\text{J}}}{\partial R_{\text{J}}}\right|\right) \ , \tag{2.123}$$

the resulting new action is expressed in terms of two scalar fields as

$$\begin{aligned} S_{\text{E}} &= \int d^4x\sqrt{-g_{\text{E}}}\left[\frac{M_{\text{pl}}^2}{2}R_{\text{E}} - \frac{1}{2}g_{\text{E}}^{\mu\nu}\partial_\mu\varphi\partial_\nu\varphi - \frac{1}{2}e^{-\alpha\varphi}g_{\text{E}}^{\mu\nu}\partial_\mu h\partial_\nu h - U_{\text{E}}(\varphi,h)\right] \ , \\ U_{\text{E}}(\varphi,h) &= \frac{\lambda}{4}e^{-2\alpha\varphi}h^4 + \frac{3}{4}M_{\text{pl}}^2M^2\left[1-\left(1+\frac{\xi}{M_{\text{pl}}^2}h^2\right)e^{-\alpha\varphi}\right]^2 \ . \end{aligned} \tag{2.124}$$

Note that the definition of this new scalaron φ contains not only the scalar mode induced by R_{J}^2 but also the Higgs field due to the non-minimal coupling term. As will be shown later, this combination constructed from the conformal coupling [62,63] neatly cancels the heavy modes in R_{J} and h^2 during reheating so that the dynamics of

φ is greatly simplified. By expanding the action in Eq. (2.124) around the global minimum of the potential, $(\varphi, h) = (0, 0)$, the effective Higgs self-coupling in Eq. (2.120) shows up, which leads to the same conclusion as in Eq. (2.121). The non-canonical kinetic term for the Higgs field in this frame cannot jeopardize the situation because the kinetic coupling always appears as Planck-suppressed terms $\alpha\varphi \ll 1$ around the vacuum [37, 42]. In addition to the better UV property, the emergence of the non-minimal coupling and the R^2 term in the Higgs inflation model is thought to be inevitable. On the one hand, the non-minimal coupling between Higgs and Ricci scalar is needed to improve the renormalizability of the energy-momentum tensor of the theory [136, 137]. On the other hand, appearing as the one-loop counter term to gravity [138], the quadratic curvature term acquires a large coefficient $\sim \xi^2$ by the renormalization group running [43–47, 135] because the beta function of this coefficient receives a dominant contribution proportional to ξ^2 at one-loop level for $\xi \gg 1$. Besides, the "scalaron" field can also be understood to appear as a pole in the 2-to-2 scattering amplitude of Higgs when resumming over the vacuum polarization diagrams of graviton [48], and as a σ-meson that linearizes the non-linear sigma model rewritten from the Lagrangian of the Higgs inflation [49], which will not be discussed here in detail. Discussion about the improvement of the EW vacuum metastability can also be found in Refs. [42, 135]. As mentioned in Sec. 2.2, within the possible range of top quark mass, the Higgs self-coupling can turn negative at around the inflation scale, which leads to an unbounded potential, and therefore, instability for the Higgs field. It is shown that the presence of scalaron can push λ to be positive again at a higher energy scale if $\xi M/M_{\rm pl}$ is large enough so that the Higgs stability can be secured [42] or a local minimum may be developed on the scalar potential and induce interesting cosmological consequences [135].

As a brief summary, all the ingredients shown in the action (2.118) of the mixed Higgs-R^2 inflation model are theoretically inevitable, and this model can be regarded as a promising UV-extension of the Higgs inflation with a cutoff scale $\sim M_{\rm pl}$ as long as the perturbativity condition (2.121) is satisfied. In the following, a review of the inflation dynamics in this model is presented, showing that it is an observationally favored inflation model as its single-field limits.

The inflation dynamics in the mixed Higgs-R^2 inflation model can be analyzed systematically by the multi-field formalism introduced previously within EF [38, 139]. It is shown that there is an attractor during inflation in the $\xi \gtrsim 1$ regime where the low-energy effective field theory approach is applicable because of the large mass of isocurvature mode generated by large non-minimal coupling. As a result, the system

is regarded as an effective Starobinsky model or effective Higgs inflation. To be self-consistent, the mixed Higgs-R^2 inflation will be reviewed in JF and EF sequentially.

• **Jordan frame** All the subscripts "J" are omitted for convenience. The time-time component and the trace of the Einstein equation at background level are given as

$$3M_{\rm pl}^2H^2+\frac{M_{\rm pl}^2}{M^2}\left(6H\ddot{H}-3\dot{H}^2+18H^2\dot{H}\right)+3\xi Hh\left(Hh+2\dot{h}\right)=\frac{1}{2}\dot{h}^2+\frac{\lambda}{4}h^4\ , \tag{2.125}$$

$$-\Box\left(\frac{R}{M^2}+3\xi\frac{h^2}{M_{\rm pl}^2}\right)+\left(1+\xi\frac{h^2}{M_{\rm pl}^2}\right)R=\frac{1}{M_{\rm pl}^2}\left(\lambda h^4-\dot{h}^2\right)\ , \tag{2.126}$$

where $\Box\equiv g^{\mu\nu}\nabla_\mu\nabla_\nu$ is the d'Alembert operator with respect to $g_{\mu\nu}$ in the corresponding frame, and again the Ricci scalar is regarded as an independent degree of freedom induced by higher order time derivatives of Hubble parameter H. These equations return to Eqs. (2.68) and (2.69) when $h=0$. Even with slow-roll approximation, directly solving them is generally difficult, so more information from the Higgs sector is needed to further simplify this set of equations. In the JF action (2.118), the effective potential for Higgs is simply given by

$$V_{\rm eff}=-\frac{\xi}{2}h^2R+\frac{\lambda}{4}h^4\ , \tag{2.127}$$

from which a local maximum and two local minima can be found for $R>0$

$$R>0\ ,\ V_{{\rm eff},h}=0\quad\Rightarrow\quad\begin{cases}h=0\ , & V_{{\rm eff},hh}<0\ ,\\ h_{\rm v\pm}=\pm\sqrt{\xi R/\lambda}\ , & V_{{\rm eff},hh}>0\ ,\end{cases} \tag{2.128}$$

while for $R<0$ there is only one extremum

$$R<0\ ,\ V_{{\rm eff},h}=0\quad\Rightarrow\quad h_{\rm v0}=0\ ,\quad V_{{\rm eff},hh}>0\ . \tag{2.129}$$

Like the Starobinsky model, slow-roll approximation requires $R>0$ during inflation, so the discussion here will focus on the case where Ricci scalar takes a positive sign.

In the regime $R>0$, the origin of Higgs $h=0$ is an unstable point so that the inflaton must fall into one of the minima characterized by the lower of Eq. (2.128). Without loss of generality, it is convenient to just adopt the one with positive Higgs field value and omit the "±" subscript hereafter (even for EF). Taking into account this attractor solution to eliminate the Higgs field, Eqs. (2.125) and (2.126) become

$$3M_{\rm pl}^2H^2+\frac{M_{\rm pl}^2}{M^2}\left(6H\ddot{H}-3\dot{H}^2+18H^2\dot{H}\right)=\frac{\xi}{8\lambda}\frac{\dot{R}^2}{R}-\frac{3\xi^2}{\lambda}H\dot{R}+\frac{3\xi^2}{2\lambda}\dot{H}R\ , \tag{2.130}$$

$$\ddot{R}+3H\dot{R}+\tilde{M}^2R=-\frac{\xi}{4\lambda}\frac{\tilde{M}^2}{M_{\rm pl}^2}\frac{\dot{R}^2}{R}\ , \tag{2.131}$$

where a new parameter understood as the effective mass of scalaron is defined in the following way

$$\tilde{M} \equiv M \left(1 + \frac{3\xi^2 M^2}{\lambda M_{\rm pl}^2}\right)^{-1/2} . \tag{2.132}$$

These equations can be understood as the Einstein equations of the system with a constraint given by the lower of Eq. (2.128) without any approximation. As can be easily seen, the left hand side (LHS) of Eqs. (2.130) and (2.131) are very similar to that of Eqs. (2.68) and (2.69) respectively, except that the mass M in Eq. (2.69) is replaced by $\tilde{M}$ in Eq. (2.131). During inflation, the slow-roll parameters defined in Eqs. (2.27) and (2.28) are small, i.e.

$$\epsilon_1 = -\frac{\dot{H}}{H^2} \ll 1 \ , \ \epsilon_2 = -\frac{\ddot{H}}{2H\dot{H}} \ll 1 \ . \tag{2.133}$$

As a result, the Einstein equations in the minimum with slow-roll approximation become

$$3M_{\rm pl}^2 H^2 + 18\frac{M_{\rm pl}^2}{\tilde{M}^2} H^2 \dot{H} \simeq 0 \ , \tag{2.134}$$

$$3H\dot{R} + \tilde{M}^2 R \simeq 0 \ , \tag{2.135}$$

which coincide with those in the Starobinsky model with an effective scalaron mass $\tilde{M}$. Consequently, to match the observed amplitude of scalar power spectrum, it is required that

$$\tilde{M} = M_c \ , \tag{2.136}$$

which induces a constraint equation on the model parameters in the mixed Higgs-R^2 inflation model so that the number of independent parameters reduces by one. It is also useful to rewrite the constraint (2.136) in another equivalent form [41]

$$\frac{\xi^2}{\xi_c^2} + \frac{M_c^2}{M^2} = 1 \ , \tag{2.137}$$

where the relation between ξ_c and M_c derived from Eqs. (2.73) and (2.84) is used

$$\xi_c = \sqrt{\frac{\lambda}{3}} \frac{M_{\rm pl}}{M_c} \ . \tag{2.138}$$

The analysis above is a significant insight because it indicates that the new two-field inflation is essentially the same as its single-field limits, and therefore gives the

same predictions on n_s and r. Note that, in principle, this is not guaranteed for all the parameter range. Especially, the statement is always true only when considering large non-minimal coupling and non-critical Higgs self-coupling [36, 39, 40][27]. This thesis focuses on exactly the case $\xi \gtrsim 1$ and $\lambda \sim \mathcal{O}(10^{-2})$ so the effective Starobinsky model prediction is always valid.

In order to make the discussion more concrete hereafter, it is helpful to define different regions in the parameter space according to the properties of the system. Therefore, the whole parameter space is separated into two regimes as follows:

- R^2-like regime:

$$\frac{\xi^2}{\lambda} < \frac{M_{\rm pl}^2}{3M^2} \ , \tag{2.139}$$

- Higgs-like regime:

$$\frac{\xi^2}{\lambda} > \frac{M_{\rm pl}^2}{3M^2} \ . \tag{2.140}$$

This separation condition can also be rewritten as $\xi = \xi_c/\sqrt{2}$. Additionally, violation of the perturbativity condition (2.121) defines a strongly-coupled regime that only covers part of the Higgs-like regime as long as $\lambda < 1$. Indeed, taking Eq. (2.136) into account, the Higgs-like regime without the strong coupling issue is given by $\xi_c/\sqrt{2} \simeq 3.1 \times 10^3\sqrt{\lambda/0.01} \lesssim \xi \lesssim \xi_s$ where ξ_s characterizes the boundary defined in Eq. (2.121)

$$\xi_s \equiv \left(\frac{1}{\xi_c^2} + \frac{3}{4\pi}\frac{M_c^2}{M_{\rm pl}^2}\right)^{-1/2} \lesssim \xi_c \ . \tag{2.141}$$

Therefore, there exists a parameter space within the Higgs-like region where the system is quantum mechanically under control up to the Planck scale [37, 42] as explained above such that the mixed Higgs-R^2 inflation model can be regarded as a UV-extension of the Higgs inflation. Figure 2.1 shows the parameter space in the ξ-$1/M$ plane with $\lambda = 0.01$.

[27]Note, for comparison, that in the minimally coupled case $\xi = 0$, the double inflationary h^4-R^2 model was first considered in [140] without identifying h with the Higgs field, and its scalar perturbation spectrum was derived in [141]. To obtain the correct value for the slope of the scalar power spectrum $n_s - 1$ and to satisfy the upper limit on the tensor-to-scalar ratio r, viability of such a model requires its last ~ 60 e-folds to be in the R^2-like regime that occurs for $M < \sqrt{\lambda}M_{\rm pl}$ with extremely small $\lambda \lesssim \mathcal{O}(10^{-10})$, or if h^2 is always less than $M_{\rm pl}^2$ (then the field h does not contribute to inflation at all). The same conclusion remains valid for $0 < \xi \ll 1$, $\xi h^2/M_{\rm pl}^2 \ll 1$, too.

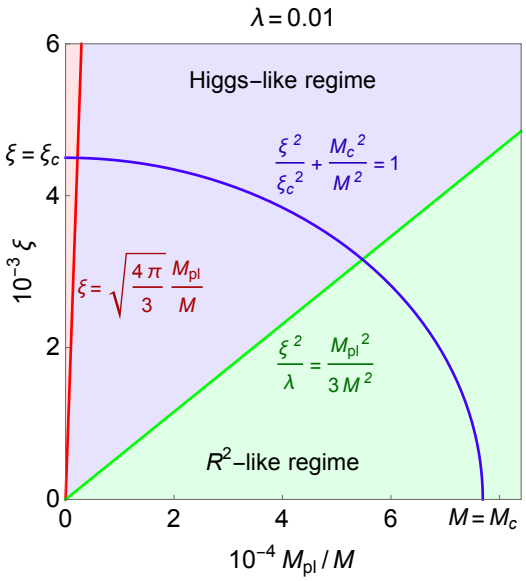

Figure 2.1: Parameter space for different regimes in the mixed Higgs-R^2 inflation model with $\lambda = 0.01$. The red region is the strongly-coupled regime where perturbative analysis is questionable (2.121). The blue and green regions are the Higgs-like and R^2-like regimes, respectively. The blue line satisfies the condition for the observed curvature power spectrum (2.136) or (2.137).

• **Einstein frame** The subscripts "E" for the quantities defined in EF will be omitted for convenience. In principle, the classical background dynamics in the system (2.124) should be systematically analyzed with the multi-field formalism introduced previously [38]. Specifically, it corresponds to the case $N = 2$ in Eq. (2.88) with

$$\phi^a = \begin{pmatrix} \varphi \\ h \end{pmatrix} \ , \quad \gamma_{ab} = \begin{pmatrix} 1 & 0 \\ 0 & e^{-\sqrt{\frac{2}{3}}\frac{\varphi}{M_P}} \end{pmatrix} \ , \tag{2.142}$$

and the potential given by Eq. (2.124), which leads to the unit vectors tangent and orthogonal to the inflation trajectory as well as the turning rate

$$\begin{aligned} T^a &= \left(\dot{\varphi}^2 + e^{-\alpha\varphi}\dot{h}^2\right)^{-1/2} \begin{pmatrix} \dot{\varphi} \\ \dot{h} \end{pmatrix} \ , \\ N^a &= \left(\dot{\varphi}^2 + e^{-\alpha\varphi}\dot{h}^2\right)^{-1/2} \begin{pmatrix} -e^{-\frac{\alpha}{2}\varphi}\dot{h} \\ e^{\frac{\alpha}{2}\varphi}\dot{\varphi} \end{pmatrix} \ , \\ \dot{\theta}_t^2 &= e^{\alpha\varphi}\left(\dot{\varphi}^2 + e^{-\alpha\varphi}\dot{h}^2\right)^{-2}\left(\dot{\varphi}U_{,h} - e^{-\alpha\varphi}\dot{h}U_{,\varphi}\right)^2 \ . \end{aligned} \tag{2.143}$$

Consequently, the effective mass for the isocurvature mode $M_{\rm eff}$ in Eq. (2.103) can be

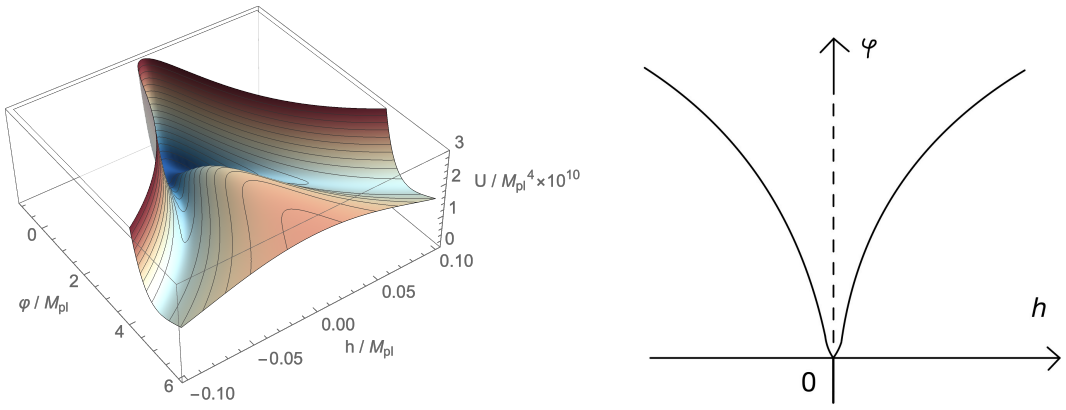

Figure 2.2: Left: An example for the shape of the potential with $U(\varphi, h)$ with model parameters $(\xi, \lambda) = (3000, 0.01)$ and constraint (2.136) satisfied. Right: A schematic picture showing the local minima and maxima on the potential from top view. the solid lines correspond to local minima while the dashed line corresponds to local maxima.

calculated as

$$M_{\rm eff}^2 = \left(\dot\varphi^2 + e^{-\alpha\varphi}\dot h^2\right)^{-1}\left(e^{-\alpha\varphi}\dot h^2 U_{,\varphi\varphi} + e^{\alpha\varphi}\dot\varphi^2 U_{,hh} - 2\dot\varphi\dot h U_{,\varphi h} - \frac{\alpha}{2}\dot\varphi^2 U_{,\varphi} - \alpha\dot\varphi\dot h U_{,h}\right)$$
$$- \frac{\dot\varphi^2 + e^{-\alpha\varphi}\dot h^2}{6M_p^2} - e^{\alpha\varphi}\left(\dot\varphi^2 + e^{-\alpha\varphi}\dot h^2\right)^{-2}\left(\dot\varphi U_{,h} - e^{-\alpha\varphi}\dot h U_{,\varphi}\right)^2 \ , \tag{2.144}$$

where the equations of motion for φ and h (see Appendix C) have been used. The second term is much smaller than Hubble during inflation $\propto \epsilon_1 H^2 \ll H^2$. If the slow-roll approximations $\ddot\phi^a \ll H\dot\phi^a$ and $H \sim \sqrt{U}/M_{\rm pl}$ are valid, the third term (turning rate) is also much smaller than H^2. The dominant contribution comes from the second derivatives of $U(\varphi, h)$ in the first term. To determine the dynamics, it is important to understand the shape of the potential. Figure 2.2 shows an example of the EF potential $U(\varphi, h)$. Similar to the situation in JF, there is one local maximum and two local minima on the potential $U(\varphi, h)$ in the Higgs direction in $\varphi > 0$ regime which are given as

$$\varphi > 0 \ , \ U_{,h} = 0 \quad \Rightarrow \quad \begin{cases} h = 0 \ , & U_{,hh} < 0 \ , \\ h_{\rm v\pm} = \pm\sqrt{3\xi(e^{\alpha\varphi} - 1)/\lambda}\tilde M \ , & U_{,hh} > 0 \ , \end{cases} \tag{2.145}$$

while only one minimum in $\varphi < 0$ regime

$$\varphi < 0 \ , \ U_{,h} = 0 \quad \Rightarrow \quad h_{\rm v0} = 0 \ , \quad U_{,hh} > 0 \ . \tag{2.146}$$

It is easy to show that Eqs. (2.145) and (2.146) are equivalent to Eqs. (2.128) and (2.129), respectively. Therefore, $U(\varphi, h)$ shows an attractor behavior. Slow-roll inflation occurs in $\varphi > 0$ regime (because $R_{\rm J} > 0$), so the inflaton will fall into

one of the valleys to achieve the effective single-field dynamics. Note that, however, because of the non-trivial field space metric shown in the action (2.124), the inflaton field actually traces neither $h_{\rm v}$ nor the geodesics of the field space, as has been explained in the discussion of multi-field formalism previously. Given the lower of Eq. (2.145) and the results in Appendix C, it can be easily shown that

$$H^2 \sim U/M_{\rm pl}^2 \sim \tilde{M}^2 \ , \ U_{,\varphi\varphi} \sim M^2 \ , \ U_{,\varphi h} \sim \sqrt{\xi} M^2 \ , \ U_{,hh} \sim \xi M^2 \ , \tag{2.147}$$

which means that the dominant contribution $U_{,hh}$ makes $M_{\rm eff} > H$ for $\xi \gtrsim 1$, especially when $\xi \gg 1$. As a result, the low-energy effective field theory approach is applicable to the regime of interest.

As a brief summary, the large isocurvature mass $M_{\rm eff}$ and small trajectory turning rate $\dot{\theta}_t$ in the attractor solution allows an effective single-field description of the mixed Higgs-R^2 inflation in EF with sound speed hardly modified $c_s \simeq 1$, which is consistent with the analysis in JF. Therefore, it is safe to integrate out the heavy degree of freedom in Eq. (2.124) to simplify the system. A simple way is to insert the lower of Eq. (2.145) into the action (2.124) which leads to an equivalent form as the Higgs inflation action in EF before the field redefinition (2.86), only with couplings replaced by [41]

$$\tilde{\lambda} \equiv \lambda \left(1 + \frac{\lambda M_{\rm pl}^2}{3\xi^2 M^2} \right) \ , \ \ \tilde{\xi} \equiv \xi \left(1 + \frac{\lambda M_{\rm pl}^2}{3\xi^2 M^2} \right) \ . \tag{2.148}$$

Consequently, similar to the single field case, the constraint from Eq. (2.63) gives

$$\sqrt{\tilde{\lambda}/3} M_{\rm pl}/\tilde{\xi} = M_c \ , \tag{2.149}$$

which results in exactly Eq. (2.137), as expected.

In conclusion, the mixed Higgs-R^2 inflation is equivalent to an effective Starobinsky model or effective Higgs inflation, predicting the most observationally favored [23] scalar spectral index n_s and tensor-to-scalar ratio r in Eqs. (2.64) and (2.65).

This chapter has reviewed the physical picture of a promising scenario for the very early Universe, inflation, as well as the realization in both single-field and multi-field models. Inflation, regarded as an accelerated expansion phase right after the "initial singularity", can wash out the inhomogeneous and anisotropic initial conditions, the spatial curvature, and the unwanted relics produced from the early time, leaving a homogeneous, isotropic, and flat Universe as observed today. Such accelerated expansion can be realized in many ways, among which this thesis focuses on the

slow-roll inflation driven by homogeneous scalar field(s) called the inflaton. During inflation, the potential energy of inflaton dominates the Universe almost as a positive cosmological constant that provides the negative pressure to inflate the space. Therefore, the inflaton slowly rolls down the potential with large Hubble friction and negligible kinetic energy, which is why it is called slow-roll inflation. On the other hand, quantum fluctuations upon the homogeneous background generated during inflation are essential for the observed CMB temperature anisotropy and LSS formation. These fluctuations are classified into scalar-, vector-, and tensor-type, described by the cosmological perturbation theory. The scalar-type perturbations are responsible for seeding the density fluctuations in the Universe imprinted on CMB and LSS. The vector-type is exponentially suppressed by cosmic expansion. The tensor-type perturbations, or primordial gravitational waves, can produce B-mode polarization that is the primary target of future experiments. Detecting the primordial tensor perturbations is not only the smoking gun of inflation but the evidence of quantization of gravity, which would significantly enhance the physical understanding of the observed Universe.

Single-field slow-roll inflation is the simplest class of inflation models that can explain the observational results. There are two models that are observationally favored most, the Starobinsky model and the Higgs inflation. The inflation dynamics is equivalent in both models, giving the best-fit values of n_s and r, while the reheating processes (which will be discussed later) are different. Nevertheless, the origin of the large coefficient of R^2 term in the Starobinsky model or the UV issues in the Higgs inflation are neither explained satisfyingly within their original frameworks. Therefore, a sensible UV extension is strongly desired to solve these problems. One way for generalization is to consider multi-field models since most proposed UV physics beyond SM contains multiple scalar fields which can participate in inflation. A two-field model, the mixed Higgs-R^2 inflation model, is introduced by directly combining the two best-fit single-field models. The analysis above shows that it can serve as a candidate of UV-extension of the Higgs inflation because the cutoff scale is pushed up to $M_{\rm pl}$ in the presence of R^2. As will be shown later, the preheating process is also free from strong coupling issue with the help of scalaron. Besides, a number of studies show that all the ingredients in this model inevitably appear from several theoretical points of view. Furthermore, the inflation dynamics in this model can be described as an effective Starobinsky model or effective Higgs inflation in the regime of large non-minimal coupling and non-critical Higgs self-coupling, giving favorable

predictions on CMB observation. Therefore, the mixed Higgs-R^2 inflation model is indeed a likely UV-extension of the Higgs inflation.

The remaining important question is how to connect the mixed Higgs-R^2 inflation with the successful Hot Big Bang cosmology, i.e. the reheating process after inflation, which is essential to finally determine the pivot scale of curvature perturbation to confront the prediction of inflation with observation. This question will be discussed in the rest of this thesis as the main topic.

Chapter 3

Particle Production and Reheating

Reheating is an essential part for a successful inflationary universe model, through which high-energy relativistic particles are produced and thermalized in the "empty" space by transferring the inflaton energy to other matter fields, converting the cold Universe into a radiation-dominated one after the quasi-exponential expansion[28]. Eventually, all the degrees of freedom in SM are populated, and the Universe evolves in the way described by the conventional Hot Big Bang theory. As an integral part of the cosmic thermal history that is highly affecting the estimation of the required duration of inflation, the investigation of reheating is necessary to strengthen the observational constraints on inflation [10, 11][29] by accurately expressing the pivot scale of curvature perturbation in terms of the e-fold number of inflation (see Fig. 3.1). However, reheating suffers from the difficulty of detection due to the wash-out effects on the trace of reheating physics from thermalization and late-time non-linear evolution. Therefore, understanding reheating and seeking possible relevant observables are of great significance[30].

Reheating process is highly model-dependent. Usually, it is required to occur above the scale of a few MeV [154, 155] in order not to spoil the success of explaining the abundance of light primordial elements by BBN. According to the current understanding, reheating is generically characterized by two sequential stages for models where the end of inflation is followed by the coherent oscillation of inflaton[31]. The first stage is preheating, which is short but efficient to transfer energy from inflaton

[28] Instead, a particular class of inflation models called warm inflation [142, 143] produces particles during inflation, but it suffers from other problems [144].

[29] See e.g. Refs. [145–147] for follow-up studies.

[30] Some possible ways to probe reheating are proposed, such as by the equation of state of the early Universe and reheating temperature through primordial gravitational wave background [12, 13], and probing the gravitational waves produced from preheating (e.g. Refs. [148–153]).

[31] See other possibilities without inflaton oscillation, e.g. instant preheating [156] and reheating through gravitational particle production [157–160] in models discussed in, e.g. Refs. [56, 57, 161].

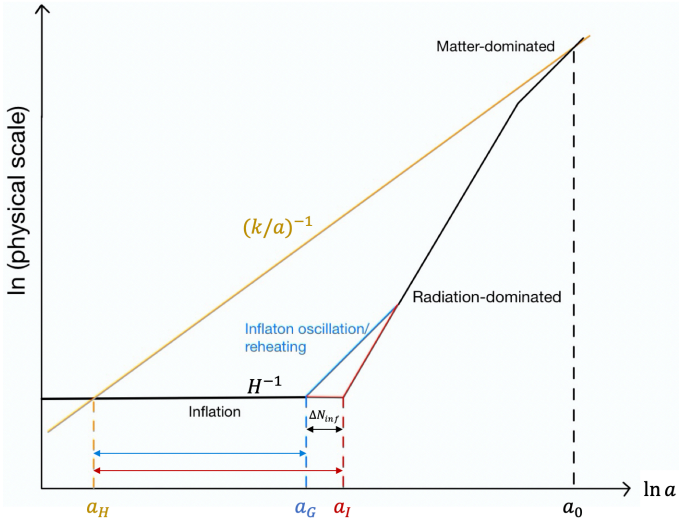

Figure 3.1: A schematic picture showing the relation between reheating and the duration of inflation. The black line is the Hubble scale H^{-1}. The blue line corresponds to the gradual reheating case while the red line is the instantaneous reheating case. The orange line is the pivot scale that enters the horizon today. a_H and a_0 denote the moments when the pivot scale exits and enters the horizon, respectively. a_G and a_I are the ending moments of inflation in the case of gradual and instantaneous reheating, respectively. Therefore, the duration of inflation for the two cases are given by $N_G = \ln(a_G/a_H)$ and $N_I = \ln(a_I/a_H)$, respectively, with $N_G < N_I$.

to relativistic particles through some dominant non-perturbative processes such as broad parametric resonance [14–17] or tachyonic instability [18–20] where the number of produced particles grows exponentially. These mechanisms usually involve non-linear processes from backreaction that complicate the whole calculation and require sophisticated numerical methods. The second stage is perturbative reheating (elementary theory of reheating), during which the inflaton experiences perturbative decay into other matter fields and loses all the energy [3, 21, 22]. Since the backreaction can terminate the preheating before all the inflaton energy is taken away in most cases, the system eventually enter the perturbative regime so that the perturbative decay of inflaton dominates the rest of reheating and determine the reheating temperature when the Hubble parameter drops below the decay rate of the inflaton.

Essentially, both non-perturbative and perturbative processes of particle production discussed here can be attributed to a time-dependent effective mass (or frequency) of the fields to be produced. Such a situation usually arises from couplings among different fields or a time-dependent background spacetime. Since the effective masses are directly related to the definition of vacuum state of the fields, a time-

dependent mass results in a time-dependent vacuum state[32] instead of a unique one, sometimes called instantaneous vacuum. Consequently, such a field cannot always stay in its "vacuum", which indicates a particle production process in the case where the mass changes non-adiabatically with time because particle number is just an adiabatic invariant. On the other hand, the notation of "particle" may not be physically well-defined in a time-dependent background. A universal concept of "particle" does not always exist (nor necessary) because it generally depends on the state of motion of observers or detectors, even in Minkowski spacetime [162–164]. The issue of the definition of vacuum, therefore, is crucial for the discussion of particle production.

This chapter reviews particle production in a time-dependent background and its application to reheating after the end of inflation. The general theory of such particle production is briefly presented in Sec. 3.1, followed by its application to perturbative and non-perturbative particle production. In particular, in the non-perturbative case, more attention is drawn to tachyonic instability because it plays an important role during preheating in the mixed Higgs-R^2 inflation model, one of the main original works presented in this thesis. In Sec. 3.2, the reheating processes in two special cases are studied, namely in the Starobinsky model and the Higgs inflation. Notably, in the Higgs inflation case, the strong coupling issue during preheating is discussed, which questions the validity of the reheating process at the very beginning stage, so further investigation of the subsequent evolution in this model will be omitted.

3.1 Particle Production

Particle production is inevitably involved many physical processes of great interest, such as black hole evaporation [165, 166], Schwinger effect [167], and reheating after inflation. In the case of reheating, the inflaton field(s) or the corresponding degree(s) of freedom serves as a background energy source of the particle production by varying the effective masses of the produced fields, which results in the change of vacuum state or production of particles. Through such a process, the inflaton field transfers its energy to relativistic particles to reheat the Universe.

Before the application to concrete models, the basic idea and calculation of particle production with time-dependent effective mass will be introduced, based on which the

[32] In Heisenberg picture which is used in this thesis, since the quantum state is time-independent, a more appropriate description is that a state being the vacuum at one moment cannot remain as the vacuum of the system for all time due to the change of the operators. Nevertheless, the phrase "time-dependent vacuum" will be used sometimes and should be understood in the sense explained above.

production processes can be classified into perturbative and non-perturbative regimes. In the non-perturbative regime, further classification can be made according to the realization mechanisms, such as parametric resonance and tachyonic instability. In the following, the main interest lies in the production of scalar particles in a time-dependent background. The discussion is mainly based on Refs. [64, 168].

3.1.1 Scalar Fields in Time-Dependent Background

The idea and calculation here are based on the theory of quantum fields in a time-dependent background. Specifically, after the end of inflation, the inflaton field exits the slow-roll regime and, as a typical example, starts to oscillate coherently. Since the inflaton energy still dominates the Universe, its non-trivial evolution predominantly affects the quantum fields in this background. This effect can be summarized in a general form of the equation of motion for scalar fields. After quantizing the scalar fields, the particle production can be interpreted as the mixing of positive and negative modes induced by the time-dependent effective masses, as will be shown in the following.

3.1.1.1 Classical Scalar Fields

Consider a scalar field $\chi(t, \mathbf{x})$ without homogeneous background part as the target for production whose equation of motion can generally be written as

$$-\Box\chi(t, \mathbf{x}) + m_{\rm eff}^2(t)\chi(t, \mathbf{x}) = 0 \ . \tag{3.1}$$

To illustrate this point, three simplified but typical examples are considered in the following.

• **Example One** In Minkowski spacetime, a massless field $\chi(t, \mathbf{x})$ is directly coupled to a homogeneous scalar field $\phi(t)$ with an effective potential $V(\phi)$ which is minimized at σ_ϕ. Then the corresponding action around σ_ϕ after the shift $\phi - \sigma_\phi \to \phi$ is

$$S = \frac{1}{2}\int d^4x \left[\dot{\phi}^2 - m_\phi^2\phi^2 - \eta^{\mu\nu}\partial_\mu\chi\partial_\nu\chi - g_\phi^2\left(\phi + \sigma_\phi\right)^2\chi^2\right] \ , \tag{3.2}$$

where $\eta_{\mu\nu}$ is the Minkowski metric, $V(\phi)$ is assumed to be quadratic around σ_ϕ, and g_ϕ is a small coupling constant. The equation of motion for $\chi(t, \mathbf{x})$ is then

$$\ddot{\chi} - \nabla^2\chi + m_{\rm eff}^2(t)\chi = 0 \ , \tag{3.3}$$

where $m_{\rm eff}^2(t) \equiv g_\phi^2\phi^2(t) + 2g_\phi^2\sigma_\phi\phi(t) + g_\phi^2\sigma_\phi^2$. This is exactly in the same form as Eq. (3.1). The oscillation of $\phi(t)$ around the minimum induces a time-dependent

effective mass for $\chi(t,\mathbf{x})$ which is responsible for the production of χ-particles as will be shown later. Therefore, if the inflaton field directly couples to other matter fields, particle production will occur during the coherent oscillation phase after the end of inflation. Actually, it is easy to show from Eq. (2.25) that the coherently oscillating $\phi(t)$ with the quadratic potential $-m_\phi^2\phi^2$ can be understood as a condensate of massive particles with mass m_ϕ and zero momentum. The particle production is then the decay of such particles into the target field $\chi(t,\mathbf{x})$.

• **Example Two** In a curved spacetime, a scalar field $\chi(t,\mathbf{x})$ with mass m_χ is non-minimally coupled with gravity. The relevant part of action is given by

$$S=\frac{1}{2}\int d^4x\sqrt{-g}\left[\xi\chi^2R-g^{\mu\nu}\partial_\mu\chi\partial_\nu\chi-m_\chi^2\chi^2\right]\ , \tag{3.4}$$

where ξ is the non-minimal coupling which can take any real value. Assuming the flat FLRW background, the equation of motion for $\chi(t,\mathbf{x})$ is as follows

$$\ddot{\chi}+3H\dot{\chi}-\nabla^2\chi/a^2+m_{\rm eff}^2(t)\chi=0\ , \tag{3.5}$$

where $m_{\rm eff}^2(t)\equiv m_\chi^2-\xi R(t)$ receives the contribution from non-minimal coupling. This equation is of the same form as Eq. (3.1). Thus, the non-adiabatic variation of $R(t)$ can also be responsible for particle production as long as the modes with wavelengths comparable or larger than the curvature scale $k_p^2\lesssim|\xi R|$ are considered. In the short wavelength limit $k_p^2\gg|\xi R|$, the non-minimal coupling is negligible.

• **Example Three** In Minkowski spacetime, a non-canonical scalar field $\chi_1(t,\mathbf{x})$ is coupled with a homogeneous scalar field $\phi(t)$ through the kinetic term

$$S=-\frac{1}{2}\int d^4x\ f_{\rm nc}^2(\phi)\eta^{\mu\nu}\partial_\mu\chi_1\partial_\nu\chi_1\ . \tag{3.6}$$

By redefining a new field $\chi=f_{\rm nc}(\phi)\chi_1$, the kinetic term is canonicalized and an effective mass term appears

$$S=-\frac{1}{2}\int d^4x\left[\eta^{\mu\nu}\partial_\mu\chi\partial_\nu\chi-m_{\rm eff}^2(t)\chi^2\right]\ , \tag{3.7}$$

where $m_{\rm eff}^2(t)\equiv\ddot{f}_{\rm nc}(\phi)/f_{\rm nc}^2(\phi)$. The equation of motion for $\chi(t,\mathbf{x})$ is then naturally the same as Eq. (3.1). In other words, a non-canonical kinetic term that may arise in a conformal transformation can also induce particle production effectively as a time-dependent mass term.

The three examples above may imply that Eq. (3.1) is a general form of the equation of motion for fields that are coupled to gravity or other homogeneous fields

through the potential or the kinetic term. Even if the target field has a homogeneous part and self-interaction, the perturbative expansion can still result in the same form except that $m_{\text{eff}}(t)$ consists of not only $R(t)$ or $\phi(t)$ but the homogeneous part of the target field. It is obvious that the energy of $\chi(t, \mathbf{x})$ is not conserved. The time-dependent effective mass then serves as an energy source, so $\chi(t, \mathbf{x})$ becomes a driven oscillator whose amplitude can be amplified if $m_{\text{eff}}(t)$ is appropriately chosen. Besides, it is easy to generalize these examples to massive target field cases. For the purpose of this thesis, it is sufficient to focus on such type of equations as Eq. (3.1) for the study of particle production.

3.1.1.2 Quantization and Vacuum State

The action for $\chi(t, \mathbf{x})$ in a curved spacetime with corresponding equation of motion (3.1) can be written as

$$S_\chi = -\frac{1}{2}\int d^4x\sqrt{-g}\left(g^{\mu\nu}\partial_\mu\chi\partial_\nu\chi + m^2_{\text{eff}}(t)\chi^2\right) \ , \tag{3.8}$$

where $m_{\text{eff}}(t)$ can result from couplings with homogeneous fields or gravity, as explained previously. When considering a flat FLRW metric as background spacetime, this action can be further simplified by using the conformal time η in Eq. (2.3) instead of the physical time t. By redefining $\tilde{\chi} \equiv a(\eta)\chi$, the action (3.8) becomes

$$S_\chi = \frac{1}{2}\int d^3x d\eta \left[\tilde{\chi}'^2 - (\nabla\tilde{\chi})^2 - \tilde{m}^2_{\text{eff}}\tilde{\chi}^2\right] \equiv \int d^3x d\eta \ \mathcal{L}_{\tilde{\chi}} \ , \tag{3.9}$$

which is simply the action for a scalar field $\tilde{\chi}(\eta, \mathbf{x})$ in Minkowski spacetime with a time-dependent effective mass defined by

$$\tilde{m}^2_{\text{eff}}(\eta) \equiv a^2(\eta)\left[m^2_{\text{eff}}(\eta) - R(\eta)/6\right] \ . \tag{3.10}$$

The corresponding equation of motion for $\tilde{\chi}(\eta, \mathbf{x})$ is then

$$\tilde{\chi}'' - \nabla^2\tilde{\chi} + \tilde{m}^2_{\text{eff}}(\eta)\tilde{\chi} = 0 \ . \tag{3.11}$$

The benefit to work with Eq. (3.11) is that the effect from Hubble expansion is formally absent so the system can be simply analyzed as if in Minkowski spacetime. Thus, the canonical quantization can be done in the usual way. Given the Lagrangian $\mathcal{L}_{\tilde{\chi}}$, the conjugate momentum for $\tilde{\chi}$ is defined as

$$\tilde{\pi}(\eta, \mathbf{x}) \equiv \delta\mathcal{L}_{\tilde{\chi}}/\delta\tilde{\chi}' = \tilde{\chi}' \ . \tag{3.12}$$

For a real scalar field $\tilde{\chi}(\eta, \mathbf{x})$, it can be expanded in Fourier modes as

$$\tilde{\chi}(\eta, \mathbf{x}) = \int \frac{d^3k}{(2\pi)^3} e^{i\mathbf{k}\cdot\mathbf{x}} \tilde{\chi}(\eta, \mathbf{k}) \ , \tag{3.13}$$

where $\tilde{\chi}(\eta, \mathbf{k})$ can be generally written as

$$\tilde{\chi}(\eta, \mathbf{k}) = u_k(\eta) a_{\mathbf{k}} + u_k^*(\eta) a_{-\mathbf{k}}^\dagger \ , \tag{3.14}$$

with $k = |\mathbf{k}|$, and $a_{\mathbf{k}}^\dagger$ and $a_{\mathbf{k}}$ are the creation and annihilation operators, respectively, satisfying the commutation relations

$$\left[a_{\mathbf{k}}, a_{\mathbf{p}}^\dagger\right] = (2\pi)^3 \delta^{(3)}(\mathbf{k} - \mathbf{p}) \ , \ \ [a_{\mathbf{k}}, a_{\mathbf{p}}] = \left[a_{\mathbf{k}}^\dagger, a_{\mathbf{p}}^\dagger\right] = 0 \ . \tag{3.15}$$

Since the scalar field $\tilde{\chi}(\eta, \mathbf{x})$ and its conjugate momentum $\tilde{\pi}(\eta, \mathbf{x})$ should satisfy the canonical commutation relations

$$[\tilde{\chi}(\eta, \mathbf{x}), \tilde{\pi}(\eta, \mathbf{y})] = i\delta^{(3)}(\mathbf{x} - \mathbf{y}) \ , \ \ [\tilde{\chi}(\eta, \mathbf{x}), \tilde{\chi}(\eta, \mathbf{y})] = [\tilde{\pi}(\eta, \mathbf{x}), \tilde{\pi}(\eta, \mathbf{y})] = 0 \ , \tag{3.16}$$

the Wronskian to normalize the mode function $u_k(\eta)$ is then

$$W\left[u_k, u_k^*\right] = u_k u_k^{*\prime} - u_k' u_k^* = i \ . \tag{3.17}$$

The commutator for the Fourier modes can also be found easily

$$[\tilde{\chi}(\eta, \mathbf{k}), \tilde{\pi}(\eta, \mathbf{p})] = i\delta^{(3)}(\mathbf{k} + \mathbf{p}) \ , \ \ [\tilde{\chi}(\eta, \mathbf{k}), \tilde{\chi}(\eta, \mathbf{p})] = [\tilde{\pi}(\eta, \mathbf{k}), \tilde{\pi}(\eta, \mathbf{p})] = 0 \ , \tag{3.18}$$

where it is a plus sign in the Dirac delta function on the right hand side opposite to a minus sign as in Eq. (3.15). Inserting the Fourier transformation back to Eq. (3.11) leads to the equation of motion for the mode function

$$\begin{aligned} u_k'' + \tilde{\omega}_k^2(\eta) u_k &= 0 \ , \\ \tilde{\omega}_k^2(\eta) &\equiv k^2 + \tilde{m}_{\text{eff}}^2(\eta) \ , \end{aligned} \tag{3.19}$$

where the effective frequency is also time-dependent due to $\tilde{m}_{\text{eff}}(\eta)$. To understand the vacuum structure and particle production process, it is necessary to solve Eq. (3.19), an equation for parametric oscillator. However, analytical solutions for this type of equations are only known for limited cases, one of which is the well-known Mathieu equation (see Appendix D) that is useful for the study of reheating. Nevertheless, a general discussion about the vacuum state in the presence of a time-dependent frequency $\tilde{\omega}_k(\eta)$ is still possible and beneficial.

Let $|_{\eta_0}0\rangle$ denote the normalized vacuum state at some moment $\eta = \eta_0$ associated with the mode function u_k and the pair of creation/annihilation operators $a^\dagger_{\mathbf{k}}$ and $a_{\mathbf{k}}$. By definition, $|_{\eta_0}0\rangle$ is an eigenstate of the annihilation operator with vanishing eigenvalue $a_{\mathbf{k}}|_{\eta_0}0\rangle = 0$ as well as the Hamiltonian operator for the system with the minimal eigenvalue. As usual, the Hamiltonian can be obtained by a Legendre transformation of the Lagrangian $\mathcal{L}_{\tilde{\chi}}$ in Eq. (3.9) as

$$\begin{aligned}\hat{H}_{\tilde{\chi}} &= \frac{1}{2}\int d^3x \left[\tilde{\pi}^2 + (\nabla\tilde{\chi})^2 + \tilde{m}^2_{\rm eff}\tilde{\chi}^2\right] \ , \\ &= \frac{1}{2}\int \frac{d^3k}{(2\pi)^3}\left[F_k(\eta)a_{\mathbf{k}}a_{-\mathbf{k}} + F^*_k(\eta)a^\dagger_{\mathbf{k}}a^\dagger_{-\mathbf{k}} + \left(a^\dagger_{\mathbf{k}}a_{\mathbf{k}} + a_{\mathbf{k}}a^\dagger_{\mathbf{k}}\right)E_k(\eta)\right] , \end{aligned} \tag{3.20}$$

where $\hat{(\ )}$ is used for Hamiltonian to distinguish from the Hubble parameter H, and

$$\begin{aligned} E_k(\eta) &\equiv |u'_k|^2 + \tilde{\omega}^2_k(\eta)\,|u_k|^2 \ , \\ F_k(\eta) &\equiv u'^2_k + \tilde{\omega}^2_k(\eta)u^2_k \ . \end{aligned} \tag{3.21}$$

On the one hand, the expectation value of $\hat{H}$ in vacuum state $|_{\eta_0}0\rangle$ at time $\eta = \eta_0$ is simply calculated as

$$\langle_{\eta_0}0|\hat{H}_{\tilde{\chi}}(\eta_0)|_{\eta_0}0\rangle = \frac{1}{2}(2\pi)^3\delta^{(3)}(0)\int\frac{d^3k}{(2\pi)^3}E_k(\eta_0) \ , \tag{3.22}$$

where the divergence is due to the infinite total volume of space, so that the comoving energy density is given by

$$\rho(\eta_0) = \frac{1}{2}\int\frac{d^3k}{(2\pi)^3}E_k(\eta_0) \ , \tag{3.23}$$

which should be minimized. It is easy to show that $E_k(\eta_0)$ is minimized if the mode function satisfies the following conditions up to an unimportant arbitrary phase

$$u_k(\eta_0) = 1/\sqrt{2\tilde{\omega}_k(\eta_0)} \ , \ u'_k(\eta_0) = -i\sqrt{\tilde{\omega}_k(\eta_0)/2} \ . \tag{3.24}$$

The resulting Hamiltonian at this moment becomes

$$\begin{aligned}\hat{H}_{\tilde{\chi}}(\eta_0) &= \frac{1}{2}\int\frac{d^3k}{(2\pi)^3}\left(a^\dagger_{\mathbf{k}}a_{\mathbf{k}} + a_{\mathbf{k}}a^\dagger_{\mathbf{k}}\right)\tilde{\omega}_k(\eta_0) \ , \\ &= \frac{1}{2}\int\frac{d^3k}{(2\pi)^3}\left(2a^\dagger_{\mathbf{k}}a_{\mathbf{k}} + (2\pi)^3\,\delta^{(3)}(0)\right)\tilde{\omega}_k(\eta_0) \ , \end{aligned} \tag{3.25}$$

where, on the second line, the first term corresponds to the occupation number operator which vanishes when sandwiched by $\langle_{\eta_0}0|$ and $|_{\eta_0}0\rangle$ while the second is the zero-point energy. However, this cannot always hold true for a time-dependent $\tilde{\omega}_k(\eta)$.

In other words, the mode function $u_k(\eta)$ cannot minimize $E_k(\eta)$ in the upper of Eq. (3.21) while satisfying Eq. (3.19) for all the time. On the other hand, $|_{\eta_0}0\rangle$ is an eigenstate of $\hat{H}_{\tilde{\chi}}(\eta_0)$ only if $F_k(\eta_0) = 0$, i.e. requiring that

$$u_k'^2(\eta_0) + \tilde{\omega}_k^2(\eta_0)u_k^2(\eta_0) = 0 \ , \tag{3.26}$$

whose solution is formally written as

$$u_k(\eta) \propto \exp\left[\pm i \int^{\eta} \tilde{\omega}_k(\eta_1)d\eta_1\right] \ . \tag{3.27}$$

Obviously, the conditions (3.24) satisfy Eq. (3.26) so $|_{\eta_0}0\rangle$ is indeed a vacuum state at the moment $\eta = \eta_0$. However, it is easy to show that the solution (3.27) is generally not the solution for Eq. (3.19) unless $\tilde{\omega}_k(\eta) = \text{const}$. In other words, $|_{\eta_0}0\rangle$ cannot remain as the eigenstate of $\hat{H}_{\tilde{\chi}}$ while satisfying Eq. (3.19) for all the time.

In summary, the "vacuum" in a general time-dependent background is instantaneous and not unique. There is no preferred choice of physical vacuum state for all time and, therefore, the concept of "particle" in such background. Intuitively speaking, for example, in a general curved spacetime, this ambiguity comes from the finite scale determined by the four-dimensional curvature. The modes with scales much smaller than the curvature scale cannot "feel" the non-trivial geometry of the spacetime, so the situation is similar to Minkowski background. However, for modes with scales comparable or larger than the curvature scale, the change of the background geometry becomes significant, and the plane wave approximation used in Minkowski spacetime is no longer valid so that the usual definition of a localized particle as a wavepacket fails at large scales.

In some special cases, for example when the change of $\tilde{m}_{\text{eff}}(\eta)$ is slow enough, there may be a better[33] choice of vacuum, called adiabatic vacuum. This prescription relies on the WKB approximation. Assuming the ansatz of the solution of Eq. (3.19) to be in the form

$$u_k(\eta) = \frac{1}{\sqrt{W_k(\eta)}} \exp\left[i \int^{\eta} W_k(\eta_1)d\eta_1\right] \ , \tag{3.28}$$

it can be found that $W_k(\eta)$ must satisfy the following condition

$$W_k^2 = \tilde{\omega}_k^2 - \frac{1}{2}\left[\frac{W_k''}{W_k} - \frac{3}{2}\frac{W_k'^2}{W_k^2}\right] \ . \tag{3.29}$$

[33] See Refs. [64, 168] for details.

If the background $\tilde{\omega}_k(\eta)$ varies adiabatically, i.e. the typical time scale of background evolution much larger than that of the mode function u_k, Eq. (3.29) can be treated as a recurrence. The zeroth order is ${}^{(0)}W_k = \tilde{\omega}_k$ while the second order is

$$ {}^{(2)}W_k = \tilde{\omega}_k \left(1 - \frac{1}{4}\frac{\tilde{\omega}_k''}{\tilde{\omega}_k^3} + \frac{3}{8}\frac{\tilde{\omega}_k'^2}{\tilde{\omega}_k^4} \right) \ , \tag{3.30} $$

which is valid under the condition of adiabaticity

$$ -\frac{1}{4}\frac{\tilde{\omega}_k''}{\tilde{\omega}_k^3} + \frac{3}{8}\frac{\tilde{\omega}_k'^2}{\tilde{\omega}_k^4} \ll 1 \ . \tag{3.31} $$

In principle, it is possible to reach arbitrary order of recurrence but not necessary. This series is an asymptotic series where the terms of higher order increase strictly more slowly than those of lower order as going to the interested limit but the summation diverges. For this kind of asymptotic series, there usually exists an optimal truncation order where the error reaches minimum[34]. The adiabatic vacuum at $\eta = \eta_0$ is then determined by putting the optimal order solution ${}^{(N)}W_k$ back into the ansatz to find out the N-th order mode function ${}^{(N)}u_k(\eta)$ and requiring the exact solution $u_k(\eta)$ to satisfy the initial conditions

$$ u_k(\eta_0) = {}^{(N)}u_k(\eta_0) \ , \ u_k'(\eta_0) = {}^{(N)}u_k'(\eta_0) \ . \tag{3.32} $$

Note that the adiabatic vacuum is an exact state in the sense that the approximated mode function ${}^{(N)}u_k(\eta_0)$ is just for the matching at $\eta = \eta_0$, as shown above. The quantized field is still the exact mode function $u_k(\eta)$. The matching also makes the adiabatic vacuum not unique because the matching process can be taken at different $\eta \neq \eta_0$. Once $\tilde{\omega}_k$ is constant, all the vacuum prescriptions coincide.

3.1.1.3 Bogoliubov Transformation and Particle Production

Consider two periods around $\eta = \eta_0$ and $\eta = \eta_1$ when the background evolves adiabatically. As a result, there exist sensible concepts of (adiabatic) vacuum (and particle) at these moments which are denoted by $|_{\eta_0}0\rangle$ and $|_{\eta_1}0\rangle$. The mode function associated with the former is $u_k(\eta)$ as previously mentioned, while $w_k(\eta)$ denotes the mode function for the latter together with a new pair of creation/annihilation operators $b_{\mathbf{k}}^\dagger$ and $b_{\mathbf{k}}$. Consequently, there are two different expansions for the quantum field $\tilde{\chi}(\eta, \mathbf{k})$ as

$$ \tilde{\chi}(\eta, \mathbf{k}) = u_k(\eta) a_{\mathbf{k}} + u_k^*(\eta) a_{-\mathbf{k}}^\dagger = w_k(\eta) b_{\mathbf{k}} + w_k^*(\eta) b_{-\mathbf{k}}^\dagger \ . \tag{3.33} $$

[34] See e.g. discussion on an alternative method based on Stokes phenomenon [169, 170].

Generically, the mode function $w_k(\eta)$ associated with $|_{\eta_1}0\rangle$ can be written as

$$w_k(\eta) = \alpha_k u_k(\eta) + \beta_k u_k^*(\eta) \ , \tag{3.34}$$

where α_k and β_k are complex constants called the Bogoliubov coefficients which should satisfy the normalization condition

$$|\alpha_k|^2 - |\beta_k|^2 = 1 \ . \tag{3.35}$$

And $w_k(\eta)$ also satisfies the same form of initial conditions (3.24) at $\eta = \eta_1$ as it minimizes the Hamiltonian at that moment. Accordingly, it is easy to show that the two pairs of creation and annihilation operators satisfy the following relation

$$b_{\mathbf{k}} = \alpha_k^* a_{\mathbf{k}} - \beta_k^* a_{\mathbf{k}}^\dagger \ . \tag{3.36}$$

These relations (3.34) and (3.36) are known as Bogoliubov transformation [171].

The Bogoliubov transformation is useful to clarify the relation between different vacuum states. For example, consider the state $|_{\eta_0}0\rangle$ and the Hamiltonian (3.20). Since $u_k(\eta)$ satisfies the initial conditions (3.24), the expectation value of Hamiltonian at $\eta = \eta_0$ is given by Eq. (3.22) with $E_k(\eta_0)$ replaced by $\tilde{\omega}_k(\eta_0)$. Therefore, there is no particle present at this time but only zero-point energy. In the Heisenberg picture, the state is fixed but the operators evolve. At a later moment $\eta = \eta_1$, the Hamiltonian can be expressed as the first line of Eq. (3.25) except for η_0, $a_{\mathbf{k}}$, and $a_{\mathbf{k}}^\dagger$ replaced by η_1, $b_{\mathbf{k}}$, and $b_{\mathbf{k}}^\dagger$ respectively, because $w_k(\eta)$ also satisfies the same form of initial conditions (3.24) at $\eta = \eta_1$. If now the Hamiltonian is sandwiched by $|_{\eta_1}0\rangle$, it only leads to the same result as before, i.e. only the existence of zero-point energy. However, the state is still $|_{\eta_0}0\rangle$ so the expectation value of $\hat{H}_{\tilde{\chi}}(\eta_1)$ is then calculated as follows

$$\begin{aligned}
\langle_{\eta_0}0|\hat{H}_{\tilde{\chi}}(\eta_1)|_{\eta_0}0\rangle &= \frac{1}{2}\int \frac{d^3k}{(2\pi)^3}\langle_{\eta_0}0|b_{\mathbf{k}}^\dagger b_{\mathbf{k}} + b_{\mathbf{k}} b_{\mathbf{k}}^\dagger|_{\eta_0}0\rangle\tilde{\omega}_k(\eta_1) \ , \\
&= (2\pi)^3\,\delta^{(3)}(0)\int \frac{d^3k}{(2\pi)^3}\left(|\beta_k|^2 + \frac{1}{2}\right)\tilde{\omega}_k(\eta_1) \ ,
\end{aligned} \tag{3.37}$$

where the Bogoliubov transformation (3.36) has been applied and $(2\pi)^3\delta^{(3)}(0)$ comes from the infinite spatial volume. As a result, particles are produced in the state $|_{\eta_0}0\rangle$ as the system evolves in time and the comoving energy density[35] of the produced particles at $\eta = \eta_1$ is given by

$$\rho_{\tilde{\chi}} = \int \frac{d^3k}{(2\pi)^3}|\beta_k|^2\tilde{\omega}_k(\eta_1) \ . \tag{3.38}$$

[35]Here, the zero-point energy is simply subtracted. However, it can be seen that the zero-point energy is time-dependent so simple subtraction may be not justified. See Ref. [168] for more detail.

As can be seen clearly, the Bogoliubov coefficient β_k is directly related to the comoving number density of the produced particles in the following way

$$n_{\tilde{\chi}} = \int \frac{d^3k}{(2\pi)^3} n_k = \int \frac{d^3k}{(2\pi)^3} |\beta_k|^2 \ , \tag{3.39}$$

where $n_k = |\beta_k|^2$ is the occupation number of $\tilde{\chi}$ in momentum space. Note that if $|\beta_k|^2$ decreases slower than k^{-3} for large k, the integration above diverges, which indicates that the Bogoliubov transformation is not well-defined.

From above, the physical interpretation of the Bogoliubov transformation can be understood as follows. If ω_k tends to be constant in the far past and far future, well-defined vacuum states always exist and the positive- and negative-frequency modes $\exp(\mp i\tilde{\omega}_k\eta)$ (or mode functions) are well separated from each other. However, if $\omega_k(\eta)$ is time-dependent in some middle period, these two modes are mixed (as in Eq. (3.34)) and vacuum fluctuations are excited, which results in particle production.

After reviewing the technique of Bogoliubov transformation to calculate the production of scalar particles in a time-dependent background, this technique will be applied to two types of particle production in the following, the perturbative and the non-perturbative production that are important for the investigation of reheating at post-inflationary epoch.

3.1.2 Perturbative Production

Perturbative particle production is relevant when the coupling between target fields and the background field is weak enough. For example in Eq. (3.19), the perturbative production occurs when the effective mass $|\tilde{m}_{\rm eff}(\eta)|$ is much smaller than the interested scale k so that it could be treated as perturbation. The discussion here is mainly based on the discussion in Refs. [16, 64, 159, 172].

Rewrite Eq. (3.19) as

$$\begin{aligned} u_k'' + \omega_k^2 u_k &= -\left[\tilde{m}_{\rm eff}^2(\eta) - m_\chi^2\right] u_k \equiv S_{\tilde{\chi}}(\eta) u_k \ , \\ \omega_k^2 &\equiv k^2 + m_\chi^2 \ , \end{aligned} \tag{3.40}$$

where $\tilde{m}_{\rm eff}^2(\eta)$ can contain different types of contributions as explained at the beginning of this section, including the mass of χ, the non-minimal coupling, and the coupling with other fields. Therefore, the perturbative particle production is valid when $\chi(\eta, \mathbf{x})$ is light and the couplings with background are weak. This equation can

be solved by the Green's function method together with iteration due to the smallness of $S_{\tilde{\chi}}$. Assuming the boundary conditions

$$\begin{cases} u_k(\eta) = e^{-i\omega_k\eta}/\sqrt{2\omega_k} \ , & \eta \to -\infty \ , \\ u_k(\eta) = \alpha_k e^{-i\omega_k\eta}/\sqrt{2\omega_k} + \beta_k e^{i\omega_k\eta}/\sqrt{2\omega_k} \ , & \eta \to +\infty \ , \end{cases} \tag{3.41}$$

where α_k and β_k are nothing but the Bogoliubov coefficients normalized as Eq. (3.35), the solution of Eq. (3.40) is written as

$$u_k(\eta) = \frac{1}{\sqrt{2\omega_k}} e^{-i\omega_k\eta} + \frac{1}{\omega_k}\int_{-\infty}^{\eta} \sin\left[\omega_k\left(\eta - \tilde{\eta}\right)\right] S_{\tilde{\chi}}(\tilde{\eta}) u_k(\tilde{\eta}) d\tilde{\eta} \ , \tag{3.42}$$

from which the Bogoliubov coefficients at $\eta \to +\infty$ can be derived as

$$\begin{aligned} \alpha_k &= 1 + \frac{i}{\sqrt{2\omega_k}}\int_{-\infty}^{+\infty} e^{i\omega_k\eta} S_{\tilde{\chi}}(\eta) u_k(\eta) d\eta \ , \\ \beta_k &= -\frac{i}{\sqrt{2\omega_k}}\int_{-\infty}^{+\infty} e^{-i\omega_k\eta} S_{\tilde{\chi}}(\eta) u_k(\eta) d\eta \ . \end{aligned} \tag{3.43}$$

Because $S_{\tilde{\chi}}(\eta)$ is perturbation, the integration (3.42) can be solved by iteration. Given the zeroth order $u_k^{(0)}(\eta) = e^{-i\omega_k\eta}/\sqrt{2\omega_k}$ which corresponds to $\alpha_k = 1$ and $\beta_k = 0$, the next order is obtained by just substituting $u_k^{(0)}(\eta)$ for $u_k(\eta)$ in Eq. (3.43), so the leading contribution to comoving number density of produced particles at $\eta \to +\infty$ are of second order in $S_{\tilde{\chi}}(\eta)$ as

$$n_{\tilde{\chi}} = \int \frac{d^3k}{(2\pi)^3} |\beta_k|^2 = \frac{1}{8\pi^2}\int_0^{\infty} \frac{k^2 dk}{\omega_k^2} \iint_{-\infty}^{+\infty} d\eta_1 d\eta_2 \ e^{-2i\omega_k(\eta_1 - \eta_2)} S_{\tilde{\chi}}(\eta_1) S_{\tilde{\chi}}(\eta_2) \ . \tag{3.44}$$

In the massless case where $m_\chi = 0$, this integration can be further simplified because ω_k^2 reduces to k^2 and cancels that on the numerator. As a result, the comoving number density of the produced massless particles is given as

$$n_{\tilde{\chi},\mathrm{m}_\chi=0} = \frac{1}{16\pi}\int_{-\infty}^{+\infty} S_{\tilde{\chi}}^2(\eta) d\eta \ . \tag{3.45}$$

The role of the mass is to suppress the particle production process, which can be more clearly seen in concrete examples later. The corresponding comoving energy density of the produced particles $\rho_{\tilde{\chi}}$ can also be calculated. Since Eq. (3.40) is linear in u_k, this process corresponds to one particle from the source decaying into two $\tilde{\chi}$ particles, i.e. $\dot{n}_{\tilde{\chi}} = -2\dot{n}_{\mathrm{bg}}$. The decay rate of the background field is then

$$\Gamma_{\mathrm{bg}\to\tilde{\chi}\tilde{\chi}} = -\dot{n}_{\mathrm{bg}}/n_{\mathrm{bg}} = \dot{n}_{\tilde{\chi}}/(2n_{\mathrm{bg}}) \ , \tag{3.46}$$

where the subscript "bg" denotes the particle from the background source that decays. For example, in Eq. (3.2), the interaction $\Delta\mathcal{L}_{\phi\to\chi\chi} = -g_\phi^2\sigma_\phi\phi\chi^2$ induces the decay of one ϕ-particle into two χ-particles.

Observing that $S_{\tilde{\chi}}(\eta)$ is given by the small general couplings between χ and other fields, it indicates that this perturbative approach can be applied in both JF and EF. Especially in the latter, another way to obtain the decay rate is calculating the S-matrix of the corresponding process with Feynman diagram as done in quantum field theory in Minkowski spacetime. The known result for the tree-level decay rate of ϕ into massless χ via $\Delta\mathcal{L}_{\phi\to\chi\chi} = -g_\phi^2\sigma_\phi\phi\chi^2$ calculated in this way is

$$\Gamma_{\phi\to\chi\chi} = \frac{g_\phi^4\sigma_\phi^2}{8\pi m_\phi} \ , \tag{3.47}$$

which is constant and independent of the number density of the produced particles. This decay rate can be shown to coincide with the result obtained in the first method.

To incorporate the perturbative decay into reheating after inflation, the decay rate is often treated as a friction term in the equation of motion for the inflaton field, for instance, in Eq. (2.24) the single-field case

$$\ddot{\phi} + (3H + \Gamma_{\phi\to\chi\chi})\,\dot{\phi} + V_{,\phi} = 0 \ . \tag{3.48}$$

Since the produced massless (or $m_\chi \ll m_\phi$) χ-particles are relativistic, accordingly, the Boltzmann equation for the radiation energy density $\rho_{\rm rad}$ and the Friedmann equation are given as

$$\dot{\rho}_{\rm rad} + 4H\rho_{\rm rad} = \Gamma_{\phi\to\chi\chi}\rho_\phi \ , \tag{3.49}$$

$$3M_{\rm pl}^2H^2 = \rho_\phi + \rho_{\rm rad} \ . \tag{3.50}$$

As a result, perturbative reheating transfers the energy of inflaton into other relativistic particles until the completion of perturbative reheating which is characterized by the moment when the Hubble expansion rate falls below the decay rate of inflaton, denoted as t_r. After that, the Universe is dominated by radiation so the energy density is related to the temperature of the Universe as

$$3M_{\rm pl}^2H^2(t_r) = \rho_{\rm rad}(t_r) = \pi^2 g_r T_r^4/30 \ , \tag{3.51}$$

where T_r is one of the most important quantities in reheating defined as the reheating temperature, and $g_r = 106.75$ is the effective number of relativistic species. Since $H(t_r) = \Gamma_{\phi\to\chi\chi}$, it leads to

$$T_r = \left(\frac{90}{g_r\pi^2}\right)^{1/4}\sqrt{M_{\rm pl}\Gamma_{\phi\to\chi\chi}} \ \simeq 0.54\sqrt{M_{\rm pl}\Gamma_{\phi\to\chi\chi}} \ . \tag{3.52}$$

As for the interaction, $\Delta\mathcal{L}_{\phi\phi\to\chi\chi} = -g_\phi^2\phi^2\chi^2/2$, the scattering rate typically decreases faster than the Hubble rate does as the amplitude of ϕ becomes smaller so this process soon becomes inefficient, which means that this channel cannot reheat the Universe by itself. Therefore, in the model where $\sigma_\phi = 0$, the channel $\phi \to \chi\chi$ is absent and it is likely that the reheating never completes solely with the scattering $\phi\phi \to \chi\chi$. If there are other ways for the inflaton to decay, e.g. to light fermions, then reheating the Universe is still possible.

Reheating through perturbative particle production is usually referred to as the elementary theory of reheating [21, 22], which plays a vital role at the last stage of reheating in most cases, determining the reheating temperature. Before entering the perturbative regime as the inflaton oscillation becomes small, more efficient particle production processes are of interest.

3.1.3 Non-Perturbative Production

The perturbative approach introduced above fails when the combination of the couplings and the amplitude of background oscillation is large, for example, $|\xi R| \gtrsim 1$. In this regime, the non-perturbative effects such as parametric resonance and tachyonic instability dominate the particle production processes, leading to highly efficient particle production. Reheating through such non-perturbative particle production is usually referred to as preheating [14, 16]. Although preheating is short and cannot affect the reheating temperature much, violent preheating may leave imprints on other observables, such as the equation of state of the early Universe and high-frequency gravitational waves that may be detected in the future, as mentioned previously. The calculation of particle production can be realized within the framework of the Bogoliubov transformation introduced previously with more careful treatment. The discussion in the following is mainly based on Refs. [14, 16, 17, 168] for parametric resonance and Refs. [173, 174] for tachyonic instability, specifically focusing on the case where the background field acts as a harmonic oscillator without considering backreaction.

3.1.3.1 Parametric Resonance

Parametric resonance is based on the theory of the Mathieu equation, especially the stability chart shown in Appendix D. Generally speaking, parametric resonance can be classified into two types according to the width of the resonance bands, narrow and broad resonance. As to be shown, the former can be understood as an "enhanced version" of perturbative decay by Bose condensation effect [175] which leads

to a qualitatively different result from the perturbative particle production, while the latter as the successive scatterings of the mode function on parabolic potentials [16].

Without loss of generality, consider Eq. (3.1) with $m^2_{\rm eff}(t) \equiv g^2_\phi\phi^2(t) + 2g^2_\phi\sigma_\phi\phi(t) + g^2_\phi\sigma^2_\phi$ as shown in Example One in last section[36] with $m_\chi = 0$. The time-dependence comes from the first and second terms; the former dominates when $|\phi| \gg |\sigma_\phi|$ while the latter dominates if $|\phi| \ll |\sigma_\phi|$. The non-minimal coupling case is completely analogous to the latter. Quantizing the $\chi(t,\mathbf{x})$ field

$$\chi(t,\mathbf{x}) = \int \frac{d^3k}{(2\pi)^3} e^{i\mathbf{k}\cdot\mathbf{x}} \left[\chi_k(t) a_{\mathbf{k}} + \chi^*_k(t) a^\dagger_{-\mathbf{k}}\right] \ , \tag{3.53}$$

the equation of motion for $\chi_k(t)$, according to Eq. (3.1), can be written in a flat FLRW background as

$$\begin{cases} \ddot{\chi}_k + 3H\dot{\chi}_k + \left[k^2_p + g^2_\phi\phi^2(t)\right]\chi_k = 0 \ , & \phi_0 \gg |\sigma_\phi| \ , \\ \ddot{\chi}_k + 3H\dot{\chi}_k + \left[k^2_p + g^2_\phi\sigma^2_\phi + 2g^2_\phi\sigma_\phi\phi(t)\right]\chi_k = 0 \ , & \phi_0 \ll |\sigma_\phi| \ . \end{cases} \tag{3.54}$$

For simplicity, the Hubble expansion is neglected in the following[37] and brief discussion on such effect will be presented subsequently. Then, the background field $\phi(t)$ can be assumed to take the following simple form

$$\phi(t) = \phi_0 \sin(m_\phi t) \ , \tag{3.55}$$

where $\phi_0 > 0$ is the constant amplitude and m_ϕ is the mass of $\phi(t)$. As a result, Eq. (3.54) can be rewritten in the same form as Mathieu equation (D.1) in Appendix D

$$\chi_{k,zz} + \left[A_k - 2q\cos(2z)\right]\chi_k = 0 \ , \tag{3.56}$$

where the dimensionless variables z, A_k and q are given by

$$\begin{cases} A_k = k^2/m^2_\phi + 2q \ , \ q = g^2_\phi\phi^2_0/(4m^2_\phi) \ , \ z = m_\phi t, & \phi_0 \gg |\sigma_\phi| \ , \\ A_k = 4\left(k^2 + g^2_\phi\sigma^2_\phi\right)/m^2_\phi \ , \ q = 4g^2_\phi\sigma_\phi\phi_0/m^2_\phi \ , \ z = m_\phi t/2 + \pi/4, & \phi_0 \ll |\sigma_\phi| \ . \end{cases} \tag{3.57}$$

[36] As mentioned earlier, the analysis here can be generalized to the case where the target field has a homogeneous part and self-interaction. In that case, the particles are resonantly produced by the oscillation of its own homogeneous part. See e.g. the discussion in Refs. [14, 16] for case with presence of $\lambda\phi/4$, and in Ref. [17] where the conformally invariant theory $\lambda\phi^4/4 + g^2_\phi\phi^2\chi^2/2$ is analyzed for the production of both ϕ- and χ-particles.

[37] The situation in Eq. (3.11) may indicate that it is possible to avoid the cosmic expansion but the non-trivial time-dependence of $a(t)$ and the usage of η can spoil the simple behavior of $\phi(t)$ or $R(t)$ in the effective mass, as implied in Eq. (3.10). Another kind of field redefinition for simplification is discussed in the broad resonance case.

Therefore, the analysis in Appendix D is applicable to the particle production processes through parametric resonance. According to different locations of the parameters of interest in the stability chart in Fig. D.2, the discussion is categorized into two different regimes, narrow and broad resonance.

• **Narrow Resonance** Consider $\max\{g_\phi\phi_0, g_\phi|\sigma_\phi|\} \ll m_\phi$, which means that $q \ll 1$. This case is within the narrow resonance regime. As discussed in Appendix D, the instability bands shows up when $A_k \simeq n^2$ with $n \in \mathbb{Z}_+$ among which the most important one is $n = 1$ because its width is the largest $1 - q \lesssim A_k \lesssim 1 + q$. For the choice of k within this instability band, the solution grows exponentially $\chi_k(t) \propto \exp\left[\mu_k^{(1)} z\right]$, where, according to Eq. (D.15), the instability index $\mu_k^{(1)}$ is given by

$$\mu_k^{(1)} \simeq \left[q^2/4 - \left(\sqrt{A_k} - 1\right)^2\right]^{1/2} \simeq \begin{cases} \left[q^2/4 - (k/m_\phi - 1)^2\right]^{1/2} , & \phi_0 \gg |\sigma_\phi| , \\ \left[q^2/4 - (2k/m_\phi - 1)^2\right]^{1/2} , & \phi_0 \ll |\sigma_\phi| , \end{cases} \tag{3.58}$$

from which it can be extracted that resonance only occurs in the modes with very narrow range of momentum

$$\begin{cases} (1 - q/2)\, m_\phi \lesssim k \lesssim (1 + q/2)\, m_\phi , & \phi_0 \gg |\sigma_\phi| , \\ (1/2 - q/4)\, m_\phi \lesssim k \lesssim (1/2 + q/4)\, m_\phi , & \phi_0 \ll |\sigma_\phi| . \end{cases} \tag{3.59}$$

In both cases, the maximal instability index is $\mu_{k,\max}^{(1)} = q/2$ when the produced particles are on-shell, i.e. $k = m_\phi$ and $k = m_\phi/2$, respectively. As a result, the number density n_k of the maximally produced modes χ_k grows as $\propto \exp\left[2\mu_{k,\max}^{(1)} z\right] = \exp(qz)$ because

$$n_k = \frac{\omega_{k,\text{eff}}}{2}\left(\frac{|\dot{\chi}_k|^2}{\omega_{k,\text{eff}}^2} + |\chi_k|^2\right) - \frac{1}{2} , \tag{3.60}$$

where $\omega_{k,\text{eff}}(t)$ is the effective frequency for χ_k. At the same time, other off-shell particles with $k \pm \Delta k$ where $\Delta k \sim q$ are also produced. One example of narrow resonance for the $\phi_0 \gg \sigma_\phi$ case is shown in Fig. 3.2.

In particular for the case $\phi_0 \ll |\sigma_\phi|$, it can be compared with the perturbative decay process $\phi \to \chi\chi$ induced by the interaction $\Delta\mathcal{L}_{\phi\to\chi\chi} = -g_\phi^2\sigma_\phi\phi\chi^2$ to understand their difference. In the perturbative regime, the decay rate is given by Eq. (3.47) for $m_\chi = 0$, which results in exponential decay of number density of ϕ but not exponential growth of that of χ. However, in the narrow resonance case, the exponential growth rate of n_χ is given as $\mu_{k,\max}^{(1)} m_\phi \simeq 2g_\phi^2\sigma_\phi\phi_0/m_\phi$, according to the analysis above. Therefore, it can be firstly noticed that these two effects may coexist but dominate

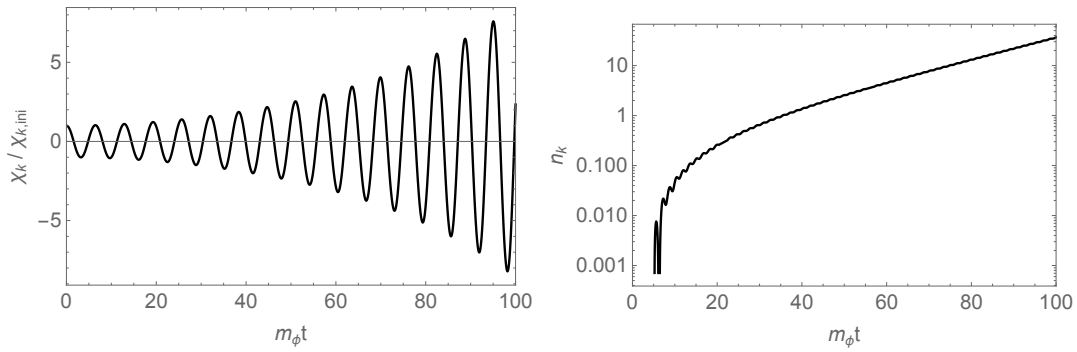

Figure 3.2: An example of narrow resonance for the $\phi_0 \gg |\sigma_\phi|$ case in Eq. (3.57) with $A_k = 1$ and $q = 0.05$. $\chi_{k,\mathrm{ini}}$ is the initial value of χ_k. The left panel shows the evolution of χ_k while the right shows the occupation number n_k.

different time regimes. When $\phi_0 \gtrsim g_\phi^2 \sigma_\phi/(16\pi)$ is satisfied at early time, narrow resonance is more important and the number density of χ grows exponentially because the growth rate $\mu^{(1)}_{k,\mathrm{max}} m_\phi$ is larger than $\Gamma_{\phi\to\chi\chi}$. As the energy of ϕ decreases due to particle production (and cosmic expansion), ϕ_0 becomes small enough that the perturbative decay rate exceeds the exponential growth rate of narrow resonance, which means that the amplitude ϕ_0 decays at a time scale shorter than that necessary for narrow resonance to occur. Since this moment, the perturbative decay plays a more important role. The second difference between the two effects is that only on-shell particles are considered in the former but both on-shell and off-shell χ are produced in the latter as mentioned previously. The third is that the growth of n_χ is proportional to n_χ itself in the narrow resonance case, i.e. enhanced by Bose condensation effect, while the perturbative decay is not. This can be roughly seen in the following way. If the effective decay rate is enhanced by the Bose effect, it can be estimated as

$$\Gamma_{\phi\to\chi\chi,\mathrm{eff}} \sim 2\Gamma_{\phi\to\chi\chi} n_k \ , \tag{3.61}$$

where the factor 2 comes from the production of *two* χ-particles, and $n_k \gg 1$ is assumed so that such effect is significant. According to Eq. (3.59), further assume that only particles with $k \simeq m_\phi/2$ are produced with $\Delta k \simeq q m_\phi/2$ as the width. Then the occupation number in momentum space can be estimated as

$$n_{k=m_\phi/2} \simeq \frac{n_\chi}{(4\pi k^2 \Delta k)/(2\pi)^3} \simeq \frac{2\pi^2 \phi_0}{g_\phi^2 \sigma_\phi} \frac{n_\chi}{n_\phi} \ , \tag{3.62}$$

where $n_\phi = m_\phi \phi_0^2/2 \gg 1$ can be effectively understood as the number density of ϕ in the condensate induced by the coherent oscillation. As a result, only after some period

when a certain amount of χ-particles have been produced $n_\chi \gtrsim g_\phi^2 \sigma_\phi n_\phi/(2\pi^2\phi_0)$, the occupation number can be large enough to have significant effect. The equation for the comoving number density of χ-particles is then given as

$$\dot{n}_\chi \simeq 2\Gamma_{\phi\to\chi\chi,\text{eff}}\, n_\phi \simeq \Gamma_{\phi\to\chi\chi}\frac{8\pi^2\phi_0}{g_\phi^2\sigma_\phi}n_\chi = \frac{\pi g_\phi^2\sigma_\phi\phi_0}{m_\phi}n_\chi \ , \tag{3.63}$$

from which it is easy to see that n_χ grows exponentially with a growth rate $\sim \mu^{(1)}_{k,\max} m_\phi$ as shown in the narrow resonance. Fermions, on the contrary, do not experience such enhancement because of Pauli principle.

So far, the Hubble expansion is neglected in the analysis. However, in more realistic cases, $H \neq 0$, e.g. during reheating, which may affect the resonance particle production process. It can be seen from above that the narrow resonance should be sensitive to such effect because the instability band is narrow as in Eq. (3.59). The expansion of the Universe redshifts the momentum of the mode functions as k/a, which will easily move the resonant modes out of the instability band to terminate the process. On the other hand, the cosmic expansion and the perturbative or resonant decay of ϕ reduce the amplitude ϕ_0 as shown in Eq. (3.48). Therefore, the exponential growth rate $\mu^{(1)}_{k,\max} m_\phi$ should at least exceed $3H$ for the narrow resonance to be considered. From another point of view [176], a damping term in the Mathieu equation diminishes the instability bands in narrow resonance regime.

It is also worth mentioning that the rescattering of produced particles can also remove themselves from the instability bands due to self-interaction in some cases. The backreaction from created particles can also change the parameters A_k and q to prevent narrow resonance from continuing. Once the narrow resonance becomes insufficient due to some or all of these effects, the perturbative decay takes over and completes reheating.

In conclusion, narrow resonance may dominate the reheating process before the perturbative reheating takes over, but it is pretty "fragile" and sensitive to many other factors, e.g. cosmic expansion.

• **Broad Resonance** Consider $g_\phi\phi_0 \gg m_\phi$, which means that $q \gg 1$. This case corresponds to the broad resonance regime, which is much more efficient than the narrow resonance. In the models considered in Eqs. (3.57), it is easy to see that $A > 2q$, which corresponds to the region above the thick black line in Fig. D.2. The broad resonance regime then refers to $A \gtrsim 2q \gg 1$ where the widths of instability bands are large, which enables modes with a broad range of k to experience explosive production, especially when $2q$ is close to A, i.e. small k. In this sense, the lower of

Eq. (3.57) is of less interest than the upper because $A \gg 2q$ is always true for the former due to $\phi_0 \ll |\sigma_\phi|$. Therefore, the following discussion focuses on the latter case.

In broad resonance, particle production occurs every time when the adiabatic condition for $\omega^2_{k,\text{eff}}(t) = k^2 + g^2\phi^2(t)$ is violated,

$$\left|\dot{\omega}_{k,\text{eff}}/\omega^2_{k,\text{eff}}\right| \gtrsim 1 \ , \tag{3.64}$$

which occurs around the zero-crossing points of $\phi(t)$, i.e. $t \simeq n\pi/m_\phi$ where $n \in \mathbb{Z}$. At these moments, $\omega_{k,\text{eff}}$ becomes very small because $2q$ is almost as large as A_k, and the mode function χ_k is significantly enhanced, just like swung up by the low frequency. Two examples of broad reasonance are shown in Fig. 3.3. During each half-oscillation of $\phi(t)$, the mode function χ_k oscillates many times. Only around the zero-crossing points of $\phi(t)$, the frequency of χ_k changes drastically to small value and particle number increases rapidly. Given Eq. (3.64), the momentum range that experiences exponential growth can be found as

$$k^2 \lesssim \left[g^2_\phi m_\phi \phi_0 \phi(t)\right]^{2/3} - g^2_\phi \phi^2(t) \ , \tag{3.65}$$

where $\cos(m_\phi t) \simeq 1$ has been used. Therefore, this particle production channel is opened when $0 < \phi(t) < \sqrt{m_\phi \phi_0/g_\phi}$, and the right hand side reaches maximum at $\phi(t) = \phi_* = 3^{-3/4}\sqrt{m\phi_0/g_\phi} \simeq q^{-1/4}\phi_0/3$, which leads to the maximal momentum range that experiences resonant process, $0 < k < k_{\text{br,max}} \simeq \sqrt{g_\phi m_\phi \phi_0/2}$. The typical momentum of the produced particles during the main part of broad resonance $|\phi| \lesssim 2\phi_*$ can be estimated as

$$k \sim k_*/2 = \sqrt{g_\phi m_\phi \phi_0}/2 = m_\phi q^{1/4}/\sqrt{2} \sim g_\phi \phi_* \ . \tag{3.66}$$

As a result, the produced particles are of typical momenta much larger than the mass of the background field m_ϕ but much smaller than $g_\phi\phi_0$, which indicates that, within the short production period, the typical energy scale of these particles is $\omega_* \sim k_*$. And the typical time scale of such a period can also be estimated as $\Delta t_* \sim 2\phi_*/\dot{\phi} \simeq 1/\sqrt{g_\phi m_\phi \phi_0} \simeq k_*^{-1} \sim \omega_*^{-1}$. As can be seen in Fig. 3.3, particle production only occurs during such a short time and the occupation number remains unchanged when $\omega_{k,\text{eff}}$ changes adiabatically. Another observation is that, the phase of χ_k during the non-adiabatic period behaves differently for instability bands characterized by odd and even $\sqrt{A}$, which, roughly speaking, is determined by the ratio between periods of $\chi_k(z)$ and $\cos(2z)$.

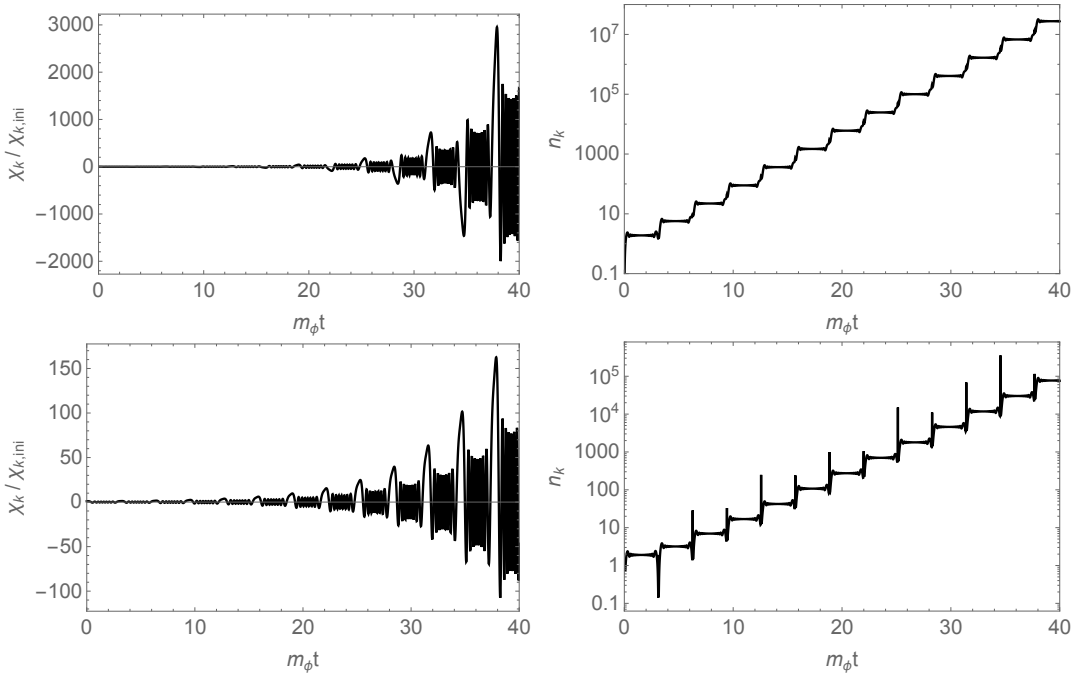

Figure 3.3: Two examples of broad resonance for the $\phi_0 \gg |\sigma_\phi|$ case in Eq. (3.57). Upper: $A_k = 19^2$ and $q = 180$. Lower: $A_k = 18^2$ and $q = 162$. $\chi_{k,\mathrm{ini}}$ is the initial value of χ_k. The left panels show the evolution of χ_k while the right show the occupation number n_k. The behaviors of the phase of χ_k during the short period of particle production are different between odd and even $\sqrt{A_k}$.

When the cosmic expansion is taken into account, the momentum and the amplitude ϕ_0 will then be redshifted such that the system does not remain in one instability band but jump over many different bands, which make the regular broad resonance become stochastic resonance [16]. "Stochastic" means that the phase of χ_k around each zero-crossing point of $\phi(t)$ behaves stochastically, unlike the one shown in Fig. 3.3, which leads to a peculiar feature of the number of χ-particles, namely occasional decrease during the production process. The stochastic resonance continues until q (or the amplitude of $\phi(t)$) and Hubble parameter H become small enough. Then the system may stay in one instability band and realize standard broad resonance.

To calculate the rate of exponential growth of χ_k at each resonance, it is important to find an analytical way to solve the equation of motion for χ_k. In Ref. [16], the resonance is successfully interpreted as successive scattering of χ_k on parabolic potentials. As analyzed previously, the adiabatic condition is violated only when $|\phi(t)| \lesssim 2\phi_*$, so the adiabatic solution is valid outside this regime. Rewrite the upper

of Eq. (3.54) by redefining $X_k(t) = a^{3/2}\chi_k(t)$ as

$$\ddot{X}_k + \Omega_{X,k}^2 X_k = 0 \ ,$$
$$\Omega_{X,k}^2 = k_p^2 + g_\phi^2\phi^2(t) - \frac{3}{4}H^2 - \frac{3}{2}\frac{\ddot{a}}{a} \ , \tag{3.67}$$

where the last two terms in $\Omega_{X,k}(t)$ are actually negligible after inflation in the circumstance considered here. Denoting the moments of zero-crossing of $\phi(t)$ as t_j with $j = 1, 2, 3, \cdots$, the adiabatic solution before and after t_j can be respectively written as

$$X_k^{(j)}(t) = \frac{\alpha_k^{(j)}}{\sqrt{2\Omega_{X,k}}} e^{-i\int^t \Omega_{X,k}(t_1)dt_1} + \frac{\beta_k^{(j)}}{\sqrt{2\Omega_{X,k}}} e^{i\int^t \Omega_{X,k}(t_1)dt_1} \ , \tag{3.68}$$

$$X_k^{(j+1)}(t) = \frac{\alpha_k^{(j+1)}}{\sqrt{2\Omega_{X,k}}} e^{-i\int^t \Omega_{X,k}(t_1)dt_1} + \frac{\beta_k^{(j+1)}}{\sqrt{2\Omega_{X,k}}} e^{i\int^t \Omega_{X,k}(t_1)dt_1} \ , \tag{3.69}$$

where α_k's and β_k's are nothing but the Bogoliubov coefficients which are constant within the adiabatic regime. In the vicinity of $t = t_j$, the approximation $\phi^2(t) \approx \phi_0^2 m_\phi^2 (t - t_j)^2$ is valid, so Eq. (3.67) describes a wave scattered by a parabolic potential

$$\frac{d^2 X_k}{d\tau^2} + (\kappa_j^2 + \tau^2) X_k = 0 \ , \tag{3.70}$$

where $\tau \equiv k_*(t - t_j)$ and $\kappa_j \equiv k_p(t_j)/k_*(t_j)$. The general solution for this equation is given as

$$X_k(\tau) = \tilde{\alpha}_k^{(j)} W\left(-\frac{\kappa_j^2}{2}, \sqrt{2}\tau\right) + \tilde{\beta}_k^{(j)} W\left(-\frac{\kappa_j^2}{2}, -\sqrt{2}\tau\right) \ , \tag{3.71}$$

where $W(a, x)$ is the parabolic cylinder function (see Appendix E) while $\tilde{\alpha}_k^{(j)}$ and $\tilde{\beta}_k^{(j)}$ are arbitrary constants. The asymptotic form of $X_k(\tau)$ for $|\tau| \gg 1$ can connect the adiabatic solutions in $t < t_j$ and $t > t_j$ regimes, which gives

$$\begin{aligned}\beta_k^{(j+1)} \simeq{}& \frac{i}{2}\left(\sqrt{1 + e^{-\pi\kappa_j^2}} - e^{-\pi\kappa_j^2/2} - \frac{1}{\sqrt{1 + e^{-\pi\kappa_j^2}} - e^{-\pi\kappa_j^2/2}}\right) e^{-i\vartheta_k/2}\beta_k^{(j)} \\ &- \frac{i}{2}\left(\sqrt{1 + e^{-\pi\kappa_j^2}} - e^{-\pi\kappa_j^2/2} + \frac{1}{\sqrt{1 + e^{-\pi\kappa_j^2}} - e^{-\pi\kappa_j^2/2}}\right) e^{i\vartheta_k/2}\alpha_k^{(j)} \ ,\end{aligned} \tag{3.72}$$

where $\vartheta_k = \arg\Gamma(1/2 - i\kappa_j^2/2)$. As a result, the number density after t_j is given by

$$n_k^{(j+1)} = \left|\beta_k^{(j+1)}\right|^2 \simeq \left(1 + 2e^{-\pi\kappa_j^2} + 2e^{-\pi\kappa_j^2/2}\sqrt{1 + e^{-\pi\kappa_j^2}}\cos\Theta^{(j)}\right) n_k^{(j)} \tag{3.73}$$

where $n_k^{(j)} = |\beta_k^{(j)}| \gg 1$ is assumed and $|\alpha_k^{(j)}|^2 - |\beta_k^{(j)}|^2 = 1$ is used, and

$$\Theta^{(j)} = 2\int_0^{t_j} \Omega_{X,k}(t)dt - \vartheta_k - \arg\alpha_k^{(j)} + \arg\beta_k^{(j)} \ , \tag{3.74}$$

whose randomness causes the stochastic behavior of the broad resonance in the presence of cosmic expansion. For the growth of n_k not to be suppressed, it is required that

$$\kappa_j^2 = \frac{A_k/a^2 - 2q}{2\sqrt{q}} \lesssim \pi^{-1} \ , \tag{3.75}$$

which coincides with the previous estimation. The instability index on the exponent $n_k^{(j+1)} = \exp\left(2\pi\mu_k^{(j)}\right) n_k^{(j)}$ is defined as

$$\mu_k^{(j)} = \frac{1}{2\pi} \ln\left(1 + 2e^{-\pi\kappa_j^2} + 2e^{-\pi\kappa_j^2/2}\sqrt{1+e^{-\pi\kappa_j^2}}\cos\Theta^{(j)}\right) \ , \tag{3.76}$$

where $\kappa_j^2 \propto g_\phi^{-1}$ so broad resonance is clearly a non-perturbative effect. The largest instability index is given by $\cos\Theta^{(j)} = 1$ as

$$\mu_{k,\max} \simeq \frac{1}{2\pi} \ln\left(1 + 2 + 2\sqrt{2}\right) \simeq 0.28 \ . \tag{3.77}$$

The above process is simply a scattering of waves scattered by a parabolic potential, so broad resonance can be understood as a successive scatterings of such kind. The final growth rate should then be the accumulation of rates of a number of such processes, which is not discussed in detail here.

In conclusion, stochastic resonance provides an efficient preheating channel at the very beginning of reheating, even in the presence of cosmic expansion. As the energy of $\phi(t)$ decreases due to Hubble expansion and energy loss for particle production, broad resonance eventually remains in one instability band instead of jumping over many and ceases as q becomes too small. Then, narrow resonance takes over at late preheating. However, the backreaction from the product of broad resonance and the expansion of the Universe complicate the situation of narrow resonance, as mentioned previously. Numerical calculation is necessary to trace the evolution of the system accurately.

3.1.3.2 Tachyonic Instability

The Mathieu equation allows another possibility to realize non-perturbative particle production at preheating, i.e. tachyonic instability, which cannot be seen in the two

cases considered earlier because $A_k > 2q$. In the situation where the interaction between background and target field is $\Delta\mathcal{L} = -g_\phi^2\sigma_\phi\phi\chi^2$ *only* that gives an effective mass $m_{\rm eff}^2(t) = 2g_\phi^2\sigma_\phi\phi(t)$, tachyonic instability may occur and lead to exponential particle production if $g_\phi^2\sigma_\phi\phi_0$ is large enough. It will be shown later that this instability plays an important role during preheating in the mixed Higgs-R^2 inflation model. Therefore, more calculation detail is presented here. Sometimes tachyonic instability is expected to be even more efficient than parametric resonance because the latter usually requires many oscillations to finally amplify the particles while the former can achieve the same within one oscillation for modes with large $g_\phi^2\sigma_\phi\phi_0$ (usually compared with momentum but a more careful discussion is needed and given below).

With the interaction mentioned above, the equation of motion for $X_k(t) = a^{3/2}\chi_k(t)$ then becomes

$$\begin{aligned} \ddot{X}_k + \Omega_{X,k}^2 X_k &= 0 \ , \\ \Omega_{X,k}^2 &= k_p^2 + m_{\rm eff}^2(t) - \frac{3}{4}H^2 - \frac{3}{2}\frac{\ddot{a}}{a} \ , \end{aligned} \tag{3.78}$$

where, again, the last terms in $\Omega_{X,k}(t)$ is negligible during reheating. As $\phi(t)$ oscillates, $\Omega_{X,k}^2(t)$ can take negative value if $2g_\phi^2\sigma_\phi\phi_0 > k_p^2$. During such a period the amplitude of χ_k grows exponentially, while outside the adiabatic solution is valid. The treatment here is similar to the case in broad resonance, namely connecting the two adiabatic regimes with one tachyonic period in between.

The moments when $\Omega_{X,k}(t)$ enters and exits the negative regime are denoted as $t_{\rm enter}(k)$ and $t_{\rm exit}(k)$, respectively. In other words, $\Omega_{X,k}(t_{\rm enter}(k)) = \Omega_{X,k}(t_{\rm exit}(k)) = 0$, and $\Omega_{X,k}(t) < 0$ during $t_{\rm enter}(k) < t < t_{\rm exit}(k)$. The adiabatic condition (see Eq. (3.29)) for $\Omega_{X,k}(t)$ is given as

$$\left| \frac{\ddot{\Omega}_{X,k}/\Omega_{X,k} - 3\dot{\Omega}_{X,k}^2/(2\Omega_{X,k}^2)}{2\Omega_{X,k}^2} \right| \ll 1 \ , \tag{3.79}$$

which is satisfied for most time except for the small vicinity of $t_{\rm enter}(k)$ and $t_{\rm exit}(k)$ because $\Omega_{X,k}$ approaches and crosses zero around these moments, leading to strong violation. Define the time when the adiabatic condition (3.79) is violated as $t_{\rm enter}^- < t < t_{\rm enter}^+$ and $t_{\rm exit}^- < t < t_{\rm exit}^+$ around $t = t_{\rm enter}(k)$ and $t = t_{\rm exit}(k)$, respectively. Then adiabatic solutions are valid outside these time ranges so they can be written

in different time regimes, $t < t^-_{\rm enter}$, $t^+_{\rm enter} < t < t^-_{\rm exit}$, $t > t^+_{\rm exit}$, respectively as

$$X_k(t) = \frac{\alpha_k}{\sqrt{2\Omega_{X,k}}} \exp\left(-i\int_{t_0}^{t}\Omega_{X,k}(t')dt'\right) + \frac{\beta_k}{\sqrt{2\Omega_{X,k}}} \exp\left(i\int_{t_0}^{t}\Omega_{X,k}(t')dt'\right) \ , \tag{3.80}$$

$$X_k(t) = \frac{a_k}{\sqrt{2|\Omega_{X,k}|}} \exp\left(-\int_{t_{\rm enter}(k)}^{t}|\Omega_{X,k}(t')|dt'\right) + \frac{b_k}{\sqrt{2|\Omega_{X,k}|}} \exp\left(\int_{t_{\rm enter}(k)}^{t}|\Omega_{X,k}(t')|dt'\right) \ , \tag{3.81}$$

$$X_k(t) = \frac{\tilde{\alpha}_k}{\sqrt{2\Omega_{X,k}}} \exp\left(-i\int_{t_{\rm exit}(k)}^{t}\Omega_{X,k}(t')dt'\right) + \frac{\tilde{\beta}_k}{\sqrt{2\Omega_{X,k}}} \exp\left(i\int_{t_{\rm exit}(k)}^{t}\Omega_{X,k}(t')dt'\right) \ , \tag{3.82}$$

where the Bogoliubov coefficients $\alpha_k, \beta_k, a_k, b_k, \tilde{\alpha}_k$ and $\tilde{\beta}_k$ are approximately constant[38] and t_0 is an initial time when α_k and β_k are defined. The normalization conditions are given by $|\alpha_k|^2 - |\beta_k|^2 = 1$, $a_k b_k^* - a_k^* b_k = i$, and $|\tilde{\alpha}_k|^2 - |\tilde{\beta}_k|^2 = 1$.

These solutions break down during $t^-_{\rm enter} < t < t^+_{\rm enter}$ and $t^-_{\rm exit} < t < t^+_{\rm exit}$ for which exact solution is needed to impose appropriate matching conditions at $t = t_{\rm enter}(k)$ and $t_{\rm exit}(k)$ between the adiabatic solutions such that the late-time occupation number $n_k = |\tilde{\beta}_k|^2$ produced by the non-adiabatic change of $\Omega_{X,k}(t)$ can be obtained as in the broad resonance case. For this purpose, the trick introduced in Ref. [173] (also in the Landau-Lifshitz's textbook [174]) is adopted to find the exact solution at the moments of zero-crossing of $\Omega_{X,k}(t)$. In the following, the mode equation (3.78) is solved when the adiabatic condition is violated to determine the "transfer matrices" between the Bogoliubov coefficients.

First, the matching condition at $t \simeq t_{\rm enter}(k)$ is examined. For t sufficiently close to the zero-crossing point, $t = t_{\rm enter}(k)$, Taylor expansion can be applied to $\Omega^2_{X,k}$ as

$$\Omega^2_{X,k} \approx 0 + \left.\frac{d(\Omega^2_{X,k})}{dt}\right|_{t=t_{\rm enter}(k)} [t - t_{\rm enter}(k)] \equiv \tilde{A}_k \left[t - t_{\rm enter}(k)\right] \ , \tag{3.83}$$

with $\tilde{A}_k < 0$, so that the equation of motion for X_k becomes

$$\ddot{X}_k + \tilde{A}_k \left[t - t_{\rm enter}(k)\right] X_k \approx 0 \ . \tag{3.84}$$

This equation is the same as the stationary Schrödinger equation with a linear potential. The exact solution to it is known to be Airy functions (see Appendix F), i.e.

$$X_k(t) = \tilde{B}_{1k}{\rm Ai}\left(\tilde{A}_k^{1/3}\left[t_{\rm enter}(k) - t\right]\right) + \tilde{B}_{2k}{\rm Bi}\left(\tilde{A}_k^{1/3}\left[t_{\rm enter}(k) - t\right]\right) , \tag{3.85}$$

[38] In general, the notations α_k and β_k are typically used for Bogoliubov coefficients so they also appear more than one times in the previous sections, but they should not cause confusion, which should be understood. Strictly speaking, Bogoliubov coefficients can be time-dependent but, in the adiabatic case, they are approximately constant as used throughout this thesis.

where $\tilde{B}_{1k}$ and $\tilde{B}_{2k}$ are complex constants. For $t < t_{\rm enter}(k)$, the argument in Eq. (3.85) is negative, then the leading term of the asymptotic expansion of the Airy function at $\left|\tilde{A}_k^{1/3}\left[t_{\rm enter}(k) - t\right]\right| \gg 1$ reads

$$X_k(t) \to \frac{|\tilde{A}_k|^{1/6}}{\sqrt{2\pi\Omega_{X,k}}}\Bigg[\left(\frac{1-i}{2}\tilde{B}_{1k} + \frac{1+i}{2}\tilde{B}_{2k}\right)\exp\left(-i\int_{t_{\rm enter}(k)}^{t}\Omega_{X,k}(t')dt'\right) + \left(\frac{1+i}{2}\tilde{B}_{1k} + \frac{1-i}{2}\tilde{B}_{2k}\right)\exp\left(i\int_{t_{\rm enter}(k)}^{t}\Omega_{X,k}(t')dt'\right)\Bigg] . \tag{3.86}$$

On the other hand, for $t > t_{\rm enter}(k)$, the argument in Eq. (3.85) is positive, so, with the leading term of the asymptotic expansion of the Airy function at $\tilde{A}_k^{1/3}\left[t_{\rm enter}(k) - t\right] \gg 1$, Eq. (3.85) is approximated as

$$X_k(t) \to \frac{|\tilde{A}_k|^{1/6}}{\sqrt{2\pi|\Omega_{X,k}|}}\left[\frac{\tilde{B}_{1k}}{\sqrt{2}}\exp\left(-\int_{t_{\rm enter}(k)}^{t}|\Omega_{X,k}(t')|dt'\right) + \sqrt{2}\tilde{B}_{2k}\exp\left(\int_{t_{\rm enter}(k)}^{t}|\Omega_{X,k}(t')|dt'\right)\right] . \tag{3.87}$$

With these results, the adiabatic solutions on both sides of $t = t_{\rm enter}(k)$, i.e. Eqs. (3.80) and (3.81), can be connected through $\tilde{B}_{1k}$ and $\tilde{B}_{2k}$. It should be noted that, to do so, it is required that there is a regime where both adiabatic condition and Taylor expansion of $\Omega_{X,k}(t)$ are valid, which implies that the following conditions should be satisfied

$$\left|\tilde{A}_k^{1/3}[t_{\rm enter}(k) - t]\right| \gg 1, \quad \left|\tilde{A}_k\right| \gg \frac{1}{2}\frac{d^2(\Omega_{X,k}^2)}{dt^2}\bigg|_{t=t_{\rm enter}(k)}|t - t_{\rm enter}(k)| \ , \tag{3.88}$$

as well as Eq. (3.79), which will be concretely examined in the discussion on tachyonic preheating in the mixed Higgs-R^2 inflation model [51]. According to Eqs. (3.80), (3.81), (3.86), and (3.87), the matching conditions for $t < t_{\rm enter}(k)$ and $t > t_{\rm enter}(k)$ are given respectively as

$$\begin{pmatrix}\alpha_k \\ \beta_k\end{pmatrix} = \frac{|\tilde{A}_k|^{1/6}}{2\sqrt{\pi}}\begin{pmatrix}(1-i)e^{i\theta_k} & (1+i)e^{i\theta_k} \\ (1+i)e^{-i\theta_k} & (1-i)e^{-i\theta_k}\end{pmatrix}\begin{pmatrix}\tilde{B}_{1k} \\ \tilde{B}_{2k}\end{pmatrix}, \quad \theta_k \equiv \int_{t_0}^{t_{\rm enter}(k)}\Omega_{X,k}(t)dt \ , \tag{3.89}$$

$$\begin{pmatrix}a_k \\ b_k\end{pmatrix} = \frac{|\tilde{A}_k|^{1/6}}{2\sqrt{\pi}}\begin{pmatrix}\sqrt{2} & 0 \\ 0 & 2\sqrt{2}\end{pmatrix}\begin{pmatrix}\tilde{B}_{1k} \\ \tilde{B}_{2k}\end{pmatrix} . \tag{3.90}$$

Here θ_k is the phase accumulation from t_0 to the entry of the tachyonic regime. As a result of Eqs. (3.89) and (3.90), the transfer matrix between $(\alpha_k, \beta_k)^\top$ and $(a_k, b_k)^\top$ is then

$$\begin{pmatrix}a_k \\ b_k\end{pmatrix} = \frac{1}{2\sqrt{2}}\begin{pmatrix}(1+i)e^{-i\theta_k} & (1-i)e^{i\theta_k} \\ 2(1-i)e^{-i\theta_k} & 2(1+i)e^{i\theta_k}\end{pmatrix}\begin{pmatrix}\alpha_k \\ \beta_k\end{pmatrix} . \tag{3.91}$$

In a similar way, the matching condition at $t \simeq t_{\rm exit}(k)$ can be obtained. For t sufficiently close to the zero-crossing point at the end of the tachyonic regime, $t = t_{\rm exit}(k)$, again Taylor expansion of $\Omega^2_{X,k}$ is valid, approximately giving

$$\Omega^2_{X,k} \approx 0 + \left.\frac{d(\Omega^2_{X,k})}{dt}\right|_{t=t_{\rm exit}(k)} [t - t_{\rm exit}(k)] \equiv \tilde{C}_k[t - t_{\rm exit}(k)] \ , \tag{3.92}$$

with $\tilde{C}_k > 0$, so that the equation of motion for X_k becomes

$$\ddot{X}_k + \tilde{C}_k[t - t_{\rm exit}(k)]X_k \approx 0 \ . \tag{3.93}$$

In the same way as done above, the exact solution is expressed in terms of the Airy functions,

$$X_k(t) = \tilde{D}_{1k}{\rm Ai}\left(\tilde{C}_k^{1/3}[t_{\rm exit}(k) - t]\right) + \tilde{D}_{2k}{\rm Bi}\left(\tilde{C}_k^{1/3}[t_{\rm exit}(k) - t]\right) \ , \tag{3.94}$$

where $\tilde{D}_{1k}$ and $\tilde{D}_{2k}$ are complex constants. Once more, before the exit of tachyonic regime, the asymptotic expressions of the mode functions for $\left|\tilde{C}_k^{1/3}[t_{\rm exit}(k) - t]\right| \gg 1$ can be written as

$$\begin{aligned} X_k(t) \to \frac{\tilde{C}_k^{1/6}}{\sqrt{2\pi\Omega_{X,k}}} \Bigg[&\left(\frac{1+i}{2}\tilde{D}_{1k} + \frac{1-i}{2}\tilde{D}_{2k}\right) \exp\left(-i\int_{t_{\rm exit}(k)}^{t} \Omega_{X,k}(t')dt'\right) \\ &+ \left(\frac{1-i}{2}\tilde{D}_{1k} + \frac{1+i}{2}\tilde{D}_{2k}\right) \exp\left(i\int_{t_{\rm exit}(k)}^{t} \Omega_{X,k}(t')dt'\right)\Bigg] \ . \end{aligned} \tag{3.95}$$

On the other hand, after the exit, Eq. (3.94) can be approximated, for $\tilde{C}_k^{1/3}[t_{\rm exit}(k) - t] \gg 1$, as

$$X_k(t) \to \frac{\tilde{C}_k^{1/6}}{\sqrt{2\pi|\Omega_{X,k}|}} \left[\frac{\tilde{D}_{1k}}{\sqrt{2}} \exp\left(\int_{t_{\rm exit}(k)}^{t} |\Omega_{X,k}(t')|dt'\right) + \sqrt{2}\tilde{D}_{2k} \exp\left(-\int_{t_{\rm exit}(k)}^{t} |\Omega_{X,k}(t')|dt'\right)\right] \ . \tag{3.96}$$

By matching the exponents, the adiabatic solutions on both sides of the exit, i.e. Eqs. (3.81) and (3.82), can be connected with the constants $\tilde{D}_{1k}$ and $\tilde{D}_{2k}$ respectively as

$$\begin{pmatrix} \tilde{\alpha}_k \\ \tilde{\beta}_k \end{pmatrix} = \frac{\tilde{C}_k^{1/6}}{2\sqrt{\pi}} \begin{pmatrix} 1+i & 1-i \\ 1-i & 1+i \end{pmatrix} \begin{pmatrix} \tilde{D}_{1k} \\ \tilde{D}_{2k} \end{pmatrix} , \tag{3.97}$$

$$\begin{pmatrix} a_k \\ b_k \end{pmatrix} = \frac{\tilde{C}_k^{1/6}}{2\sqrt{\pi}} \begin{pmatrix} 0 & 2\sqrt{2}e^{\Omega_k} \\ \sqrt{2}e^{-\Omega_k} & 0 \end{pmatrix} \begin{pmatrix} \tilde{D}_{1k} \\ \tilde{D}_{2k} \end{pmatrix} , \quad \Omega_k \equiv \int_{t_{\rm enter}(k)}^{t_{\rm exit}(k)} |\Omega_{X,k}(t)|dt \ . \tag{3.98}$$

Here Ω_k is the "phase" accumulation during the tachyonic regime from $t_{\rm enter}(k)$ to $t_{\rm exit}(k)$, which is responsible for the exponential growth of the particle number. Consequently, with Eqs. (3.97) and (3.98), the transfer matrix between $(a_k, b_k)^\top$ and

$(\tilde{\alpha}_k, \tilde{\beta}_k)^\top$ is easily found to be

$$\begin{pmatrix} \tilde{\alpha}_k \\ \tilde{\beta}_k \end{pmatrix} = \frac{1}{2\sqrt{2}} \begin{pmatrix} (1-i)e^{-\Omega_k} & 2(1+i)e^{\Omega_k} \\ (1+i)e^{-\Omega_k} & 2(1-i)e^{\Omega_k} \end{pmatrix} \begin{pmatrix} a_k \\ b_k \end{pmatrix} . \tag{3.99}$$

Eventually, combining Eqs. (3.91) and (3.99) leads to the desired transfer matrix between the two pairs of Bogoliubov coefficients before and after the tachyonic regime as

$$\begin{pmatrix} \tilde{\alpha}_k \\ \tilde{\beta}_k \end{pmatrix} = \begin{pmatrix} e^{-i\theta_k}(e^{\Omega_k} + e^{-\Omega_k}/4) & ie^{i\theta_k}(e^{\Omega_k} - e^{-\Omega_k}/4) \\ -ie^{-i\theta_k}(e^{\Omega_k} - e^{-\Omega_k}/4) & e^{i\theta_k}(e^{\Omega_k} + e^{-\Omega_k}/4) \end{pmatrix} \begin{pmatrix} \alpha_k \\ \beta_k \end{pmatrix} . \tag{3.100}$$

As a result, the occupation number of the produced particles with a given k can be computed as

$$n_k = \left|\tilde{\beta}_k\right|^2 = \left|-ie^{-i\theta_k}\alpha_k(e^{\Omega_k} - e^{-\Omega_k}/4) + e^{i\theta_k}\beta_k(e^{\Omega_k} + e^{-\Omega_k}/4)\right|^2 . \tag{3.101}$$

As usual, the initial condition within the adiabatic regime is set to be vacuum, i.e. $\alpha_k = 1$ and $\beta_k = 0$, which simplifies the expression above as follows

$$n_k = \left|\tilde{\beta}_k\right|^2 = \left|e^{\Omega_k} - e^{-\Omega_k}/4\right|^2 \approx e^{2\Omega_k} , \tag{3.102}$$

where, in the last line, it is assumed that the tachyonic instability strength is strong $\Omega_k \gg 1$ for the given k, so the exponential suppressed term is omitted, which is consistent with the expectation from the simple adiabatic approximation, $n_k \simeq \exp(2\Omega_k)$, because the adiabatic approximation cannot accurately trace the small term.

From the discussion above, to have strong enough tachyonic effect $\Omega_k > 1$, it is required that $k_p \ll |m_{\text{eff}}|$ in order to provide large amplitude $|\Omega_{X,k}|$ in the tachyonic regime and long duration of this period, which ensures significant contribution to Ω_k. In such a case, the occupation number n_k for these modes grows rapidly. However, although the occupation number is larger for modes with smaller k_p, the contribution from these modes to the energy density, which is of more physical importance, will be suppressed by the small k itself because the volume element of phase space is proportional to k^2dk. Therefore, it is expected that the typical momentum of the produced particles that constitute the most of energy density will be of order $k_p/|m_{\text{eff}}| \sim \mathcal{O}(10^{-1}) - \mathcal{O}(1)$. In other words, strong tachyonic instability should not be characterized solely by Ω_k but the energy density of the produced particles, although the former may be used for rough estimation conveniently. In the strong instability case, the background energy will be transferred away extremely rapidly, causing a sharp decrease of ϕ_0 , which, in turn, reduces or terminates the tachyonic

instability process. The cosmic expansion effect in more realistic models is therefore not important. For the mode X_k with large $k_p^2 \gtrsim m_{\text{eff}}^2$, it is obvious that the tachyonic effect will be negligible or disappear completely. Especially when k_p is slightly smaller than the amplitude of the effective mass, the tachyonic regime is so small and the transition time is so short that the adiabatic solution during the tachyonic period may not even exist.

The non-perturbative particle production processes are efficient in most cases such that the energy density of the products grows rapidly in this regime, which is described by the results shown previously. These analytical estimations can clearly show the behavior of the number density and energy density of the produced particles, and the tendency of the future evolution of the system. If the non-perturbative process lasts long enough, the energy density of the produced particles can become comparable with that of the background fields. Since then, the backreaction gradually gets more and more important as large amount of produced particles take part in the non-linear interactions with background fields, such as rescattering which can redistribute the momenta of the particles. When these effects are no longer negligible, a sophisticated numerical technique is needed, such as lattice simulation, to fully incorporate the particle production process.

3.2 Reheating: Case Study

Typical types of perturbative and non-perturbative particle production processes have been introduced in detail in the last section, which provides a powerful tool to investigate the reheating process in the early Universe after the end of inflation. Reheating, as the crucial transition period between inflation and Hot Big Bang, is very important for accurately fixing the pivot scale of curvature perturbation observed on CMB, and also has a lot of connection with other physics in the early Universe such as gravitational waves and baryogenesis. Therefore, given an inflation model, it is necessary to clarify the ambiguity during this period as much as possible in order to confront existing experimental data and seek possible observables in the future.

Here, the reheating processes in the Starobinsky model and the Higgs inflation are discussed by applying the methods introduced previously. The final reheating temperature of the Starobinsky model will be given. As for the Higgs inflation, due to the strong coupling issue, the validity of the theory at the very beginning of reheating is questioned, so the traditional treatment with parametric resonance and

perturbative particle production will not be discussed in detail. Instead, the cause of such issue will be presented, which is beneficial for the investigation of the first stage of preheating in the mixed Higgs-R^2 inflation model in the next chapter.

3.2.1 Reheating in Starobinsky Model

The inflation dynamics in the Starobinsky model [3] has been discussed in Chapter 2, which shows that the inflationary predictions in this model fit the results of current observation [23] very well if the only one model parameter takes the value $M = M_c$. After the end of inflation, the reheating process begins [3, 29, 30, 172]. Consider the action (2.66) with an additional massive scalar field χ with non-minimal coupling (as given in Eq. (3.4) in Example Two)

$$S_{\rm J} = \frac{1}{2}\int d^4x\sqrt{-g_{\rm J}}\left[M_{\rm pl}^2 R_{\rm J} + \frac{M_{\rm pl}^2}{6M^2}R_{\rm J}^2 + \xi\chi^2 R_{\rm J} - g_{\rm J}^{\mu\nu}\partial_\mu\chi\partial_\nu\chi - m_\chi^2\chi^2\right] , \tag{3.103}$$

where the target field $\chi(t, \mathbf{x})$ is treated as perturbation and produced during reheating. As long as ξ is not very close to $-1/6$, the main reheating channel is the decay of scalaron into χ-particles [177][39]. In the following, the reheating process is discussed in both JF and EF. In the former, the particle production can be understood as the result of time-dependent background spacetime, while in the latter, it results from the effective mass given by a background scalar field.

• **Jordan frame** All the subscripts "J" are omitted for convenience. Following the same procedure from Eq. (3.8), the mode function u_k for $\tilde{\chi} = a\chi$ here obeys the same equation as Eq. (3.40) with $S_{\tilde{\chi}}$ given by

$$S_{\tilde{\chi}}(\eta) = (\xi + 1/6)\, a^2(\eta)R(\eta) + \left[1 - a^2(\eta)\right] m_\chi^2 , \tag{3.104}$$

where the time variable has been transformed to conformal time η and $a(\eta)$ is the scale factor in flat FLRW metric. It can be seen that, after the JF dynamics of $R(\eta)$ and $a(\eta)$ are determined in the Starobinsky model during reheating, the production of χ-particles can be calculated with methods introduced earlier. Different production channels can be realized depending on the value of non-minimal coupling ξ. For quite large $|\xi| \gtrsim 3$ with $m_\chi = 0$ or $|\xi| \gtrsim 10$ with $m_\chi \sim \mathcal{O}(M)$, broad resonance can occur to amplify the target field exponentially [98], for which the detailed discussion is omitted here. The reason, as has been explained at the end of the discussion of parametric

[39] Ref. [178] considers the case where the scalaron decays into two gauge boson via trace anomaly of energy-momentum tensor at one-loop level. This is the dominant channel when scalar fields are only conformally coupled with gravity, i.e. $\xi = -1/6$.

resonance, is that the amplitude of $R(\eta)$ will decrease rapidly due to energy loss, so the resonance becomes narrow and finally perturbative reheating takes over and determines the reheating temperature at late time. For very large $|\xi|$, tachyonic preheating may also be possible, but the consideration of such unnaturally large $|\xi|$ here lacks good motivation. Therefore, the discussion below focuses on small $|\xi| \lesssim 1$. For the same reason, main interest lies in late time and the perturbative decay rate of the background.

In JF, the scalar degree of freedom responsible for inflaton is hidden in the Ricci scalar whose non-trivial dynamics is determined by the Einstein equations (2.68) and (2.69). Different from inflation, $M^2 \gg |\dot{H}|, H^2$ is satisfied during reheating, so Eq. (2.68) can be rewritten as

$$2H\ddot{H} - \dot{H}^2 + M^2H^2 = -6H^2\dot{H} \approx 0 \ , \tag{3.105}$$

where the friction term $-6H^2\dot{H}$ is treated as perturbation, which leads to the solution

$$H \simeq \frac{4}{3t}\left[1 + \frac{4}{3H_{\rm end}t} + \frac{\sin(Mt)}{Mt}\right]^{-1} \cos^2\left(\frac{M}{2}t\right) \ , \tag{3.106}$$

where $H_{\rm end} \simeq M/\sqrt{6}$ is the Hubble parameter at the end of inflation, i.e. the beginning of reheating, as discussed in Chapter 2. Besides, the second term in the square brackets can actually be neglected due to the late time approximation $Mt \gg 1$, but the third term should be kept because its contribution to the time derivative of H is important. The time average of H gives $\langle H\rangle_{\rm ave} = 2/(3t)$ which means that the Universe is effectively matter-dominated in a time-averaged sense. Then the scale factor can be solved easily as

$$a(t) \simeq t^{2/3}\left[1 + \frac{2\sin(Mt)}{3Mt} + \frac{8}{9H_{\rm end}t}\right] \ , \tag{3.107}$$

where the proportional factor has been removed for convenient since the absolute size of $a(t)$ has no physical meaning in the flat FLRW metric. Again the third term in the square brackets can be neglected. As for Eq. (2.69), by redefining $R \to a^{3/2}R$ to simplify the situation, it is easy to find that

$$R \simeq -4Mt^{-1}\sin(Mt) \ , \tag{3.108}$$

up to leading order. Therefore, similar to many single-field inflation models, the inflaton degree of freedom oscillates after inflation and such oscillation induces particle production to reheat the Universe. This oscillating scalar degree of freedom is nothing

but the scalaron. The expression (3.108) can also be derived with $H(t)$ and $a(t)$ found above.

Consider some moment at late time $t_0 \gg M^{-1}$ after many scalaron oscillations and some duration $\Delta t = (t - t_0)$ such that $t_0 \gg \Delta t \gg M^{-1}$. Then, the Ricci scalar and the scale factor can be further approximated as

$$\begin{aligned} R(t) &\simeq -\frac{4M}{t_0}\sin(Mt)\ , \\ a(t) &\simeq 1 + \frac{2}{3Mt_0}\sin(Mt)\ , \end{aligned} \tag{3.109}$$

with proper normalization, and so the conformal time $d\eta \simeq dt$. Since ξ is small, the time derivative of particle number density $\dot{n}_{\tilde{\chi}}$ which is important to obtain the scalaron decay rate can be calculated in a perturbative way through Eq. (3.44). From the approximation above, the product of source term in the time integration can be written as

$$S_{\tilde{\chi}}(\eta_1)S_{\tilde{\chi}}(\eta_2) \simeq -\frac{4\tilde{m}^4}{9M^2t_0^2}\left[e^{iM(t_1+t_2)} - e^{iM(t_1-t_2)} - e^{-iM(t_1-t_2)} + e^{-iM(t_1+t_2)}\right]\ , \tag{3.110}$$

where the complex form is used instead of trigonometric functions for calculation convenience and $\tilde{m}^2 \equiv m_\chi^2 + 3(\xi + 1/6)M^2$. Combining with $\exp[-2i\omega_k(t_1 - t_2)]$ in Eq. (3.44), the time integration of terms with $(2\omega_k + M)$ in the exponent leads to Dirac delta function $\delta(2\omega_k + M)$ that vanishes because $\omega_k > 0$ and $M > 0$. Therefore, only the terms with $\exp[-i(2\omega_k - M)(t_1 - t_2)]$ survive. As a result, the time derivative of number density is calculated as

$$\begin{aligned} \dot{n}_{\tilde{\chi}}(t) &\simeq \frac{1}{\pi}\frac{\tilde{m}^4}{9M^2t_0^2}\int_0^{+\infty} dk \frac{k^2}{k^2 + m_\chi^2}\delta\left(2\omega_k - M\right)e^{i(2\omega_k - M)t}\ , \\ &= \frac{1}{2\pi}\frac{\tilde{m}^4}{9M^2t_0^2}\left(1 - \frac{4m_\chi^2}{M^2}\right)^{1/2}\ . \end{aligned} \tag{3.111}$$

Naturally, the time derivative of the energy density of scalaron is $\dot{\rho}_{\rm bg} \simeq -M\dot{n}_{\tilde{\chi}}/2$, while the time-averaged background energy density can be approximated as $\langle\rho_{\rm bg}\rangle_{\rm ave} \approx 4M_{\rm pl}^2/(3t_0^2)$, which gives the background decay rate as

$$\Gamma_{{\rm bg}\to\tilde{\chi}\tilde{\chi}} = \frac{\dot{\rho}_{\rm bg}}{\langle\rho_{\rm bg}\rangle_{\rm ave}} = \frac{1}{8\pi}\frac{\tilde{m}^4}{3M_{\rm pl}^2M}\left(1 - \frac{4m_\chi^2}{M^2}\right)^{1/2} \xrightarrow{m_\chi \ll M} \frac{3}{16\pi}\frac{M^3}{M_{\rm pl}^2}\left(\xi + \frac{1}{6}\right)^2\ . \tag{3.112}$$

As can be seen, the mass m_χ suppresses the decay rate and the decay channel is forbidden for $M < 2m_\chi$. The reheating temperature for the case $m_\chi \approx 0$, according

to Eq. (3.52), is then

$$T_r \simeq 0.54\sqrt{\frac{3}{8\pi}}\left(\xi+\frac{1}{6}\right)\left(\frac{M}{M_{\rm pl}}\right)^{3/2} M_{\rm pl}\ , \tag{3.113}$$

which coincides with the result calculated in Ref. [177, 179]. For minimally coupled case $\xi = 0$, $T_r \sim 10^9$ GeV.

• **Einstein frame** All the subscripts "E" are omitted for convenience. Given the JF action (3.103), it is easy to conformally transform to EF. The resulting action is just the same as the EF action in the mixed Higgs-R^2 inflation model, i.e. Eq. (2.124), except that $h(t)$ is replaced by $\chi(t,\mathbf{x})$ and the Higgs potential $-\lambda h^4/4$ by the mass term $-m_\chi^2\chi^2/2$. Moreover, during reheating, $\alpha|\varphi| \ll 1$ is satisfied so small field approximation for φ is valid, which directly results in $\varphi(t) \propto \sin(Mt)$. In addition, the coupling between φ and χ comes from the conformal factor in kinetic term and mass term of χ as well as the potential. Since $m_\chi \ll M$, the leading contribution from the potential is $\Delta\mathcal{L} = \xi M^2\varphi\chi^2/(\alpha M_{\rm pl}^2)$ that, by repeating the procedure above, yields

$$\Gamma = \frac{3}{16\pi}\frac{\xi^2 M^3}{M_{\rm pl}^2}\ , \tag{3.114}$$

which is almost the same as Eq. (3.112) except for the 1/6. Actually, the coupling through kinetic term gives the contribution of 1/6, which can be seen e.g. in Ref. [180]. This term will give dominant effect if $|\xi| \ll 1$. On the other hand, the decay rate calculated here coincides with that in Eq. (3.47) as expected. Therefore, the perturbative particle production in a time-dependent background can indeed be understood as the quantum mechanical decay of the massive particles with zero momentum from the coherent oscillation of background field.

Given the reheating temperature, the duration of inflation can be calculated. Rewrite the e-fold number of inflation as

$$\begin{aligned} N_{\rm inf} = \ln\left(\frac{a_{\rm end}}{a_k}\right) &= \ln\left(\frac{a_0 M_{\rm pl}}{k}\right) + \ln\left(\frac{a_{\rm end}}{a_r}\right) + \ln\left(\frac{a_r}{a_0}\right) + \ln\left(\frac{H_k}{M_{\rm pl}}\right)\ , \\ &= \ln\left(\frac{a_0 M_{\rm pl}}{k}\right) - \Delta N_r + \ln\left[\frac{T_0}{T_r}\left(\frac{g_0}{g_r}\right)^{1/3}\right] + \ln\left(\frac{M_c}{2M_{\rm pl}}\right)\ , \end{aligned} \tag{3.115}$$

where $a_{\rm end} = a(t_{\rm end})$, a_0, and a_r denote the scale factor at the end of inflation, present, and the end of reheating, respectively, and k is the pivot scale while a_k and $H_k \simeq M_c/2$ are the corresponding scale factor and Hubble parameter such that $k = a_k H_k$. The

second term ΔN_r represents the duration of reheating process in terms of e-fold number. Here, it has been implicitly assumed that the thermalization after reheating is realized within one Hubble time and the total entropy is conserved between the end of thermalization and today. At present and the end of reheating, the effective number of relativistic species are given by $g_0 = 43/11$ and $g_r = 106.75$, respectively, with corresponding temperatures $T_0 \simeq 2.7K$ as observed and T_r ($\sim 10^9$ GeV in the Starobinsky model with minimally coupled scalar field). Furthermore, the pivot scale is chosen to be $k/a_0 = 0.002$ Mpc^{-1} as in Ref. [23][40]. With the end of reheating characterized by $H \simeq \Gamma_{\mathrm{bg}\to\tilde{\chi}\tilde{\chi}}$, the duration of reheating can be found as $\Delta N_r \simeq 18$. As a result, the e-fold number of inflation in the Starobinsky model is given by [54]

$$N_{\mathrm{inf}} \simeq 54 \ . \tag{3.116}$$

Since the reheating process is basically perturbative in the Starobinsky model because the interaction is essentially gravitational, the reheating temperature is relatively low and the duration is thus long, resulting in "short" inflation. This feature provides one way to distinguish the Starobinsky model from other inflationary models whose inflationary prediction is the same as the former, e.g. the Higgs inflation.

3.2.2 Reheating in Higgs Inflation

The reheating process in the Higgs inflation is rather non-trivial. One important reason is that the SM Higgs field couples with all other SM fields, especially the strong couplings with quarks and gauge bosons, which enables the Higgs field to decay much more efficiently than the scalaron does in the Starobinsky model. The traditional methods to study reheating in the Higgs inflation are carried out in earlier works [31–33], where it is found that the resonant production of the transverse mode of the weak gauge bosons is the dominant channel of reheating. However, it is recognized later that the effective mass of the longitudinal mode of the gauge bosons shows large spiky features contributed by the Higgs field velocity and acceleration due to the presence of large non-minimal coupling $\xi \sim \mathcal{O}(10^3)$, which induces even more efficient particle production that can complete reheating quickly [34, 35][41]. However, the energy scale of these spikes actually exceeds the cutoff scale of the theory during reheating, as mentioned earlier, which casts doubt on the validity or reliability of its predictions.

[40] The $\Delta^2_{\mathcal{R}}$ and $n_s - 1$ were presented in Ref. [23] for $k = 0.05$ Mpc^{-1}, so $N_{0.05} = N_{\mathrm{inf}} - 3.2$ where N_{inf} is given in Eq. (3.116) for $k = 0.002$ Mpc^{-1}.

[41] This phenomenon is also noticed in Refs. [113, 181]. See comments in Ref. [34].

In the following, the origin of such spikes is discussed in both JF and EF. Due to the UV issue in this situation, it is ambiguous to investigate the subsequent reheating process further, so such analysis is not presented in this thesis.

To study the behavior of the effective mass of the longitudinal mode of weak gauge bosons and its production, it is straightforward to directly introduce the realistic $\mathrm{SU}(2)_L \times \mathrm{U}(1)_Y$ gauge fields. However, for the present purpose and simplicity, it is sufficient to study the case of a local U(1) gauge field because the most important effect here holds true in the realistic case. Actually, it can be even simpler to just investigate the phase direction of the Higgs field that serves as the Nambu-Goldstone (NG) mode to constitute the longitudinal mode of the gauge field, but here the full version of local U(1) case is shown for completeness. Therefore, consider the JF action in Eq. (2.79) plus a local U(1) gauge field A_μ as follows

$$S_{\rm J} = \int d^4x\sqrt{-g_{\rm J}}\left[\left(\frac{M_{\rm pl}^2}{2} + \xi\left|\mathcal{H}_{\rm SM}\right|^2\right)R_{\rm J} - g_{\rm J}^{\mu\nu}D_\mu\mathcal{H}_{\rm SM}^\dagger D_\nu\mathcal{H}_{\rm SM} - \lambda\left|\mathcal{H}_{\rm SM}\right|^4 - \frac{1}{4}g_{\rm J}^{\mu\rho}g_{\rm J}^{\nu\sigma}F_{\mu\nu}F_{\rho\sigma}\right] , \tag{3.117}$$

where $F_{\mu\nu} = \partial_\mu A_\nu - \partial_\nu A_\mu$ and $D_\mu = \partial_\mu - ig_A A_\mu$. This action is invariant under the transformation $A_\mu \to A_\mu - \partial_\mu\theta$ and $\mathcal{H}_{\rm SM} \to e^{-ig_A\theta}\mathcal{H}_{\rm SM}$, where the field $\theta(t,\mathbf{x})$ in phase direction of SM Higgs plays a role as NG mode. In the following discussion, the unitary gauge $\mathcal{H}_{\rm SM} = h/\sqrt{2}$ will be used as before.

• **Jordan frame** It is convenient to omit all the subscripts "J" in the present discussion. In the Fourier space,

$$A_\mu(\mathbf{x},t) = \int\frac{d^3k}{(2\pi)^3}e^{i\mathbf{k}\cdot\mathbf{x}}A_\mu(\mathbf{k},t) , \tag{3.118}$$

the action for A_μ, with the time-component A_0 eliminated by the constraint from its equation of motion, then can be rewritten in two parts as follows

$$\begin{aligned} S_{A_T} &= \int dt\frac{d^3k}{(2\pi)^3}\left[\frac{a}{2}|\dot{\mathbf{A}}_T|^2 - \frac{a}{2}\left(k_p^2 + m_A^2\right)|\mathbf{A}_T|^2\right] , \\ S_{A_L} &= \int dt\frac{d^3k}{(2\pi)^3}\left[\frac{a}{2}\frac{m_A^2}{k_p^2+m_A^2}|\dot{A}_L|^2 - \frac{a}{2}m_A^2|A_L|^2\right] , \end{aligned} \tag{3.119}$$

where $m_A^2 \equiv g_A^2h^2$, and the spatial part of A_μ is decomposed into transverse and longitudinal modes as $\mathbf{A} = \mathbf{A}_T + \mathbf{k}A_L/k$. As can be seen above, the transverse mode behaves just similarly as χ in the previous section, but the longitudinal mode receives contribution from the Higgs to the kinetic term. Defining $f_{\rm nc}(t) = m_A\sqrt{a/(k_p^2+m_A^2)}$,

according to Example Three at the beginning of this chapter, the effective mass of A_L is modified when canonicalizing the kinetic term as

$$m_{L,\text{eff}}^2 = m_A^2 - \ddot{f}_{\text{nc}}/f_{\text{nc}} \ , \tag{3.120}$$

where $\ddot{f}_{\text{nc}}/f_{\text{nc}}$ introduces time derivatives of m_A in the effective mass, which is different from the transverse mode case and plays an essential role to generate the large spikes. It is not necessary to show the complete expression for $m_{L,\text{eff}}^2$ because the dominant contribution can be found by analyzing the motion of $h(t)$ during reheating. To see that, it is better to take the small field limit $k_p \gg m_A$, leading to

$$-\frac{\ddot{f}_{\text{nc}}}{f_{\text{nc}}} \to -\frac{9}{4}H^2 - \frac{3}{2}\dot{H} - 3H\frac{\dot{h}}{h} - \frac{\ddot{h}}{h} \ . \tag{3.121}$$

This expression can be further simplified by the equation of motion for h at background level derived from Eq. (3.117) as

$$\ddot{h} + 3H\dot{h} - \xi R h + \lambda h^3 = 0 \ , \tag{3.122}$$

from which it can be seen that $\xi \gg 1$ induces a large effective mass $\xi|R| \gg H^2$ for the Higgs field such that it oscillates rapidly after inflation. Replacing $\ddot{h}$ in Eq. (3.121) with Eq. (3.122), it becomes

$$-\frac{\ddot{f}_{\text{nc}}}{f_{\text{nc}}} \to -\frac{9}{4}H^2 - \frac{3}{2}\dot{H} - \xi R + \lambda h^2 \ , \tag{3.123}$$

where, focusing on the regime of zero-crossing of $h(t)$, the dominant contribution comes from the third term with $\xi \gg 1$. Therefore, a significant enhancement appears due to the presence of large non-minimal coupling, which can also be understood as an enhancement to the velocity and acceleration of Higgs around zero-crossing in Eq. (3.122). Consequently, the effective mass of the longitudinal mode of gauge field becomes spiky, inducing extremely efficient particle production. One example is shown in Fig. 3.4.

• **Einstein frame** The same phenomenon can be found in EF. The only difference is that m_A^2 is divided by a conformal factor, which does not alter the main conclusion. Since the calculation is (almost) the same as above [34], it will be omitted here to avoid redundancy. It can be estimated that the amplitude of the spike in the effective mass of the longitudinal mode of the gauge field at the beginning of preheating is

$$m_{\text{sp}} = \Delta t_{\text{sp}}^{-1} \sim \sqrt{\lambda} M_{\text{pl}} \ , \tag{3.124}$$

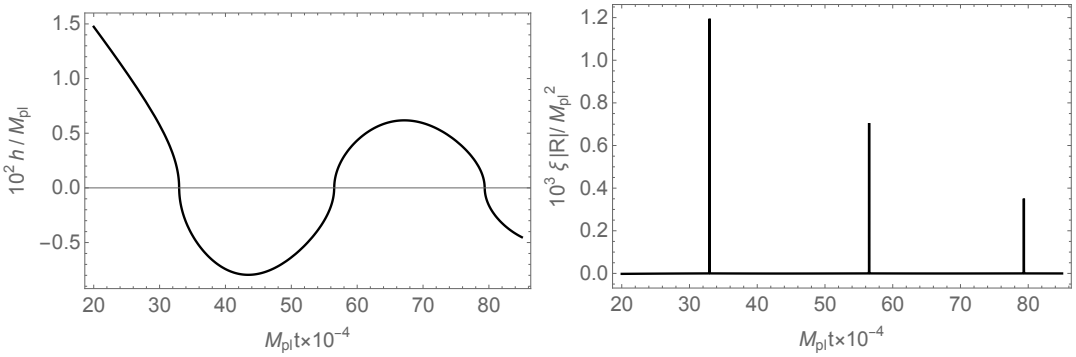

Figure 3.4: One example of the JF dynamics during reheating in the Higgs inflation with $(\xi, \lambda) = (4000, 0.01)$. Left: h oscillates rapidly, especially around the zero-crossing. Right: $\xi|R|$ shows large spikes at the moments that coincide with the zero-crossing points of h .

which is much larger than the cutoff scale of the theory [34]. This phenomenon is true in either frame. The origin is $\xi \gg 1$ which, in JF, is the large non-minimal coupling of Higgs to gravity while, in EF, modifies the structure of the kinetic term of Higgs. Fortunately, the physics are identical, connected by the conformal transformation [62, 63] introduced in Sec. 2.2.

If a spike of such a large scale does not spoil the validity of the theory, it certainly induces extremely violent particle production, exciting particles with momentum $\sim m_{\rm sp}$ that contribute most of the energy density of produced particles. As a result, the energy density of produced A_L can be roughly estimated as $\rho_{A_L} \sim m_{\rm sp}^4 \sim \lambda^2 M_{\rm pl}^4$ which is much larger than the inflation scale $\sim M_c^2 M_{\rm pl}^2$ if λ is non-critical. Consequently, it is argued that the particle production process caused by the spikes can deplete the inflaton energy within just one Higgs oscillation and complete preheating [34]. Of course, the thermalization and the backreaction are not taken into account in the consideration. A numerical study should be involved to have a comprehensive understanding. However, such a large scale is indeed likely to ruin the reliability of the theory, which strongly implies that a UV-extended theory is desired to give unambiguous observational predictions on inflation and reheating. In this sense, it is well-motivated to consider the UV-extended model, the mixed Higgs-R^2 inflation model, because, as explained in the previous chapter, its cutoff scale is pushed up to Planck scale by R^2 and, as will be shown in next chapter, the spike scale will be largely lowered also by R^2, which ensures the validity of the theoretical predictions in this model.

This chapter has reviewed the theory of particle production in a time-dependent

background and its application to reheating in two promising single-field models in order for the preparation of discussion about the reheating process in the mixed Higgs-R^2 inflation model as the main topic in this thesis. Generally speaking, the effects of non-trivial background dynamics can be understood in a unified manner as a time-varying effective mass of the target fields as in Eq. (3.1), including a general curved spacetime, a homogeneous field, and a non-canonical kinetic term, which can be encountered in various inflationary models. A time-dependent effective mass indicates that the vacuum state of the target field is not unique, and the positive- and negative-frequency modes are mixed, especially when the time-dependence is non-adiabatic, to which the particle production is attributed. According to the type and size of couplings, the particle production processes can be categorized into perturbative and non-perturbative ones. The former is treated with perturbation theory and is able to recover the result calculated in quantum field theory. The latter is governed by the Mathieu equation and can further be classified into narrow resonance, broad resonance, and tachyonic instability.

In the two inflationary models considered here, the Starobinsky model and the Higgs inflation, the inflaton degree of freedom coherently oscillates after the end of inflation, inducing particle production to reheat the Universe. In the former, the reheating process is mainly perturbative, and the reheating temperature is relatively low. In the latter case, the large non-minimal coupling leads to the peculiar behavior of Higgs during reheating, i.e. sharp transitions at each zero-crossing. As a result, the effective mass of the longitudinal mode of gauge fields is greatly enhanced and shows large spikes, inducing extremely violent particle production that can complete preheating rapidly. However, such reheating process and its predictions are ambiguous and questionable due to the UV issue resulted from the low cutoff scale and large spiky mass of the longitudinal mode of gauge fields. Since the spike scale exceeds the cutoff of the theory, it is difficult to ensure its validity. Therefore, a UV-extended Higgs inflation is desired from this point of view.

The mixed Higgs-R^2 inflation model can be an excellent candidate as the UV-extension of Higgs inflation. One of the most important reasons is that the cutoff scale is lifted to $M_{\rm pl}$ thanks to the presence of the R^2 term. And the inflation dynamics in this model can be understood as an effective Starobinsky model or effective Higgs inflation, so it is favored by the current observation. However, this is not enough for a successful inflation model. The reheating process should also be investigated carefully in order to ultimately settle down the UV issue and improve the observa-

tional constraints, which is the main subject of this thesis and will be discussed in the following chapter based on the original works [41, 51, 53].

Chapter 4

Reheating in Mixed Higgs-R^2 Inflation Model

The mixed Higgs-R^2 inflation model, as a UV-extended candidate of the Higgs inflation, shows improved UV properties while keeping the observationally favored inflation predictions [36–40,42], which strongly motivates the investigation of the reheating process after the mixed Higgs-R^2 inflation which provides the initial conditions for the Hot Big Bang in this model. The main purpose is to carefully examine the possible existence of unwanted UV issues during reheating as in the Higgs inflation [34], and to clarify the ambiguity in the inflation predictions due to the uncertainty in reheating so that the observational constraints on the broad parameter space in this model can be improved, through which the degeneracy between the two-field model and its single-field limits can be broken. The discussion here focuses on parameters outside the strongly-coupled regime in Fig. 2.1, i.e. with condition (2.121) satisfied.

As will be shown shortly, the effective single-field description of the model is no longer valid during reheating. The multi-field dynamics of the two scalar degrees of freedom becomes crucial to determine the evolution of the system, which leads to rich reheating phenomena but great complication, especially at the bifurcation point around the global minimum $(\varphi, h) = (0, 0)$ in the potential (see Fig. 2.2). Based on the original works [41, 51, 53], different stages of reheating with different model parameters will be discussed in detail[42]. The first stage of preheating involves the spiky features in the effective mass of the longitudinal mode of gauge bosons. It can be analytically shown that the energy scale of those spikes is largely weakened by the multi-field dynamics in the presence of R^2 so that the particle production associated with this phenomenon becomes inefficient to have significant effects during preheating [41]. There are two possibilities for the subsequent evolution, the occurrence of

[42]Preheating process in similar models is studied in, e.g. Ref. [182].

tachyonic preheating that can complete preheating almost instantaneously [50–52], and perturbative reheating that plays an essential role if the tachyonic instability is inefficient enough or simply absent [53]. The conditions for efficient tachyonic preheating are derived, and the reheating temperature for different model parameters in both cases is found, which is done by combining analytical and numerical methods. In these studies, the backreaction from the produced particles to the background dynamics is not considered because the analysis is mainly analytical while sophisticated numerical computation is needed to consider the non-linear effects consistently. Nevertheless, the study is limited to the regime where the backreaction is not important and the analytical results have clear physical meaning for understanding the situation. Therefore, the phrase "*complete preheating*" used hereafter means that the energy density of the produced particles during preheating becomes comparable with that of background, instead of completely depleting the energy of inflaton. More detail will be discussed in the corresponding section. Another concern may be related to the renormalization group running of the model parameters, such as λ and the neglected Higgs mass. Especially, as shown in Ref. [135], the Higgs mass may become as large as $\sim M_{\rm pl}/\xi$ at inflation scale, which may have non-trivial effects on the current results. However, it is not the case, as can be seen in the clear analysis in the same Ref. [135].

The chapter is constructed as follows. At the beginning of each discussion, the background dynamics for the corresponding stage are analyzed, which constitutes the basis of subsequent investigation on reheating. The behavior of spiky features in the effective mass of NG mode is clarified in Sec. 4.1, proving that the single-field UV issue disappears in the mixed Higgs-R^2 inflation model. In Sec. 4.2, a comprehensive analytical investigation together with numerical calculation of the tachyonic preheating in this model is presented, including the conditions for occurrence, efficiency, and the necessary degree of fine-tuning. Finally, in Sec. 4.3, perturbative reheating is discussed in the case where the tachyonic instability is unable to complete preheating, determining the final reheating temperature and duration.

4.1 First Stage of Preheating

Similar to the Higgs inflation case [34], at the first stage of preheating in the mixed Higgs-R^2 inflation model, the particle production is induced by the spikes exhibited in the effective mass of the phase direction of Higgs (or the NG mode) that constitutes

the longitudinal mode of gauge bosons. In the single-field case, due to the large non-minimal coupling $\xi \gg 1$, the mass scale of the spikes $\sim \sqrt{\lambda} M_{\rm pl}$ is much higher than the cutoff scale of the theory $\sim M_{\rm pl}/\xi$, which is considered out of quantum mechanical control and the perturbation theory is expected to fail. However, with the inclusion of R^2 term, the situation is shown analytically and numerically to change significantly by the multi-field nature, i.e. considerable reduction of the spike scale [41]. On the one hand, this result confirms that the UV issue in the single-field case no longer exists in this UV-extended model, while on the other hand, it proves that the spike preheating is far from sufficient to complete preheating. Other reheating mechanisms, therefore, are needed to reheat the Universe after mixed Higgs-R^2 inflation.

The analysis below focuses on the global U(1) Higgs which is sufficient for the present purpose, but it is expected that the conclusion remains unchanged for the fully gauged $\mathrm{SU}(2)_L \times \mathrm{U}(1)_Y$ case. Therefore, the "Higgs" field is written in the form

$$\mathcal{H}_{\rm SM}(t, \mathbf{x}) = h(t) e^{i\theta_h(t,\mathbf{x})}/\sqrt{2} \ , \tag{4.1}$$

in the action (2.118) where the NG mode $\theta_h(t, \mathbf{x})$ is treated as perturbation. In order to study quantum creation of this NG mode due to the spikes, the main goal is then to find out the behavior of its effective mass.

• **Jordan frame** Here, all the subscripts "J" for JF are omitted for simplicity. With Eq. (4.1), the relevant part of the Lagrangian in JF reads

$$\sqrt{-g}\mathcal{L} \supset -\frac{1}{2}\sqrt{-g} h^2 g^{\mu\nu} \partial_\mu \theta_h \partial_\nu \theta_h = \frac{1}{2}\dot{\theta}_c^2 - \frac{1}{2a^2}(\nabla\theta_c)^2 + \frac{1}{2}\frac{\ddot{f}_{\rm nc}}{f_{\rm nc}}\theta_c^2 \ , \tag{4.2}$$

where the canonical field θ_c and $f_{\rm nc}(t)$ are defined as

$$\theta_c(t, \mathbf{x}) \equiv a^{3/2}(t) h(t) \theta_h(t, \mathbf{x}) \equiv f_{\rm nc}(t) \theta_h(t, \mathbf{x}) \ , \tag{4.3}$$

in the flat FLRW background, which is a special case of Example Three at the beginning in Chapter 3. As a result, the effective mass of the canonicalized NG mode is given by

$$m_{\theta_c}^2 = -\frac{\ddot{f}_{\rm nc}}{f_{\rm nc}} = -\frac{9}{4}H^2 - \frac{3}{2}\dot{H} + \frac{V_{{\rm eff},h}}{h} \sim -\xi R \ , \tag{4.4}$$

where the equation of motion for Higgs has been used for simplification and the effective potential $V_{\rm eff}$ is given in Eq. (2.127). In the last estimation, the dominant contribution is easily found to be in the same form as the single-field case with $\xi \gg 1$. Therefore, it is important to understand the background evolution of $R(t)$ in the two-field case which is determined by Eqs. (2.125) and (2.126).

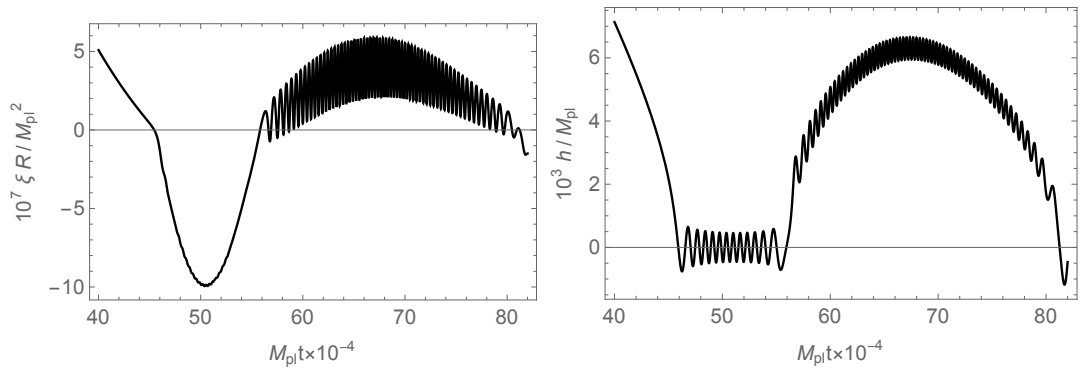

Figure 4.1: One example of the first oscillation of ξR (left) and h (right) after the end of the mixed Higgs-R^2 inflation in JF with $(\xi, \lambda) = (4000, 0.01)$. Compared with the single-field case, the shape zero-crossing of Higgs is replaced by a series of small oscillations around the origin.

Analogous to the single-field case, the spikes are expected to appear whenever h approaches a zero-crossing point. One example of the evolution of ξR and h in their first oscillation after the end of the mixed Higgs-R^2 inflation is shown in Fig. 4.1, which shows that the accelerated transition of Higgs around $h \simeq 0$ in the single-field case becomes several small oscillations at the origin due to the presence of R^2. This observation allows analytical calculation of the behavior of Ricci scalar and Higgs with simple approximation. More importantly, the left panel of Fig. 4.1 shows much regular behavior of $R(t)$ with much smaller amplitude than that in Fig. 3.4, which implies that the spiky features in $m^2_{\theta_c}$ must be weakened significantly. To be specific, Eq. (2.126) can be written in the following form when $h \simeq h_{\rm v0} = 0$

$$-\Box R + M^2 R \simeq 0 \ , \tag{4.5}$$

where the energy of Higgs is appropriately assumed to be negligible during the small oscillations around the origin, which indicates that $R(t)$ is actually a harmonic oscillator with frequency M in this period instead of $\tilde{M}$, i.e. $R(t) \propto \sin(Mt)$ regardless of the cosmic expansion within the first oscillation. The amplitude of this oscillator is then essential for the determination of the spike scale of $m^2_{\theta_c}$. The simplest way to do that is to trace the energy of the system. Since the energy of Higgs at this moment is negligible, the total energy is naturally dominated by the scalaron oscillation because there has not been any particle production at this stage. The energy loss compared with the beginning of inflation is simply due to the Hubble friction, which can be assumed to be an undetermined constant coefficient

$$\rho_R = C_1^2 \rho_{\rm inf} \ , \tag{4.6}$$

where C_1 can be fixed by fitting the numerical calculation. This task is left to the discussion in EF in the following.

• **Einstein frame** All subscripts "E" will be omitted for convenience. Since the Higgs field remains unchanged in the conformal transformation (2.122), the relevant part of the Lagrangian in EF can be obtained simply by inserting $h \to he^{i\theta_h}$ into the action (2.124), which leads to

$$\sqrt{-g}\mathcal{L} \supset -\frac{1}{2}\sqrt{-g}e^{-\alpha\varphi}h^2 g^{\mu\nu}\partial_\mu\theta_h\partial_\nu\theta_h = \frac{1}{2}\dot{\theta}_c^2 - \frac{1}{2a^2}(\nabla\theta_c)^2 + \frac{1}{2}\frac{\ddot{f}_{\rm nc}}{f_{\rm nc}}\theta_c^2 + \cdots , \tag{4.7}$$

where the canonical field $\theta_c(t,\mathbf{x})$ and $f_{\rm nc}(t)$ are defined as

$$\theta_c(t,\mathbf{x}) \equiv a^{3/2}(t)e^{-\alpha\varphi(t)/2}h(t)\theta_h(t,\mathbf{x}) \equiv f_{\rm nc}(t)\theta_h(t,\mathbf{x}) \ . \tag{4.8}$$

As can be seen, the only difference from the case in JF is that the conformal factor in Eq. (2.122) enters the definition of $f_{\rm nc}(t)$. Similarly, the effective mass of the NG mode is easily read off as

$$m_{\theta_c}^2 = -\frac{\ddot{f}_{\rm nc}(t)}{f_{\rm nc}(t)} = -\frac{\alpha}{2}U_{,\varphi} + \frac{e^{\alpha\varphi}}{h}U_{,h} - \frac{3}{4}\frac{U}{M_{\rm pl}^2} + \frac{5}{24}\frac{1}{M_{\rm pl}^2}\left(\dot{\varphi}^2 + e^{-\alpha\varphi}\dot{h}^2\right) \ , \tag{4.9}$$

where the background equations (C.6), (C.7), and (C.8) in Appendix C have been used to simplify the situation. While the last two terms are always of the order of the Hubble parameter, the first two terms can be much larger $\sim \xi M^2$ when the scalar field trajectory deviates from the valley (2.145). Again, the detailed evolution of scalaron and Higgs is essential to determine the properties of $m_{\theta_c}^2$ so the background analysis in EF is necessary for the study to proceed.

In EF, the two scalar degrees of freedom for inflaton become more explicit as in the action (2.124). The effective single field description breaks down during reheating; therefore, the full equations of motion for φ and h shown in Appendix C should be taken into account. Given Eqs. (C.6), (C.7), and (C.8), it can be seen that the system is highly complicated due to the couplings between scalaron and Higgs, so numerical results may be needed to gain an intuition of the dynamics for analytical understanding. Figures 4.3 exhibit typical examples of evolution of h (top panels) and φ (bottom panels) for three benchmark points shown in Fig. 4.2 which are specifically chosen as:

$$\text{(A)}\ \ \xi/\xi_c \simeq 0.9996,\ \ M_c/M \simeq 0.0282 \quad \leftrightarrow \quad \xi = \xi_s \simeq 4439,\ \ M_{\rm pl}/M \simeq 2.17\times 10^3,$$

$$\text{(B)}\ \ \xi/\xi_c \simeq 0.9975,\ \ M_c/M \simeq 0.0709 \quad \leftrightarrow \quad \xi = 4430,\ \ M_{\rm pl}/M \simeq 5.45\times 10^3,$$

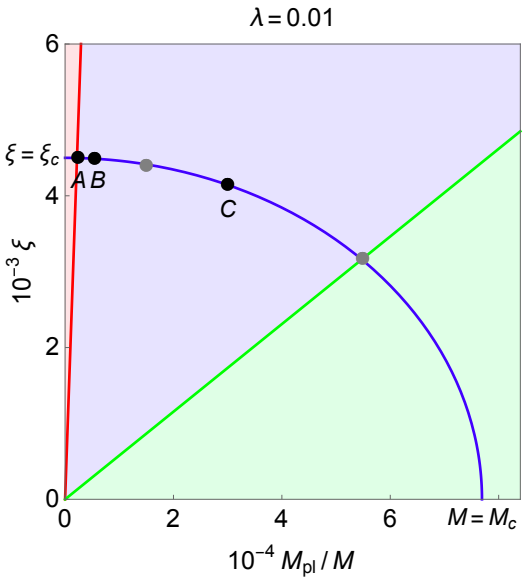

Figure 4.2: Parameter space for the mixed Higgs-R^2 inflation model with $\lambda = 0.01$. The black points (A), (B), and (C) along the blue line represent three benchmark points chosen for examples of the evolution of φ and h in Figs. 4.3 and 4.4, while all five parameter points (three black and two gray) are for the numerical fitting in Fig. 4.5.

$$\text{(C)}\ \ \xi/\xi_c \simeq 0.9208,\ \ M_c/M \simeq 0.39 \qquad \leftrightarrow \qquad \xi \simeq 4089,\ \ M_{\rm pl}/M = 3\times 10^4,$$

which satisfy the observational constraint (2.137). Note that parameter point (A) lies on the boundary to the strongly-coupled regime. The initial condition for Figs. 4.3 is just before the end of inflation as $\varphi = 1.2M_{\rm pl}$, $\dot{\varphi} = 0$, while h satisfies $\partial U/\partial h = 0$ and $\dot{h} = 0$ at $t = 0$, but it has been confirmed that the results remain unchanged if larger number of e-folds before the end of inflation is taken. As shown in Figs. 4.3, the scalar fields are once trapped in the only narrow valley for $\varphi < 0$ with the time scale $\sim M^{-1}$ and the h field oscillates rapidly with the effective mass squared $\sim \alpha|\varphi|\xi M^2$ around the streamline $h_{\rm v0} = 0$ at the bottom of the valley. The frequency of the Higgs field can be very large if $\alpha|\varphi| \sim 1$. Figures 4.4 show the time evolution of $m^2_{\theta_c}$ for our benchmark parameters (A), (B), and (C). It is straightforward to see that the effective mass gets larger when φ gets negative and, at the same time, $h \simeq 0$. Also, more or less, the spiky shape still appears even in the case where the R^2 term is present. However, the amplitude and width are obviously different from the single-field case. It can be observed that the height of the spikes gets lower and their width gets wider as M (or ξ) decreases, i.e. more R^2-like case. This is natural because no spikes should be expected in the R^2-limit. More specifically, the heights and the widths of the spikes for all five parameter points in Fig. 4.2 are shown as a function

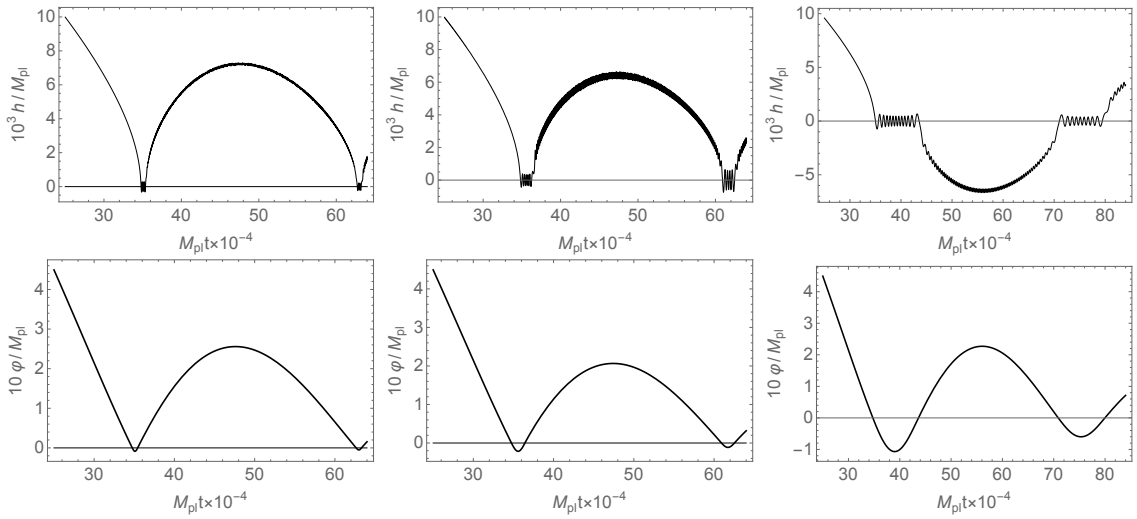

Figure 4.3: Time evolution of the Higgs field h (top) and scalaron φ (bottom) for the parameter points (A) (left), (B) (middle), and (C) (right) with $\lambda = 0.01$. See Fig. 4.2 for the three parameter points.

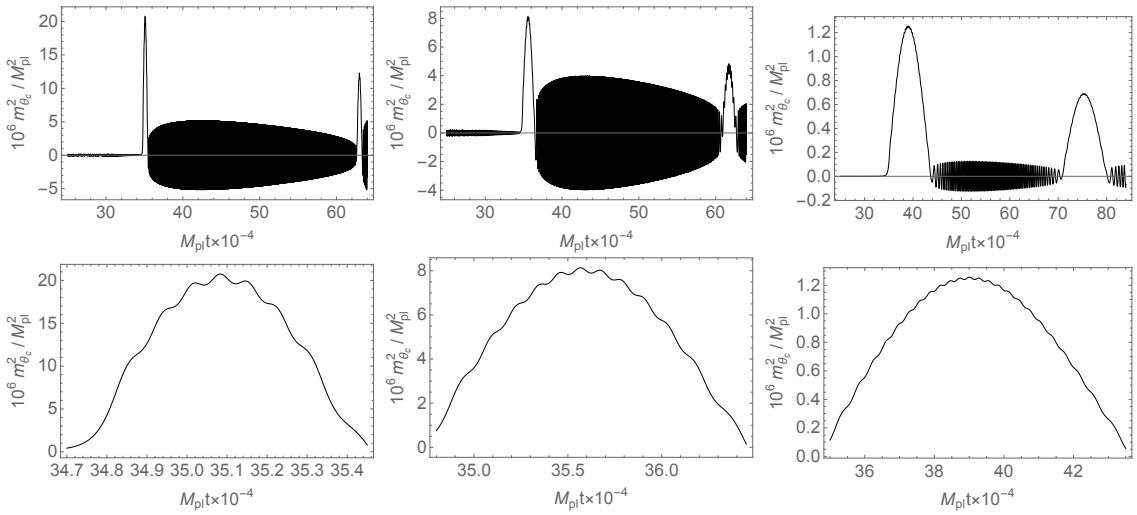

Figure 4.4: Time evolution of the effective mass squared for the phase direction $m^2_{\theta_c}$ for the parameter points (A) (left), (B) (middle), and (C) (right) with $\lambda = 0.01$. The top panels show the evolution over the full time range shown in Figs. 4.3, while the bottom panels are magnifications of the top panels around the first peak.

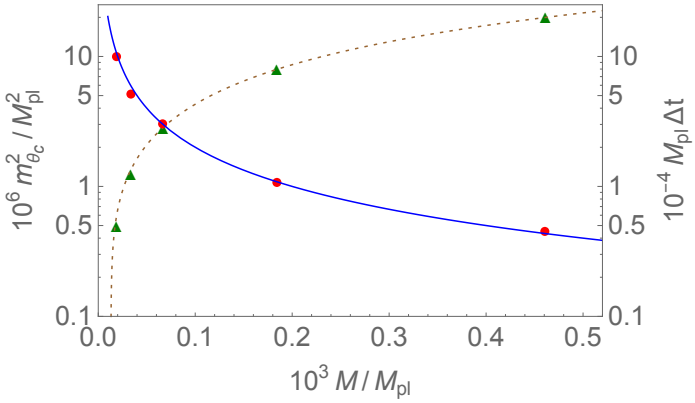

Figure 4.5: Peak amplitude and timescale of the spike in the effective mass squared $m_{\theta_c}^2$ at the first oscillation after the end of mixed Higgs-R^2 inflation. The green triangles and the red disks are the numerically obtained peak amplitude and timescale of the mass spike, respectively, while the brown dashed line and the blue solid line are analytic estimates (4.17) and (4.18) with $C_1 \simeq 0.25$ and $C_{\rm t} \simeq 2$.

of M in Fig. 4.5, under the observational constraint (2.137). The width of the spikes is defined as the full width at half maximum. Therefore, the numerical results show that the spikes become more "spiky" as the system becomes more Higgs-like, but even at the boundary $\xi = \xi_s$ of the strongly-coupled regime, the amplitude of the spike is largely weakened compared with the one in the Higgs inflation.

With the observation above, the analytical understanding of the behavior of the spikes can be easily found with appropriate approximation as follows. During inflation, the energy density of the Universe is dominated by the potential in Eq. (2.124). With the effective single-field condition, i.e. the valley for $\varphi > 0$ given in the lower of Eq. (2.145), the asymptotic potential height for $\alpha\varphi \gg 1$ is then

$$U_{\rm inf} = 3M_{\rm pl}^2 \tilde{M}^2/4 \ . \tag{4.10}$$

On the other hand, small field approximation is valid during reheating, i.e. $\alpha|\varphi| \ll 1$, which greatly simplifies the potential $U(\varphi, h)$ by expanding it around the origin

$$U(\varphi, h) \approx \frac{\lambda}{4} h^4 + \frac{1}{2} M^2 \left(\varphi - \frac{\xi h^2}{\alpha M_{\rm pl}^2} \right)^2 \ . \tag{4.11}$$

Focusing on the regime $\varphi < 0$ where the spikes appear, there is only one minimum along $h_{\rm v0} = 0$ as shown in Eq. (2.146) and Fig. 2.2, where the potential is

$$U(\varphi, h = 0) = U_0(\varphi) = M^2 \varphi^2/2 \ , \tag{4.12}$$

which leads to the mass of the scalaron around the valley

$$m_\varphi^2 = M^2 \ . \tag{4.13}$$

Therefore, the scalaron field, as is also shown previously in the analysis in JF, behaves simply as a harmonic oscillator with mass M in this regime, which helps to estimate the duration of $\varphi < 0$ regime, or equivalently, the width of the spikes. Since the potential energy also dominates the kinetic one when φ field climbs up the valley during $\varphi < 0$ and reaches its maximal amplitude $\varphi = \varphi_1 < 0$, the potential energy (4.12) at the first oscillation can be related to $U_{\rm inf}$ in the following way

$$U_0(\varphi_1) = C_1^2 U_{\rm inf} \ , \tag{4.14}$$

which yields

$$\alpha|\varphi_1| = C_1 \frac{\tilde{M}}{M} = C_1 \sqrt{\frac{\lambda M_{\rm pl}^2}{3\xi^2 M^2 + \lambda M_{\rm pl}^2}} \ . \tag{4.15}$$

Here $C_1 \lesssim 1$ represents the dissipation of the potential energy from the plateau region during inflation to φ reaching the largest negative value φ_1 after a half oscillation. With the relation shown above, the maximal amplitude of the effective mass $m_{\theta_c}^2$, which corresponds to the height of spikes, can be estimated at the point $(\varphi, h) = (\varphi_1, 0)$ as

$$\left(m_{\theta_c}^{\rm sp}\right)^2 \simeq M^2 \left[\frac{C_1}{2}(6\xi + 1)\frac{\tilde{M}}{M} - \frac{C_1^2}{16}\left(\frac{\tilde{M}}{M}\right)^2 \right] \ , \tag{4.16}$$

where, as can be checked, the dominant contribution comes from the second term in Eq. (4.9) for $\xi \gg 1$. For larger $M (> \sqrt{\lambda} M_{\rm pl}/\xi)$, this result gives $\left(m_{\theta_c}^{\rm sp}\right)^2 \simeq C_1 \sqrt{3\lambda} M M_{\rm pl}$. Note that in this expression for sufficiently large $M \simeq \sqrt{\lambda} M_{\rm pl}$ and $\xi > \xi_s$[43] for which the single-field Higgs inflation approximation gets better, the formula in the Higgs inflation case is recovered $\left(m_{\theta_c}^{\rm sp}\right)^2 \simeq \sqrt{3} C_1 \lambda M_{\rm pl}^2$ [34], which is consistent with the explanation in Chapter 2 that the Higgs inflation actually enters the strongly-coupled regime in Fig. 2.1. Taking the observational constraint (2.137) into account, Eq. (4.16) becomes

$$\left(m_{\theta_c}^{\rm sp}\right)^2 \approx C_1 \sqrt{3\lambda(M^2 - M_c^2)} M_{\rm pl} \ , \tag{4.17}$$

for $\xi \gg 1$. In the Higgs-like regime, $M \gg M_c$ so the spikes may be large, while in the R^2-like regime, $M \simeq M_c$ which suppresses the height of the spikes. As mentioned

[43] These parameters obviously do not respect the perturbativity condition Eq. (2.121).

above, the duration of the first spike is determined by the period when the scalaron stays in the $\varphi < 0$ regime, i.e. $\sim M^{-1}$. Therefore, the width of the spikes can be simply estimated as

$$\Delta t_{\rm sp} = C_{\rm t} M^{-1} \ . \tag{4.18}$$

Again, the formula for the Higgs inflation $\Delta t_{\rm sp} \simeq (\sqrt{\lambda} M_{\rm pl})^{-1}$ can be recovered at $M \simeq \sqrt{\lambda} M_{\rm pl}$ when the single-field Higgs inflation approximation gets better. Note that Eqs. (4.16) and (4.18) are not valid any more when M significantly exceeds the spike timescale inverse in the Higgs inflation case $M \gg \sqrt{\lambda} M_{\rm pl}$. Also in Fig. 4.5, the analytical estimates (4.17) and (4.18) are shown with $C_1 \simeq 0.25$ and $C_{\rm t} \simeq 2$ fitted with the measured peak amplitude and timescale of the spikes. The green triangles and the red disks are the values of the amplitude and the timescale estimated from the numerical time evolution, respectively, while the brown dashed line and the blue solid line are the predictions of the analytic estimates (4.17) and (4.18), respectively. It can be seen that the numerical results coincide with the analytic estimates well. A rough estimate of C_1 could help to understand the fitted value. For the single-field Higgs- or R^2-inflation, the potential shape becomes $\propto (1-e^{-\alpha\varphi})^2$. Thus, the slow-roll condition $\max\{|\epsilon_1|, |\epsilon_2|\} < 1$ breaks down at the moment $e^{-\alpha\varphi} = 2\sqrt{3} - 3$ when the inflaton potential energy is $\simeq 0.287$ times its value at the plateau. This value is just close to $\simeq 0.25$ found previously, so it is expected that similar physical picture applies in the two field case.

As a result, the height of the spike shown in Eq. (4.17) can no longer exceed the cutoff scale of the theory $\sim M_{\rm pl}$ in the mixed Higgs-R^2 inflation model, which further confirms that this two-field model is free from the UV issues encountered in the Higgs inflation and serves as a promising UV-extension candidate of the latter.

Having the analytical behavior of the first spike in $m^2_{\theta_c}$ after the end of the mixed Higgs-R^2 inflation, the estimation of particle production induced by such a spike becomes possible, which is essential to examine the efficiency of this preheating channel. Particle production from subsequent oscillations is neglected because the main interest lies in the effect of the strongest spike that appears in the single-field Higgs inflation.

For the estimate of particle production from non-adiabatic change of effective mass, the technique introduced in Chapter 3 can be used. Specifically in the case of a strong spike which is like Dirac delta function, a special point is that there is a jump in the junction conditions for the first-order derivative of mode functions, just as solving the Schrödinger equation with a delta potential. The main goal is still to

find the Bogoliubov coefficient β_k that is directly related to the occupation number of produced particles with momentum k. The general results for such a case can be found in the Appendix C of Ref. [183]. If the strong spike is described by the following cosh-type spike function

$$m_{\theta_c}^2(t) = \frac{m}{2\Delta t}\frac{1}{\cosh^2(t/\Delta t)} \ , \tag{4.19}$$

and the produced field is in the vacuum for $t \to -\infty$, its number density after the spike is then given by

$$n_{\theta_c} = \int \frac{d^3k}{(2\pi)^3}\, f_{\theta_c} \ , \quad f_{\theta_c} = \cos^2\left(\frac{\pi}{2}\sqrt{1+2m\Delta t}\right) \Big/ \sinh^2(\pi k \Delta t) \ . \tag{4.20}$$

Since the full width at half maximum is used to estimate $\Delta t_{\rm sp}$, it may be identified as $\Delta t_{\rm sp} = \Delta t \times 2\ln\left(\sqrt{2}+1\right)$. With $\left(m_{\theta_c}^{\rm sp}\right)^2 \simeq m/(2\Delta t)$, the energy density of the produced phase direction can be approximately calculated as

$$\rho_{\theta_c} \simeq \int \frac{d^3k}{(2\pi)^3}\, k f_{\theta_c} \sim 4.5\times 10^{-3}\Delta t_{\rm sp}^{-4} \simeq 2.8\times 10^{-4}\left(\frac{C_{\rm t}}{2}\right)^{-4} M^4 \ , \tag{4.21}$$

where the cosine-squared in the numerator of Eq. (4.20) to be 0.5.[44] The estimate (4.21) is in agreement with the general result for particle creation in cosmology obtained in Ref. [159] and with more detailed expression for the rate of particle creation in Ref. [172]. In particular, the particle production efficiency should reach maximum at the boundary to the strongly-coupled condition $M \simeq \sqrt{4\pi/\lambda}\tilde{M}$, giving the energy density

$$\rho_{\theta_c} \simeq 4.5\times 10^2\left(\frac{\lambda}{0.01}\right)^{-2}\left(\frac{C_{\rm t}}{2}\right)^{-4}\tilde{M}^4 \simeq 7.6\times 10^{-8}\left(\frac{\lambda}{0.01}\right)^{-2}\left(\frac{C_{\rm t}}{2}\right)^{-4}\tilde{M}^2 M_{\rm pl}^2 \ , \tag{4.22}$$

which is much smaller than the energy density carried by the inflaton just after the end of inflation $\rho_{\rm inf} \simeq U_{\rm inf} = 3M_{\rm pl}^2\tilde{M}^2/4$. For smaller M, the energy density of the phase direction becomes even smaller. Note that this discussion does not rely on the observational condition (2.137). Therefore it can be concluded that, even when R^2 term is added so that the cutoff scale of the theory becomes $M_{\rm pl}$, the spike still appears and is a real physical phenomenon, but the preheating of the Universe does not complete with the production of the NG bosons from a single spike.

Investigation of the effective mass of the NG mode for the mixed Higgs-R^2 inflation model based on Ref. [41] is presented above, finding that the effective mass

[44] In fact, for $M \gg \tilde{M}$, the parameter dependence $m\Delta t \sim \left(m_{\theta_c}^{\rm sp}\right)^2(\Delta t_{\rm sp})^2 \propto M_{\rm pl}/M$ makes the argument of the cosine function much larger than unity.

exhibits spikes over the preheating process as in the Higgs inflation [34]. The remarkable difference is that the cutoff scale of this UV-extended model is lifted to $M_{\rm pl}$ thanks to the scalaron originated from the R^2 term, while the energy scale of the spike $(m^{\rm sp}_{\theta_c})^2$ is substantially suppressed and well below the cutoff as found previously, contrary to the case of the Higgs inflation, which ensures the reliability of the theoretical predictions in this model. The properties of the spikes are well described by the analytic formula (4.17) and (4.18) which shows that the amplitude of the spikes becomes lower and the width becomes larger when the model is more R^2-like. Conversely, the spike is higher and sharper when the system approaches the Higgs-limit. The model is healthy even at the boundary $\xi = \xi_s$, and the properties of the spikes in the Higgs inflation are recovered once the parameter is deep inside the strongly-coupled regime. Therefore, the spiky behavior of the NG mode is concluded as a genuine physical phenomenon associated with the production of the longitudinal mode of gauge bosons.

According to the estimation in Eq. (4.20), even in the extreme case with the parameters being on the boundary to the strongly-coupled regime, the produced energy density of NG boson is much smaller than the total energy density of the Universe. Thus, the reheating cannot be completed within only one spike (see Eq. (4.22)). This conclusion is sharply distinct from the one in the Higgs inflation. Although the analysis is given for the global U(1) scalar $\mathcal{H}_{\rm SM}$, it is expected that the conclusion remains unchanged for the realistic $\mathrm{SU}(2)_L \times \mathrm{U}(1)_Y$ case. As a result, as will be shown later, the subsequent evolution of the Universe with other reheating mechanisms such as tachyonic instability [50–52] and perturbative decay of the scalaron and Higgs [53] should be the main channel of the depletion of the inflaton quanta. Similar analysis can be done in other UV-extension models of the Higgs inflation.

4.2 Occurrence of Tachyonic Preheating

Despite the close relation with the Higgs inflation, the preheating mechanisms are surprisingly different in the mixed Higgs-R^2 inflation model. In the Higgs inflation, reheating is driven by the post-inflationary oscillation of the SM Higgs field. More specifically, the oscillation with large non-minimal coupling $\xi \gg 1$ induces high spikes in the effective mass of the longitudinal modes of weak gauge bosons [34] as shown in the previous chapter, which may complete reheating exceptionally quickly regardless of the possible UV issues. This phenomenon occurs before the resonant production of the transverse mode of weak gauge bosons studied in earlier works [31–33]. However,

as shown previously, the multi-field dynamics in the mixed Higgs-R^2 inflation model essentially changes such a situation, largely weakening the violent particle production induced by spikes. Thus, the conclusion for spike preheating no longer holds [41], which can be seen in the analytical results of the energy density of produced particles in Eq. (4.22). At the same time, the UV issue in the Higgs inflation is completely avoided because of the hierarchy between the cutoff $\sim M_{\rm pl}$ and the spike scale in Eq. (4.17).

The inefficiency of such spike preheating in the mixed Higgs-R^2 inflation model naturally suggests the necessity to identify the dominant process for the completion of reheating in subsequent evolution. Soon after the work [41], Bezrukov *et al.* [50] numerically showed that, with some special choices of model parameters in the Higgs-like regime, the preheating in this model could be completed by tachyonic instability of the (physical) Higgs field and the longitudinal modes of weak gauge bosons right after the first stage mentioned above. The shape of the two-dimensional potential of the (physical) Higgs field h and the scalaron φ consists of the two potential valleys in $\varphi > 0$ regime where inflation takes place and the potential hill between them at $h = 0$, as seen in Fig. 2.2, forming a bifurcation point. If appropriate model parameters are chosen, the system can climb up the potential hill around $h = 0$ during the oscillations of φ around the origin. As a result, the dynamics of the background fields at reheating as a whole becomes chaotic in the sense introduced in Ref. [184] (see also Ref. [185]). Also, the Higgs field, as well as the longitudinal modes of gauge bosons, are tachyonic in this regime[45]. Thus, tachyonic preheating can take place[46], and it is indeed found to be strong enough to complete preheating at some parameter points in Ref. [50]. This possibility is intriguing, but it is not quantitatively clear which choices of model parameters allow this tachyonic preheating and how much fine-tuning is needed among them until a deeper understanding of this physical picture is obtained in Ref. [51].

On the other hand, such a two-dimensional potential shape (e.g. in Fig. 2.2) may raise some subtleties in the following study, which should be clarified before proceeding to the detailed discussion of tachyonic preheating. In order to focus on the dynamics of the physical Higgs field, a simplified model is adopted, taking it as a real singlet field h. As mentioned above, this toy model apparently shows two distinct trajectories along the valleys of the scalar potential in the regime $\varphi > 0$. It is then

[45] Actually, the tachyonic effect exists even if the inflaton cannot climb up the hill exactly, as already see in Fig. 4.4 where $m^2_{\theta_c}$ oscillates between positive and negative values in $\varphi > 0$ regime.

[46] Tachyonic preheating was first studied in theories with spontaneous symmetry breaking [18–20]. Tachyonic instability for the spectator field can also be induced by large field space curvature, see, e.g. Ref. [186].

natural to see that this model gives rise to domain walls in the Higgs direction during or after inflation. However, these domain walls are just temporary instead of being static as in a singlet scalar field theory with a double-well potential and will disappear in the flat spacetime limit when $\varphi \to 0$. They vanish even during reheating when scalaron enters the negative regime $\varphi < 0$. Note also that the realistic SM Higgs field does not yield any domain walls either.

Another important point that needs clarifying is that the backreaction from produced particles to the background fields is not taken into account in the following semi-analytical investigation, which is the main limitation of the present study. Nevertheless, the study here focuses on the first scalaron oscillation, right after the first stage of preheating in the previous section, when the tachyonic instability is expected to be the strongest and extremely efficient channel of particle production, so that the backreaction can be neglected temporarily. As pointed out in Ref. [50] and shown later in the lattice simulation in Ref. [52][47], even if the model parameters do not allow tachyonic preheating at the first scalaron oscillation, tachyonic instability can still be effective at subsequent oscillations. In such cases, the backreaction of produced particles on the background scalar field dynamics can be important, and the simplified treatment in the present discussion is not directly applicable. Furthermore, in this section, *the preheating is completed* if the energy density of produced particles becomes comparable to the background energy density because the thermalization of the produced particles and the transition of the Universe to the radiation-dominated stage without late-time scalar field (re)domination is not investigated.

In the following, the instability of the physical Higgs field is analyzed with both analytical and numerical methods. Firstly, the conditions on model parameters with which the tachyonic effect is prominent are found and serve as the critical ingredient for the subsequent discussion. Secondly, based on these parameter choices, the efficiency of the tachyonic instability is analyzed, and calculation of the energy density of produced particles is presented, which is necessary for the estimate of the degree of fine-tuning needed to complete preheating solely by the tachyonic instability in the last part of the discussion.

This discussion can be carried out in either JF or EF, but as will be briefly shown shortly, the analysis in two frames is somewhat the same in a trivial way because most attention is drawn to the regime $h \simeq 0$.

• **Jordan frame** Here, the subscripts "J" are omitted for convenience. As in Sec. 4.1, the equation of motion for $R(t)$ is given as Eq. (4.5). Therefore, the behavior of the

[47] Ref. [52] showed up on arXiv on the same day as Ref. [51]. The results are not in conflict.

Ricci scalar is straightforward $R(t) \propto \sin(Mt)$ where the cosmic expansion can be safely neglected within one oscillation. This simple form not only holds for $R(t) < 0$ as previously but for the case of interest here because $h \simeq 0$ on the hill where the strongest tachyonic instability occurs. As a result, the equation of motion for the physical Higgs field is the same as Eq. (3.122) or approximately

$$\ddot{h} + 3H\dot{h} - \xi R h \approx 0 \ , \tag{4.23}$$

where higher-order terms in h are neglected. The effective mass $-\xi R(t)$ is ordinary during $R(t) < 0$ but obviously becomes tachyonic when $R(t) > 0$, which is the very origin of the tachyonic instability in the Higgs field. Recalling Eq. (4.4), the dominant contribution to the effective mass of the NG mode takes exactly the same form, indicating that comparable strength of tachyonic instability should also be found in the longitudinal mode of weak gauge bosons. This will be discussed in more detail later.

As mentioned above, the situation described here is trivially the same as that in EF, which can be easily seen in the definition of φ in the conformal transformation (2.123). Explicitly, it can be rewritten as

$$e^{\alpha\varphi} = 1 + \frac{R}{3M^2} + \frac{\xi h^2}{M_{\rm pl}^2} \ , \tag{4.24}$$

where the last term on the right hand side can be dropped if $h \simeq 0$. Meanwhile, small field $\alpha|\varphi| \ll 1$ is good approximation during reheating, so $e^{\alpha\varphi} \simeq 1 + \alpha\varphi$. As a result, a simple relation can be found $R(t) \simeq 3M^2\alpha\varphi(t)$ in the situation considered here. In other words, $R(t)$ is basically equivalent to $\varphi(t)$ in EF, which is the reason why it is said to be trivial.

Thus, it is sufficient to focus on the analysis in EF as follows.

• **Einstein frame** Subscripts "E" are all omitted for simplicity. In the post-inflationary epoch, the effective single-field description is no longer viable and the system obeys the Friedmann equation (C.6), the equations of motion for scalaron (C.7), and the Higgs field (C.8). As mentioned previously, small field approximation is valid so it is convenient to work on the simplified potential in Eq. (4.11). For $\varphi > 0$, the potential is described by the valleys that are continued from the inflationary trajectory and the hill at $h = 0$ between them. The valleys provide a relation between the Higgs field and the scalaron through the lower of Eq. (2.145) as

$$h^2 = h_{\rm v\pm}^2 \simeq 3\xi\tilde{M}^2\alpha\varphi/\lambda \ , \tag{4.25}$$

where $\alpha\varphi \ll 1$ is used. The potential along the valley is then given by

$$U(\varphi, h_{\rm v\pm}) = U_{\rm v}(\varphi) = \tilde{M}^2\varphi/2 \ , \tag{4.26}$$

with the effective mass for the valley and the "isocurvature" mass (or the Higgs mass) being

$$m^2_{\varphi,{\rm v}} \equiv U_{{\rm v},\varphi\varphi} = \tilde{M}^2 \ , \quad m_h^2 \equiv U_{,hh} = 6\alpha\xi M^2\varphi \ . \tag{4.27}$$

On the contrary, if the scalar fields climb up the hill at $h = 0$ in the regime $\varphi > 0$, the potential then becomes

$$U(\varphi, h = 0) = U_{\rm hill}(\varphi) = M^2\varphi^2/2 \ , \tag{4.28}$$

which is the same as $U_0(\varphi)$ in Eq. (4.12), and the masses are also given similarly

$$m_\varphi^2 = M^2, \quad m_h^2 = -3\alpha\xi M^2\varphi, \tag{4.29}$$

where the latter is exactly the same as that in JF as expected, providing the source of tachyonic instability since $m_h^2 < 0$. On the other hand, the behaviors of φ and h in the regime $\varphi < 0$ are simply oscillating in the only one valley $h_{\rm v0} = 0$ with masses given respectively as

$$m_\varphi^2 = M^2 \ , \quad m_h^2 = 3\alpha\xi M^2|\varphi| \ , \tag{4.30}$$

which is partly shown in previous section.

These expressions are useful for the analytic estimate of the dynamics in the preheating stage, which will be studied subsequently. Note that in both cases $m_h^2 \gg m_\varphi^2$ holds for early reheating unless $\xi \lesssim 1$.

4.2.1 Conditions for Tachyonic Instability

During inflation, the scalaron and the Higgs field slowly roll down the potential along the valley described by the lower of Eq. (2.145) in $\varphi > 0$ regime driving the quasi-exponential expansion of the Universe. After the end of inflation, the two fields oscillate around the global minimum $(\varphi, h) = (0, 0)$ and start to reheat the Universe. At the first stage of preheating, scalaron φ climbs up the valley described by Eq. (2.146) in $\varphi < 0$ regime while the Higgs h rapidly oscillates around its origin with small amplitude. The spike preheating during this half-period of φ has already been studied in Sec. 4.1, finding that the efficiency is negligible. After that, the scalar fields come back to the global minimum and encounter the bifurcation point in the

Higgs direction that gives the distinctive feature in the evolution of the system, as seen in Fig. 2.2.

Without fine-tuning in the model parameters (which is referred to as "usual" cases below), the two scalar fields again enter one of the valleys in $\varphi > 0$ regime with small and rapid oscillations in the Higgs direction as pointed out in Ref. [41, 139][48]. It is easy to see from Eqs. (4.27) and (4.30) that $\varphi(t)$ is slowly oscillating around the origin with two discrete frequencies M and $\tilde{M}$ in the regimes $\varphi < 0$ and $\varphi > 0$, respectively. This shows the hierarchy between the frequencies of scalaron and Higgs during the oscillation period, as mentioned earlier.

Remarkably, as pointed out in Ref. [50], if the model parameter is chosen carefully, the Higgs field can keep $h \simeq 0$ when the scalaron evolves from negative to positive field value, i.e. the inflaton climbs up the hill in $\varphi > 0$ regime. Consequently, the Higgs field feels tachyonic instability during this period, which is the main topic in this section. Note also that the Toda-Brumer necessary criterion [188, 189] for the appearance of classical global dynamical chaos in the background field evolution $\det ||U_{,\varphi h}|| < 0$ is fulfilled in this regime.

Figures 4.6 show four examples of the field evolution obtained numerically. These figures are obtained by solving the full homogeneous equations of motion and Friedmann equation without any small field approximation. The upper panels show a realization of the "usual" cases. They clearly show that even when the inflation takes place with $h > 0$, the Higgs field can develop both positive and negative field values at the first oscillation of the scalaron during reheating. The lower panels show the hill-climbing case with fine-tuning. In the most fine-tuned case, it is possible to climb down to the origin $h = 0$ without falling into the potential valleys during the period when $\varphi > 0$. In a less fine-tuned case, due to the tachyonic instability of the Higgs field, the system falls into one of the potential valleys, and the Higgs field oscillates with a relatively large amplitude. Figures 4.7 show the evolution of the mass squared of the Higgs field in the cases of the lower panels in Figs. 4.6. They explicitly show that the Higgs field is tachyonic during the hill-climbing epoch.

The derivation of the condition for hill-climbing is based on the observation of Figs. 4.6. During the first scalaron oscillation in the regime $\varphi < 0$, the Higgs field evolution can be characterized by the number of its oscillations around the origin $h = 0$ and by its final phase when the scalaron comes back to the origin, which is denoted as $t = t_{\text{enter},0}$. As the parameter ξ or M changes continuously, the phase also changes continuously. Exact hill-climbing occurs when the phase is close to a multiple

[48] Similar behaviors are also found in other models [187].

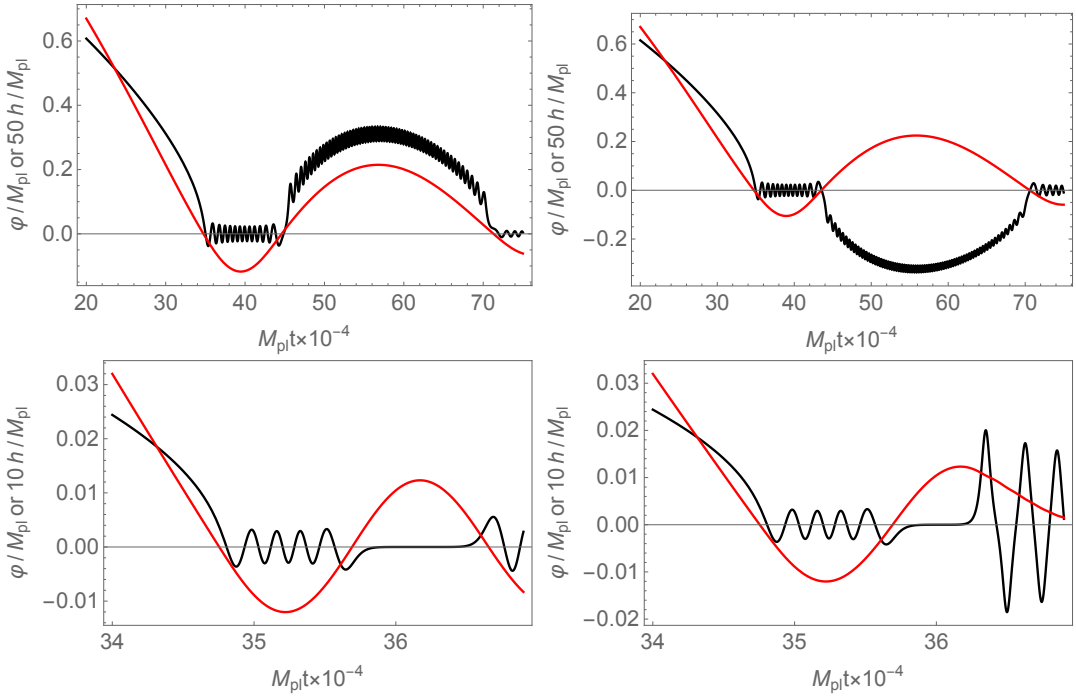

Figure 4.6: Evolution of the scalaron (red) and the Higgs (black) in the post-inflationary epoch. The parameters are chosen as $\lambda = 0.01$ with observational constraint (2.137) satisfied. Upper left: $\xi = 4000$. The Higgs enters the valley with positive Higgs field value. Upper right: $\xi = 4100$. The Higgs enters the valley with negative Higgs field value. Lower left: $\xi \simeq \xi_{N=9}$ where ξ_N is defined in Eq. (4.36). Higgs stays on the "hill" during the whole period of $\varphi > 0$. Lower right: $\xi = \xi_{N=9}(1-\epsilon)$ where $\epsilon \sim \mathcal{O}(10^{-12})$. Higgs exits the tachyonic regime halfway. Note that in order to obtain such fine-tuned evolution numerically, a 16-digit or more precision of ξ is needed, but the values themselves do not have any meanings since other parameters that are determined by observations do not have such a high precision.

of π. Therefore, the parameter is related to the number of oscillations of the Higgs field during the period when $\varphi < 0$. The frequency (or mass) of the Higgs oscillation and the time duration of the scalaron being in the regime $\varphi < 0$ can be estimated with Eq. (4.30) as

$$\Delta t_{\rm osc} \simeq \frac{1}{2}\frac{2\pi}{M} = \frac{\pi}{M} \ , \quad m_h^2 = 3\alpha\xi M^2|\varphi(t)| \ , \tag{4.31}$$

which is closely related to the width of spikes in the mass of the longitudinal mode of the gauge bosons. Strictly speaking, the mass of the Higgs field during this period is time-dependent, but here it is useful to introduce a numerical constant of order of unity, C_{m_h}, to estimate the averaged Higgs mass during the part of its oscillation when $\varphi < 0$ as

$$\overline{m_h} = M(3\xi\alpha)^{1/2}\langle|\varphi(t)|^{1/2}\rangle_{\rm ave} = C_{m_h}M(3\xi\alpha|\varphi_1|)^{1/2} \ , \tag{4.32}$$

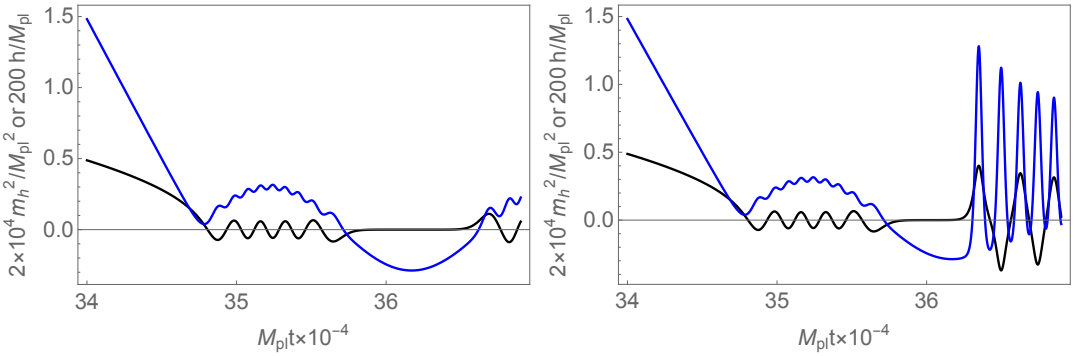

Figure 4.7: Time evolution of the mass squared of the Higgs field $m_h^2 \equiv U_{,hh}$ (blue) along with the Higgs field evolution (black). The parameters are the same as the lower panels of Fig. 4.6. Left: Higgs field stays on the "hill" during the whole period of $\varphi > 0$. Right: Higgs field exits the tachyonic regime halfway.

where the highest point at $\varphi_1(< 0)$ after the first zero-crossing is given in Eq. (4.15). As a result, the evaluation of the accumulated phase of the Higgs field oscillation during this period is simply $\overline{m_h}\Delta t_{\rm osc} = \pi C_{m_h}(3C_1\xi\tilde{M}/M)^{1/2}$. Then, it can be conjectured that the exact hill-climbing of the scalaron after first oscillation happens when the following condition is satisfied

$$N\pi - \Delta\phi = \pi C_{m_h}\sqrt{3C_1\xi\tilde{M}/M}\ , \tag{4.33}$$

where $N \in \mathbb{Z}_+$ represents of the number of half-oscillations of the Higgs field, and $\Delta\phi < \pi$ is a small phase shift needed for the exact hill-climbing. Using Eq. (2.132) and $\tilde{M} = M_c$, the equation above can be rewritten as

$$N = \frac{\Delta\phi}{\pi} + C_{m_h}\sqrt{3C_1\xi}\left(1 - \frac{3}{\lambda}\frac{M_c^2}{M_{\rm pl}^2}\xi^2\right)^{1/4}\ , \tag{4.34}$$

$$= \frac{\Delta\phi}{\pi} + (3\lambda)^{1/4}C_{m_h}\sqrt{C_1\frac{M_{\rm pl}}{M}}\left(1 - \frac{M_c^2}{M^2}\right)^{1/4}\ , \tag{4.35}$$

in terms of ξ and M, respectively. Then, ξ can be solved in terms of N as

$$\xi_N = \sqrt{\frac{\lambda}{6}}\frac{M_{\rm pl}}{M_c}\left[1 \pm \sqrt{1 - \frac{4}{3\lambda C_{m_h}^4 C_1^2}\frac{M_c^2}{M_{\rm pl}^2}\left(N - \frac{\Delta\phi}{\pi}\right)^4}\right]^{1/2}\ , \tag{4.36}$$

where "+" corresponds to the Higgs-like regime while "−" the R^2-like regime. Hereafter, parameters ξ_N and the corresponding $M_N(\xi_N)$ (obtained through Eq. (2.137)) that can realize exact hill-climbing in the first scalaron oscillation are referred to as the "critical parameters". Introducing a new parameter θ as

$$\cos\theta \equiv \xi/\xi_c\ , \quad \sin\theta \equiv M_c/M\ , \quad (0 < \theta < \pi/2)\ , \tag{4.37}$$

so that it satisfies Eq. (2.137), Eq. (4.34) can be rewritten as

$$N = \frac{\Delta\phi}{\pi} + C_{m_h}\sqrt{\frac{3C_1\xi_c}{2}\sin(2\theta)}\ . \tag{4.38}$$

Here $0 < \theta < \pi/4$ covers the Higgs-like regime (including the non-perturbative regime) whereas $\pi/4 < \theta < \pi/2$ covers the R^2-like regime. With this parameterization, two regimes can be treated on the same footing. From Eq. (4.38), the maximal number of the Higgs half-oscillations in the $\varphi < 0$ period is estimated as

$$N_{\rm max} \simeq C_{m_h}\sqrt{3C_1\xi_c/2} \simeq 40C_{m_h}\ , \tag{4.39}$$

in either the Higgs-like and R^2-like regime, that also corresponds to the number of the exact hill-climbing cases in each regime.

With the help of these relations, all the parameters that realize the exact hill-climbing can be found numerically. Figure 4.8 shows the parameter θ and the corresponding number of Higgs half-oscillations during the $\varphi < 0$ period for the exact hill-climbing. It is easy to see that Eq. (4.38) gives a qualitatively good explanation on the appearance of the hill-climbing behavior. The maximal N is numerically found to be $N_{\rm max} = 26$, which is explained by taking $C_{m_h} \simeq 0.64$. Actually, for deep Higgs-like regime $M \gg M_c$, Eq. (4.35) provides a surprisingly simple relation between the consecutive parameters as

$$M_N/M_{N+1} \approx (N+1)^2/N^2\ , \tag{4.40}$$

while similarly, Eq. (4.34) leads to

$$\xi_N/\xi_{N+1} \approx N^2/(N+1)^2\ , \tag{4.41}$$

for the parameters in deep R^2-like regime $\xi \ll \xi_c$. Therefore, once a critical parameter is found, the next parameter value for exact hill-climbing can be identified easily through these relations.

Note that would the cosmic expansion and coupling between the scalaron and the Higgs field be neglected, so that scalaron oscillations become harmonic and those of the Higgs field quasi-harmonic with the adiabatically changing frequency $m_h(t) \propto |\varphi(t)|^{1/2}$, an estimate of the numerical constant C_{m_h} would be obtained as $C_{m_h} = \pi^{-1}\int_0^\pi \sqrt{\sin x}\, dx = 4\pi^{-1/2}\,\Gamma(3/4)/\Gamma(1/4) \approx 0.7628$ - not a bad approximation. However, the θ parameters for the exact hill-climbing in Fig. 4.8 are calculated with much greater precision.

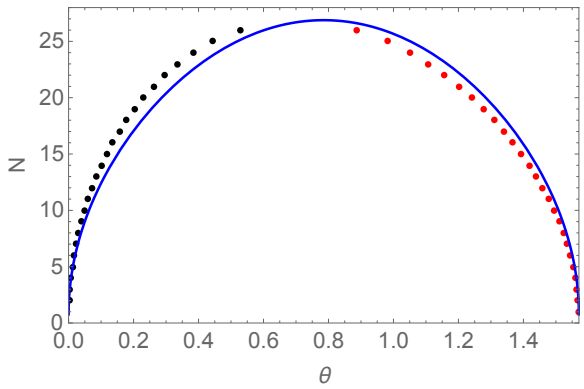

Figure 4.8: The value, N, of the number of the Higgs field half-oscillations during the $\varphi < 0$ period for each exact hill-climbing case. The black dots are critical parameters in Higgs-like regime (Branch 1) and the red for R^2-like (Branch 2). All the parameters θ that realize the exact hill-climbing have their corresponding N. The blue line represents the relation Eq. (4.38) with $C_{m_h} = 0.64$ and $\Delta\phi = 2.4$.

In Fig. 4.8, the critical parameters for the exact hill-climbing present to be classified into two branches corresponding to the Higgs-like and R^2-like regimes. They will be referred to as Branch 1 and Branch 2, respectively. Accordingly, these critical parameters will be labeled as θ_N^i (or M_N^i, ξ_N^i) with $i = 1, 2$ being the label for each branch from now on. Based on the distribution of these parameters, it is also convenient to describe the system with M_N^1 (or $(M_N^1)^{-1}$) for Branch 1 and ξ_N^2 for Branch 2. In Branch 1, as $(M_N^1)^{-1}$ increases, N goes from 1 to 26, and in Branch 2, as ξ_N^2 increases, N goes from 1 to 26. In the former case, the small number of Higgs oscillations for a smaller $(M_N^1)^{-1}$ is due to the small $\Delta t_{\rm osc}$. In the latter case, the small number of Higgs oscillations for a smaller ξ_N^2 results from the small m_h even with large $\Delta t_{\rm osc}$. Note that parameters with $N < 8$ in Branch 1 lie within the strongly-coupled regime with Eq. (2.121) and will not be considered any further. So far, all the parameter values that realize the exact hill-climbing have been found. By definition, they lead to full tachyonic instability of the Higgs after the second zero-crossing of φ. In the following, the efficiency of such instability is estimated and examined to see whether preheating can be completed within the first scalaron oscillation solely by this effect.

4.2.2 Efficiency of Tachyonic Preheating

The calculation of the efficiency of the tachyonic instability in the exact hill-climbing case is presented here to study the possibility of completing preheating by this phenomenon. Parameters are then chosen to be the critical parameters that realize such

cases. The caveat here is that backreaction is not taken into account, as mentioned previously, and hence the results given here do not reflect the exact evolution of the system but give an estimate on whether or not the energy density of the produced particles can be comparable to that of the background. In particular, it is not examined whether the energy density of the homogeneous field oscillation completely disappears or whether the produced particles are thermalized. It is assumed that once the energy density of the produced particles becomes comparable to that of the whole system, backreaction is significant enough to drain the remaining oscillation energy into particles, and the system approaches the thermal state.

4.2.2.1 Equation of Motion for Higgs Perturbation

As the first step, the evolution of fluctuations around the homogeneous background of the scalaron and the Higgs field is investigated. The linearized equations of motion for the fluctuation of scalaron $\delta\varphi_k$ and Higgs δh_k in the Fourier space are given by Eqs.(C.12) and (C.13) in Appendix C. At this moment, the discussion focuses on the physical Higgs field (and scalaron), and neglects the phase direction of the Higgs field or the gauge fields which will be briefly discussed later. Redefining two new fields $\delta\tilde{\varphi}_k \equiv a^{3/2}\delta\varphi_k$ and $\delta\tilde{h}_k \equiv a^{3/2}\delta h_k$ to remove the Hubble friction terms, the equations of motion become

$$\begin{aligned}
&\delta\ddot{\tilde{\varphi}}_k + \left(k_p^2 + U_{,\varphi\varphi} - \frac{\alpha^2}{2}e^{-\alpha\varphi}\dot{h}^2 - \frac{9}{4}H^2 - \frac{3}{2}\dot{H}\right)\delta\tilde{\varphi}_k \\
&\qquad = -\alpha e^{-\alpha\varphi}\dot{h}\dot{\delta}\tilde{h}_k + \left(\frac{3\alpha}{2}He^{-\alpha\varphi}\dot{h} - U_{,\varphi h}\right)\delta\tilde{h}_k, \qquad (4.42)\\
&\delta\ddot{\tilde{h}}_k + \left(k_p^2 + e^{\alpha\varphi}U_{,hh} + \frac{3\alpha}{2}H\dot{\varphi} - \frac{9}{4}H^2 - \frac{3}{2}\dot{H}\right)\delta\tilde{h}_k \\
&\qquad = \alpha\left(\dot{\varphi}\dot{\delta}\tilde{h}_k + \dot{h}\dot{\delta}\tilde{\varphi}_k\right) - \left(\frac{3\alpha}{2}H\dot{h} + \alpha e^{\alpha\varphi}U_{,h} + e^{\alpha\varphi}U_{,\varphi h}\right)\delta\tilde{\varphi}_k, \qquad (4.43)
\end{aligned}$$

where the remaining friction terms and the coupling between the two fluctuations are placed on the right hand side. These terms come from the non-canonical kinetic term and off-diagonal elements in the mass matrix.

Although, in principle, the full mode equations (4.42) and (4.43) can be solved numerically, it costs too much to investigate the whole parameter space. Instead, analytical evaluation of the parameter dependence of the efficiency of the tachyonic preheating is conducted. Note that, since $U_{,\varphi\varphi} \simeq M^2 > H^2, |\dot{H}|, \dot{h}^2/M_{\rm pl}^2$, the scalaron field does not experience tachyonic instability. Moreover, since $\dot{h} = U_{,h} = U_{,\varphi h} = 0$ holds in the exact hill-climbing case, the mixing between the scalaron and Higgs fluctuations vanishes. Therefore, the scalaron fluctuations are never amplified during

this period. For this reason, discussion focuses only on the Higgs fluctuation $\delta\tilde{h}_k$ hereafter.

The mode equation for the Higgs fluctuations (4.43) can be further simplified. Since the mixing between Higgs and scalaron fluctuations vanishes as mentioned above, it is safe to omit the terms involving the scalaron fluctuations. Also, after inflation, the background value of $\alpha\varphi$ (and $h/M_{\rm pl}$) are at most $\mathcal{O}(10^{-1})$. Consequently, the non-canonical part of the Higgs kinetic term in Eq. (2.124) does not play any important role as $\exp(\alpha\varphi) \simeq 1$. In addition, the tachyonic mass directly coming from the potential dominates over the other "mass" terms so the latter are neglected in the following arguments. Taking the inequalities $|U_{,hh}| \gg M^2 > \tilde{M}^2 \gtrsim H^2, |\dot{H}|$ into account, the Hubble induced terms are negligibly small compared to the tachyonic mass of the Higgs field. Moreover, from the Friedmann equation (C.6), it can be seen that $H\dot{\varphi} < M_{\rm pl}H^2$. In particular, since the energy density of the system is mostly stored in the potential in late hill-climbing period (when particle production is the most efficient), the following hierarchy should be satisfied $\dot{\varphi}^2 \ll U(\varphi, h) \simeq 3H^2M_{\rm pl}^2$. Thus, the mass term is well approximated as $k_p^2 + U_{,hh} = \omega_{h,k}^2$. It can also be seen that the friction term is smaller than the scalaron mass, $|\alpha\dot{\varphi}| < H < M$. Since the time scale of interest is $\sim M^{-1}$, the friction terms can never be important. In summary, the mode equation for the Higgs fluctuations are simplified into the one with a time-dependent tachyonic mass as

$$\ddot{\tilde{\delta h}}_k + \omega_{h,k}^2\tilde{\delta h}_k \approx 0 \ , \quad \omega_{h,k}^2 \equiv k_p^2 + m_h^2 = k_p^2 + U_{,hh} \ , \quad m_h^2 = -3\alpha\xi M^2\varphi(t) \ , \quad (4.44)$$

which is exactly in the same form as the general case shown in Eq. (3.1). Therefore, the technique introduced in Chapter 3 can be used for the analytic investigation of particle production in the following, in particular the one for tachyonic instability in Sec. 3.1.3.2.

4.2.2.2 Tachyonic Higgs Mass for Exact Hill-Climbing

As shown in Chapter 3, given the equation of motion with a time-dependent effective mass, its behavior is crucial for the calculation of particle production. In the exact hill-climbing case, the background field evolution in $\varphi > 0$ can be characterized as follows. First, the scalaron crosses zero from the regime $\varphi < 0$ at $t = t_{\rm enter,0}$, as mentioned previously. Then the scalaron climbs up the potential hill when $\varphi > 0$ with the Higgs field $h \simeq 0$. Once the scalaron reaches the highest point $\varphi = \varphi_2$, it reverses its direction and starts to go down the potential hill, still keeping $h \simeq 0$. Finally, the scalaron crosses zero again at $t = t_{\rm exit,0}$. The duration of this period is

then given by $\Delta t \equiv t_{\rm exit,0} - t_{\rm enter,0}$ and the mass of Higgs m_h^2 becomes tachyonic during $t_{\rm enter,0} < t < t_{\rm exit,0}$. These are the two most important quantities for the estimation of particle production from tachyonic instability, so they will be evaluated analytically in the subsequent discussion.

The scalaron field value at the highest point can be evaluated in the same way as $\varphi_1(< 0)$ in Sec. 4.1. Since the kinetic energy vanishes at the highest point $\varphi_2(> 0)$, the following relation is satisfied

$$U_0(\varphi_2) = C_2^2 U_0(\varphi_1) = C_2^2 C_1^2 U_{\rm inf} \ , \tag{4.45}$$

where a new numerical parameter C_2 is introduced to take into account the energy loss during hill-climbing. Then, it is easy to find that

$$\alpha\varphi_2 = C_2 C_1 M_c / M_N^i \ , \tag{4.46}$$

where $\tilde{M} = M_c$ is taken into account. The evolution of the scalaron is governed by the potential $U(\varphi)_{\rm hill} \simeq (M_N^i)^2\varphi^2/2$. Thus, the duration of the hill-climbing can be evaluated by half period of the scalaron oscillation around the origin, $\Delta t \simeq \pi/M_N^i$, which is the same as $\Delta t_{\rm osc}$ in the previous subsection. The time evolution of the scalaron during the exact hill-climbing is approximated as

$$\varphi(t) \simeq \varphi_2 \sin\left(\pi \frac{t - t_{\rm enter,0}}{\Delta t}\right) = \frac{C_2 C_1}{\alpha}\frac{M_c}{M_N^i} \sin\left(\pi \frac{t - t_{\rm enter,0}}{\Delta t}\right) \ . \tag{4.47}$$

Combining this with Eq. (4.29), the tachyonic Higgs mass squared is obtained as

$$m_h^2 \simeq -m_{h,\rm max}^2 \sin\left(\pi \frac{t - t_{\rm enter,0}}{\Delta t}\right) \ , \tag{4.48}$$

where $m_{h,\rm max}$ is the absolute value of the Higgs mass at φ_2 given as

$$m_{h,\rm max}^2 = |U_{,hh}|_{\varphi=\varphi_2,h=0} = 3C_2C_1\xi_N^i M_N^i M_c = 3C_2C_1\xi_c M_c^2 \cot\theta_N^i \ , \tag{4.49}$$

$$\simeq \begin{cases} \sqrt{3\lambda} C_2 C_1 M_{\rm pl} M_N^1 \ , & \text{for Branch 1,} \\ 3C_2C_1M_c^2\xi_N^2 \ , & \text{for Branch 2.} \end{cases} \tag{4.50}$$

It is easy to find $m_{h,\rm max}^2/M_N^{i2} = (3/2)C_2C_1\xi_c \sin(2\theta_N^i)$, which, according to Eq. (4.38), implies that the absolute value of the Higgs mass at φ_2 is larger than (or at least comparable to) the scalaron mass for the exact hill-climbing case. This is the source of efficient particle production through tachyonic instability.

By solving the full background equations of motion numerically, the scalaron field value at the highest point φ_2 is estimated for each exact hill-climbing case as far as

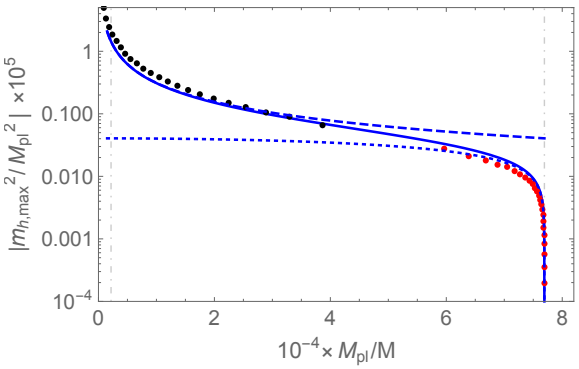

Figure 4.9: Absolute value of the Higgs mass squared at the highest point $\varphi = \varphi_2$ in the exact hill-climbing case for $M = M_N^1$ (black) and $M = M_N^2$ (red). The solid line shows Eq. (4.49) with $C_1 = 0.25$ and $C_2 = 0.72$. The dashed and dotted lines show the asymptotic formula for Branch 1 and 2 in Eq. (4.50), respectively. The left dot-dashed boundary is the unitary bound while the right is $\xi = 0$.

the numerical precision allows. The results confirm that the analytical estimation of the highest point of the scalaron (4.46) and its time evolution (4.47) works well. Figure 4.9 shows that the absolute value of the Higgs mass squared at φ_2 obtained from numerical calculation is well fit by taking $C_2 \simeq 0.72$ in Eq. (4.49). Note that this value is even closer to the rough estimate $C_{m_h} \approx 0.7628$ obtained in the previous subsection neglecting the cosmic expansion and coupling between the scalaron and the Higgs field than to the numerical value of C_{m_h} itself.

It is easy to see that the tachyonic mass is much stronger in the Higgs-like regime than in the R^2-like regime, which is considered natural for the following reason. According to Eq. (4.23) or Eq. (4.29), the amplitude of m_h^2 is proportional to ξ that decreases and vanishes as the system approaches the R^2-limit where there is no tachyonic effect as well-known. On the other hand, the duration Δt is proportional to M^{-1} which, instead, increases when getting closer to the R^2-limit. As a result, the Higgs field can stay in the tachyonic regime for a longer time in R^2-like regime than Higgs-like. So, up to this point, it still seems difficult to determine the dependence of the strength of instability on the model parameter M within each branch, which will be clarified with more careful calculation in the following. However, as a naive expectation, the system with critical parameters should experience a stronger tachyonic effect in the Higgs-like regime than R^2-like as a whole.

4.2.2.3 Particle Production Through Tachyonic Instability

Based on the previous analysis on the equation of motion and effective mass for the Higgs field, the particle production through tachyonic instability during exact hill-

climbing can be investigated analytically. Since the tachyonic mass squared changes from 0 to $-m_{h,\max}^2 = -3C_2C_1\xi_c M_c^2 \cot\theta_N^i$, modes with the wavenumber $k_p < m_{h,\max}$ feels the instability, and the number of particles for such modes is exponentially amplified. Assuming that particle production is not efficient when $\omega_{h,k}^2$ is positive[49], the comoving occupation number of Higgs particles n_k with moving momentum k can be estimated at the time when the scalaron comes back to the origin as in Eqs. (3.98) and (3.102).

Before taking these results for granted, it should be verified that there exists a regime around $t_{\rm enter}(k)$ and $t_{\rm exit}(k)$ where the adiabatic condition (3.79) and the validity of Taylor expansion (3.88) are satisfied simultaneously, based on which the expression for occupation number n_k in the case of tachyonic particle production is derived. In the specific situation considered here, $t_{\rm enter}(k)$ and $t_{\rm exit}(k)$ are the moments when $\omega_{k,h}(t)$ crosses zero and the mode k enters and exits the tachyonic regime, respectively, and naturally $t_{\rm enter}(0) = t_{\rm enter,0}$ and $t_{\rm exit}(0) = t_{\rm exit,0}$. The examination is performed for the regime around $t = t_{\rm enter}(k)$ in the following, which can be easily extended to the $t = t_{\rm exit}(k)$ case. With Eq. (4.48) and $\Delta t \simeq \pi/M$, the frequency of $\tilde{\delta h}$ is written as

$$\omega_{h,k}^2 = k_p^2 + m_h^2 \approx k_p^2 - m_{h,\max}^2 \sin\left[M(t - t_{\rm enter,0})\right] \ . \tag{4.51}$$

Note that $m_{h,\max} > M$ is satisfied for $\sin 2\theta \gtrsim \xi_c^{-1}$, which is the case of interest, (close to) the exact hill-climbing cases. The dominant contribution to the energy density of the produced particles is expected to come from the modes with $k_p^2 \lesssim m_{h,\max}^2$ and $m_{h,\max}^2 - k_p^2 \sim m_{h,\max}^2$. The modes with $m_{h,\max}^2 - k_p^2 \ll m_{h,\max}^2$ do not have a long time for the tachyonic period so Ω_k does not become so large. For modes with $k_p^2 \ll m_{h,\max}^2$, the energy carried by each mode is not so large to give dominant contributions to the total energy density. On the one hand, the left hand side of Eq. (3.79) is expanded with respect to $(t - t_{\rm enter}(k))$ as

$$\left| \frac{\ddot{\omega}_{h,k}/\omega_{h,k} - 3\dot{\omega}_{h,k}^2/(2\omega_{h,k}^2)}{2\omega_{h,k}^2} \right| \simeq \frac{5}{16M\sqrt{m_{h,\max}^4 - k_p^4}} |t - t_{\rm enter}(k)|^{-3} \ , \tag{4.52}$$

[49] Of course, particle production from parametric resonance can happen even when $\omega_{h,k}^2$ is positive with the Higgs oscillation. However, since it takes $\gtrsim \mathcal{O}(10^2)$ oscillations for parametric resonance to amplify the particles as suggested from the Higgs inflation case [31, 32] (note that these studies do not include the spike contribution as mentioned in Sec. 3.2, though), it is expected that the tachyonic instability is stronger if it takes place. Note that the present purpose is to identify if the tachyonic instability alone can complete preheating, so other particle production channels are not considered.

where $\dot{a}$ is omitted since the cosmic expansion is negligible within the time scale of this dynamics. For the modes with $k_p \sim m_{h,\max}$, the adiabatic condition reads

$$|t - t_{\rm enter}(k)| \gg (m_{h,\max}^2 M)^{-1/3} \ . \tag{4.53}$$

On the other hand, from the first inequality of Eq. (3.88), the asymptotic expansion of the Airy function is valid for

$$|t - t_{\rm enter}(k)| \gg \left(\sqrt{1 - \frac{k_p^4}{m_{h,\max}^4}}\, m_{h,\max}^2 M\right)^{-1/3} \sim (m_{h,\max}^2 M)^{-1/3} \ , \tag{4.54}$$

while from the second inequality of Eq. (3.88) the linear approximation of the potential is found to be valid for

$$|t - t_{\rm enter}(k)| \ll 2M^{-1}\sqrt{\frac{m_{h,\max}^4}{k_p^4} - 1} \sim M^{-1} \ . \tag{4.55}$$

Therefore, from Eqs. (4.53), (4.54), and (4.55), it can be easily seen that there indeed exists such a regime where it is permissible to use the matching condition before and after the non-adiabatic period around $t = t_{\rm enter}(k)$ for the case of interest, i.e. $m_{h,\max} > M$ and $k_p \sim m_{h,\max}$, as performed in Sec. 3.1.3.2. In other words, it is safe to use the conclusion given in Eqs. (3.98) and (3.102). The occupation number for modes with momentum k at $t = t_{\rm exit,0}$ is then calculated as

$$n_k(t_{\rm exit,0}) \simeq \left|e^{\Omega_k} - e^{-\Omega_k}/4\right|^2 \simeq e^{2\Omega_k} \ , \quad \Omega_k \equiv \int_{t_{\rm enter}(k)}^{t_{\rm exit}(k)} |\omega_{h,k}(t)| dt \ . \tag{4.56}$$

The comoving energy density of the produced particles at $t = t_{\rm exit,0}$ is then as follows

$$\rho_{\delta h}(t_{\rm exit,0}) = \int \frac{d^3k}{(2\pi)^3}\omega_{h,k}(t) n_k(t)\bigg|_{t=t_{\rm exit,0}} = \int \frac{d^3k}{(2\pi)^3}\frac{k}{a(t)}\left|e^{\Omega_k} - \frac{e^{-\Omega_k}}{4}\right|^2\bigg|_{t=t_{\rm exit,0}} \ . \tag{4.57}$$

As a rough estimate, focus on the typical mode $k_t/a(t_{\rm exit,0}) \simeq m_{h,\max}/2$. Consequently, the exponent can be approximated as $\Omega_{k_t} \sim m_{h,\max}\Delta t$ (by omitting the time dependence of m_h^2 and offset k^2 in $\omega_{h,k}^2$) and the resulting energy density can be estimated as $\rho_{\delta h} \sim m_{h,\max}^4 \exp(2\Omega_{k_t})/32\pi^2 \sim m_{h,\max}^4 \exp(2m_{h,\max}\Delta t)/32\pi^2$. Substituting for θ_N^i using $m_{h,\max}\Delta t \simeq 2\pi N$ and Eqs. (4.38) and (4.49), it is easy to find that

$$\begin{aligned}
\rho_{\delta h}(t_{\rm exit,0}) &\sim \frac{9\xi_c^2 M_c^4 \cot^2\theta_N^i}{32\pi^2}\exp\left(\pi\sqrt{6\xi_c \sin(2\theta_N^i)}\right) \\
&\sim \frac{\exp(2\pi N)}{32\pi^2} \times \begin{cases} 9\lambda^2 (M_{\rm pl}/N)^4 \ , & \text{for Branch 1} \ , \\ (N\tilde{M})^4 \ , & \text{for Branch 2} \ , \end{cases}
\end{aligned} \tag{4.58}$$

where in the second approximation $\Delta\phi$ is omitted and $C_{m_h} = C_1 = C_2 = 1$ is taken for simplicity. It is interesting to see that the exponential amplification is larger for larger N in both branches while the resultant particle production is more effective for Branch 1 as a whole due to larger $m_{h,\max}$. This is consistent with our naive expectation that the tachyonic preheating is more effective in the Higgs-like regime. It is also a bit surprising to see that the tachyonic amplification of Higgs fluctuation can happen even in relatively deep R^2-like regime. This is because the scalaron mass is smaller for the R^2-like regime, which leads to a longer duration of exact hill-climbing and thus efficient particle production against the smaller tachyonic Higgs mass.

In order to see if the tachyonic preheating is strong enough to complete preheating, comparison between the energy density of the produced particles and the background energy density is needed, with the latter given as

$$\rho_{\rm tot} \simeq C_2^2 C_1^2 U_{\rm inf} = \frac{3C_2^2 C_1^2}{4}\tilde{M}^2 M_{\rm pl}^2 \ . \tag{4.59}$$

If the former, calculated without taking backreaction into account, is larger than $\rho_{\rm tot}/2$, the tachyonic preheating is efficient enough and the backreaction cannot be neglected any further. This condition is regarded as the completion of preheating in the discussion of tachyonic preheating in this thesis. Figure 4.10 shows $\Omega \equiv \ln\bigl(32\pi^2\rho_{\delta h}/m_{h,\max}^4\bigr)/2$, which corresponds to our analytical estimation on the effective amplification factor Ω_{k_t}, together with $\ln\bigl(16\pi^2\rho_{\rm tot}/m_{h,\max}^4\bigr)/2$ for each exact hill-climbing case as functions of N for both branches. The latter represents the smallest exponential growth factor needed for preheating to be completed. Here, the value of φ_2 is numerically obtained (see Fig. 4.9) to determine the coefficient in $m_h^2(t) = -3\alpha\xi_N M_N^2\varphi_2 \sin(M(t - t_{\rm enter,0}))$ and $\rho_{\delta h}$ is evaluated by integrating Eqs. (4.56) and (4.57).

It can be seen in Fig. 4.10 that the values of Ω in Branch 1 are very close to those in Branch 2 with corresponding N, as predicted in Eq. (4.58), and they are fit well with $\Omega \simeq \pi N - 2$. By comparing Ω and $\ln\bigl(16\pi^2\rho_{\rm tot}/m_{h,\max}^4\bigr)/2$, whether preheating is completed can be determined. In the Higgs-like regime (Branch 1), the tachyonic instability always completes preheating for the exact hill-climbing case, which is because the characteristic energy density $m_{h,\max}^4/32\pi^2$ without the exponential amplification itself is already as large as the background energy density. On the other hand, due to small $m_{h,\max}^4/32\pi^2$ in the R^2-like regime (Branch 2), preheating is not completed by the tachyonic instability even in the exact hill-climbing case for $N \leq 4$. However, thanks to the long enough Δt at sufficiently large N, preheating is completed by the tachyonic instability for the exact hill-climbing case. Note that $N = 4$ looks on the

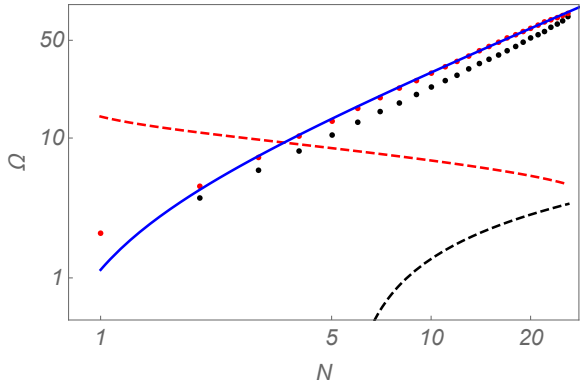

Figure 4.10: Rough estimate of the exponential amplification factor Ω for each exact hill-climbing case. Numerical results for Branch 1 (black dots) and Branch 2 (red dots) are fitted well with $\Omega \simeq \pi N - 2$ (blue line), which is consistent with Eq. (4.58). The black and red dashed lines represent $\ln\left(16\pi^2\rho_{\rm tot}/m_{h,\rm max}^4\right)$ for Branch 1 and Branch 2, respectively. Tachyonic instability is efficient enough to complete preheating for any N in Branch 1, but not for $N \leq 4$ in Branch 2.

edge of the completion of preheating, but the analysis in Fig. 4.10 is relatively qualitative and should not be taken at face value. Indeed, as long as the current numerical precision allows, no parameter space is found in which tachyonic instability completes preheating around θ_4^2. As will be seen later, at least a fine-tuning much more severe than $\mathcal{O}(10^{-5})$ is needed around this value of N.

More accurate analytical calculation also leads to conclusion that agrees with the discussion above. Safely neglecting the cosmic expansion, Ω_k is calculated for a general k and ξ by assuming that the inflaton can always climb up the hill exactly as

$$\begin{aligned}
\Omega_k &= \int_{t_{\rm enter}(k)}^{t_{\rm exit}(k)} |\omega_{h,k}(t)| dt = \int_{t_{\rm enter}(k)}^{t_{\rm exit}(k)} \left| k^2 - m_{h,\rm max}^2 \sin[M(t - t_{\rm enter,0})] \right| dt \\
&= 4\sqrt{3C_2C_1} \left(\frac{\lambda}{3}\right)^{1/4} \sqrt{\frac{M_{\rm pl}}{M}} \left(1 - \frac{M_c^2}{M^2}\right)^{1/4} f\left(\frac{k^2}{m_{h,\rm max}^2}\right) \\
&\approx \begin{cases} 4\sqrt{3C_2C_1}\sqrt{\xi}\, f_E\left(\dfrac{k^2}{m_{h,\rm max}^2}\right) , & \xi \ll \xi_c \ \text{ or } \ M \simeq M_c \ , \\ 4\sqrt{3C_2C_1}\left(\dfrac{\lambda}{3}\right)^{1/4} \sqrt{\dfrac{M_{\rm pl}}{M}}\, f_E\left(\dfrac{k^2}{m_{h,\rm max}^2}\right) , & \xi \lesssim \xi_c \ \text{ or } \ M \gg M_c \ , \end{cases}
\end{aligned} \tag{4.60}$$

where $k \leq m_{h,\rm max}$ and $f_E(x) \equiv (1-x)^{1/2} E[\arccos(x)/2, 2/(1-x)]$ is defined on the domain $0 < x < 1$ with $E[\phi, x] = \int_0^\phi (1 - x\sin^2 t)^{1/2} dt$ is the elliptic integral of the second kind. It can be shown that the function $f_E(x)$ can be well approximated simply by $\tilde{f}_E(x) = 0.6(1-x)$ in the domain of interest, so $\tilde{f}_E(x)$ will be used to

simplify the calculation below. As a result, the number density of produced particles is given by

$$n_k \simeq e^{2\Omega_k} = \exp\left[8\sqrt{3C_2C_1}\left(\frac{\lambda}{3}\right)^{1/4}\sqrt{\frac{M_{\rm pl}\xi}{M\xi_c}} \times 0.6\left(1-\frac{k^2}{m_{h,\max}^2}\right)\right] . \tag{4.61}$$

Taking the numerical values $C_1 = 0.25$ and $C_2 = 0.72$ and the typical value $\lambda = 0.01$ in the equation above leads to

$$n_k = \exp\left[0.85\sqrt{\frac{M_{\rm pl}\xi}{M\xi_c}}\left(1-\frac{k^2}{m_{h,\max}^2}\right)\right] . \tag{4.62}$$

With the help of this result, the comoving energy density of produced particles $\rho_{\delta h}$ can be easily found out as a function of M for Branch 1 and of ξ for Branch 2 as follows

$$\begin{aligned}
\rho_{\delta h} &= \int \frac{d^3k}{(2\pi)^3}\,\omega_{h,k}n_k \simeq \frac{m_{h,\max}^4}{2\pi^2}\int_0^1 k^3 \exp\left[0.85\sqrt{\frac{M_{\rm pl}\xi}{M\xi_c}}\,(1-k^2)\right]dk \\
&\simeq 3.4\times10^{-5}M_{\rm pl}M^3\frac{\xi}{\xi_c}\left[\exp\left(0.85\sqrt{\frac{M_{\rm pl}\xi}{M\xi_c}}\right) - 0.85\sqrt{\frac{M_{\rm pl}\xi}{M\xi_c}} - 1\right] \qquad (4.63) \\
&\simeq \begin{cases} 5.9\times10^{-4}M_c^4\xi\left(-1+e^{3.5\sqrt{\xi}} - 3.5\sqrt{\xi}\right) , & \xi \ll \xi_c , \\ 3.4\times10^{-5}M_{\rm pl}M^3\left(-1+e^{0.85\sqrt{M_{\rm pl}/M}} - 0.85\sqrt{\dfrac{M_{\rm pl}}{M}}\right) , & M \gg M_c , \end{cases} \qquad (4.64)
\end{aligned}$$

where $\rho_{\delta h}$ is evaluated by approximating $m_h^2 = 0$ at later times $t > t_{\rm exit,0}$. This result is shown in Fig. 4.11.

With this more accurate analytic investigation, it can be seen that $\rho_{\delta h}$ gets larger than the half of the background energy density $C_1^2\rho_{\rm inf}/2$ for $\xi \gtrsim 50$, meaning the completion of preheating. Conversely, the smallest ξ_N sufficient to complete preheating solely by tachyonic instability is around $\xi_N \simeq 50$ which corresponds to $N = 4$ in Branch 2, which is consistent with the previous conclusion from rough estimation. Therefore, for $N \leq 4$ in Branch 2, preheating cannot be completed solely by tachyonic instability within the first scalaron oscillation.

Thus far, the analysis has been for the physical Higgs only, but the effect on the longitudinal modes of the weak gauge bosons or the NG modes can be evaluated in a similar way as mentioned earlier. Their contribution to the preheating process is estimated to be comparable with that of the Higgs field. Here, a brief discussion is presented on the tachyonic instability in the phase direction for the global U(1) case.

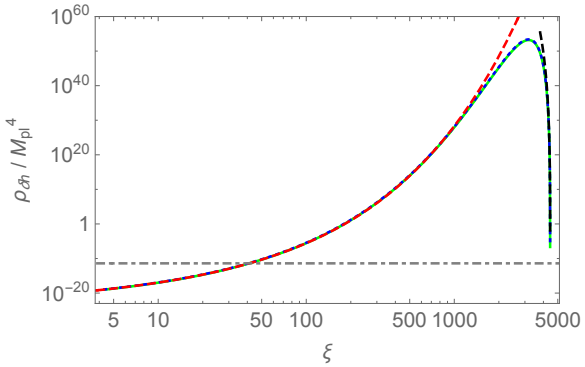

Figure 4.11: The energy density of produced Higgs fluctuations as a function of ξ for $5 < \xi < \xi_c$. Light green: $\rho_{\delta h}$ calculated with the precise function $f_E(x)$ in Ω_k in Eq. (4.60). Blue dotted: $\rho_{\delta h}$ in Eq. (4.63) with approximated $\tilde{f}_E(x)$. Red dashed and black dashed lines are asymptotic behavior in $\xi \ll \xi_c$ and $M \gg M_c$ limits in Eq. (4.64), respectively. Gray dotted-dashed: $C_1^2 \rho_{\rm inf}/2$.

The implication to the SM SU(2)$_L\times$ U(1)$_Y$ case can be read off as done in Sec. 4.1. Note that the tachyonic instability for the longitudinal mode of the weak gauge boson is observed in Ref. [50].

As calculated in Eq. (4.9) the effective mass for the canonicalized NG mode, during the hill-climbing epoch (when $\varphi < M_{\rm pl}, h \simeq 0$, and the kinetic terms are negligible), $m_{\theta_c}^2$ can be further simplified as

$$m_{\theta_c}^2 \simeq -\frac{1}{\sqrt{6}}\frac{M^2}{M_{\rm pl}}(1+6\xi)\varphi \ . \tag{4.65}$$

Therefore, comparing with the physical Higgs mass (Eq. (4.29)), it is easy to find that

$$\frac{m_{\theta_c}^2}{m_h^2} = 1 + \frac{1}{6\xi} \ , \tag{4.66}$$

which is of order unity unless $\xi \ll 1$. Since the smallest ξ_N^i is no less than the order of unity as seen in Eq. (4.34), the efficiency of tachyonic instability for the NG mode is concluded to be comparable to that for the physical Higgs fluctuations. The same is expected to apply to the longitudinal mode of gauge bosons, whose mass receives a dominant contribution from the mass of the NG mode [34].

While the mass for physical Higgs fluctuations around the potential valley is positive, the mass for the phase direction is given by

$$m_{\theta_c}^2 \simeq -\frac{\alpha}{2}\varphi\tilde{M}^2 + \frac{5}{24}\frac{1}{M_{\rm pl}^2}\left(\dot{\varphi}^2 + \dot{h}^2\right) \tag{4.67}$$

for $\varphi \ll M_{\rm pl}$, which can be tachyonic, especially when the kinetic energy is small. Therefore, the NG mode and the longitudinal mode of gauge bosons are more likely

to receive a tachyonic contribution from field oscillations around the potential valley than from physical Higgs fluctuations, which is also seen in Ref. [50]. However, the amplitude of the tachyonic mass is comparable to the time scale of the oscillations around the valley. Hence, it is expected that such tachyonic instability for the NG mode and the longitudinal mode of gauge bosons do not give a significant contribution compared to the particle production during the hill-climbing. Tachyonic mass of the physical Higgs could also be realized during oscillations around the valleys with a large amplitude, but for the same reason, such effect is expected to be relatively small. A detailed investigation will not be presented in this thesis.

As a brief summary, the NG mode and the longitudinal mode of gauge bosons also experience tachyonic instability during hill-climbing with almost the same efficiency as the physical Higgs fluctuations. Therefore, taking into account their contributions, the total particle production will be enhanced accordingly. However, since the tachyonic particle production is an exponential effect, the basic results shown previously remain quantitatively unchanged even if the enhancement is taken into account.

To conclude this part, a rough estimate of the duration of preheating in the exact hill-climbing case can be given, except for $N \leq 4$ in Branch 2 and $N \leq 7$ in Branch 1. Here, it is assumed that the radiation-dominated epoch starts right after the completion of preheating, and the scalar field oscillation will not dominate the Universe again. As mentioned above, the tachyonic effect occurs within one scalaron oscillation after the end of inflation. Then from Eq. (4.27) and (4.30), there is an upper bound of duration for each critical case[50]

$$\Delta t_{\rm pre} \simeq \pi \left(\frac{2}{M} + \frac{1}{2M_c} \right) \ . \tag{4.68}$$

In such a short period, the Hubble parameter is approximately constant and given as $H \sim C_1 C_2 M_c/2$. As a result, the number of e-folds for tachyonic effect to complete preheating is estimated as

$$\Delta N_{\rm pre} \simeq H \Delta t_{\rm pre} \sim C_1 C_2 \pi \left(\frac{1}{4} + \frac{M_c}{M} \right) \ , \tag{4.69}$$

where $0.03 \lesssim M_c/M \leq 1$ for $0 \leq \xi \leq \xi_s$. Therefore, the e-fold number of preheating is very small $0.2 \lesssim \Delta N_{\rm pre} \lesssim 0.7$ which can be regarded as almost instantaneous in cosmological sense but varies around 0.5 with respect to the change of model

[50] As will be shown shortly, preheating can be completed by tachyonic instability even for a duration shorter than one scalaron oscillation.

parameters. On the other hand, similar to Eq. (3.115), through the following relation

$$k = a_k H_k = \frac{a_k}{a_{\rm end}} \frac{a_{\rm end}}{a_{\rm pre}} \frac{a_{\rm pre}}{a_0} a_0 H_k \tag{4.70}$$

where $a_{\rm pre}$ denotes the scale factor at the end of preheating (here the onset of radiation-dominated epoch is assumed to be the end of preheating), the number of e-folds of inflation is calculated as

$$\begin{aligned} N_{\rm inf}(k) =& \ln\left(\frac{a_0 M_{\rm pl}}{k}\right) + \ln\left(\frac{a_{\rm end}}{a_{\rm pre}}\right) + \ln\left(\frac{a_{\rm pre}}{a_0}\right) + \ln\left(\frac{H_k}{M_{\rm pl}}\right) \\ =& \ln\left(\frac{a_0 M_{\rm pl}}{k}\right) - \Delta N_{\rm pre}(\theta) + \ln\left[\frac{T_0}{T_{\rm pre}}\left(\frac{g_0}{g_{\rm pre}}\right)^{1/3}\right] + \ln\left(\frac{M_c}{2M_{\rm pl}}\right) \end{aligned} \tag{4.71}$$

where, again, it is assumed that thermalization after preheating is realized almost instantaneously and the total entropy is conserved between the end of thermalization and today. The inflation scale $H_k \simeq M_c/2$ because it is effective R^2-inflation. The effective number of relativistic species at the end of preheating simply takes the value $g_{\rm pre} = 106.75$ while $T_{\rm pre}$ is the temperature at the end of preheating which can be estimated by

$$\frac{g_{\rm pre}\pi^2}{30} T_{\rm pre}^4 \approx \frac{3}{4} C_1^2 C_2^2 M_{\rm pl}^2 M_c^2 \tag{4.72}$$

which gives $T_{\rm pre} \approx 1.7 \times 10^{28}$ K. Using the pivot scale as before $k/a_0 = 0.002$ Mpc^{-1}, it is not difficult to find that

$$N_{\rm inf} \simeq 59 - \Delta N_{\rm pre}(\theta) \tag{4.73}$$

which is shown in Fig. 4.12. Compared with the prediction of the Starobinsky model $N_{\rm inf} \simeq 54$ given in last chapter[51], the resulting $N_{\rm inf}$ for the exact hill climbing is larger, which can be used to distinguish them once the experimental accuracy is high enough to distinguish $\delta N \sim 5$. On the other hand, if further distinction among parameters for the exact hill climbing is desired, an accuracy at least up to $\Delta N \sim \mathcal{O}(0.1)$ is necessary. Note that this argument is based on the assumption that the Universe becomes radiation-dominated right after the completion of preheating, which does not apply if the rescattering and backreaction prevent the system from entering the radiation domination instantaneously.

[51] The difference in $N_{\rm inf}$ between JF and EF exists, but it is of the order of the next order correction to the slow-roll approximation which is taken into account here. Therefore, the difference between the two frames will be neglected.

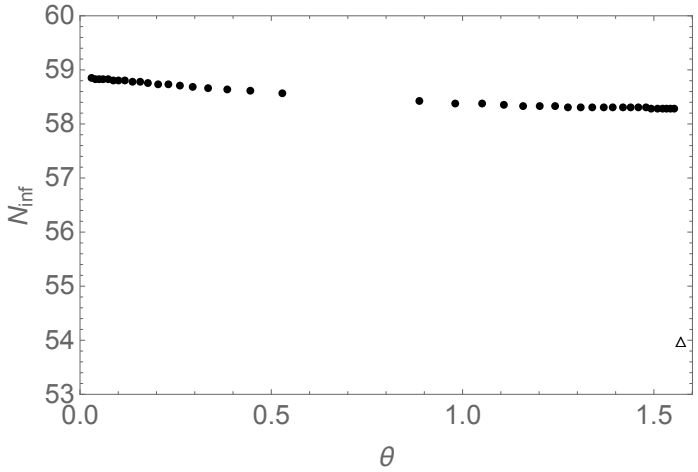

Figure 4.12: The number of e-folds of inflation with pivot scale $k = 0.002$ Mpc^{-1} for the exact hill-climbing parameters that are out of strongly-coupled regime and can complete preheating solely by tachyonic instability. The triangle represents the prediction of the Starobinsky model.

4.2.3 Necessary Degree of Fine-Tuning

In the previous subsection, the exact hill-climbing cases are studied, which requires model parameters extremely close to the critical ones θ_N^i (or ξ_N^i, M_N^i) to realize fully efficient tachyonic instability. However, once they deviate from these values, the Higgs field does not exactly go along the hill but falls to the valley in the middle of going uphill (or downhill), resulting in the termination of the tachyonic particle production. Then, the maximal deviation from the exact hill-climbing allowed for the tachyonic instability to be still sufficiently effective to complete preheating characterizes how much fine-tuning among the model parameters is necessary to produce the Higgs fluctuations whose energy density is comparable to the background. From Fig. 4.10 (or 4.11), comparing the amplification factor for the exact hill-climbing and the necessary amplification factor to complete preheating, it is natural to expect that weaker fine-tuning is required for smaller N in Branch 1 while the necessary fine-tuning is more severe for smaller N in Branch 2. This expectation is natural in the sense that the tachyonic effect is weaker for R^2-like limit because it is well-known that there is no such effect in the Starobinsky model. In the following, a quantitative study of the required amount of fine-tuning to complete preheating is presented.

First of all, note that the actual dynamics of the scalaron and Higgs in the non-exact hill-climbing case are too complicated to be described analytically. Just as the exact hill-climbing cases where the actual trajectory is not always along $h = 0$ in the $\varphi > 0$ regime, especially around $t_{\rm enter,0}$ and $t_{\rm exit,0}$, Eq. (4.47) is used as an

approximation by assuming that $h = 0$ is satisfied as long as $\varphi > 0$. Fortunately, it is shown that it serves as an appropriate simplification so that analytical analysis can be carried out. In the present case, i.e. deviating from critical parameters θ_N^i, the Higgs field leaves the origin at some "unknown" moment between two zero-crossing points of the scalaron, which becomes even more difficult for analytical description. Certainly, the "unknown" moment should be determined by the parameter choice, but the specific dependence requires too much effort that may not be necessary at this moment. Therefore, combining analytical and numerical methods can be a reasonable choice for the investigation.

The following simplifications on the scalar field dynamics are adopted. Since the falling down from the hilltop to the valley is driven by the tachyonic mass squared of $\mathcal{O}(m_{h,\max}^2)$, the time scale of this dynamics is much smaller than the whole dynamics of the hill-climbing $\Delta t \sim M^{-1}$. Therefore, the time evolution for $\varphi(t)$ can be approximated as

$$\varphi(t) \simeq \varphi_2 \sin(M(t - t_{\text{enter},0})) \ , \quad h(t) \simeq 0 \ , \quad \text{for} \quad t_{\text{enter},0} < t < t_{\text{drop}} \ , \tag{4.74}$$

where t_{drop} is the time when the Higgs field falls down to the potential valley. The scalar fields oscillate around the potential valley after $t = t_{\text{drop}}$ [50]. However, since the tachyonic instability is typically stronger than the parametric resonance (see footnote 49) and lasts sufficiently long, particle production during this epoch is simply neglected here. It is expected that the true amount of the particle production is not much different from our following estimate.

Practically, the following procedure is adopted in the study. The evolution of the scalaron $\varphi(t)$ and the Higgs field $h(t)$ is obtained by solving the full background equations of motion (C.6), (C.7), and (C.8) numerically. Then the mass for the Higgs fluctuation is evaluated as

$$m_h^2(t) = e^{\alpha\varphi(t)} U_{,hh}(\varphi(t), h(t)) \ . \tag{4.75}$$

Here, the conformal factor $e^{\alpha\varphi(t)}$ is recovered just for slight improvement. With this treatment, it is found that the tachyonic mass for the Higgs fluctuation almost follows the case of exact hill-climbing until t_{drop}, and then gets shut off almost instantly. Figure 4.13 shows a schematic sketch of the time evolution. Omitting the other contributions in the mode equation (4.43) as well as particle production after falling down to the valley, the occupation number of the Higgs fluctuation at late times is evaluated as

$$n_k = |\exp(\Omega_k) - \exp(-\Omega_k)/4|^2, \quad \Omega_k \equiv \int_{t_{\text{enter}}(k)}^{t_{\text{drop}}(k)} \sqrt{m_h^2(t) - k_p^2}. \tag{4.76}$$

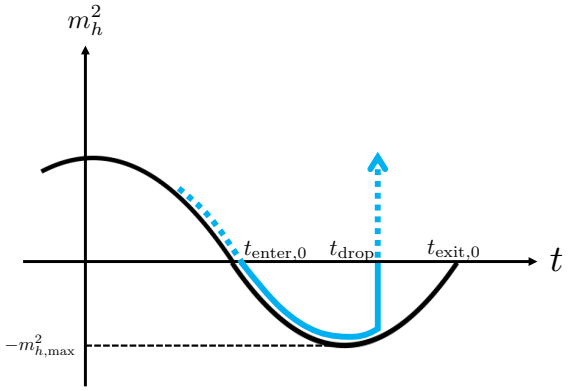

Figure 4.13: Schematic picture of the time evolution of the mass squared of the Higgs fluctuation. Blue: evolution of m_h^2 for non-exact hill-climbing. Black: evolution of m_h^2 for exact hill-climbing as comparison. The tachyonic mass for the Higgs fluctuation almost follows the exact hill-climbing case until $t = t_{\mathrm{drop}}$ and then gets shut off almost instantly.

Here in the numerical calculation, a k-dependent drop-off time, $t_{\mathrm{drop}}(k)$, is defined as the time when $\omega_k^2(t)$ crosses zero. With these simplifications, the comoving energy density of the produced Higgs fluctuation is numerically calculated when its mass becomes sufficiently small as follows[52]

$$\rho_{\delta h} = \int_0^{m_{h,\mathrm{max}}} \frac{d^3k}{(2\pi)^3} k n_k \ , \tag{4.77}$$

where cosmic expansion is neglected and the scale factor is normalized to be unity $a = 1$. Analytical estimation of $\rho_{\delta h}$ and discussion about t_{drop} is given in Appendix C in Ref. [51] by assuming t_{drop} to be free parameter, which will not be shown here.

By imposing a conservative criterion,

$$\rho_{\delta h} \gtrsim U_0(\varphi_1)/2 = C_1^2 U_{\mathrm{inf}}/2 \ , \tag{4.78}$$

together with Eq. (4.77), the parameter range around each exact hill-climbing case θ_N^i that gives sufficient amount of particle production can be identified. Define the upper and lower bound of the parameter θ around θ_N^i for successful preheating as θ_{N+}^i and θ_{N-}^i, respectively, as well as $\Delta\theta_{\mathrm{eff},N}^i \equiv \theta_{N+}^i - \theta_{N-}^i$. In order to express the degree of fine-tuning quantitatively, a new quantity $\Delta\theta_N^i$ that describes the typical

[52] For a practical purpose, $k = m_{h,\mathrm{max}}/100$ is taken as the lower limit of the integration in numerical calculation.

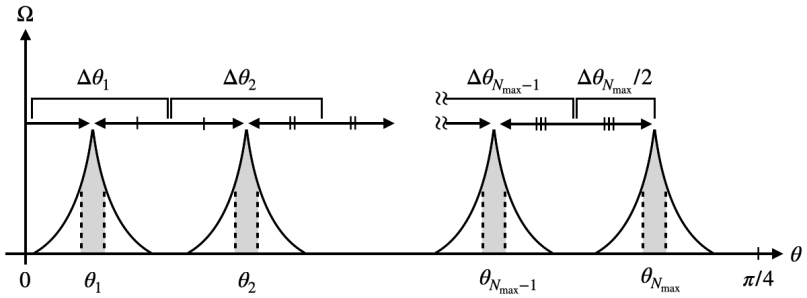

Figure 4.14: Definition of the effective width of each θ_N, $\Delta\theta_N$. Gray bands: the parameter region where the preheating successfully finishes in one stroke.

distance between two neighboring values of θ_N^i is needed, which is defined as

$$\Delta\theta_N^i \equiv \frac{\theta_{N+1}^i - \theta_{N-1}^i}{2} \quad \text{for} \quad N = 2, 3, \cdots N_{\max} - 1,$$
$$\Delta\theta_1^1 \equiv \frac{\theta_1^1 + \theta_2^1}{2}, \quad \Delta\theta_1^2 \equiv \frac{\pi}{2} - \frac{\theta_1^2 + \theta_2^2}{2}, \quad \Delta\theta_{N_{\max}}^i = \left|\theta_{N_{\max}}^i - \theta_{N_{\max}-1}^i\right|, \tag{4.79}$$

with $N_{\max} = 26$. See Fig. 4.14 for a schematic picture of these definition. As a result, the degree of fine-tuning for the N-th exact hill-climbing case in Branch i is defined as $\Delta\theta_{\text{eff},N}^i/\Delta\theta_N^i$.

Based on these analytic formulation, the following numerical analysis is carried out. Scan the parameter θ around each critical parameter θ_N^i, and solve the background equations of motion (C.6), (C.7), and (C.8) for each value of θ. With these results, the occupation number n_k in Eq. (4.76) and the energy density of the Higgs fluctuation produced through the tachyonic instability in Eq. (4.77) is calculated. The criterion (4.78) helps to determine the boundary values of θ for successful preheating θ_{N+}^i and θ_{N-}^i, and the required degree of fine-tuning $\Delta\theta_{\text{eff},N}^i/\Delta\theta_N^i$. The result is shown in Fig. 4.15, which is the main result of the investigation of tachyonic preheating in the mixed Higgs-R^2 inflation model in this thesis. It can be seen that only $\mathcal{O}(10^{-1})$ fine-tuning is required for smaller N in Branch 1, which is because the typical Higgs mass squared is large for these cases and a relatively small amplification factor Ω_k is enough for the successful preheating as seen in Fig. 4.10. As θ gets closer to $\pi/2$ (for larger N in Branch 1 and for smaller N in Branch 2), the necessary fine-tuning becomes more severe. For the most severe case, $N = 5$ in Branch 2, a fine-tuning of $\mathcal{O}(10^{-5})$ is needed. This result can be understood intuitively that a larger θ (smaller ξ) corresponds to smaller tachyonic Higgs mass $|m_h^2|$ during hill-climbing (see Fig. 4.9), and hence the Higgs field needs to stay at the hilltop for a longer period in order to have a stronger tachyonic effect, which naturally requires more fine-tuning and is consistent with the expectation from Fig. 4.10. Although the analysis here is based on

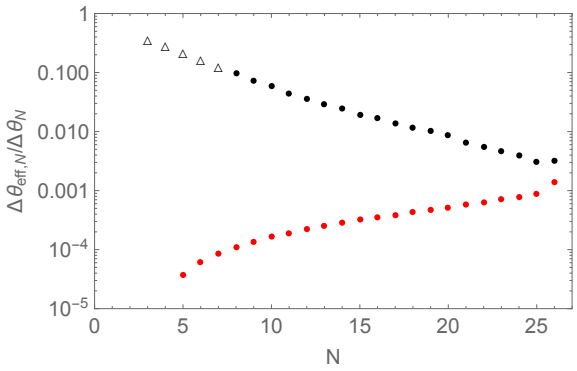

Figure 4.15: Necessary degree of fine-tuning $\Delta\theta^i_{\mathrm{eff},N}/\Delta\theta^i_N$ for the successful tachyonic preheating for Branch 1 (black) and 2 (red). The five black empty triangles are for the cases beyond the unitarity bound. In Branch 2, the data points for $N \leq 4$ do not exist because the tachyonic preheating is not efficient even for the exact hill-climbing trajectories. The sudden lift for $N = 26$ comes from the definition of $\Delta\theta^i_{N_{\max}}$ in Eq. (4.79): the interval $\Delta\theta^i_N$ increases as N increases, and hence $\Delta\theta^i_{N_{\max}} = \left|\theta^i_{N_{\max}} - \theta^i_{N_{\max}-1}\right|$ underestimates the width around $\theta^i_{N_{\max}}$, which results in the sudden lift.

a relatively simplified formulation, it is expected that the actual degree of fine-tuning obtained by full numerical calculations with the full mode equations (4.42) and (4.43) is not significantly different from this results, because the exponential amplification of the Higgs particles takes place when the background Higgs field is climbing up the hill along $h \simeq 0$.

Before concluding this section, some issues in the above analysis should be mentioned. The numerical calculation above starts from ~ 1 e-fold before the end of inflation while using the inflationary attractor as the lower of Eqs. (2.145) corresponding to the large number of e-folds during inflation as the initial condition. If an earlier moment during inflation is chosen to start the computation using the same initial condition, the face values of ξ^i_N might appear slightly different from those shown above because numerical errors accumulate with calculation time. Correspondingly, the numerical initial condition corresponding to the attractor should be formulated with much better accuracy. At the same time, it is more and more challenging to find the exact value of ξ^i_N when beginning the computation from a larger number of e-folds before the end of inflation. From this point of view, it is argued here that a slight change of the face values of ξ^i_N for numerical calculations scanning different numbers of inflationary e-folds does not mean that the presented results depend on the choice of initial conditions. Moreover, estimating the degree of fine-tuning is independent of the precision of ξ^i_N, so the main results are robust in this respect.

In this section, a study of the tachyonic preheating in the mixed Higgs-R^2 inflation model is presented based on Ref. [51]. Although some degree of fine-tuning is necessary for this preheating mechanism to work, the resulting dynamics in the Universe can be interesting.

The analytic conditions for the tachyonic instability of physical Higgs fluctuations to occur are derived by investigating the Higgs field oscillations around the potential valley in the negative scalaron regime $\varphi < 0$. All the critical parameters θ^i_N which can realize exact hill-climbing of scalaron are found numerically, providing the condition for the most efficient particle production. Beyond the results in Ref. [50], it is pointed out here [51] that tachyonic preheating can take place in both Higgs-like regime $\xi \lesssim \xi_c$ (Branch 1) and R^2-like regime $M \gtrsim M_c$ (Branch 2). Analytic calculation of particle production from the tachyonic instability shows that, for all these fine-tuned parameter points, tachyonic particle production is strong enough to complete preheating except for $N \leq 4$ in Branch 2. However, successful tachyonic preheating in this model requires some degree of fine-tuning among the model parameters. Even a slight deviation from $\theta = \theta^i_N$ can significantly reduce the strength of the tachyonic effect. In order to estimate the necessary degree of fine-tuning, detailed scan over model parameters is performed around each θ^i_N to find the interval $\Delta\theta^i_{\mathrm{eff},N}$ such that the preheating can be completed within $\theta \sim \theta^i_N \pm \Delta\theta^i_{\mathrm{eff},N}/2$. The main result is given in Fig. 4.15, which shows that the necessary fine-tuning becomes more severe as ξ gets smaller (closer to the R^2-limit). This result is natural because no tachyonic effect is expected in the Starobinsky model.

While the main focus is on the amplification of physical Higgs fluctuations instead of those in the phase direction or longitudinal gauge bosons, it is found that the amplification of the latter is comparable to that of physical Higgs fluctuations by investigating their effective mass, which suggests that the efficiency of the total particle production is enhanced by a factor of the order of unity, but the results above should remain basically unchanged, and the required fine-tuning can be read off from Fig. 4.15.

Throughout the analysis in this section, the backreaction from produced particles on the homogeneous background is not taken into account. The main interest here lies in the growth of inhomogeneities until their energy becomes comparable to that of background inflaton oscillations. As for the standard criterion for the end of reheating, it is defined as the onset of the radiation-dominated epoch where the contributions from the homogeneous background fields, i.e. the correlated quantum particles with zero spatial momentum in quantum language, become negligible. To

determine whether the particles produced by the tachyonic instability are relativistic and all the energy in the homogeneous fields is transferred to inhomogeneities requires considering the backreaction, which is beyond the investigation here. There are two possibilities expected. One is that, after a complete tachyonic period, the amplitude of the coherent oscillation of the background fields becomes very small (so do the masses of the produced particles), and the produced particles are relativistic with typical momentum $k \sim |m_{h,\max}|$. In this case, the preheating is almost instantaneous and thermalization comes afterward. The other possibility is that the backreaction terminates the tachyonic instability midway and rescattering between perturbations and background fields (turbulence) begins to take effect. In this case, however, the preheating takes a longer time. Specifically, elastic (re)scattering that conserves the number of particles is insufficient for reheating and thermalization. Deeply inelastic scatterings with specially engineered initial conditions that increase the energy of particles at the cost of a decrease of particle number are needed for this purpose. Without such special conditions, a natural hypothesis is that the final reheating temperature $T_{\rm pre}$ cannot be larger than the initial momenta of particles coming from the background before rescattering, i.e. $k/a_e \geq T_{\rm pre}$. As a conservative estimation, if the momentum of the produced particles is estimated as

$$\frac{k^2}{a_e^2} = |m_h^2|_{\varphi=\varphi_2} = \left| 3\xi M^2 C_1 C_2 \frac{M_c}{M} \right| \ , \tag{4.80}$$

and the reheating temperature

$$T_{\rm pre} = \left(\frac{90 C_1^2 C_2^2}{4 g_{\rm pre} \pi^2} M_{\rm pl}^2 M_c^2 \right)^{1/4} \ , \tag{4.81}$$

the following condition is obtained

$$M \gtrsim \sqrt{1 + 0.67 \left(\frac{0.01}{\lambda} \right)} M_c \tag{4.82}$$

which corresponds to $\xi \gtrsim \xi^{i=2}_{N=26}$ for $\lambda = 0.01$. Based on this hypothesis, the result means that for R^2-like regime, the instantaneous preheating by rescattering is not possible. Finally, in the case where preheating is not sufficient, late-time domination of scalar field oscillation is possible and perturbative decay is needed to finish reheating, which will be shown in next section based on Ref. [53].

In addition, the current discussion focuses on the period right after the second zero-crossing of scalaron φ after the end of inflation, during hill-climbing of the scalaron along the potential hill at $h \simeq 0$. The possibility of having the tachyonic effect after

a number of scalaron oscillations (in the presence/absence of the one studied here) is not addressed [50]. Indeed, to consider subsequent oscillations, other channels of particle production during field oscillations around the potential valley and possible backreaction from produced particles (by early tachyonic instability or other channels) should be involved because they can be too important to neglect. Besides, as the amplitude of scalaron oscillation decays with time as the Universe expands, the tachyonic effect from later oscillations is expected to be weaker than the one studied in this section, so it is more difficult for them to complete preheating compared with the latter.

A lattice simulation of preheating in this model for R^2-regime is performed in Ref. [52], which can take into account the rescattering between produced particles and background. Those results are not in conflict with the results shown in this section and the expectations mentioned above, although the tachyonic instability occurs in later scalaron oscillations instead of the first. However, lattice calculation still cannot capture all the possible effects, for example, the perturbative decay of the background field and produced particles that may affect the rescattering process. This issue will also be discussed later based on Ref. [53].

4.3 Perturbative Reheating

The preheating process in the mixed Higgs-R^2 inflation model has been investigated in detail in preceding sections. At the first stage of preheating, the non-adiabatic change of effective mass of NG modes is inefficient to significantly affect the whole reheating process due to the presence of the R^2 term. Right after that, a possible preheating channel appears, i.e. tachyonic instability experienced by the physical Higgs and the longitudinal mode of gauge bosons, which can be extremely efficient depending on the choice of model parameters. In EF, this is due to a bifurcation point around the global minimum of the two-dimensional scalar potentials. The quantitative understanding of the conditions for the occurrence of tachyonic instability as well as its efficiency and the necessary degree of fine-tuning is obtained by the analytical and numerical calculation in the last section, showing that the critical parameters that realize efficient tachyonic preheating appear in both Higgs- and R^2-like regimes. To complete preheating solely by the tachyonic instability appearing in the first scalaron oscillation, $\sim \mathcal{O}(10^{-1}) - \mathcal{O}(10^{-2})$ fine-tuning is needed for the Higgs-like regime while a much severe one $\sim \mathcal{O}(10^{-3}) - \mathcal{O}(10^{-5})$ is required, which suggests that efficient tachyonic preheating is not easy to realize, especially in R^2-like regime. Moreover,

the backreaction from the produced particles is not considered in previous sections, which is possible to terminate the tachyonic instability midway. Therefore, subsequent non-tachyonic mechanisms should be involved to continue the reheating process of the Universe in the case of insufficient preheating.

In the lattice simulation carried out in Ref. [52], the tachyonic preheating is studied by taking into account the backreaction from the produced particles as a classical rescattering effect between the homogeneous background and the inhomogeneous modes in the R^2-like regime. The strength of the rescattering also depends on the model parameter, getting stronger for more Higgs-like parameters and weaker for more R^2-like choices. After a few hundreds of scalaron oscillations, it was found that some fraction of the homogeneous background can remain apart from the relativistic particles. Since radiation is redshifted much faster than the homogeneous background field by cosmic expansion, it is expected that the homogeneous part can once again dominate the Universe and finally decay away perturbatively. The observation indicates a possibility that the reheating temperature T_r may only be determined by the final perturbative process regardless of the details of preheating, which further motivates the investigation of perturbative reheating at the late time. As will be shown later, the perturbative decay not only plays a role at the late time but may reduce the strength of the rescattering process in the middle of preheating.

The following discussion is based on Ref. [53]. First, the perturbative decay rates of the homogeneous scalaron field and Higgs field are calculated and those for the inhomogeneous Higgs. Then, the role of perturbative decay is studied during and after tachyonic preheating in the mixed Higgs-R^2 inflation model. In the latter case, the perturbative reheating finally determines the reheating temperature and duration, which is discussed when tachyonic preheating is inefficient or simply absent. The investigation focuses on the case $\xi \gg \mathcal{O}(10)$ where the adiabatic approximation is valid to calculate the Higgs decay rate, as will be explained later. For $\xi \lesssim \mathcal{O}(10)$, it is expected to approach the R^2-limit that is well studied in the literature and reviewed in the last chapter.

4.3.1 Decay Rate

The decay rates of scalaron and Higgs are the essential quantities in this section, which will be analyzed in both JF and EF together with the background dynamics, especially the decay rate of scalaron. The last section focuses on the hill-climbing dynamics, i.e. $h = 0$ in both positive and negative scalaron regimes in the EF language. In the following, on the contrary, only the dynamics around the attractor solution are

considered, i.e. $h = h_{\rm v0} = 0$ in $\varphi < 0$ regime while $h = h_{\rm v,\pm}$ in $\varphi > 0$ regime which is given in Eq. (2.145). This case is realized with "non-critical" parameters that, opposite to the critical ones, cannot realize tachyonic instability at the first scalaron oscillation right after the end of inflation.

4.3.1.1 Background Dynamics in Valleys

• **Jordan frame** All the subscripts "J" for JF will be omitted for convenience. Since the effective single-field description fails during reheating, there are two scalar degrees of freedom should be taken care of and the field dynamics deviate from the valleys. Therefore, in the Higgs field, apart from the non-dynamical valley part $h_{\rm v\pm}(t)$ and $h_{\rm v0}$, there is another independent component which, denoted as $h_{\rm osc}(t)$, is defined in the decomposition of $h(t)$ as follows

$$h(t) \approx h_{\rm v}(t) + h_{\rm osc}(t) \ , \tag{4.83}$$

where $h_{\rm v}$ generally denotes the valleys in either positive and negative R regime. Since the direction orthogonal to the valley is much heavier than the valley direction, it is expected that $h_{\rm osc}$ is a small[53] but fast oscillating part (see e.g. Fig. 4.1) satisfying $|h_{\rm v}| \gg |h_{\rm osc}|$ in $R > 0$ (or $\varphi > 0$ in EF) regime. This decomposition and hierarchy break down around the transition moments[54] when R (or φ in EF) crosses zero but that regime is not of main interest here. As a result, the equation of motion for $h_{\rm osc}$ is then given by

$$-\Box h_{\rm osc} + \frac{\partial V_{{\rm eff},h}}{\partial h_{\rm osc}} h_{\rm osc} \approx 0 \ , \tag{4.84}$$

where $V_{\rm eff}$ is given in Eq. (2.127).

On the other hand, rewrite Eq. (2.126) as follows

$$-\Box\tilde{R} + \tilde{M}^2\tilde{R} = -\frac{\dot{h}^2}{M_{\rm pl}^2} + \left(\frac{h^2}{M_{\rm pl}^2} + \frac{3\xi}{\lambda}\frac{\tilde{M}^2}{M_{\rm pl}^2}\right)\left(\lambda h^2 - \xi R\right) \ , \tag{4.85}$$

where $\tilde{R}(t)$ is defined as a combination of $R(t)$ and $h^2(t)$

$$\tilde{R} \equiv R/M^2 + 3\xi h^2/M_{\rm pl}^2 \ . \tag{4.86}$$

[53] When the amplitude of Higgs oscillation is large, the effective mass of Higgs can become tachyonic as explained previously. Since perturbative decay is the main topic here which plays an important role especially at late time when the amplitude of Higgs oscillation *is* small, only small Higgs oscillation is considered here.

[54] Similar situation is considered in Ref. [187].

Focusing on small oscillations of Higgs around the valleys, the Planck-suppressed kinetic term on the right hand side of Eq. (4.85) can be neglected. During $R < 0$, the only attractor is $h = h_{\rm v0} = 0$, so Eq. (4.5) is recovered from Eq. (4.85), giving the same solution for $R(t)$ as Eq. (3.108) in the Starobinsky model, i.e. $\tilde{R}$ behaving as a harmonic oscillator with frequency M, as expected, except that the value of M here can be different from M_c. In $R > 0$ regime, the attractor solution is given as the lower of Eq. (2.128), which results in

$$-\Box\tilde{R} + \tilde{M}\tilde{R} \simeq 0 \ , \tag{4.87}$$

where the combination $(\lambda h^2 - \xi R)$ vanishes due to the valley constraint in the lower of Eq. (2.128) apart from the small deviation due to small Higgs oscillations. It can be seen that $\tilde{R}$ is oscillating with frequency $\tilde{M}$ instead of M. Therefore, the evolution of $\tilde{R}$ is similar to φ in EF (see discussion on φ dynamics in Sec. 4.2), oscillating with two discrete masses depending on the sign of R. This is not coincident, as mentioned once previously in Eq. (4.24), in small field regime $\alpha|\varphi| \gg 1$ which is always valid during reheating,

$$\alpha\varphi \simeq \frac{R}{3M^2} + \frac{\xi h^2}{M_{\rm pl}^2} = 3\tilde{R} \ . \tag{4.88}$$

Actually, this result provides an important observation. Since Higgs field has high-frequency part and $\tilde{R}$ contains a term $\propto h^2$, there, in principle, are high-frequency modes within $\tilde{R}$ but they are not seen in the analysis above (neither in φ as will be shown in the analysis in EF later), which means that these high-frequency oscillations are canceled by that from R (see e.g. Fig. 4.1). More specifically, if $R(t)$ is decomposed into $R = R_{\rm v} + R_{\rm osc}$, the following relation should be satisfied

$$R_{\rm osc} \simeq -6\xi\frac{M^2}{M_{\rm pl}^2}h_{\rm v}h_{\rm osc} \ . \tag{4.89}$$

Applying the relations (2.128), (2.129), and (4.89) to the lower of Eq. (4.84), the equation of motion for $h_{\rm osc}$ then becomes

$$\begin{cases} -\Box h_{\rm osc} - \xi R\, h_{\rm osc} \approx 0 \ , & R < 0 \ , \\ -\Box h_{\rm osc} + 2\xi\dfrac{M^2}{\tilde{M}^2} R\, h_{\rm osc} \approx 0 \ , & R > 0 \ , \end{cases} \tag{4.90}$$

where higher order terms are neglected. According to these equations, the perturbative production of $\delta h(t, \mathbf{x})$ particles due to the oscillating mass $\propto R(t)$ can be calculated easily by the technique introduction in Sec. 3.1. This serves as the dominant channel for scalaron decay.

Again, the resulting decay rate of scalaron into Higgs particles here coincides with that calculated in EF. Actually, for the case with kinetic coupling as in action (2.124), it is more convenient to obtain the decay rate in JF as seen in the calculation in the Starobinsky model in Sec. 3.2, in the sense that the kinetic coupling and the potential coupling in EF should be dealt with separately.

When calculating the decay rate of Higgs, more caution should be taken because the effective mass of the Higgs field is time-dependent, which also leads to the time-dependence of the decay rate. Strictly speaking, a time-dependent decay rate is not always well-defined. Therefore, this study focuses on the adiabatic regime, i.e. the frequency of $h_{\rm osc}$ being much larger than that of scalaron, so that the Higgs mass is approximately constant during each its oscillation. This condition can be achieved with $\xi \gg 1$ which is exactly of main interest here, as mentioned earlier. Large non-minimal coupling also allows a clear separation of $h_{\rm v}$ and $h_{\rm osc}$.

The calculation of the Higgs decay involves more effort than above because Higgs couples with all other fundamental particles in SM. Therefore, more than one decay channels are important and should be taken into account. Not surprisingly, the analysis of Higgs decay is almost the same in JF and EF because the only difference is that some of the interaction terms between Higgs and other matter fields receive a conformal factor $\exp(-2\alpha\varphi)$ from the conformation transformation to EF. This conformal factor is approximately unity in small field limit $\alpha|\varphi| \ll 1$, so it does not affect the results.

In the following, the analysis turns to EF based on Ref. [53].

• **Einstein frame** For simplicity, the subscripts "E" are omitted here. The background analysis here is similar to that in JF. In small field limit, the analysis at the beginning of Sec. 4.2 applies. Especially, the equation of motion for φ can be approximately written as

$$\ddot{\varphi} + 3H\dot{\varphi} + m_\varphi^2 \varphi \approx 0 \ , \tag{4.91}$$

where Planck-suppressed terms are neglected and m_φ is given by

$$m_\varphi^2 = \begin{cases} M^2 & , \varphi < 0 \ , \\ \tilde{M}^2 & , \varphi > 0 \ . \end{cases} \tag{4.92}$$

This is exactly the same as $\tilde{R}$ as expected. Note that when $\xi \lesssim 1800$, the difference between two mass scale is small $(M - \tilde{M})/\tilde{M} \lesssim 10\%$ so φ is basically oscillating with an unchanged frequency. Only when entering the Higgs-like regime, the difference

between M and $\tilde{M}$ is significant. Since the Universe is matter-dominated before the completion of reheating due to the fact that the oscillating scalar field acts as non-relativistic matter, the Hubble parameter is simply $H \approx 2/(3t)$. As a result, Eq. (4.91) can be solved analytically as

$$\varphi(t) = \begin{cases} \tilde{\varphi}_1 \dfrac{\sin(Mt)}{Mt} & , \varphi < 0 \ , \\ \tilde{\varphi}_2 \dfrac{\sin(\tilde{M}t)}{\tilde{M}t} & , \varphi > 0 \ , \end{cases} \tag{4.93}$$

where φ is required to be regular at $t = 0$. The amplitudes $\tilde{\varphi}_1 < 0$ and $\tilde{\varphi}_2 > 0$ are amplitudes determined by initial conditions. The valley part of Higgs $h_{\rm v}$ is then determined by φ through Eq. (4.25). On the other hand, the equation of motion for the Higgs field, neglecting Planck-suppressed terms, is given as

$$\ddot{h}_{\rm osc} + 3H\dot{h}_{\rm osc} m^2_{h_{\rm osc}} h_{\rm osc} \approx 0 \ , \tag{4.94}$$

where the mass term is given as

$$m^2_{h_{\rm osc}} \equiv \begin{cases} -3\xi M^2 \alpha\varphi & , \varphi < 0 \ , \\ 6\xi M^2 \alpha\varphi & , \varphi > 0 \ , \end{cases} \tag{4.95}$$

which can be easily shown to coincide with Eq. (4.90). Obviously, the effective mass of $h_{\rm osc}$ depends on $\varphi(t)$. For $\xi \gg \mathcal{O}(10)$, $m^2_{h_{\rm osc}} \gg m^2_\varphi$ so that Higgs oscillates many times within one scalaron period, while for $\xi \lesssim \mathcal{O}(10)$, they are comparable. Figures 4.16 show two examples where it can be easily seen that the hierarchy of oscillation frequencies between Higgs and scalaron is large for $\xi \gg \mathcal{O}(10)$ while small for $\xi \lesssim \mathcal{O}(10)$. In the former case, adiabatic approximation is valid because scalaron is approximately constant within one Higgs oscillation so analytical solution is easy to find. The adiabatic solution for $h_{\rm osc}$, in the case $\xi \gg \mathcal{O}(10)$, can be solved as

$$h_{\rm osc} = \begin{cases} \dfrac{A_h}{\sqrt{2m_{h_{\rm osc}}}} \cos\left(-2\sqrt{3\xi\alpha|\varphi_a|} E\left[\dfrac{\pi}{4} - \dfrac{Mt}{2}, 2 \right] + \delta_i \right) & , \varphi < 0 \ , \\ \dfrac{A_h}{\sqrt{2m_{h_{\rm osc}}}} \cos\left(-2\sqrt{6\xi\alpha\varphi_a} \dfrac{M}{\tilde{M}} E\left[\dfrac{\pi}{4} - \dfrac{\tilde{M}t}{2}, 2 \right] + \delta_i \right) & , \varphi > 0 \ , \end{cases} \tag{4.96}$$

where A_h and the phase δ_i are determined by the initial conditions, φ_a is the amplitude of φ, and $E[\phi, x]$ is, again, the elliptic integral of the second kind. On the contrary, this approximation breaks down for the latter so analytical description is difficult to find. Therefore, analysis will be given only for $\xi \gg \mathcal{O}(10)$. For $\xi \lesssim \mathcal{O}(10)$, it is expected that the situation quickly approaches to that of R^2-inflation as ξ decreases.

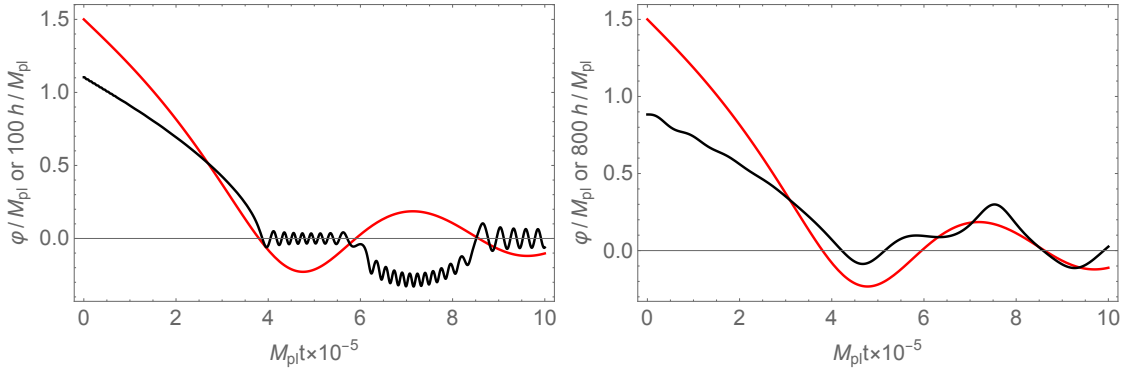

Figure 4.16: Background dynamics of the scalaron (red) and Higgs (black). Left: $(\xi, \lambda) = (1000, 0.01)$. Right: $(\xi, \lambda) = (10, 0.01)$. When $\xi \lesssim \mathcal{O}(10)$, the frequency of the small oscillation of Higgs is comparable with the scalaron frequency so the small oscillations "disappear" on the right panel.

In addition, φ indeed shows no small and fast oscillations upon the oscillation of frequency m_φ, which confirms the results in JF.

Another important issue is the energy distribution between homogeneous scalaron and Higgs. Although the discussion focuses on non-critical parameters that realize small $|h_{\rm osc}|$, it is still possible to have non-negligible effects with different parameter choices. In $\varphi < 0$ regime, most energy is stored in the scalaron. Whenever scalaron changes from negative to positive value during oscillations, some fraction of energy is transferred into the physical Higgs due to the bifurcation point. For parameters close to the critical choices, a larger amplitude of Higgs oscillation around the valley is expected, which implies that a larger amount of energy is transferred from scalaron to Higgs. On the contrary, if the parameter choice is far from the critical case, the amplitude of coherent Higgs oscillation is small, so there is little energy stored in the Higgs background. See Appendix G for more discussion. Later, this observation will play an important role when determining the reheating temperature by perturbative decay.

4.3.1.2 Decay Rate of Higgs and Scalaron

Hereafter, Higgs self-coupling is fixed to $\lambda = 0.01$ for definiteness. In order to estimate the perturbative decay rate of scalaron and Higgs, it is necessary to write down the relevant interaction terms among them and SM particles. See Appendix H for detail. In JF, it is assumed that all SM fields except for Higgs are minimally coupled with gravity. After the conformal transformation to EF, the scalaron couples with these matter fields through the conformal factor that is Planck-suppressed. In the small

φ limit, it can be neglected at the leading order. Therefore, the dominant channel for scalaron is the decay into Higgs particles through the non-minimal coupling term. Of course, it is well-known that such decay exists even when $\xi = 0$, although it is much less efficient than the large ξ case. On the other hand, the Higgs field directly couples with scalaron through the non-minimal coupling and other SM particles such as quarks and weak bosons with large coupling constants, which allows Higgs to decay much more efficiently. In this thesis, the interactions between the gauge sector and the fermion sector are not taken into account because the main goal is to deplete the energy of the homogeneous background.

The calculation will be done in the unitary gauge, as mentioned previously. When the homogeneous Higgs field oscillates around the origin, however, especially at $h = 0$, it is known that the unitary gauge is not well defined. Thus, it may be necessary to work in other well-defined gauges when studying reheating process. Nevertheless, as shown in Ref. [34], crossing $h = 0$ does not spoil the calculation in the unitary gauge. Therefore, the unitary gauge will still be adopted in the following calculation. The derivation of the decay rates for Higgs is presented in Appendix H. The results will be directly used here.

Before proceeding, the notations are clarified as follows. As in Appendix H, the field redefinition $\tilde{W}_\mu^\pm \equiv a^{3/2} W_\mu^\pm$, $\tilde{Z}_\mu \equiv a^{3/2} Z_\mu$, $\tilde{t} \equiv a^{3/2} t$, and $\tilde{b} \equiv a^{3/2} b$ are used to absorb $\sqrt{-g}$ in the decay rate calculation. The decay of Higgs considered here is mainly through two channels, to weak gauge bosons and to top and bottom quarks due to the large coupling constants. The gauge boson channels are only opened in the $\varphi > 0$ regime when the conditions (with $g \approx 0.55$ and $g' \approx 0.42$ evaluated at $\sim 10^{12}$GeV)

$$\xi^2 > \xi_c^2 \left(1 - \frac{2\lambda}{g^2}\right) \equiv \xi_W \simeq 4291 \ , \tag{4.97}$$

$$\xi^2 > \xi_c^2 \left(1 - \frac{2\lambda}{g^2 + g'^2}\right) \equiv \xi_Z \simeq 4347 \ , \tag{4.98}$$

are satisfied for $W^\pm$ and Z respectively, which means that it is allowed only in the deep Higgs-like regime. The decay rates are given by

$$\Gamma_{h\to\tilde{W}\tilde{W}} = \frac{\lambda}{8\pi} \frac{M^3}{\tilde{M}^2} (6\xi\alpha\varphi)^{1/2} \left(1 - \frac{g^2}{2\lambda}\frac{\tilde{M}^2}{M^2} + \frac{3g^4}{16\lambda^2}\frac{\tilde{M}^4}{M^4}\right) \sqrt{1 - \frac{g^2}{2\lambda}\frac{\tilde{M}^2}{M^2}} \ , \tag{4.99}$$

$$\Gamma_{h\to\tilde{Z}\tilde{Z}} = \frac{\lambda}{16\pi} \frac{M^3}{\tilde{M}^2} (6\xi\alpha\varphi)^{1/2} \left(1 - \frac{g^2 + g'^2}{2\lambda}\frac{\tilde{M}^2}{M^2} + \frac{3\left(g^2 + g'^2\right)^2}{16\lambda^2}\frac{\tilde{M}^4}{M^4}\right) \sqrt{1 - \frac{g^2 + g'^2}{2\lambda}\frac{\tilde{M}^2}{M^2}} \ . \tag{4.100}$$

in the adiabatic regime when motion of φ is sufficiently slow in the time scale of the Higgs oscillation. As for the quark channels, they are open for both $\varphi > 0$ and

$\varphi < 0$ regimes. Specifically, the top and bottom quarks are massless during $\varphi < 0$ so the channels are always opened, while during $\varphi > 0$ bottom quark channel is never forbidden due to the small Yukawa coupling y_b but top quark channel should satisfy

$$\xi^2 > \xi_c^2 \left(1 - \frac{\lambda}{y_t^2}\right) \equiv \xi_t^2 \simeq 4351^2 \ , \tag{4.101}$$

where $y_t \approx 0.05$ and $y_b \approx 0.01$ are evaluated at $\sim 10^{12}$GeV. The decay rates in the adiabatic regime are given as follows

$$\Gamma_{h\to\tilde{t}\bar{\tilde{t}}} = \begin{cases} \dfrac{3y_t^2}{16\pi} \left(3\xi\alpha|\varphi|\right)^{1/2} M \ , & \varphi < 0 \ , \\ \dfrac{3y_t^2}{16\pi} \left(6\xi\alpha\varphi\right)^{1/2} M \left(1 - \dfrac{y_t^2}{\lambda}\dfrac{\tilde{M}^2}{M^2}\right)^{3/2} , & \varphi > 0 \ , \end{cases} \tag{4.102}$$

$$\Gamma_{h\to\tilde{b}\bar{\tilde{b}}} = \begin{cases} \dfrac{3y_b^2}{16\pi} \left(3\xi\alpha|\varphi|\right)^{1/2} M \ , & \varphi < 0 \ , \\ \dfrac{3y_b^2}{16\pi} \left(6\xi\alpha\varphi\right)^{1/2} M \left(1 - \dfrac{y_b^2}{\lambda}\dfrac{\tilde{M}^2}{M^2}\right)^{3/2} , & \varphi > 0 \ . \end{cases} \tag{4.103}$$

These expressions are not only applicable for the decay of homogeneous Higgs field but the Higgs particles produced during reheating, which will be discussed later.

As for the scalaron decay [3, 29, 30, 172], the dominant channel is decaying into Higgs particles. According to Eqs. (3.112) and (4.90), the decay rate for scalaron to Higgs particles can be easily found for both $\varphi > 0$ and $\varphi < 0$ regimes. The decay is kinematically allowed only when $\xi \ll 1$ or φ becoming small when it gets close to origin or at very late time, as is shown by

$$\Gamma_{\varphi\to\delta\tilde{h}\delta\tilde{h}} = \begin{cases} \dfrac{3}{16\pi}\dfrac{M^3}{M_{\rm pl}^2}\left(\dfrac{1}{6} + \xi\right)^2 \left(1 - 12\xi\alpha|\varphi|\right)^{1/2} \ , & \varphi < 0 \ , \\ \dfrac{3}{16\pi}\dfrac{\tilde{M}^3}{M_{\rm pl}^2}\left(\dfrac{1}{6} - 2\xi\dfrac{M^2}{\tilde{M}^2}\right)^2 \left(1 - 24\xi\dfrac{M^2}{\tilde{M}^2}\alpha\varphi\right)^{1/2} , & \varphi > 0 \ , \end{cases} \tag{4.104}$$

where $\delta\tilde{h} \equiv a^{3/2}\delta h$ is the redefined Higgs perturbation as in Sec. 4.2. Therefore, the scalaron is expected to play an important role at late time in the determination of the final reheating temperature. The decay during $\varphi < 0$ vanishes when $\xi = -1/6$ as expected, which corresponds to the usual conformally coupled case. However, for $\varphi > 0$ this result does not admit negative non-minimal coupling because the existence of the valleys with finite $|h_{\rm v}|$ is assumed, which is inconsistent with $\xi < 0$. Instead, the decay rate for $\varphi > 0$ vanishes when $\xi \simeq 1/12$. The minimally coupled case $\xi = 0$ does not mean the decay channel is closed. In this case, the results here coincide with

e.g. Refs. [177, 179]. In the case considered here, the 1/6 can actually be omitted because $\xi \gg \mathcal{O}(10)$. Additionally, only when $m_\varphi > 2m_{\delta h} = 2m_{h_{\rm osc}}$, the decay is kinematically allowed, as can be easily seen. In the case where $\xi \gg 1$, the decay process can only occur when $|\varphi|$ becomes sufficiently small, which can be realized in two possible situations. The first one is when φ gets close to the origin during oscillation. The second is at late time when $|\varphi|$ becomes small due to the Hubble expansion and decay of energy through Higgs.

One more concern should be addressed. Decay rates should not exceed the oscillation frequency of the corresponding field, as required by the validity of perturbative calculation. From the expressions above, this requirement for $h \to 2\tilde{W}$ and $h \to 2\tilde{Z}$ simply lead to conservation of the perturbativity condition (2.121). For $y_t < 1$ and $y_b < 1$, the perturbative condition is automatically satisfied as well as this requirement. The same conclusion can be drawn for the scalaron decay rate in $\varphi < 0$ regime. Therefore, from this point of view, the strongly-coupled regime does not mean something terrible but simply perturbative expansion is not valid anymore. However, this is not true for the scalaron decay rate in $\varphi > 0$. Therefore, it is still not clear whether the lower of Eq. (4.104) can really be applied to calculation here. Fortunately, this channel is kinematically forbidden until a very late time which is almost irrelevant for the calculation that will be presented, especially for larger ξ. Therefore, it does not change the conclusion of this section.

4.3.2 Presence of Tachyonic Preheating

The discussion here focuses on the case where strong tachyonic instability occurs at the early stage of preheating and results in an early radiation-dominated era. In this case, the perturbative decay of the background fields will affect the tachyonic preheating in two ways, as shown below. Firstly, the decay of Higgs particles produced by the tachyonic effect can reduce their backreaction strength on the homogeneous background, for example, the rescattering effect considered in Ref. [52]. Secondly, even if the tachyonic preheating and the backreaction can transfer most of the energy from the homogeneous background into relativistic particles, as long as there is some fraction of homogeneous field (mainly scalaron) remains, it will finally dominate the Universe again as it is redshifted by the cosmic expansion in a slower manner than relativistic particles. As a result, perturbative decay eventually determines the reheating temperature regardless of the detail of preheating.

4.3.2.1 During tachyonic preheating

First, how perturbative decay affects the efficiency of the rescattering process between homogeneous and inhomogeneous modes after moderate tachyonic particle production will be discussed. This is a quantum effect that is not considered in the classical lattice simulation in Ref. [52].

As discussed previously, the Higgs particles can efficiently decay into top (and bottom) quarks as the homogeneous Higgs does, especially when $\varphi < 0$, which is seen in Eqs. (4.102) and (4.103). For example, during the first scalaron oscillation,

$$\begin{aligned}\Gamma_{\delta h\to t\bar{t}} = \frac{3y_t^2}{16\pi}\left(3\xi\alpha|\varphi|\right)^{1/2} M \simeq& \frac{3y_t^2}{16\pi}\left(3\xi C_1\frac{M_c}{M}\right)^{1/2} M \ , \\ \simeq& 0.86\times\left(\frac{M^2}{M_c^2}-1\right)^{1/4} M_c > H \simeq 0.12 M_c \ , \end{aligned} \tag{4.105}$$

for $\xi \gtrsim 100$ on which the following discussion will focus (see Figs. 4.17 for two examples)[55]. Focus on the regime $\varphi < 0$ only in the following. The typical time scale of the decay $\delta h \to t\bar{t}$ in the unit of M_c can be calculated as

$$\begin{aligned}\frac{1}{M_c t} \sim M_c^{-1}\overline{\Gamma}_{\delta h\to t\bar{t}} =& \frac{3y_t^2}{16\pi}\overline{\left(3\xi\alpha|\varphi|\right)^{1/2}}\frac{M}{M_c} \ , \\ \approx& \frac{3y_t^2}{16\pi}\sqrt{3C_1}C_{m_h}\left(\frac{\lambda}{3}\right)^{1/4}\sqrt{\frac{M_{\rm pl}}{M_c}}\left(\frac{M^2}{M_c^2}-1\right)^{1/4} \ , \end{aligned} \tag{4.106}$$

where Eq. (4.15) is used as well as $C_{m_h} = 0.64$ in Eq. (4.32) for time-averaged $\sqrt{|\varphi|}$. The result of Eq. (4.106) is shown in Fig. 4.18. Since $C_1 = 0.25$ is only valid for the first scalaron oscillation, $C_1 = 0.005$ is also considered to capture the decay of scalaron amplitude at late time. As can be seen, for most part of the parameter space, the time scale $M_c\Gamma^{-1}_{\delta h\to t\bar{t}}$ is less than ~ 50 scalaron oscillations which is much shorter than the preheating time scale shown in the examples in Ref. [52]. Therefore, the number of Higgs particles that participate in the rescattering process will decrease considerably.

Although the Higgs particles can decay into relativistic particles of other species, these decay products cannot efficiently interact with the homogeneous scalaron because they are coupled only through the conformal factor that is Planck-suppressed. Consequently, it is expected that the efficiency of the preheating process consisting of

[55] Possible reduction of the decay rate $\Gamma_{\delta h\to t\bar{t}}$ is the Lorentz factor if the Higgs particles produced by tachyonic instability are relativistic. However, this depends on the momentum distribution of δh which is determined by the detail of the tachyonic preheating. This is beyond the scope here. If most of the Higgs particles are indeed relativistic, then this decay channel may be neglected.

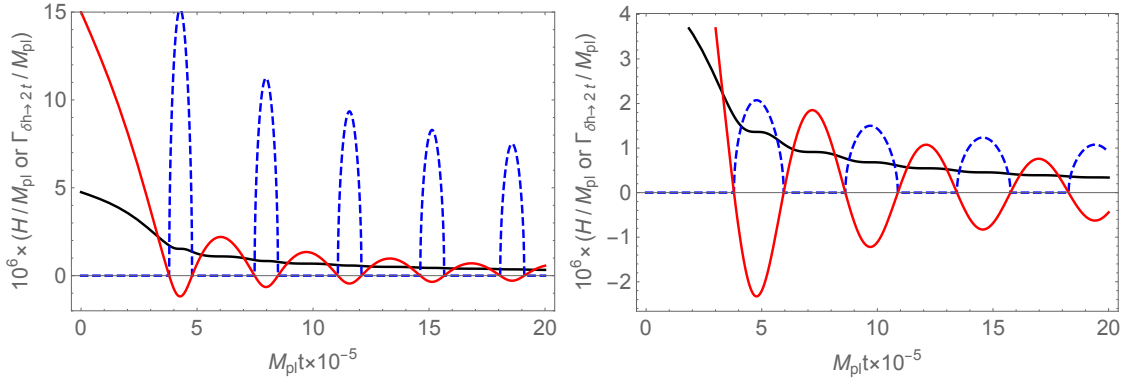

Figure 4.17: Comparison of Hubble scale H (black, solid) and the decay rate $\Gamma_{\delta h\to t\bar{t}}$ (blue, dashed). The evolution of the scalaron (red) is only for reference. Left: $(\xi, \lambda) = (4000, 0.01)$. Right: $(\xi, \lambda) = (200, 0.01)$. The decay rate vanishes when $\varphi > 0$ for the large mass of top quarks from Higgs non-zero vev. Only for $\xi \sim \xi_s$ (see Eq. (4.101)), this channel is allowed during $\varphi > 0$.

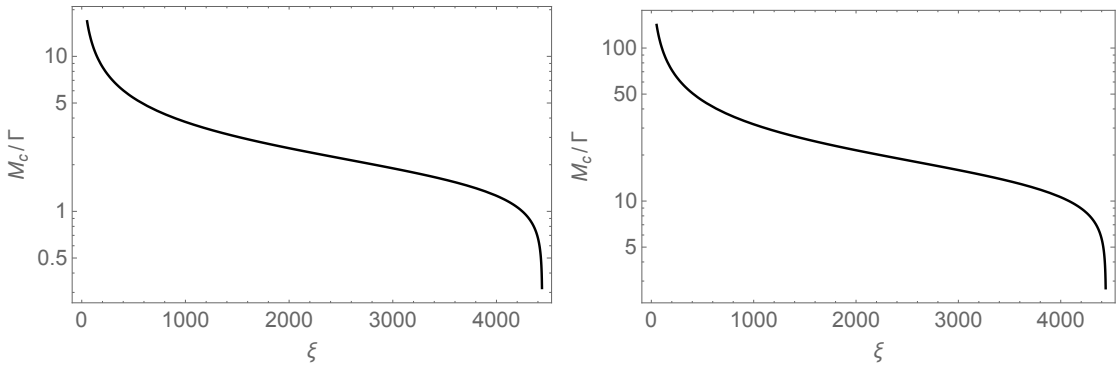

Figure 4.18: Decay time scale of the produced Higgs particles δh into top quarks according to Eq. (4.106). Left: $C_1 = 0.25$. Right: $C_1 = 0.005$.

moderate tachyonic instability and rescattering can receive a non-negligible reduction due to the decay of the produced Higgs particles, which may also allow the perturbative decay process to dominate the last stage of reheating and eventually determine the reheating temperature T_r.

4.3.2.2 After tachyonic preheating

Next, consider the case where a significant amount of energy has already been transferred from the homogeneous background fields to relativistic particles. It is interesting to study whether the homogeneous part can dominate over the radiation at a late time when the preheating processes can no longer significantly increase the energy fraction of the relativistic particles. If the answer is positive, it is also important to investigate how much the initial radiation energy affects the final reheating temper-

ature that is determined by late-time perturbative decay of the homogeneous part. These questions are addressed with numerical methods in the following discussion.

To determine of the reheating temperature, it is necessary to find out the Hubble scale at the moment when reheating is completed. Here, completion of reheating is referred to as the onset of the radiation-domination with no homogeneous fields that can dominate the Universe again, which is actually ambiguous to define in a numerical calculation for the following reasons. Due to the accumulation of error, it is challenging to obtain reliable long-time numerical calculation to check whether the Universe becomes matter-dominated again at a late time. For example, it is usually too long for the numerical calculation to run for a scalaron decay time scale Γ_φ^{-1}. Fortunately, in the perturbative decay process considered here, the decay rate for scalaron is approximately constant at the late time while the Hubble parameter H decays with time, so the homogeneous background fields will certainly be completely depleted eventually. Another reason is that the termination time chosen for the numerical calculation as the completion of reheating affects the Hubble scale (so the reheating temperature) due to the cosmic expansion. Therefore, too early (late) time will result in overestimation (underestimation) of the reheating temperature to some extent. In the following, a simple criterion is adopted to make sure that the equation of state parameter w converges to $1/3$ properly, i.e. the ratio between the energy densities of radiation and homogeneous background fields $\rho_{\rm rad}/\rho_{\rm bg} > 20$, which avoids the long-time numerical calculation and too much overestimation of T_r.

In the numerical calculation, the equations of motion for the background fields with the decay rates taken into account as friction terms are solved, together with the Boltzmann equation for the radiation energy density, and the Friedmann equation, which are given by

$$\begin{aligned}
&\ddot{\varphi} + \left(3H + \Gamma_{\varphi\to\delta\tilde{h}\delta\tilde{h}}\right)\dot{\varphi} + \frac{\partial U}{\partial\varphi} + \frac{\alpha}{2}e^{-\alpha\varphi}\dot{h}^2 = 0 \ , \\
&\ddot{h} + \left(3H + \Gamma_{h_0\to\tilde{t}\bar{\tilde{t}}} + \Gamma_{h_0\to\tilde{b}\bar{\tilde{b}}} + \Gamma_{h_0\to\tilde{W}\tilde{W}} + \Gamma_{h_0\to\tilde{Z}\tilde{Z}}\right)\dot{h} + e^{\alpha\varphi}\frac{\partial U}{\partial h} - \alpha\dot{\varphi}\dot{h} = 0 \ , \\
&\frac{d\rho_{\rm rad}}{dt} + 4H\rho_{\rm rad} = \Gamma_{\varphi\to\delta\tilde{h}\delta\tilde{h}}\dot{\varphi}^2 + \left(\Gamma_{h_0\to\tilde{t}\bar{\tilde{t}}} + \Gamma_{h_0\to\tilde{b}\bar{\tilde{b}}} + \Gamma_{h_0\to\tilde{W}\tilde{W}} + \Gamma_{h_0\to\tilde{Z}\tilde{Z}}\right)\dot{h}^2 \ , \\
&3M_{\rm pl}^2H^2 = \rho_{\rm bg} + \rho_{\rm rad} \ ,
\end{aligned} \tag{4.107}$$

where $\rho_{\rm rad}$ is the energy density of radiation while $\rho_{\rm bg}$ is the energy density of the background fields given as

$$\rho_{\rm bg} = \dot{\varphi}^2/2 + e^{-\alpha\varphi}\dot{h}^2/2 + U(\varphi, h) \ . \tag{4.108}$$

Also, step functions are used to impose the kinematic constraint for each decay channel. The equation of state parameter w and the reheating temperature T_r are estimated numerically through

$$w = -1 - \frac{2}{3}\frac{\dot{H}}{H^2} \,, \tag{4.109}$$

$$T_r = \left(\frac{90}{g_{\rm r}\pi^2}\right)^{1/4} \sqrt{H_{\rm r} M_{\rm pl}} \,, \tag{4.110}$$

where $g_{\rm r} = 106.75$ and $H_{\rm r}$ are the effective number of relativistic species and Hubble parameter at the end of reheating. In addition, define a temperature T_φ as a reference by assuming that Higgs becomes light enough so that the decay channel $\varphi \to \delta\tilde{h}\delta\tilde{h}$ is *always* open

$$\begin{aligned}
T_\varphi \equiv & 0.2\sqrt{M_{\rm pl}\overline{\Gamma}_\varphi} \\
\approx & 0.2\sqrt{M_{\rm pl}}\left[\left(\frac{\pi}{M}+\frac{\pi}{\tilde{M}}\right)^{-1}\left(\frac{3}{16\pi}\frac{M^3}{M_{\rm pl}^2}\left(\frac{1}{6}+\xi\right)^2\frac{\pi}{M}+\frac{3}{16\pi}\frac{\tilde{M}^3}{M_{\rm pl}^2}\left(\frac{1}{6}-2\xi\frac{M^2}{\tilde{M}^2}\right)^2\frac{\pi}{\tilde{M}}\right)\right]^{1/2} \\
= & 0.2\sqrt{M_{\rm pl}}\sqrt{\frac{3}{16\pi}\frac{M^3\tilde{M}}{M_{\rm pl}^2(M+\tilde{M})}}\left[\left(\frac{1}{6}+\xi\right)^2+\frac{\tilde{M}^2}{M^2}\left(\frac{1}{6}-2\xi\frac{M^2}{\tilde{M}^2}\right)^2\right]^{1/2}
\end{aligned} \tag{4.111}$$

which returns to the standard result (see e.g. [177, 179]) when $\xi \ll 1$.

Since the situation considered here is that a preexisting preheating process has transferred a large amount of energy from $\rho_{\rm bg}$ to $\rho_{\rm rad}$, the initial conditions are set to be $\rho_{\rm rad,ini} = 9\rho_{\rm bg,ini} = 90\% \times 3M_{\rm pl}^2 H_{\rm end}^2$ where $H_{\rm end}$ is the Hubble parameter at the end of inflation. Before going to the reheating temperature, two examples of the evolution of $\rho_{\rm rad}$, $\rho_{\rm bg}$, $3M_{\rm pl}^2H^2$, and w are shown in Fig. 4.19. It can be seen that for larger ξ, the homogeneous part does not really dominate over but at most becomes comparable to the radiation. In contrast, for smaller ξ, the energy density of the homogeneous part indeed becomes larger than that of the radiation, so two intersections between them are clearly seen in the upper right panel of Fig. 4.19. This result is reasonable because for larger ξ, more decay channels are allowed, and decay rates themselves also become larger. However, if perturbative decays are not taken into account, the energy density of the radiation will simply be redshifted away quickly and the Universe will be dominated by the homogeneous background field again. Also, it can be seen that w effectively converges to 1/3 when $\rho_{\rm rad}/\rho_{\rm bg} \gtrsim 20$, which shows that this criterion is reasonable.

Finally, the reheating temperature for parameters $\xi \gg \mathcal{O}(10)$ is discussed in this setup. Specifically, scan the parameter space $35 \leq \xi \leq \xi_s$ with adaptive step length

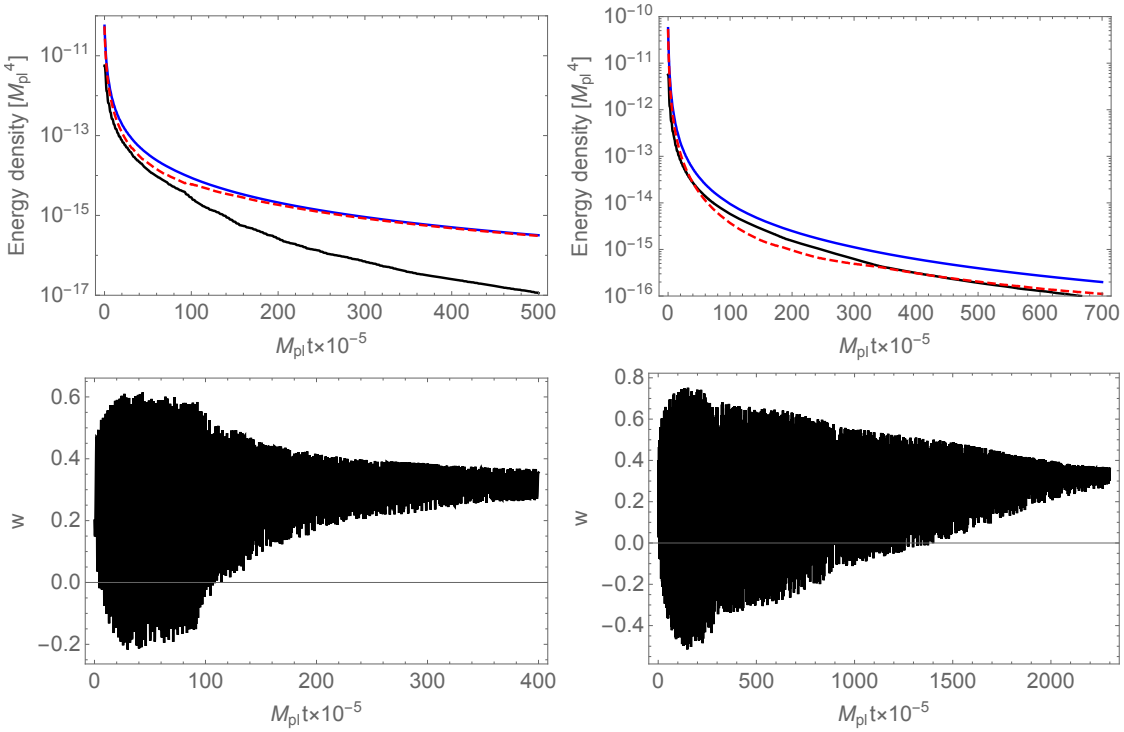

Figure 4.19: Upper: $\rho_{\rm rad}$ (red dashed), $\rho_{\rm bg}$ (black solid), and $3M_{\rm pl}^2H^2$ (blue solid). Lower: w up to $\rho_{\rm rad}/\rho_{\rm bg} \gtrsim 20$. Left: $\xi = 3000$. Right: $\xi = 1000$. Initial conditions are $\rho_{\rm rad,ini} = 9\rho_{\rm bg,ini} = 90\% \times 3M_{\rm pl}^2H_{\rm end}^2$. In order to make the intersections clearer in the upper right panel, the evolution is shown only up to $M_{\rm pl}t = 7 \times 10^7$.

and calculate the reheating temperature T_r defined at the moment when $\rho_{\rm rad}/\rho_{\rm bg}$ exceeds 20 as well as the duration of this perturbative reheating t_r. No further investigation for the cases $\xi < 35$ is presented because it takes too long for numerical calculation. From the results presented below, it can be expected that the reheating temperature quickly approaches the R^2-inflation case as ξ decreases. The result is shown in Fig. 4.20 where θ defined in Eq. (4.37) is used as the model parameter because it treats the Higgs-like and R^2-like regions "equally", which is one of the main results in this section.

It can be seen that once θ approaches the unitary bound $\theta \approx 0$, the reheating temperature rapidly increases to reach the Higgs-limit. Conversely, as $\theta \to \pi/2$, the system approaches to the R^2-limit. A similar argument also applies to the perturbative reheating duration. As for the comparison with T_φ (red line), $T_r > T_\varphi$ for most part of the parameter space because the Higgs decay plays an important role in lifting the reheating temperature. However, when θ approaches the unitary bound in Higgs-limit, T_φ becomes larger than T_r, which is understandable because it is assumed that the scalaron decay channel is always open, which is obviously NOT the

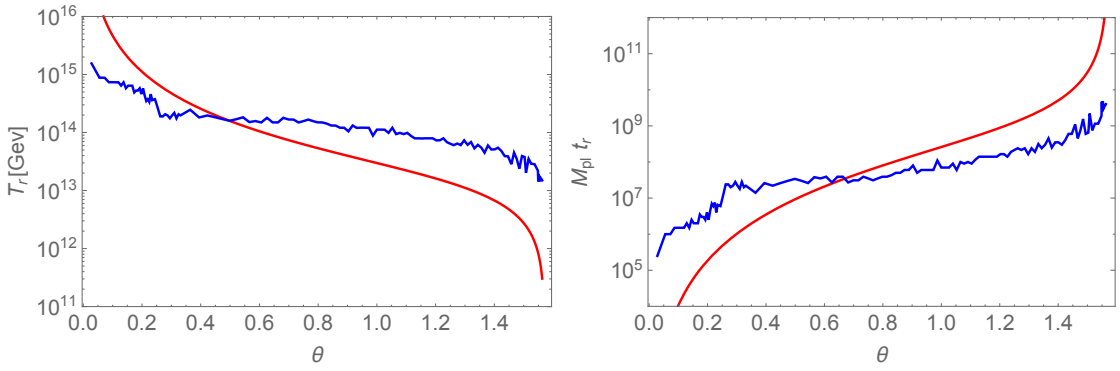

Figure 4.20: Left: reheating temperature T_r (blue) and the temperature calculated with only averaged scalaron decay rate T_φ (red) given in Eq. (4.111). Right: duration of perturbative reheating t_r (blue) and the scalaron decay time Γ_φ^{-1} (red). Both T_r and t_r are determined at the moment when $\rho_{\rm bg}$ becomes smaller than 5% of $\rho_{\rm rad}$.

realistic case since the large Higgs mass forbids the decay to occur until late time. A similar argument applies to the reheating time. Apart from these unrealistic parts, it is expected that if the calculation lasts for a long enough time, the numerical results in blue will get closer to but not coincide with the red lines in Fig. 4.20. Again, the reason is that the decay of Higgs is lifting the reheating temperature and shorten the reheating time. More importantly, the small dips and peaks on the numerical results are physical instead of pure artificial due to the error of numerical calculation. As discussed in Appendix G, the cause of these small features is the θ-dependent energy distribution between scalaron and Higgs. Suppose the model parameter is close to some critical point that realizes maximal tachyonic instability in the first scalaron oscillation. In that case, more energy is stored in the Higgs field so that the effective decay rate of the whole system becomes larger because the decay rate of Higgs is larger than that of scalaron for most parameters. Figures 4.21 show illustrative examples to make the argument more convincing. Two cases are considered: (1) nearly-critical ξ_{nc} with larger oscillation amplitude of Higgs, and (2) far-from-critical $\xi_{fc} \simeq 1.001\xi_{nc}$ with smaller oscillation amplitude of Higgs. There is no initial radiation imposed for simplicity. Since the two parameters are so close, the decay rates of Higgs and scalaron are almost the same for both cases. However, as can be easily seen in the comparison in Fig. 4.21, the nearly-critical parameter case induces a much more efficient reheating process than the latter, even with slightly smaller decay rates superficially, which can be recognized from the growth rate of $\rho_{\rm rad}$ and the converging rate of w to 1/3. On the other hand, if the parameter is far from critical values, the energy in Higgs can be minimal so that the system is effectively decaying only

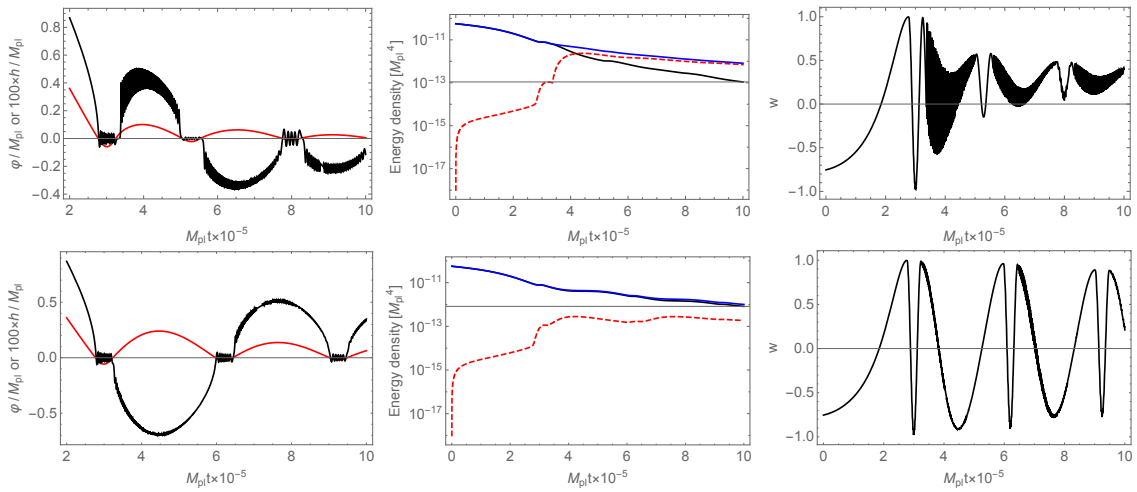

Figure 4.21: Upper: nearly-critical parameter denoted as ξ_{nc}. Lower: far-from-critical parameter denoted as $\xi_{fc} \simeq 1.001\xi_{nc}$. Left: evolution of homogeneous scalaron (red) and Higgs (blue). Middle: $\rho_{\rm rad}$ (red dashed), $\rho_{\rm bg}$ (black solid), and $3M_{\rm pl}^2H^2$ (blue solid). Right: w. There is no initial radiation energy imposed for simplicity.

through scalaron decay until the inflaton encounters a chance to transfer the energy from scalaron to Higgs. However, the chance is expected to be quite rare if the necessary degree of fine-tuning for subsequent scalaron oscillations to be critical can be analyzed similarly as the first scalaron oscillation in Sec. 4.2, and the corresponding effect would be smaller. Therefore, if the time resolution in the numerical calculation is high enough and the parameter scanning is done more finely, it is expected that the dips on the blue line in the left panel of Fig. 4.20 would be deeper while the peaks would be higher corresponding to the θ's that can realize strong tachyonic instability in the first (or at least early) scalaron oscillation after the end of inflation, with smaller wiggles corresponding to late-time critical cases. A similar argument also applies to the right panel.

4.3.3 Absence of Tachyonic Preheating

As the last part of this section, the investigation focuses on the case where tachyonic instability is weak or does not take place during preheating. As a result, there is practically no $\rho_{\rm rad}$ initially. In this case, initial conditions for $\rho_{\rm rad}$ and $\rho_{\rm bg}$ are simply changed in the previous numerical calculation.

First, two examples of the evolution of energy densities and equation of state parameter are shown in Fig. 4.22. As can be seen there, even if there is no initial radiation before the onset of the perturbative reheating, the perturbative decay of scalaron and Higgs can still reheat the Universe in a similar manner as the case

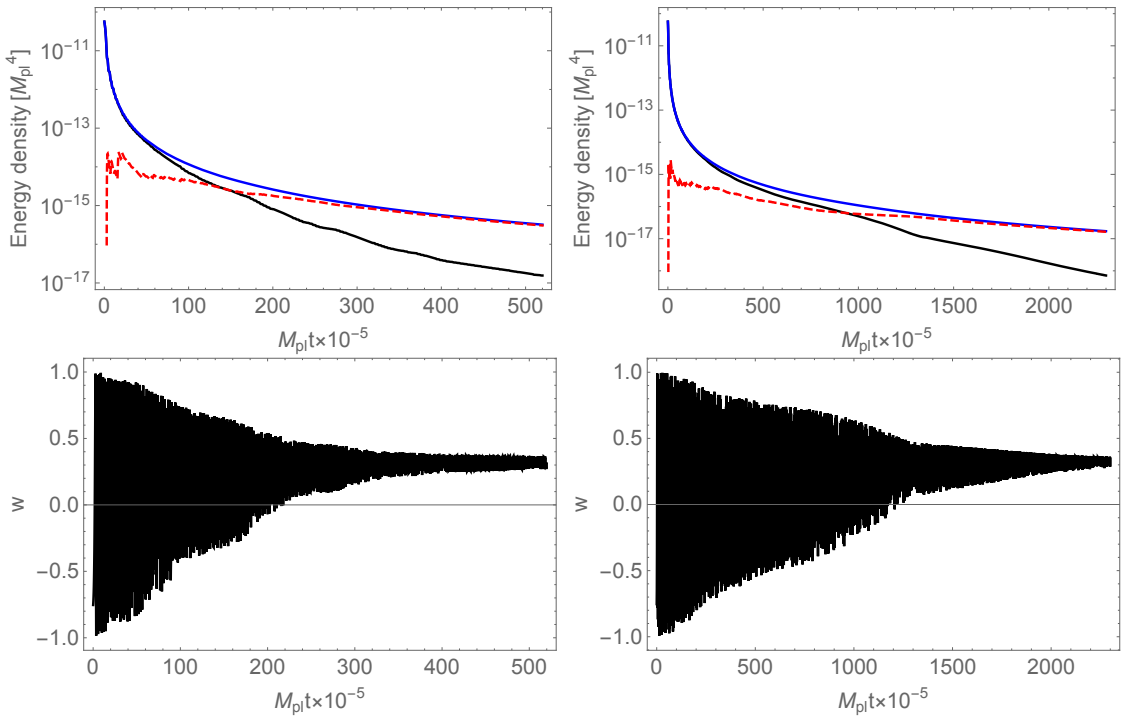

Figure 4.22: Upper: $\rho_{\rm rad}$ (red dashed), $\rho_{\rm bg}$ (black solid), and $3M_{\rm pl}^2H^2$ (blue solid). Lower: w up to $\rho_{\rm rad}/\rho_{\rm bg} \gtrsim 20$. Left: $\xi = 3000$. Right: $\xi = 1000$.

considered previously. Still, the end of reheating is defined as the moment when the condition $\rho_{\rm rad}/\rho_{\rm bg} \gtrsim 20$ becomes satisfied.

Next, the reheating temperature T_r and duration t_r are discussed in the current setup. Again the parameter space is scanned within $35 \leq \xi \leq \xi_s$ for the same reason mentioned previously. The results are shown in Fig. 4.23 together with those in Fig. 4.20 for convenient comparison. This figure is also one of the main results in this section. As can be seen in Fig. 4.23, the results from cases with and without initial radiation energy almost coincide with each other, which indicates the fact that, if preheating processes cannot completely deplete the energy of the homogeneous background fields, once the homogeneous fields dominate the Universe again and perturbative decay takes over the reheating process, the resulting reheating temperature (as well as the duration of reheating) is almost independent of the detail of preheating. Therefore, the perturbative decay indeed plays an essential role in the whole reheating process in the mixed Higgs-R^2 model.

Finally, the number of e-folds of reheating ΔN_r is calculated, which is important to confront theoretical inflation predictions with observational data. Figure 4.24 compares ΔN_r resulting from the cases with and without initial radiation. It can be seen that the difference is stable on a value slightly less than unity, which means that

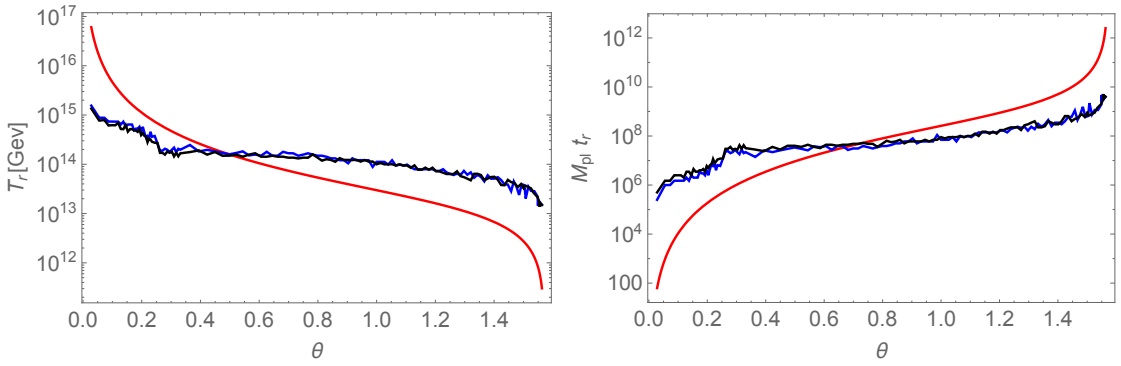

Figure 4.23: Left: T_r with (blue) and without (black) initial radiation, and $T_\varphi = 0.2\sqrt{\Gamma_\varphi M_{\rm pl}}$ (red). Right: t_r with (blue) and without (black) initial radiation, and Γ_φ^{-1} (red). Both T_r and t_r are determined at the moment when $\rho_{\rm bg}$ becomes smaller than 5% of $\rho_{\rm rad}$. The blue lines come from the results in Fig. 4.20 for convenient comparison between the cases with and without initial radiation energy.

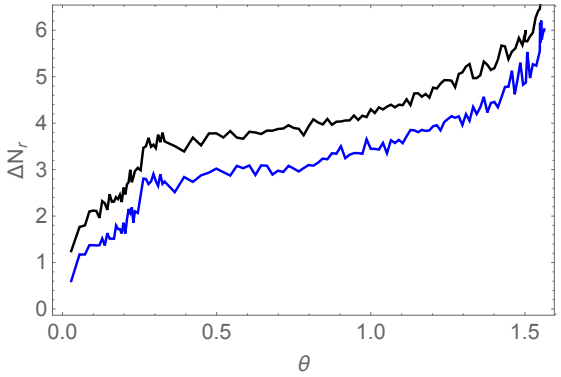

Figure 4.24: Comparison of e-fold numbers of cosmic expansion between the end of inflation and the end of reheating. Blue: number of e-fold in the case with initial radiation. Black: number of e-fold in the case without initial radiation.

if there is a large fraction of energy in relativistic particles before the domination of perturbative reheating, the number of e-folds ΔN_r needed to complete reheating can be reduced by around unity. Together with the duration of the early preheating stage itself, the information of e-fold number can identify whether the early preheating stage occurs or not. And the typical value of ΔN_r shown in Fig. 4.24 is $3 \lesssim \Delta N_r \lesssim 5$.

In this section, perturbative reheating in the mixed Higgs-R^2 inflation model is investigated, and the role of perturbative decay throughout the whole reheating process is discussed.

During perturbative reheating, the background dynamics of the scalaron and the Higgs are tightly connected with the attractor solutions, i.e. the valleys. Considering $\xi \gg \mathcal{O}(10)$, the adiabatic solution for Higgs can be analytically found because scalaron

mass is much smaller than that of Higgs. As a result, the Higgs mass is almost constant within every Higgs oscillation, which validates the calculated Higgs decay rate. The relation between the energy distribution of the background fields and the parameter choice is discussed, which creates the fine structure of the main results in Figs. 4.20, 4.23, and 4.24. Then the perturbative decay rates for scalaron and Higgs are calculated in the adiabatic regime where Higgs oscillates much faster than scalaron, based on which the possible effects of the decay on the period during and after the occurrence of tachyonic preheating are estimated. It is found that the decay of Higgs particles produced by tachyonic preheating may weaken the rescattering process between homogeneous and inhomogeneous modes in a non-negligible way, which could slow down the preheating process and allow the re-domination of the oscillating background field. More importantly, perturbative reheating determines the final reheating temperature T_r in this model. It is shown that larger ξ leads to larger T_r due to larger decay rates and more allowed decay channels. Also, the reheating temperature is typically larger than T_φ because the decay of homogeneous Higgs field increases the effective decay rate of the whole system. The early preheating stage is taken into account by imposing non-vanishing radiation energy density to the initial conditions of the system. It is found that the early preheating stage can hardly affect the final reheating temperature but still can change the number of e-folds of the perturbative reheating.

Here, the assumptions and caveats in this study should be clarified. Only parameters within $\xi_s \geq \xi \gg \mathcal{O}(10)$ are considered for the following reasons. For $\xi \lesssim \mathcal{O}(10)$, the hierarchy between scalaron and Higgs oscillation becomes small, so the adiabatic approximation breaks down, which makes it difficult to study the system analytically. In addition, the perturbative reheating process takes a long time to complete, which is challenging for numerical calculation. From the results presented above, it is expected that the system will quickly approach the R^2-inflation limit as ξ decreases. Therefore, $\xi \lesssim \mathcal{O}(10)$ is not discussed in detail here but given some simple argument. Besides, tachyonic particle production during preheating is not directly incorporated in the numerical calculation but taken into account phenomenologically as the initial radiation energy. When defining the completion of reheating, the criterion $\rho_{\rm rad}/\rho_{\rm bg} > 20$ is adopted instead of waiting for a long time, more precisely $\sim \mathcal{O}(\Gamma_{\varphi<0}^{-1})$ where $\Gamma_{\varphi<0}$ is the scalaron decay rate during $\varphi < 0$ instead of Γ_φ in Eq. (4.104). This is because the channel in $\varphi > 0$ regime is almost closed for all the time, as explained previously. Then, a simple estimation of $\Gamma_{\varphi<0}^{-1} \sim 16\pi M_c/(\lambda M^2)$ shows that even for the most efficient case $\xi = \xi_s$ the time scale is $M_{\rm pl} t_r \sim 10^5$ which is roughly the same as the

numerical results with corresponding parameter and the criterion $\rho_{\rm rad}/\rho_{\rm bg} > 20$. As ξ decreases, the time scale grows to $M_{\rm pl}t_r \sim 10^{12}$ for $\xi \simeq 100$ and even larger for smaller ξ, which is much longer than that evaluated with the adopted criterion. The results obtained here are expected to be robust because the numerical results show that the equation of state parameter converges well to 1/3. As for the produced particles, it is assumed that they are relativistic and reach thermal equilibrium right at the end of reheating defined in this investigation. Actually, when Higgs background decays in $\varphi < 0$ regime, the produced fermions (top and bottom quarks in our consideration) are massless therefore relativistic. However, they gain masses as scalaron enters $\varphi > 0$ regime and Higgs enters one of the valleys. Therefore, they are switching between being massless and massive during the oscillation of the homogeneous fields. When they become heavier during $\varphi > 0$, they can further decay into other lighter particles. This phenomenon is not studied in detail in this thesis.

This work only focuses on the case $\xi \gg \mathcal{O}(10)$. For small $\xi \lesssim \mathcal{O}(10)$, it is argued that the situation would quickly approach to R^2-limit, but a more detailed investigation should be done in the future work in this parameter range. Also, this work only incorporated the effects of tachyonic preheating phenomenologically in the sense that the effects of the early preheating stage have been taken into account only as the preexisting radiation in the numerical calculation.

This chapter constitutes the central part of this thesis, discussing the reheating process in the mixed Higgs-R^2 inflation model based on the original works [41,51,53], which is characterized by three parts, the first stage of preheating, tachyonic preheating, and the perturbative reheating. The first stage of preheating corresponds to the violent spike preheating in the Higgs inflation, but, in the two-field case, it is analytically shown that the spikes are much milder and insufficient to complete preheating. The weakened spiky phenomenon also ensures that the mixed Higgs-R^2 inflation model can serve as a UV-extension of the Higgs inflation up to the Planck scale. After that, the non-minimal coupling creates a possibility that, with fine-tuned parameters, the Higgs field and the longitudinal mode of gauge bosons experience strong tachyonic instability, which can complete preheating almost instantaneously. However, the occurrence of sufficiently strong tachyonic preheating requires severe fine-tuning, especially in the R^2-like regime. Both analytical and numerical methods are used in the investigation. In the fine-tuned case, the corresponding e-fold number of inflation is also estimated. If the tachyonic effect is not strong enough to complete preheating or totally absent, perturbative decay of the scalaron and the Higgs plays

an essential role during the reheating process. In the former, the tachyonic preheating transfers a large amount of energy from inflaton fields to radiation at the early stage, but they are redshifted much faster than the remaining coherent oscillation of background fields, so eventually, the coherent oscillation dominates the Universe again and perturbative reheating takes place. In addition, although the products of tachyonic preheating may help to destroy the homogeneous background by rescattering, the large decay rate of the Higgs field into quarks may weaken such effects. The perturbative reheating determines the final reheating temperature and duration if tachyonic preheating is inefficient. In such a case, the final reheating temperature and duration is almost independent of the detail of preheating. The Higgs-like regime generally result in higher reheating temperature and shorter duration than those in R^2-like regime, as shown previously. Although the parameter range considered here does not reach the vicinity of the R^2-limit, it is expected that the system approaches the well-known Starobinsky model as $\xi \to 0$. With all these investigations and results, a comprehensive understanding of the reheating process in the mixed Higgs-R^2 inflation model is gained, and the observational constraint on the model parameters can be improved by fixing the pivot scale of the curvature perturbations for different parameters by corresponding reheating phenomena.

Chapter 5

Conclusion

In this thesis, the origin of the Big Bang in the mixed Higgs-R^2 inflation model is investigated, namely the reheating process that provides initial conditions for the Hot Big Bang, mainly based on my original works [41, 51, 53].

In Chapter 2, a brief review of the inflation scenario is given, including the motivation and basic physical picture of inflation, the simplest class of inflation model, i.e. single-field slow-roll inflation, and the general formalism for the multi-field inflation. In the single-field case, two simple but observationally favored models are of great interest, namely the Starobinsky model with only one model parameter, and the Higgs inflation that makes use of the only observed scalar field in SM. These two models are equivalent during inflation, giving the same predictions on the scalar spectral index and the tensor-to-scalar ratio. However, the Higgs inflation suffers from UV problems that make the prediction from this model questionable. In particular, the cutoff scale of the Higgs inflation is suppressed by the large non-minimal coupling between Higgs and gravity. To solve these issues, a UV-extension is eagerly desired. As a promising candidate, the mixed Higgs-R^2 inflation model is reviewed in the last section based on Ref. [38]. In this two-field model, the scalaron and the Higgs both play the role in driving inflation. In the presence of the R^2 term, the cutoff scale is lifted to the Planck scale and still gives the same inflation prediction as its two single-field limits with large non-minimal coupling. The parameter space is broad and can be divided into Higgs-like and R^2-like regimes, while there is a strongly-coupled regime inside the former to which the Higgs-limit belongs. As long as the parameter is chosen outside this regime, the perturbativity is ensured in this model. It is shown that the effective single-field description is valid during inflation, so the mixed Higgs-R^2 inflation can be understood as an effective Starobinsky model or effective Higgs inflation. However, the UV issue in the Higgs inflation is even severer during preheating [34], which is discussed in Chapter 3.

In Chapter 3, the basics of particle production and its application to reheating are reviewed. Reheating is an indispensable part of a successful inflation model as a graceful exit of the quasi-de Sitter phase to connect with the subsequent Hot Big Bang. Also, a comprehensive understanding of reheating can clarify the ambiguity of the pivot scale of curvature perturbation to improve the observational constraint of model parameters. A typical type of particle production can be classified as the non-adiabatic time-dependence of the effective mass of the target field. Based on a general equation of motion of this type, the perturbative and non-perturbative particle production are discussed in detail according to the parameter choices, including parametric resonance and tachyonic instability in the latter case. The non-perturbative processes are usually very efficient, which plays a vital role during preheating in an inflation model, especially the broad resonance and the tachyonic instability. The perturbative process is weak and slow instead, but it can be essential at the last stage of reheating because the conditions for non-perturbative particle production are usually not satisfied anymore at the late time. As typical examples, the reheating processes in the Starobinsky model and the Higgs inflation are reviewed. In the former case, the reheating channel is dominated by perturbative reheating through the decay of the scalaron, which results in a relatively low reheating temperature. For the latter case, a violent preheating process is induced by the sizeable non-minimal coupling that leads to significant spikes in the effective mass of the longitudinal mode of weak gauge bosons. However, these spikes are too large that the energy scale exceeds the cutoff of the theory during reheating, which causes serious UV problems in the Higgs inflation model. As a result, because the theory enters the strongly-coupled regime, its predictions may not be reliable. Therefore, as a UV extension candidate, it is vital to examine the preheating process in the mixed Higgs-R^2 inflation model to ensure the absence of these issues.

In the central part of this thesis, Chapter 4, the reheating process in the mixed Higgs-R^2 inflation model is studied. The effective single-field description is no longer valid during reheating, which makes the situation much more complicated but results in rich phenomena that are not expected in its two single-field limits. Thanks to the multi-field nature of the reheating dynamics, even though the non-minimal coupling can be large, the large spikes that cause problems in the Higgs inflation are still present at the first stage of preheating but significantly reduced by the presence of scalaron. Since the Higgs-limit lies within the strongly-coupling regime in the parameter space, it is understandable that the strong coupling issue appears in the Higgs inflation but disappears in the UV-extended model as long as the model parameter is outside the

strongly-coupled regime. As a result, the spike in the effective mass of longitudinal mode of gauge bosons is physical but cannot exceed the even higher cutoff in this theory, which confirms that the mixed Higgs-R^2 inflation model is indeed suitable as the UV-extension of the Higgs inflation. For the same reason, the particle production by the spikes is far less efficient than that in the single-field case, giving very limited impact on the preheating process in the two-field model. Therefore, other mechanisms in the subsequent evolution should be involved to deplete the inflaton energy to reheat the Universe. In fact, the preheating process can be dominated by tachyonic instability if the model parameters are critical ones that can realize a significant tachyonic effect right after the spike preheating. The tachyonic effects in the Higgs field and the longitudinal mode of gauge bosons can complete preheating within one e-fold of expansion for most of the critical parameters, except for those close to the R^2-limit because naturally no tachyonic instability is expected in this limit. The resulting e-fold number of inflation is then $58 \lesssim N_{\rm inf} \lesssim 59$ which corresponds to a scalar spectral index $n_s \simeq 0.9658$. Observing this value of n_s gives strong constraint on the model parameter and breaks the degeneracy with the Starobinsky model, indicating the parameters should be one of those shown in Fig. 4.8. Of course, fine-tuning is needed for the realization of such strong tachyonic preheating. The necessary degree of fine-tuning for the R^2-regime ($\Delta\theta_{{\rm eff},N}/\Delta\theta_N \lesssim 10^{-3}$) is much more severe than the Higgs-like regime ($10^{-3} \lesssim \Delta\theta_{{\rm eff},N}/\Delta\theta_N \lesssim 10^{-1}$) because the amplitude of tachyonic mass is generally smaller in the former. Consequently, more fine-tuning is needed to stay in the tachyonic regime for a longer time to have sufficient particle production in the R^2-like regime. Since fine-tuning is needed, it seems more likely that the tachyonic preheating at the first scalaron oscillation after the end of inflation is not strong enough to complete preheating. In this case, the produced radiation by tachyonic instability is probably redshifted away, so the remaining coherent oscillation of inflaton fields dominates the Universe again. To deplete the rest of the inflaton energy, perturbative decay serves as the primary channel at the late time, determining the reheating temperature and duration. The decay rate of Higgs is typically larger than that of scalaron, so the reheating temperature in the mixed Higgs-R^2 inflation model is generically larger than that in the Starobinsky model. For most parameters between the two limits, the reheating temperature is $\sim \mathcal{O}(10^{14})$GeV and the e-fold number of reheating is typically $\Delta N_r \simeq 3-5$, which can be translated to $n_s \simeq 0.9643-0.9630$ and would be constrained by future CMB observation if the precision reaches $\Delta n_s \simeq 0.001$, although there is a partial degeneracy between the cases with and without (insufficient) tachyonic preheating. Which regime the parameter is located

in can be determined by such observation. In either case, if the measurement of n_s can be precise to $\Delta n_s \sim \mathcal{O}(10^{-4})$ level, the corresponding reheating temperature can be finally pinned down so that the mixing ratio between R^2 and Higgs can be fixed even more precisely. When getting close to the R^2-limit or Higgs-limit, the standard results are smoothly recovered. For larger non-minimal coupling, the reheating temperature becomes higher because the scalaron decay into Higgs gets significant. The energy distribution between the Higgs and the scalaron further generates some fine structures on the parameter-dependence of the reheating temperature and duration, which may increase the difficulty breaking the degeneracy among model parameters within a small neighborhood. Besides, the perturbative decay of produced particles can also slow down the rescattering process between homogeneous and inhomogeneous fields.

The results summarized in this thesis provide an analytical and comprehensive understanding of the reheating process in the strongly-motivated mixed Higgs-R^2 inflation model that can serve as the UV-extension of the Higgs inflation and give observationally favored inflation predictions. The reheating process provides the initial conditions for the subsequent evolution of the Universe. Depending on the choice of model parameters, the reheating process can be very different from its two single-field limits, leading to different reheating temperatures and duration, which can be used to break the degeneracy among different parameters and improve the observational constraint on model parameters. Since this model is within GR and SM, ruling out or verifying this model is crucial for determining whether the construction of inflation model requires new physics beyond GR and SM or not. It can be expected that more precise CMB observation in the future can narrow down the favored range of n_s to constrain the viable parameter space in the mixed Higgs-R^2 inflation model. Moreover, since the tensor-to-scalar ratio also depends on $N_{\rm inf}$, future experiments, such as Lite (Light) satellite for the studies of B-mode polarization and Inflation from cosmic background Radiation Detection (LiteBIRD), CMB-S4, and Cosmic Origins Explorer (CORE), may be able to further constrain the model. In principle, the alternating radiation- and matter-dominance shown in Sec. 4.3 is also helpful to distinguish the mixed Higgs-R^2 inflation model with other inflation models because the change of equation of state parameter can be imprinted in the spectrum of the primordial gravitational wave background [12], which might be detected by future experiment such as DECi-hertz Interferometer Gravitational wave Observatory (DECIGO).

Appendix A

Conformal Transformation

In this appendix, the rules of conformal transformation are summarized (see e.g. Ref. [64]). The convention $(-,+,+,+)$ and $R^{\mu}{}_{\nu\rho\sigma} = \partial_\rho \Gamma^{\mu}_{\nu\sigma} - \partial_\sigma \Gamma^{\mu}_{\nu\rho} + \Gamma^{\mu}_{\rho\alpha}\Gamma^{\alpha}_{\nu\sigma} - \Gamma^{\mu}_{\sigma\alpha}\Gamma^{\alpha}_{\nu\rho}$ are used.

Consider a conformal transformation for D-dimensional spacetime

$$g_{\mu\nu}(x) \to \tilde{g}_{\mu\nu}(x) = \Omega(x)^2 g_{\mu\nu}(x) \ , \tag{A.1}$$

where $\Omega(x)$ is a continuous, non-vanishing, finite, and real function. Under such a transformation, the Christoffel symbol, Ricci tensor, and Ricci scalar are transformed as follows.

$$\Gamma^{\rho}_{\mu\nu} \to \tilde{\Gamma}^{\rho}_{\mu\nu} = \Gamma^{\rho}_{\mu\nu} + \Omega^{-1}\left(\delta^{\rho}_{\mu}\nabla_\nu\Omega + \delta^{\rho}_{\nu}\nabla_\mu\Omega - g_{\mu\nu}g^{\rho\sigma}\nabla_\sigma\Omega\right) \ , \tag{A.2}$$

$$R_{\mu\nu} \to \tilde{R}_{\mu\nu} = R_{\mu\nu} - \frac{\Omega^{2-D}}{D-2} g_{\mu\nu}\Box(\Omega^{D-2}) + (D-2)\Omega\nabla_\mu\nabla_\nu(\Omega^{-1}) \ , \tag{A.3}$$

$$R \to \tilde{R} = \frac{R}{\Omega^2} - \frac{(D-1)(D-4)}{\Omega^4}\nabla_\mu\Omega\nabla^\mu\Omega - \frac{2(D-1)}{\Omega^3}\Box\Omega \ , \tag{A.4}$$

$$\Box\phi \to \tilde{\Box}\phi = \Omega^{-2}\Box\phi + \frac{D-2}{2} g^{\mu\nu}\Omega^{-4}\nabla_\mu\left(\Omega^2\right)\nabla_\nu\phi \ , \tag{A.5}$$

where $\Box \equiv g^{\mu\nu}\nabla_\mu\nabla_\nu$. Consider a scalar field, the combination

$$\left[\Box - \frac{D-2}{4(D-1)}R\right]\phi \ , \tag{A.6}$$

transforms in a simple way under the conformal transformation (A.1)

$$\left[\Box - \frac{D-2}{4(D-1)}R\right]\phi \to \left[\tilde{\Box} - \frac{D-2}{4(D-1)}\tilde{R}\right]\tilde{\phi} = \Omega^{-\frac{n+2}{2}}\left[\Box - \frac{D-2}{4(D-1)}R\right]\phi \ , \tag{A.7}$$

if the scalar field transforms as

$$\phi \to \tilde{\phi} = \Omega^{\frac{2-D}{2}} \phi \ . \tag{A.8}$$

Therefore, given a Lagrangian for a scalar field as

$$\mathcal{L} = \frac{1}{2}\sqrt{-g}\left[-\partial_\mu\phi\partial^\mu\phi - (m^2 - \xi R)\phi^2\right] \ , \tag{A.9}$$

if $m = 0$ and $\xi = -[(D-2)/(D-1)]/4$, the equation of motion for ϕ

$$\left[\Box - \frac{D-2}{4(D-1)}R\right]\phi = 0 \ , \tag{A.10}$$

is invariant under the transformation (A.1) and (A.8) because the following is also satisfied

$$\left[\tilde{\Box} - \frac{D-2}{4(D-1)}\tilde{R}\right]\tilde{\phi} = 0 \ . \tag{A.11}$$

Usually, $\xi = -[(D-2)/(D-1)]/4$ is called conformal coupling with which the scalar field is actually "minimally" affected by gravity. To be more specific, consider a simple example with Eq. (A.9) for a homogeneous ϕ and a four-dimensional flat FLRW background ($K = 0$ in Eq. (2.1)). In this case, the equation of motion for ϕ is given by

$$\ddot{\phi} + 3H\dot{\phi} + \left(m^2 - \xi R\right)\phi = 0 \ . \tag{A.12}$$

By using conformal time $d\eta = dt/a(t)$ and redefining $\chi \equiv a\phi$, the equation of motion above becomes

$$\chi'' + m^2a^2\chi - \left(\frac{1}{6} + \xi\right)a^2R\chi = 0 \ . \tag{A.13}$$

When $\xi = -1/6$ which is the conformal coupling in four-dimension, gravity only rescales the mass of ϕ while the direction coupling between R and ϕ vanishes.

Appendix B

Gauge Transformation

In this appendix, the rules of gauge transformation for four-scalar, -vector, -tensor fields are summarized. With these transformation rules, gauge-invariant quantities can be easily constructed.

The four-tensor, -vector, and -scalar fields can be decomposed into background and perturbations in the following way

$$\begin{aligned} g_{\mu\nu}(t,\mathbf{x}) &= \bar{g}_{\mu\nu}(t) + \delta g_{\mu\nu}(t,\mathbf{x}) \ , \\ v_{\mu}(t,\mathbf{x}) &= \bar{v}_{\mu}(t) + \delta v_{\mu}(t,\mathbf{x}) \ , \\ \phi(t,\mathbf{x}) &= \bar{\phi}(t) + \delta\phi(t,\mathbf{x}) \ , \end{aligned} \tag{B.1}$$

where the over-line $\bar{(\ )}$ denotes the homogeneous background and the spatially dependent parts correspond to perturbations which are small compared with the background quantities $|\delta g_{\mu\nu}| \ll |\bar{g}_{\mu\nu}|$, $|\delta v_{\mu}| \ll |\bar{v}_{\mu}|$,and $|\delta\phi| \ll |\bar{\phi}|$. Under an infinitesimal coordinate transformation

$$x^{\mu} \to \tilde{x}^{\mu} = x^{\mu} + \xi^{\mu} \quad , \quad \xi^{\mu} = (\xi^{0}, \xi^{\mathrm{V}i} + \delta^{ij}\xi^{\mathrm{S}}_{,j}) \ , \tag{B.2}$$

where $|\xi| \ll |x|$ is assumed, and $\xi^{\mathrm{V}i}_{,i} = 0$ with the notation for spatial partial derivatives $(\ )_{,i} \equiv \partial_i(\ )$, the tensor-, vector-, and scalar-type perturbations are transformed as follows

$$\begin{aligned} \delta\tilde{g}_{\mu\nu} =& \delta g_{\mu\nu} - \bar{g}_{\mu\sigma}\xi^{\sigma}_{,\nu} - \bar{g}_{\rho\nu}\xi^{\rho}_{,\mu} - \xi^{\rho}\bar{g}_{\mu\nu,\rho} \ , \\ \delta\tilde{v}_{\mu} =& \delta v_{\mu} - \bar{v}_{\nu}\xi^{\nu}_{,\mu} - \xi^{\nu}\bar{v}_{\mu,\nu} \ , \\ \delta\tilde{\phi} =& \delta\phi - \xi^{\mu}\bar{\phi}_{,\mu} \ . \end{aligned} \tag{B.3}$$

To be more specific, the metric perturbations on a flat FLRW metric are generally given by

$$ds^2 = -(1+2\Phi)dt^2 + 2a(t)B_i dx^i dt + a^2(t)\left[(1-2\Psi)\delta_{ij} + E_{ij}\right]dx^i dx^j \ , \tag{B.4}$$

where Φ is Newtonian potential, Ψ is the curvature perturbation, $B_i = B^{\rm S}_{,i} + B^{\rm V}_i$ is the shift, and $E_{ij} = 2E^{\rm S}_{,ij} + 2E^{\rm V}_{(i,j)} + h^{\rm TT}_{ij}$ is the spatial shear. These perturbations should satisfy the following conditions $\delta^{ij}B^{\rm V}_{i,j} = \delta^{ij}E^{\rm V}_{i,j} = \delta^{ij}E^{\rm S}_{,ij} = \delta^{ij}h^{\rm TT}_{ij} = \delta^{jk}h^{\rm TT}_{ij,k} = 0$. Here, the compact notation $E^{\rm V}_{(i,j)} = \left(E^{\rm V}_{i,j} + E^{\rm V}_{j,i}\right)/2$ is used. On the other hand, the perturbations in matter sector are given as

$$\begin{aligned} \rho(t,\mathbf{x}) = \bar{\rho}(t) + \delta\rho(t,\mathbf{x}) \quad &, \quad p(t,\mathbf{x}) = \bar{p} + \delta p(t,\mathbf{x}) \ , \\ u_\mu = (-1-\Phi, a v_i) \quad &, \quad u^\mu \left(1-\Phi, \delta^{ij}\left(v_j - B_j\right)/a\right) \ , \end{aligned} \tag{B.5}$$

where $v_i = v^{\rm S}_{,i} + v^{\rm V}_i$ with $v^{\rm V}_{i,i} = 0$. From Eqs. (B.3), it is straightforward to derive the following relations between two different gauges

$$\begin{aligned} \tilde{\Phi} = \Phi - \dot{\xi}^0 \ , \ \tilde{\Psi} = \Psi + H\xi^0 \ , \\ \tilde{E}^{\rm S} = E^{\rm S} - \xi^{\rm S} \ , \ \tilde{B}^{\rm S} = B^{\rm S} + \frac{1}{a}\xi^0 - a\dot{\xi}^{\rm S} \ , \\ \delta\tilde{\rho} = \delta\rho - \dot{\bar{\rho}}\xi^0 \ , \ \delta\tilde{p} = \delta p - \dot{\bar{p}}\xi^0 \ , \\ \tilde{v}^{\rm S} = v^{\rm S} + \frac{1}{a}\xi^0 \ , \ \delta\tilde{\phi} = \delta\phi - \dot{\bar{\phi}}\xi^0 \ , \\ \tilde{B}^{\rm V}_i = B^{\rm V}_i + a\delta_{ij}\dot{\xi}^{{\rm V}j} \ , \ \tilde{E}^{\rm V}_i = E^{\rm V}_i - \delta_{ij}\xi^{{\rm V}j} \ , \end{aligned} \tag{B.6}$$

while $v^{\rm V}_i$ and $h^{\rm TT}_{ij}$ are gauge-invariant automatically. From these transformation rules, it is easy to construct various gauge-invariant quantities, but not all of them are physically meaningful or useful. In other words, all physical quantities are gauge-invariant but gauge-invariant quantities are not necessarily physical.

Appendix C

Equations of Motion in Einstein Frame

In this appendix, the explicit expressions of the EF equations of motion for scalaron and Higgs in the mixed Higgs-R^2 inflation model are summarized.

Firstly, a list of first and second derivatives of the potential (2.124) is given because they are useful for the analysis and calculation.

$$\frac{U_{,\varphi}}{\alpha} = -\frac{\lambda}{2}\frac{M^2}{\tilde{M}^2}e^{-2\alpha\varphi}h^4 + \frac{3\xi}{2}M^2\left(1-2e^{-\alpha\varphi}\right)e^{-\alpha\varphi}h^2 + \frac{3}{2}M_{\rm pl}^2M^2\left(1-e^{-\alpha\varphi}\right)e^{-\alpha\varphi}\ , \tag{C.1}$$

$$U_{,h} = \lambda\frac{M^2}{\tilde{M}^2}e^{-2\alpha\varphi}h^3 - 3\xi M^2\left(1-e^{-\alpha\varphi}\right)e^{-\alpha\varphi}h\ , \tag{C.2}$$

$$\frac{U_{,\varphi\varphi}}{\alpha^2} = \lambda\frac{M^2}{\tilde{M}^2}e^{-2\alpha\varphi}h^4 - \frac{3\xi}{2}M^2\left(1-4e^{-\alpha\varphi}\right)e^{-\alpha\varphi}h^2 - \frac{3}{2}M_{\rm pl}^2M^2\left(1-2e^{-\alpha\varphi}\right)e^{-\alpha\varphi}\ , \tag{C.3}$$

$$U_{,hh} = 3\lambda\frac{M^2}{\tilde{M}^2}e^{-2\alpha\varphi}h^2 - 3\xi M^2\left(1-e^{-\alpha\varphi}\right)e^{-\alpha\varphi}\ , \tag{C.4}$$

$$\frac{U_{,\varphi h}}{\alpha} = -2\lambda\frac{M^2}{\tilde{M}^2}e^{-2\alpha\varphi}h^3 + 3\xi M^2\left(1-2e^{-\alpha\varphi}\right)e^{-\alpha\varphi}h\ . \tag{C.5}$$

Next, assuming the background spacetime to be the flat ($K = 0$) Friedmann metric (2.1), the Friedmann equation and background equations of motion for φ and h are given as follows

$$3M_{\rm pl}^2H^2 = \frac{1}{2}\dot{\varphi}^2 + \frac{1}{2}e^{-\alpha\varphi}\dot{h}^2 + U\ , \tag{C.6}$$

$$\ddot{\varphi} + 3H\dot{\varphi} + U_{,\varphi} + \frac{\alpha}{2}e^{-\alpha\varphi}\dot{h}^2 = 0\ , \tag{C.7}$$

$$\ddot{h} + 3H\dot{h} + e^{\alpha\varphi}U_{,h} - \alpha\dot{\varphi}\dot{h} = 0\ , \tag{C.8}$$

where the kinetic coupling is easily seen due to the non-canonical kinetic term of

Higgs in the action (2.124). Another useful form of the Friedmann equation is

$$-2M_{\rm pl}^2\dot{H} = \dot{\varphi}^2 + e^{-\alpha\varphi}\dot{h}^2 \ . \tag{C.9}$$

As can be seen, the kinetic term of the Higgs is suppressed by the factor $e^{-\alpha\varphi}$ that is significant during inflation $\alpha\varphi \gg 1$.

As for perturbations of scalaron and Higgs, it is usually convenient to fix a gauge before derivation. Transforming to other gauges can be done through the gauge transformation shown in Appendix B. One simple gauge choice would be the spatially flat gauge where the gauge invariant Sasaki-Mukhanov variable is simply the fluctuation of scalar field. Given the Fourier modes of $\delta\varphi$ and δh as

$$\delta\varphi(t,\mathbf{x}) = \int \frac{d^3k}{(2\pi)^3} e^{i\mathbf{k}\cdot\mathbf{x}} \left[\delta\varphi_k(t) a_{\mathbf{k}} + \delta\varphi_k^*(t) a_{-\mathbf{k}}^\dagger\right] \ , \tag{C.10}$$

$$\delta h(t,\mathbf{x}) = \int \frac{d^3k}{(2\pi)^3} e^{i\mathbf{k}\cdot\mathbf{x}} \left[\delta h_k(t) a_{\mathbf{k}} + \delta h_k^*(t) a_{-\mathbf{k}}^\dagger\right] \ , \tag{C.11}$$

their equations of motion can be derived from Eq. (2.98)

$$\ddot{\delta\varphi}_k + 3H\dot{\delta\varphi}_k + \left(k_p^2 + U_{,\varphi\varphi} - \frac{\alpha^2}{2} e^{-\alpha\varphi}\dot{h}^2\right)\delta\varphi_k = -\alpha e^{-\alpha\varphi}\dot{h}\dot{\delta h}_k - U_{,\varphi h}\delta h_k, \tag{C.12}$$

$$\ddot{\delta h}_k + (3H - \alpha\dot{\varphi})\,\dot{\delta h}_k + \left(k_p^2 + e^{\alpha\varphi}U_{,hh}\right)\delta h_k = \alpha\dot{h}\dot{\delta\varphi}_k - e^{\alpha\varphi}\left(\alpha U_{,h} + U_{,\varphi h}\right)\delta\varphi_k, \tag{C.13}$$

where $k_p \equiv k/a(t)$ is the physical wavelength.

Appendix D

Mathieu Equation

In this appendix, the basics of the Mathieu equation are summarized, mainly based on Refs. [176, 190], including the perturbative treatment and the Floquet solution.

Mathieu equation is a linear second-order ordinary differential equation describing a periodically driven oscillator which is usually written in the following form

$$y_{,zz}(z) + [A - 2q\cos(2z)]\, y(z) = 0 \ , \tag{D.1}$$

where A and q are constant parameters of the system, and the comma in subscript denotes partial derivatives. When $A > 0$ and $q = 0$, the harmonic oscillator is recovered. In this appendix, A can be either positive or negative, while only $q > 0$ is considered because a negative sign can be realized simply by a phase shift in the cosine function. Besides reheating, this equation can be encountered in the analysis of, for example, a pendulum with a periodically moving support in the vertical direction, and the Helmholtz equation in elliptic cylindrical coordinates. Mathieu function is the solution of Eq. (D.1) while sometimes it refers to the solution with period π or 2π specifically.

In the following, perturbative treatment is used to discuss the case where the excitation is small $q \ll 1$ as a first step, and then the Floquet theory is applied to a more general case to find out the stability chart of the Mathieu equation.

D.1 Perturbative Treatment

In the case $q \ll 1 \lesssim A$ in Eq. (D.1), the method of multiple scales can be used to solve the equation perturbatively. Defining $\varepsilon \equiv 2q$ for convenience, the small parameter ε indicates the existence of a long typical scale $\sim \varepsilon^{-1}$. Therefore, a possible solution can be written in the following form

$$y(z) = \tilde{y}(z, \tilde{z}) \ , \tag{D.2}$$

which is a function of the original argument z and the "slow" variable $\tilde{z} \equiv \varepsilon z$. As a result, the total derivative with respect to z becomes

$$d/dz = 1 \cdot \partial/\partial z + \varepsilon \cdot \partial/\partial \tilde{z} \ . \tag{D.3}$$

Using the Poincaré-Lindstedt method to expand the solution $\tilde{y}(z, \tilde{z})$ and the parameter A in terms of ε as follows

$$\begin{aligned} \tilde{y}(z, \tilde{z}) &= \tilde{y}_0(z, \tilde{z}) + \varepsilon \tilde{y}_1(z, \tilde{z}) + \varepsilon^2 \tilde{y}_2(z, \tilde{z}) + \mathcal{O}(\varepsilon^3) \ , \\ A &= A_0 + \varepsilon A_1 + \varepsilon^2 A_2 + \mathcal{O}(\varepsilon^3) \ , \end{aligned} \tag{D.4}$$

and combining Eq. (D.3), it is easy to write down the perturbative Mathieu equation order by order in terms of ε.

The zeroth order is simply a harmonic oscillator equation with natural frequency given by $A_0^{1/2}$

$$\tilde{y}_{0,zz} + A_0 \tilde{y}_0 = 0 \ , \tag{D.5}$$

whose solution is well-known

$$\tilde{y}_0(z, \tilde{z}) = B_1(\tilde{z}) e^{iA_0^{1/2} z} + B_2(\tilde{z}) e^{-iA_0^{1/2} z} \ , \tag{D.6}$$

where $B_1(\tilde{z})$ and $B_2(\tilde{z})$ are arbitrary complex functions of $\tilde{z}$.

The first-order equation is non-trivial and written as

$$\tilde{y}_{1,zz} + A_0 \tilde{y}_1 = \tilde{y}_0 \cos(2z) - 2\tilde{y}_{0,z\tilde{z}} - A_1 \tilde{y}_0 \ , \tag{D.7}$$

where the left hand side is simple, while the right hand side consists of several modes with different frequencies among which the term with $\cos(2z)$ is especially important for the analysis here. Specifically, by inserting the zeroth-order solution (D.6), the right hand side is given by

$$\begin{aligned} \tilde{y}_0 \cos(2z) - 2\tilde{y}_{0,z\tilde{z}} - A_1 \tilde{y}_0 = & \frac{B_1}{2} \left[e^{i\left(A_0^{1/2}+2\right)z} + e^{i\left(A_0^{1/2}-2\right)z} \right] \\ & + \frac{B_2}{2} \left[e^{-i\left(A_0^{1/2}+2\right)z} + e^{-i\left(A_0^{1/2}-2\right)z} \right] \\ & - \left(A_1 B_1 + 2iA_0^{1/2} B_{1,\tilde{z}} \right) e^{iA_0^{1/2} z} \\ & - \left(A_1 B_2 - 2iA_0^{1/2} B_{2,\tilde{z}} \right) e^{-iA_0^{1/2} z} \ . \end{aligned} \tag{D.8}$$

The third and fourth lines in Eq. (D.8) contain explicit secular terms for general A_0 which can be removed by choosing $B_1(\tilde{z})$ and $B_2(\tilde{z})$ properly to avoid unbounded solution as

$$\begin{aligned} B_{1,\tilde{z}} - i\frac{A_1}{2A_0^{1/2}}B_1 = 0 \ , \\ B_{2,\tilde{z}} + i\frac{A_1}{2A_0^{1/2}}B_2 = 0 \ . \end{aligned} \tag{D.9}$$

In these terms, the perturbative source has no effect to the solution. As for the first and second lines in Eq. (D.8), where $\cos(2z)$ plays an important role, contains secular terms only if one of the following conditions are satisfied

$$\begin{aligned} A_0 = \left(A_0^{1/2} + 2\right)^2 \ , \\ A_0 = \left(A_0^{1/2} - 2\right)^2 \ . \end{aligned} \tag{D.10}$$

Real solution for A_0 only exists in the lower of Eq. (D.10) which gives $A_0 = 1$. As a result, all four lines should be taken into account simultaneously to pick up all the secular terms whose coefficients are given by

$$\begin{aligned} B_{1,\tilde{z}} + iB_2/4 - iA_1B_1/2 = 0 \ , \\ B_{2,\tilde{z}} - iB_1/4 + iA_1B_2/2 = 0 \ , \end{aligned} \tag{D.11}$$

which should be satisfied to remove all the secular terms for the first-order equation (D.7). This set of equations can be easily transformed into two identical decoupled second-order ordinary differential equations as

$$\begin{aligned} B_{1,\tilde{z}\tilde{z}} + \left(A_1^2/4 - 1/16\right)B_1 = 0 \ , \\ (B_1 \leftrightarrow B_2) \ . \end{aligned} \tag{D.12}$$

However, even so, if $B_1(\tilde{z})$ and $B_2(\tilde{z})$ themselves are growing unboundedly, the remaining source terms proportional to them still induce instability. Obviously, the solutions are stable when $A_1^2 > 1/4$ and unbounded when $A_1^2 < 1/4$ with $A_1^2 = 1/4$ being the transition line. Therefore, the first-order equation induces an instability band around $A = 1$. More specifically, the two transition lines are

$$A = 1 \pm \varepsilon/2 = 1 \pm q \ , \tag{D.13}$$

between which is one of the instability bands for the solution. This is shown in Fig. D.1. Within this instability band, the solution of Mathieu equation grows expo-

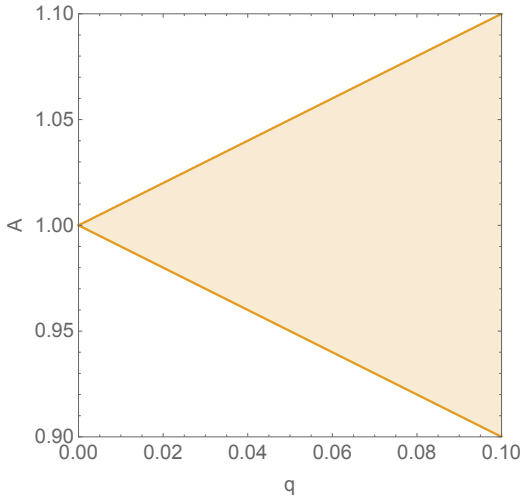

Figure D.1: The first instability band of Mathieu equation (D.1) with $0 < q \ll 1$ up to first order. The shaded region corresponds to the unstable regime given by $A_0 = 1^2$ and $1 - q < A < 1 + q$ according to Eq. (D.13).

nentially $\propto \exp\left[\mu^{(1)} z\right]$ where the superscript "(1)" denotes the first instability band, which can calculated from Eqs. (D.12). When $A_1^2 < 1/4$, the solutions for $B_1(\tilde{z})$ and $B_2(\tilde{z})$ are dominated by the term

$$\propto \exp\left(\sqrt{\frac{1}{16A_0} - \frac{A_1^2}{4A_0}}\tilde{z}\right) = \exp\left(\sqrt{\frac{q^2}{4} - A_1^2 q^2}\ z\right) \ , \tag{D.14}$$

where $A_0 = 1$ has been used for the first band. This exponent finally enters the solution $y(z)$ for Eq. (D.1). Since $A = 1 \pm 2A_1 q \simeq 1$ in this case, approximately it gives $\pm A_1 q \simeq \sqrt{A} - 1$ such that

$$\mu^{(1)} \simeq \left[q^2/4 - \left(\sqrt{A} - 1\right)^2\right]^{1/2} \ . \tag{D.15}$$

As will be shown in next section, there are infinite instability bands for Mathieu equation with $A > 0$ which are characterized by $A = n^2$ with $n \in \mathbb{Z}_+$. The bands other than $n = 1$ emerge at higher order in the perturbative treatment. For example, if the analysis above is continued to the second order, the equation for $\tilde{y}_2(z, \tilde{z})$ is given by

$$\tilde{y}_{2,zz} + A_0 \tilde{y}_2 = \tilde{y}_1 \cos(2z) - \tilde{y}_{0,\tilde{z}\tilde{z}} - 2\tilde{y}_{1,z\tilde{z}} - A_2 \tilde{y}_0 - A_1 \tilde{y}_1 \ . \tag{D.16}$$

As usual, the first-order equation (D.7) must be solved before dealing with the second-order. Using the method of variation of constants, the solution $\tilde{y}_1$ can be written in

the form as

$$\tilde{y}_1(z,\tilde{z}) = B_3(z,\tilde{z})e^{iA_0^{1/2}z} + B_4(z,\tilde{z})e^{-iA_0^{1/2}z} \ . \tag{D.17}$$

Without explicitly solving the equations for $B_3(z,\tilde{z})$ and $B_4(z,\tilde{z})$, it is easy to see that they contain the following modes

$$\begin{aligned} B_3(z,\tilde{z}) &\supset e^{\pm 2iz} \ , \ e^{-2i\left(A_0^{1/2}\pm 1\right)z} \ , \\ B_4(z,\tilde{z}) &\supset e^{\pm 2iz} \ , \ e^{+2i\left(A_0^{1/2}\pm 1\right)z} \ , \end{aligned} \tag{D.18}$$

such that the term with driving source $\tilde{y}_1\cos(2z)$ in Eq. (D.16) gives the most non-trivial mode $e^{\pm i\left(A_0^{1/2}\pm 4\right)z}$. Consequently, this mode turns out to resonantly enhance the solution if $A_0 = 4$, indicating a new instability band characterized by $A = 2^2$. Other instability bands with $n > 2$ can be found in a similar way. Also note that the width of instability bands for $q \ll 1$ decreases as q^n, so practically the first band is the most important one as it is the widest. Yet, the perturbative treatment presented above only covers the regime $0 < q \ll 1$. A more systematic way to analyze Mathieu equation is to use Floquet theory as shown in next section.

D.2 Floquet Solution and Stability Chart

For a general equation

$$y_{,zz}(z) + [A - P(z)]\, y(z) = 0 \ , \tag{D.19}$$

where $P(z)$ is a periodic function with period T_P, the solution that

$$y(z + T_P) = \sigma y(z) \ , \tag{D.20}$$

is called the Floquet solution. Clearly, if $|\sigma| > 1$, the solution $y(z)$ is unbounded for large z. In the following, the Floquet solution for Mathieu equation (D.1) is analyzed as one special case of Eq. (D.19) with $P(z) = 2q\cos(2z)$ and $T_P = \pi$.

Given a fundamental set of solutions $y_{f1}(z)$ and $y_{f2}(z)$ that satisfy the following initial conditions

$$\begin{cases} y_{f1}(0) = 1 \ , & y_{f1,z}(0) = 0 \ , \\ y_{f2}(0) = 0 \ , & y_{f2,z}(0) = 1 \ , \end{cases} \tag{D.21}$$

the resulting Wronskian is constant

$$W\left[y_{f1}, y_{f2}\right](z) = y_{f1}y_{f2,z} - y_{f1,z}y_{f2} = 1 \ , \tag{D.22}$$

and the general solution for Eq. (D.19) can be constructed as

$$y(z) = D_1 y_{f1}(z) + D_2 y_{f2}(z) \ , \tag{D.23}$$

where D_1 and D_2 are arbitrary constants. Using Eq. (D.20), it is easy to find that

$$\begin{pmatrix} y_{f1}(T_P) - \sigma & y_{f2}(T_P) \\ y_{f1,z}(T_P) & y_{f2,z}(T_P) - \sigma \end{pmatrix} \begin{pmatrix} D_1 \\ D_2 \end{pmatrix} = 0 \ , \tag{D.24}$$

which possesses non-trivial solution when the determinant of the coefficient matrix vanishes, equivalently,

$$\sigma^2 - \left[y_{f1}(T_P) + y_{f2,z}(T_P) \right] \sigma + 1 = 0 \ , \tag{D.25}$$

where the Wronskian (D.22) has been used. The discriminant of this quadratic equation is simply

$$\Delta_\sigma = \left[y_{f1}(T_P) + y_{f2,z}(T_P) \right]^2 - 4 \ . \tag{D.26}$$

If $\Delta_\sigma > 0$, there exits two different real roots $\sigma_\pm$ (assuming $\sigma_+ > \sigma_-$) which satisfy $\sigma_+ \sigma_- = 1$. Therefore, the Floquet solution (D.20) is exponentially growing in the case $\sigma_+ > 1$. If $\Delta_\sigma < 0$, only imaginary roots with modulus of unity exist so the Floquet solution is stable. The condition $\Delta_\sigma = 0$ gives the transition curves between stable and unstable regimes. In such a case, the roots are either $\sigma_+ = \sigma_- = 1$ or $\sigma_+ = \sigma_- = -1$ that correspond to solutions with period T_P and $2T_P$, respectively. Numerical calculation of $|y_{f1}(T_P) + y_{f2,z}(T_P)|$ with the initial conditions (D.21) then gives the stability chart of Mathieu equation that is shown in Fig. (D.2).

Obviously, the Mathieu equation covers the tachyonic instability regime, i.e. for $A - 2q\cos(2z) < 0$. Actually, in most case with a negative A, the system presents such kind of instability. As in the simplest example, the solution for Eq. (D.19) with $A < 0$ and $P(z) = 0$ is given by

$$y(z) = D_3 e^{|A|^{1/2} z} + D_4 e^{-|A|^{1/2} z} \ , \tag{D.27}$$

where D_3 and D_4 are arbitrary constants. Apparently, the amplitude of the first term grows exponentially as z increases if $D_3 \neq 0$. Note, however, that there exits stable regime even for $A < 0$ in Fig. D.2, for which a well-known example is the Kapitza's pendulum (a vertically forced inverted pendulum)[56].

[56] This stability was first noticed by Stephenson [191,192] and later analyzed by Kapitza [193,194]. See also Ref. [195].

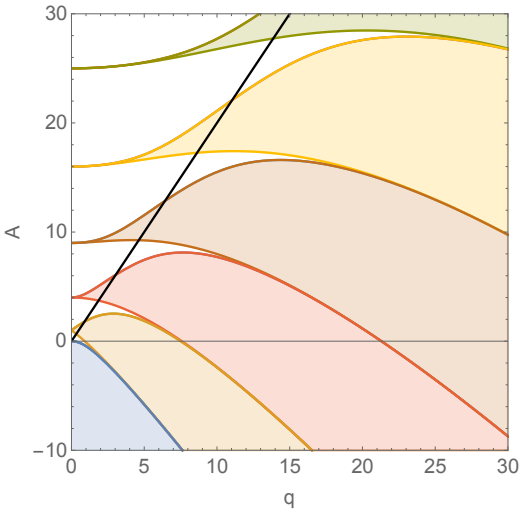

Figure D.2: The stability chart of Mathieu equation (D.1) with $q > 0$ generated by Wolfram Mathematica. The shaded region corresponds to the unstable regimes. It can be seen that the instability bands in $A > 0$ regime are characterized by $A = n^2$ with $n \in \mathbb{Z}_+$. As n increases, the bandwidth in $q \ll 1$ regime decreases. Fig. D.1 corresponds to the band with smallest positive A in $q \ll 1$ regime and of the same color in this figure. The black thick line represents $A = 2q$ which is useful when considering realistic models of reheating, e.g. in Sec.3.1.

When talking about the instability in this context, the solution $y(z)$ can really diverge. The physical reason is that the source term contains infinite energy, or the backreaction from the growth of $y(z)$ to the source is not taken into account, i.e. q being constant in the case of Eq. (D.1). Here, this situation is referred to as "global instability" by the author. However, in a more realistic case, e.g. particle production in cosmology, the source contains finite energy, and the backreaction from the production becomes vital as its energy grows. For instance, q decreases in time as the energy of the source is taken away such that $y(z)$ cannot grow unboundedly. Therefore, the backreaction should be taken into consideration carefully. In this sense, even if the chosen parameter set locates in the stable regime in Fig. D.2, the physical system may still experience (referred to by the author as) "local instability" during which the energy of the production rapidly becomes comparable with the background or the source. In such a case, the stability chart D.2 is not enough to determine the final fate of the system.

Here, only the undamped case is discussed. In a more realistic case, the damping effect shows up. For example, in cosmology, a scalar field feels some friction due to cosmic expansion. In the presence of damping, the stability chart in Fig. D.2 is modified, especially the parts of the tongues close to the vertical axis being smoothed

and separated from the axis, which makes the instability regions in the perturbative regime disappear. More detail can be found in Ref. [176].

Appendix E

Parabolic Cylinder Function

In this appendix, some useful properties of parabolic cylinder functions are summarized, mainly about the asymptotic behavior for large argument, based on Ref. [196].

Parabolic cylinder function $W(a, \pm x)$ are two linearly independent solutions for the following second order differential equation

$$W_{,xx} + \left(x^2/4 - a\right) W = 0 \ , \tag{E.1}$$

where x is a real variable and $a \in \mathbb{R}$ for the present purpose. More specifically, $W(a, \pm x)$ can be written as

$$W(a, \pm x) = \frac{(\cosh \pi a)^{1/4}}{2\sqrt{\pi}} \left(G_1(a) y_1(a, x) \mp \sqrt{2} G_3(a) y_2(a, x) \right) \ , \tag{E.2}$$

where $y_1(a, x)$ and $y_2(a, x)$ can be expressed in terms of the confluent hypergeometric function of the first kind, ${}_1F_1(a; b; z)$, as

$$\begin{aligned} y_1(a, x) &= e^{-ix^2/4} \ {}_1F_1\left(1/4 - ia/2 \ ; \ 1/2 \ ; \ ix^2/2\right) \ , \\ y_2(a, x) &= x e^{i\pi/4 - ix^2/4} \ {}_1F_1\left(3/4 - ia/2 \ ; \ 3/2 \ ; \ ix^2/2\right) \ , \end{aligned} \tag{E.3}$$

while $G_1(a)$ and $G_3(a)$ are given in terms of Gamma function as

$$\begin{aligned} G_1(a) &= \left|\Gamma\left(1/4 + ia/2\right)\right| \ , \\ G_3(a) &= \left|\Gamma\left(3/4 + ia/2\right)\right| \ . \end{aligned} \tag{E.4}$$

It is not difficult to show that, at $x = 0$,

$$\begin{aligned} W(a, 0) &= 2^{-3/4} \sqrt{G_1(a)/G_3(a)} \ , \\ W'(a, 0) &= -2^{-1/4} \sqrt{G_3(a)/G_1(a)} \ , \end{aligned} \tag{E.5}$$

so the Wronskian of these two solutions are time-independent and non-vanishing

$$W\left[W(a,x),W(a,-x)\right]=1\ , \tag{E.6}$$

which is consistent with the statement of the linear independence of $W(a,\pm x)$ at the beginning.

The asymptotic behavior when $x\gg|a|$ is usually useful in practice. Specifically, the asymptotic form is given by

$$\begin{aligned}
W(a,x)&=\sqrt{\frac{2\bar{k}}{x}}\left[s_1(a,x)\cos\left(\frac{x^2}{4}-a\ln x\ +\frac{\pi}{4}+\frac{\vartheta_k}{2}\right)\right.\\
&\qquad\left.-s_2(a,x)\sin\left(\frac{x^2}{4}-a\ln x\ +\frac{\pi}{4}+\frac{\vartheta_k}{2}\right)\right]\ ,\\
W(a,-x)&=\sqrt{\frac{2}{\bar{k}x}}\left[s_1(a,x)\sin\left(\frac{x^2}{4}-a\ln x\ +\frac{\pi}{4}+\frac{\vartheta_k}{2}\right)\right.\\
&\qquad\left.+s_2(a,x)\cos\left(\frac{x^2}{4}-a\ln x\ +\frac{\pi}{4}+\frac{\vartheta_k}{2}\right)\right]\ ,
\end{aligned} \tag{E.7}$$

where $\bar{k}\equiv\sqrt{1+e^{2\pi a}}-e^{\pi a}$ and $\vartheta_k\equiv\arg\Gamma(1/2+ia)$, while the two functions $s_1(a,x)$ and $s_2(a,x)$, for large x, are asymptotically given as

$$\begin{aligned}
s_1(a,x)&\sim 1+\frac{v_2}{1!2}x^{-2}-\frac{u_4}{2!2^2}x^{-4}+\mathcal{O}(x^{-6})\ ,\\
s_2(a,x)&\sim -\frac{u_2}{1!2}x^{-2}-\frac{v_4}{2!2^2}x^{-4}+\mathcal{O}(x^{-6})\ ,
\end{aligned} \tag{E.8}$$

with $u_r+iv_r=\Gamma(r+1/2+ia)/\Gamma(1/2+ia)$. Up to leading order in the power of x, $W(a,x)$ can be approximated as $(x>0)$

$$\begin{aligned}
W(a,x)&\to\sqrt{\frac{2\bar{k}}{x}}\ \cos\left(\frac{x^2}{4}+\frac{\vartheta_k}{2}\right)=\sqrt{\frac{\bar{k}}{2x}}\left(e^{ix^2/4+i\vartheta_k/2}+e^{-ix^2/4-i\vartheta_k/2}\right)\ ,\\
W(a,-x)&\to\sqrt{\frac{2}{\bar{k}x}}\ \sin\left(\frac{x^2}{4}+\frac{\vartheta_k}{2}\right)=-i\sqrt{\frac{1}{2\bar{k}x}}\left(e^{ix^2/4+i\vartheta_k/2}-e^{-ix^2/4-i\vartheta_k/2}\right)\ .
\end{aligned} \tag{E.9}$$

Appendix F

Airy Function

In this appendix, some useful properties of the Airy functions are summarized, mainly about the asymptotic behavior for large argument, based on Ref. [196].

Airy function $\mathrm{Ai}(x)$ and $\mathrm{Bi}(x)$ are two linearly independent solutions to the Airy equation

$$w_{,xx} - xw = 0 \ , \tag{F.1}$$

where x is kept to be real for the purpose of this thesis. The behavior of the two Airy functions is shown in Fig. F.1. The Airy functions can be expressed in terms of the modified Bessel function of the first kind, $I_\nu(z)$, as

$$\begin{aligned} \mathrm{Ai}(x) &= \frac{\sqrt{x}}{3}\left[I_{-1/3}\left(\frac{2}{3}x^{3/2}\right) - I_{1/3}\left(\frac{2}{3}x^{3/2}\right)\right] \ , \\ \mathrm{Bi}(x) &= \sqrt{\frac{x}{3}}\left[I_{-1/3}\left(\frac{2}{3}x^{3/2}\right) + I_{1/3}\left(\frac{2}{3}x^{3/2}\right)\right] \ . \end{aligned} \tag{F.2}$$

It can be easily shown that the Wronskian of $\mathrm{Ai}(x)$ and $\mathrm{Bi}(x)$ is time-independent and non-vanishing

$$W\left[\mathrm{Ai}(x), \mathrm{Bi}(x)\right] = \pi^{-1} \ , \tag{F.3}$$

where the following values have been used

$$\begin{aligned} \mathrm{Ai}(0) &= \frac{\mathrm{Bi}(0)}{\sqrt{3}} = \frac{3^{-2/3}}{\Gamma(2/3)} \ , \\ -\mathrm{Ai}'(0) &= \frac{\mathrm{Bi}'(0)}{\sqrt{3}} = \frac{3^{-1/3}}{\Gamma(1/3)} \ . \end{aligned} \tag{F.4}$$

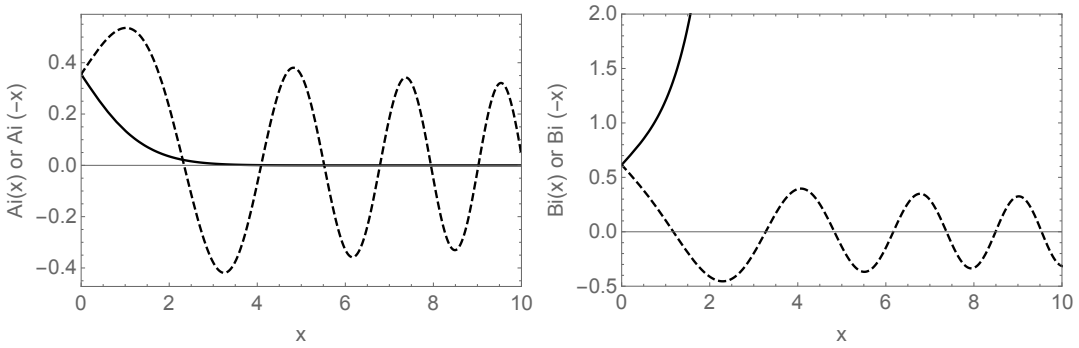

Figure F.1: Airy functions $\mathrm{Ai}(x)$ (left) and $\mathrm{Bi}(x)$ (right) with real variable. Solid: positive argument $x > 0$. Dashed: negative argument $-x < 0$. It can be seen that, for $-x < 0$ both functions oscillate with some phase difference, but for $x > 0$, there is exponential suppression in $\mathrm{Ai}(x)$ while exponential growth in $\mathrm{Bi}(x)$.

Practically, the asymptotic behavior of the Airy functions are very useful for approximation. Specifically, for $x \gg 1$, $\mathrm{Ai}(x)$ and $\mathrm{Ai}(-x)$ can be expanded asymptotically as

$$\begin{aligned}
\mathrm{Ai}(x) &\sim \frac{1}{2\sqrt{\pi}} \frac{e^{-2x^{3/2}/3}}{x^{1/4}} \left[1 - \frac{\Gamma\left(3+1/2\right)}{54\Gamma(3/2)} \frac{3}{2x^{3/2}} + \mathcal{O}\left(x^{-3}\right)\right] , \\
\mathrm{Ai}(-x) &\sim \frac{1}{\sqrt{\pi}} \frac{1}{x^{1/4}} \left[\sin\left(\frac{2}{3}x^{3/2} + \frac{\pi}{4}\right) + \mathcal{O}\left(x^{-3/2}\right)\right] ,
\end{aligned} \tag{F.5}$$

where the exponential suppression is obvious in the positive argument case. On the other hand, the asymptotic expansion of $\mathrm{Bi}(x)$ and $\mathrm{Bi}(-x)$ are given by

$$\begin{aligned}
\mathrm{Bi}(x) &\sim \frac{1}{\sqrt{\pi}} \frac{e^{2x^{3/2}/3}}{x^{1/4}} \left[1 + \frac{\Gamma\left(3+1/2\right)}{54\Gamma(3/2)} \frac{3}{2x^{3/2}} + \mathcal{O}\left(x^{-3}\right)\right] , \\
\mathrm{Bi}(-x) &\sim \frac{1}{\sqrt{\pi}} \frac{1}{x^{1/4}} \left[\cos\left(\frac{2}{3}x^{3/2} + \frac{\pi}{4}\right) + \mathcal{O}\left(x^{-3/2}\right)\right] ,
\end{aligned} \tag{F.6}$$

where it is easy to see the exponential enhancement in the positive argument case.

The property of $\mathrm{Ai}(x)$ and $\mathrm{Bi}(x)$ that the behavior changes from oscillation to exponential suppression/enhancement when the argument changes sign is exactly desired when investigating a tachyonic regime between two adiabatic ones. Therefore, the Airy functions are essential for the study of tachyonic preheating, as shown in the main text.

Appendix G

Energy Distribution between Higgs and Scalaron

In this appendix, the energy distribution between Higgs and scalaron in EF during (p)reheating is discussed. This point is significant on at least two aspects considered here. Firstly, in Sec. 4.1 and 4.2, a simple trick is used to calculate the amplitude of the first oscillation of the homogeneous background so that analytical calculation of the particle production of spiky preheating and tachyonic preheating is easily carried out. This trick relies on the fact that the kinetic energy of Higgs is negligible when φ reaches its maximal amplitude during the oscillation, i.e. $\dot{\varphi} = 0$. It can be true because $h \simeq 0$ in both cases. Secondly, as discussed in the main text in Sec. 4.3, the energy distribution is important to determine the efficiency of the perturbative decay for different parameter choices. The reason is as follows. The decay rate of Higgs is much larger than that of scalaron. If a large fraction of energy is stored in the Higgs field, it is expected that the decay would be more efficient than the case where most energy is stored in the scalaron. As will be shown below, the closer to (but not coinciding with[57]) the critical parameters that can realize strong tachyonic preheating in the first scalaron oscillation after the end of inflation, the more energy is stored in the Higgs field, which results in a more efficient perturbative reheating and higher reheating temperature as discussed in the main text. Therefore, when scanning the parameter space to obtain the reheating temperature from perturbative decay, dips and peaks can be seen due to the changing "distance" from the critical parameters. Of course, if subsequent oscillations are also taken into account, a large amount of energy transferred from the scalaron to the Higgs is possible for more parameters. In

[57] If backreaction is taken into account, tachyonic instability in the critical case might be terminated midway, which could cause large amplitude of Higgs oscillation and so large energy stored in Higgs field, but this case is not considered in this thesis.

this case, the effect is expected to be relatively weak because the energy of the system is decreasing in time generically.

The discussion is separated into two parts for (1) $\varphi < 0$ regime during the first scalaron oscillation, and (2) subsequent oscillations, respectively, and is restricted to $\xi \gg \mathcal{O}(10)$ because it could be done analytically for the reason mentioned in Sec. 4.3. Since Higgs is approximately a harmonic oscillator in this case, its kinetic energy can be used to characterize the total energy stored in Higgs.

G.1 Negative Scalaron Regime during First Oscillation

In the regime $\varphi < 0$ during the first scalaron oscillation, the kinetic energy of Higgs is subdominant compared with the potential energy for most of the time, which can be shown as follows. The effective mass of Higgs is given in the upper of Eq. (4.95) while the typical amplitude is $h_{\rm osc} \sim M_{\rm pl}/\xi_c$. Therefore, the averaged kinetic energy can be estimated as

$$E_{h,\rm kin} \sim m_{h_{\rm osc}}^2 \frac{M_{\rm pl}^2}{\xi_c^2} \sim \frac{\xi}{\xi_c^2} M^2 M_{\rm pl}^2 \alpha |\langle\varphi\rangle_{\rm ave}| \ . \tag{G.1}$$

where $\langle\varphi\rangle_{\rm ave}$ denotes the time averaged value of φ during this period. On the other hand, the potential energy density is given by

$$U_0(\varphi) \sim M_{\rm pl}^2 M^2 \left(\alpha\langle\varphi\rangle_{\rm ave}\right)^2 \ . \tag{G.2}$$

The ratio between the kinetic and potential energy is then

$$\frac{E_{h,\rm kin}}{U_0(\varphi<0)} \sim \frac{\xi}{\xi_c^2} \frac{1}{\alpha|\langle\varphi\rangle_{\rm ave}|} \ll 1 \tag{G.3}$$

which is consistent with our expectation. Therefore, the conclusion in Sec. 4.1 and 4.2 can be safely used that the amplitude of φ when $\varphi < 0$ for the first time is given by Eq. (4.15).

G.2 Subsequent Oscillations

The energy of the homogeneous Higgs field in the subsequent oscillations is largely affected by the period $\varphi > 0$ in the first scalaron oscillation. The argument is based on the particular shape of the potential shown in Fig. 2.2. If the system starts with a nearly-critical parameter, by climbing up the potential hill around $h = 0$ in $\varphi > 0$

regime and falling to one of the valleys during oscillation, scalaron can easily generate a large amplitude of Higgs oscillation $|h_{\rm osc}| \sim |h_{\rm v}|$ around the valley, which means that more energy is transferred to the Higgs. On the contrary, it is difficult for the Higgs to "return" energy to the scalaron as long as the Higgs stays in the valleys when $\varphi > 0$ in later evolution, which is the general case because fine-tuning is needed to climb up the hill (again) [51]. Consequently, if a large fraction of energy is transferred to the Higgs field in the first scalaron oscillation, this amount of energy will decay through Higgs, which is efficient. On the other hand, starting with a far-from-critical parameter, the oscillation amplitude of Higgs stays small long enough until an opportunity for the inflaton to climb up the hill in some subsequent oscillations. After that moment, the perturbative decay process can become more efficient, but the whole reheating period must be more extended than the former case because the possible maximal efficiency of the tachyonic instability decreases as the amplitude of scalaron oscillation gets smaller. Thus, the following discussion focuses on the regime $\varphi > 0$ in the latter part of the first scalaron oscillation.

Firstly, consider the case where $|h_{\rm osc}| \sim |h_{\rm v}|$ when the model parameter is nearly-critical. Specifically, the kinetic energy of Higgs is estimated as

$$E_{h,\rm kin} \sim m_{h_{\rm osc}}^2 h_{\rm osc}^2 \sim m_{h_{\rm osc}}^2 h_{\rm v}^2 \sim \mathcal{O}(10) \times \frac{\xi^2}{\lambda} \tilde{M}^2 M^2 \left(\alpha\varphi\right)^2 \ , \tag{G.4}$$

while the potential energy is given by

$$U_{\rm v}(\varphi > 0) \sim M_{\rm pl}^2 \tilde{M}^2 \left(\alpha\varphi\right)^2 \ . \tag{G.5}$$

As a result, the ratio between them is given by

$$\frac{E_{h,\rm kin}}{U_{\rm v}(\varphi > 0)} \sim \mathcal{O}(10) \times \frac{\xi^2}{\lambda} \frac{M^2}{M_{\rm pl}^2} = \mathcal{O}(10) \times \frac{1}{3} \left(\frac{M^2}{\tilde{M}^2} - 1 \right) \ . \tag{G.6}$$

For the case of interest $\xi \gg \mathcal{O}(10)$, this could be much larger than order of unity, which means that a large fraction of energy is stored in the homogeneous Higgs field. Of course, the calculation above is just order estimate because generally speaking $|h_{\rm osc}|$ cannot really exceed or equal $|h_{\rm v}|$. Even if it does in some specific case, it is beyond the scope of the discussion here. Next, consider the case where $|h_{\rm osc}| \ll |h_{\rm v}|$ when the model parameter is far from being critical. Repeating the calculation above while setting $|h_{\rm osc}| \sim M_{\rm pl}/\xi_c$ results in the following estimate

$$\frac{E_{h,\rm kin}}{U_{\rm v}(\varphi > 0)} \sim \frac{m_{h_{\rm osc}}^2 M_{\rm pl}^2/\xi_c^2}{M_{\rm pl}^2 \tilde{M}^2 (\alpha\varphi)^2} \sim \frac{\xi}{\xi_c^2} \frac{M^2}{\tilde{M}^2} \frac{1}{\alpha\varphi} \leq \left. \frac{\xi}{\xi_c^2} \frac{M^2}{\tilde{M}^2} \frac{1}{\alpha\varphi} \right|_{\xi=\xi_s} \simeq \frac{0.3}{\alpha\varphi} \sim \mathcal{O}(1) \ . \tag{G.7}$$

In conclusion, there is a larger fraction of energy stored in Higgs for model parameters closer to critical cases while a smaller fraction for parameters far from the critical points.

Appendix H

Derivation of Decay Rate of Higgs

In this appendix, the derivation of the decay rates for the Higgs field into SM particles is presented in the adiabatic regime when the scalaron motion is sufficiently slow in the time scale of the Higgs oscillation. Only the decay of Higgs into $W^{\pm}$, Z bosons and top, bottom quarks is considered here. Also, $\lambda = 0.01$ is fixed for definiteness.

In the JF, the Lagrangian for relevant sector is written as

$$\mathcal{L}_{\rm J} \supset -g_{\rm J}^{\mu\nu} \left(D_{{\rm J}\mu}\mathcal{H}_{\rm SM}\right)^{\dagger} D_{{\rm J}\nu}\mathcal{H}_{\rm SM} - \lambda|\mathcal{H}_{\rm SM}|^4 + K_{\rm J,gauge} - \frac{y_t}{\sqrt{2}}h\bar{t}t - \frac{y_b}{\sqrt{2}}h\bar{b}b \ , \tag{H.1}$$

where $D_{{\rm J}\mu} = \nabla_{{\rm J}\mu} + \frac{i}{2}g'B_\mu + igW_\mu^a\tau^a$ is the covariant derivative with $\sigma^a = 2\tau^a$ the Pauli matrices, and $K_{\rm J,gauge}$ is the gauge invariant kinetic terms of the gauge fields given as

$$\begin{aligned} K_{\rm J,gauge} =& -\frac{1}{4}g_{\rm J}^{\mu\rho}g_{\rm J}^{\nu\sigma}B_{\mu\nu}B_{\rho\sigma} - \frac{1}{4}g_{\rm J}^{\mu\rho}g_{\rm J}^{\nu\sigma}W_{\mu\nu}^a W_{\rho\sigma}^a \ , \\ B_{\mu\nu} \equiv& \ \partial_\mu B_\nu - \partial_\nu B_\mu \ , \\ W_{\mu\nu}^a \equiv& \ \partial_\mu W_\nu^a - \partial_\nu W_\mu^a - g\epsilon^{abc}W_\mu^b W_\nu^c \ , \end{aligned} \tag{H.2}$$

and the last two terms for the mass terms for top and bottom quarks. By the one-loop renormalization group running (see for example Ref. [197]), the gauge couplings take the values $g \approx 0.55$, $g' \approx 0.42$, and the Yukawa couplings $y_t \approx 0.5$, $y_b \approx 0.01$ at energy scale $\sim 10^{12}$ GeV which corresponds to the energy scale at the end of inflation in the mixed Higgs-R^2 inflation model. Transform Eq. (H.1) to EF through conformal transformation (2.122) and write down the relevant terms for gauge fields up to quadratic order in unitary gauge as

$$e^{\alpha\varphi}\mathcal{L}_{\rm E,g} \supset -\frac{g^2}{8}g_{\rm E}^{\mu\nu}h^2\left(2W_\mu^+W_\nu^- + \frac{Z_\mu Z_\nu}{\cos^2\theta_w}\right) \ , \tag{H.3}$$

and for top and bottom quarks as

$$e^{2\alpha\varphi}\mathcal{L}_{\mathrm{E,Y}} \supset -\frac{y_t}{\sqrt{2}}h\bar{t}t - \frac{y_b}{\sqrt{2}}h\bar{b}b \ , \tag{H.4}$$

where, Z_μ, $W^\pm_\mu$, and the photon A_μ are defined by rotating the gauge fields as

$$\begin{aligned} Z_\mu \equiv& \cos\theta_w W^3_\mu - \sin\theta_w B_\mu \ , \\ A_\mu \equiv& \sin\theta_w W^3_\mu + \cos\theta_w B_\mu \ , \\ W^\pm_\mu \equiv& \frac{1}{\sqrt{2}}\left(W^1_\mu \mp iW^2_\mu\right) \ , \end{aligned} \tag{H.5}$$

with $\tan\theta_w = g'/g$.

Consider the decomposition (4.83). When $\varphi > 0$, the approximation $|h_{\mathrm{v}}| \gg |h_{\mathrm{osc}}|$ is valid, so up to first order in h_{osc} the relevant terms are given by

$$e^{\alpha\varphi}\mathcal{L}_{\mathrm{E,g}} \supset -\frac{g^2}{8}g^{\mu\nu}_{\mathrm{E}}h^2_{\mathrm{v}}\left(2W^+_\mu W^-_\nu + \frac{Z_\mu Z_\nu}{\cos^2\theta_w}\right) - \frac{g^2}{4}g^{\mu\nu}_{\mathrm{E}}h_{\mathrm{v}}h_{\mathrm{osc}}\left(2W^+_\mu W^-_\nu + \frac{Z_\mu Z_\nu}{\cos^2\theta_w}\right), \tag{H.6}$$

$$e^{2\alpha\varphi}\mathcal{L}_{\mathrm{E,Y}} \supset -\frac{y_t}{\sqrt{2}}h_{\mathrm{v}}\bar{t}t - \frac{y_b}{\sqrt{2}}h_{\mathrm{v}}\bar{b}b - \frac{y_t}{\sqrt{2}}h_{\mathrm{osc}}\bar{t}t - \frac{y_b}{\sqrt{2}}h_{\mathrm{osc}}\bar{b}b \ , \tag{H.7}$$

where gauge fields and quarks gain masses due to the non-vanishing vev of Higgs, and there are decay channels for Higgs to decay into these particles. When $\varphi < 0$, $h_{\mathrm{v}} = 0$ which leads to

$$e^{\alpha\varphi}\mathcal{L}_{\mathrm{E,g}} \supset -\frac{g^2}{8}g^{\mu\nu}h^2_{\mathrm{osc}}\left(2W^+_\mu W^-_\nu + \frac{Z_\mu Z_\nu}{\cos^2\theta_w}\right) \ , \tag{H.8}$$

$$e^{2\alpha\varphi}\mathcal{L}_{\mathrm{E,Y}} \supset -\frac{y_t}{\sqrt{2}}h_{\mathrm{osc}}\bar{t}t - \frac{y_b}{\sqrt{2}}h_{\mathrm{osc}}\bar{b}b \ . \tag{H.9}$$

where gauge fields and quarks become massless because the vev of Higgs becomes zero. In Eq. (H.8), there is no three-leg interaction terms for the homogeneous Higgs to decay into $W^\pm$ and Z bosons so this channel is only relevant for $\varphi > 0$ regime. On the other hand, the Yukawa interaction terms always exist for quarks. Based on these results, the decay rates of the homogeneous Higgs field into $W^\pm$, Z, t and b can be calculated. Note that the non-Abelian nature of the gauge fields is not taken into account because it is not important to the lowest order of gauge coupling. In addition, as mentioned in the main text, the conformal factor $\exp(\alpha\varphi)$ and $\exp(2\alpha\varphi)$ are irrelevant in small fields approximation which is of interest during reheating. Therefore, the difference between JF and EF disappear.

As seen from above, the first two terms in Eq. (H.6) gives the effective masses for the gauge bosons. In the flat FLRW background, $\sqrt{-g_{\mathrm{E}}} = a^3$. To eliminate these

factors, it is convenient to redefine the fields as $\tilde{W}^{\pm}_{\mu} \equiv a^{3/2} W^{\pm}_{\mu}$ and $\tilde{Z}_{\mu} \equiv a^{3/2} Z_{\mu}$, such that the effective masses are

$$m^2_{\tilde{W}} \equiv \frac{g^2}{4} h^2_{\rm v} \ , \tag{H.10}$$

$$m^2_{\tilde{Z}} \equiv \frac{g^2}{4\cos^2\theta_w} h^2_{\rm v} = \frac{g^2+g'^2}{4} h^2_{\rm v} \ . \tag{H.11}$$

As a result, the decay rates for Higgs to gauge bosons in $\varphi > 0$ regime can be calculated as

$$\Gamma_{h\to\tilde{W}\tilde{W}} = \frac{\lambda}{8\pi}\frac{M^3}{\tilde{M}^2}\left(6\xi\alpha\varphi\right)^{1/2}\left(1 - \frac{g^2}{2\lambda}\frac{\tilde{M}^2}{M^2} + \frac{3g^4}{16\lambda^2}\frac{\tilde{M}^4}{M^4}\right)\sqrt{1-\frac{g^2}{2\lambda}\frac{\tilde{M}^2}{M^2}} \ , \tag{H.12}$$

$$\Gamma_{h\to\tilde{Z}\tilde{Z}} = \frac{\lambda}{16\pi}\frac{M^3}{\tilde{M}^2}\left(6\xi\alpha\varphi\right)^{1/2}\left(1 - \frac{g^2+g'^2}{2\lambda}\frac{\tilde{M}^2}{M^2} + \frac{3\left(g^2+g'^2\right)^2}{16\lambda^2}\frac{\tilde{M}^4}{M^4}\right)\sqrt{1-\frac{g^2+g'^2}{2\lambda}\frac{\tilde{M}^2}{M^2}} \ . \tag{H.13}$$

These decay channels are open only when the conditions

$$\xi^2 > \xi^2_c\left(1 - \frac{2\lambda}{g^2}\right) \equiv \xi^2_W \simeq 4291^2 \tag{H.14}$$

$$\xi^2 > \xi^2_c\left(1 - \frac{2\lambda}{g^2+g'^2}\right) \equiv \xi^2_Z \simeq 4347^2 \tag{H.15}$$

are satisfied respectively, which means that the decay of homogeneous Higgs into $W^{\pm}$ and Z is possible only in the deep Higgs-like regime.

As for the fermion section, redefining $\tilde{t} \equiv a^{3/2} t$ and $\tilde{b} \equiv a^{3/2} b$ to absorb the factor $\sqrt{-g_{\rm E}}$, the masses of the new fermion fields are given as

$$m_{\tilde{t}} \equiv \frac{y_t}{\sqrt{2}} h_{\rm v} \tag{H.16}$$

$$m_{\tilde{b}} \equiv \frac{y_b}{\sqrt{2}} h_{\rm v} \ . \tag{H.17}$$

Unlike the gauge sector, the Higgs background can decay into top and bottom quarks in both positive and negative φ regimes. The decay width can be calculated as

$$\Gamma_{h\to\tilde{t}\bar{\tilde{t}}} = \begin{cases} \dfrac{3y_t^2}{16\pi}\left(3\xi\alpha|\varphi|\right)^{1/2} M \ , & \varphi < 0 \ , \\ \dfrac{3y_t^2}{16\pi}\left(6\xi\alpha\varphi\right)^{1/2} M \left(1 - \dfrac{y_t^2}{\lambda}\dfrac{\tilde{M}^2}{M^2}\right)^{3/2} , & \varphi > 0 \ , \end{cases} \tag{H.18}$$

$$\Gamma_{h\to\tilde{b}\bar{\tilde{b}}} = \begin{cases} \dfrac{3y_b^2}{16\pi}\left(3\xi\alpha|\varphi|\right)^{1/2} M \ , & \varphi < 0 \ , \\ \dfrac{3y_b^2}{16\pi}\left(6\xi\alpha\varphi\right)^{1/2} M \left(1 - \dfrac{y_b^2}{\lambda}\dfrac{\tilde{M}^2}{M^2}\right)^{3/2} , & \varphi > 0 \ . \end{cases} \tag{H.19}$$

Because the quarks are massless during $\varphi < 0$, the channels are always open during that period. On the contrary, the decay to top quarks is allowed during $\varphi > 0$ only when

$$\xi^2 > \xi_c^2 \left(1 - \frac{\lambda}{y_t^2}\right) \equiv \xi_t^2 \simeq 4351^2 \tag{H.20}$$

while the bottom quark channel is always open due to the small coupling y_b.

Bibliography

[1] E. W. Kolb and M. S. Turner, *The Early Universe*, vol. 69. Frontiers in Physics, 1990.

[2] V. Mukhanov, *Physical Foundations of Cosmology*. Cambridge University Press, Oxford, 2005.

[3] A. A. Starobinsky, "A New Type of Isotropic Cosmological Models Without Singularity," *Phys. Lett.* **91B** (1980) 99–102. [Adv. Ser. Astrophys. Cosmol. 3, 130 (1987)].

[4] A. H. Guth, "The Inflationary Universe: A Possible Solution to the Horizon and Flatness Problems," *Phys. Rev.* **D23** (1981) 347–356.

[5] K. Sato, "First Order Phase Transition of a Vacuum and Expansion of the Universe," *Mon. Not. Roy. Astron. Soc.* **195** (1981) 467–479.

[6] A. D. Linde, "A New Inflationary Universe Scenario: A Possible Solution of the Horizon, Flatness, Homogeneity, Isotropy and Primordial Monopole Problems," *Phys. Lett.* **108B** (1982) 389–393.

[7] A. Albrecht and P. J. Steinhardt, "Cosmology for Grand Unified Theories with Radiatively Induced Symmetry Breaking," *Phys. Rev. Lett.* **48** (1982) 1220–1223.

[8] K. Sato and J. Yokoyama, "Inflationary cosmology: First 30+ years," *Int. J. Mod. Phys.* **D24** no. 11, (2015) 1530025.

[9] A. R. Liddle and D. H. Lyth, *Cosmological inflation and large scale structure*. Cambridge University Press, 2000.

[10] A. R. Liddle and S. M. Leach, "How long before the end of inflation were observable perturbations produced?," *Phys. Rev. D* **68** (2003) 103503, arXiv:astro-ph/0305263.

[11] J. Martin and C. Ringeval, "First CMB Constraints on the Inflationary Reheating Temperature," *Phys. Rev. D* **82** (2010) 023511, arXiv:1004.5525 [astro-ph.CO].

[12] N. Seto and J. Yokoyama, "Probing the equation of state of the early universe with a space laser interferometer," *J. Phys. Soc. Jap.* **72** (2003) 3082–3086, arXiv:gr-qc/0305096.

[13] K. Nakayama, S. Saito, Y. Suwa, and J. Yokoyama, "Probing reheating temperature of the universe with gravitational wave background," *JCAP* **06** (2008) 020, arXiv:0804.1827 [astro-ph].

[14] L. Kofman, A. D. Linde, and A. A. Starobinsky, "Reheating after inflation," *Phys. Rev. Lett.* **73** (1994) 3195–3198, arXiv:hep-th/9405187.

[15] Y. Shtanov, J. H. Traschen, and R. H. Brandenberger, "Universe reheating after inflation," *Phys. Rev.* **D51** (1995) 5438–5455, arXiv:hep-ph/9407247 [hep-ph].

[16] L. Kofman, A. D. Linde, and A. A. Starobinsky, "Towards the theory of reheating after inflation," *Phys. Rev. D* **56** (1997) 3258–3295, arXiv:hep-ph/9704452.

[17] P. B. Greene, L. Kofman, A. D. Linde, and A. A. Starobinsky, "Structure of resonance in preheating after inflation," *Phys. Rev. D* **56** (1997) 6175–6192, arXiv:hep-ph/9705347.

[18] G. N. Felder, J. Garcia-Bellido, P. B. Greene, L. Kofman, A. D. Linde, and I. Tkachev, "Dynamics of symmetry breaking and tachyonic preheating," *Phys. Rev. Lett.* **87** (2001) 011601, arXiv:hep-ph/0012142.

[19] G. N. Felder, L. Kofman, and A. D. Linde, "Tachyonic instability and dynamics of spontaneous symmetry breaking," *Phys. Rev. D* **64** (2001) 123517, arXiv:hep-th/0106179.

[20] L. Kofman, "Tachyonic preheating," in *8th International Symposium on Particles Strings and Cosmology*, pp. 167–182. Chapel Hill, NC, U.S.A., 10-15 April 2001. arXiv:hep-ph/0107280.

[21] A. D. Dolgov and A. D. Linde, "Baryon Asymmetry in Inflationary Universe," *Phys. Lett.* **116B** (1982) 329.

[22] L. F. Abbott, E. Farhi, and M. B. Wise, "Particle Production in the New Inflationary Cosmology," *Phys. Lett.* **117B** (1982) 29.

[23] **Planck** Collaboration, Y. Akrami *et al.*, "Planck 2018 results. X. Constraints on inflation," arXiv:1807.06211 [astro-ph.CO].

[24] A. A. Starobinsky, "The Perturbation Spectrum Evolving from a Nonsingular Initially De-Sitter Cosmology and the Microwave Background Anisotropy," *Sov. Astron. Lett.* **9** (1983) 302.

[25] J. L. Cervantes-Cota and H. Dehnen, "Induced gravity inflation in the standard model of particle physics," *Nucl. Phys. B* **442** (1995) 391–412, arXiv:astro-ph/9505069.

[26] F. L. Bezrukov and M. Shaposhnikov, "The Standard Model Higgs boson as the inflaton," *Phys. Lett. B* **659** (2008) 703–706, arXiv:0710.3755 [hep-th].

[27] A. Barvinsky, A. Kamenshchik, and A. Starobinsky, "Inflation scenario via the Standard Model Higgs boson and LHC," *JCAP* **11** (2008) 021, arXiv:0809.2104 [hep-ph].

[28] K. Kamada, T. Kobayashi, T. Takahashi, M. Yamaguchi, and J. Yokoyama, "Generalized Higgs inflation," *Phys. Rev. D* **86** (2012) 023504, arXiv:1203.4059 [hep-ph].

[29] A. A. Starobinsky, "Nonsingular model of the Universe with the quantum-gravitational de Sitter stage and its observational consequences," in *Quantum Gravity.* Proceedings of the 2nd Seminar on Quantum Gravity, INR Press, Moscow, 13-15 October 1981, pp. 58–72, (INR Press, Moscow, 1982). Reprinted in: Markov, M.A. and West, P.C., eds., Quantum Gravity, (Plenum Press, New York, 1984), pp. 103–128.

[30] A. Vilenkin, "Classical and Quantum Cosmology of the Starobinsky Inflationary Model," *Phys. Rev. D* **32** (1985) 2511.

[31] F. Bezrukov, D. Gorbunov, and M. Shaposhnikov, "On initial conditions for the Hot Big Bang," *JCAP* **06** (2009) 029, arXiv:0812.3622 [hep-ph].

[32] J. Garcia-Bellido, D. G. Figueroa, and J. Rubio, "Preheating in the Standard Model with the Higgs-Inflaton coupled to gravity," *Phys. Rev. D* **79** (2009) 063531, arXiv:0812.4624 [hep-ph].

[33] J. Repond and J. Rubio, "Combined Preheating on the lattice with applications to Higgs inflation," *JCAP* **07** (2016) 043, arXiv:1604.08238 [astro-ph.CO].

[34] Y. Ema, R. Jinno, K. Mukaida, and K. Nakayama, "Violent Preheating in Inflation with Nonminimal Coupling," *JCAP* **02** (2017) 045, arXiv:1609.05209 [hep-ph].

[35] E. I. Sfakianakis and J. van de Vis, "Preheating after Higgs Inflation: Self-Resonance and Gauge boson production," *Phys. Rev. D* **99** no. 8, (2019) 083519, arXiv:1810.01304 [hep-ph].

[36] Y.-C. Wang and T. Wang, "Primordial perturbations generated by Higgs field and R^2 operator," *Phys. Rev. D* **96** no. 12, (2017) 123506, arXiv:1701.06636 [gr-qc].

[37] Y. Ema, "Higgs Scalaron Mixed Inflation," *Phys. Lett. B* **770** (2017) 403–411, arXiv:1701.07665 [hep-ph].

[38] M. He, A. A. Starobinsky, and J. Yokoyama, "Inflation in the mixed Higgs-R^2 model," *JCAP* **05** (2018) 064, arXiv:1804.00409 [astro-ph.CO].

[39] A. Gundhi and C. F. Steinwachs, "Scalaron-Higgs inflation," *Nucl. Phys. B* **954** (2020) 114989, arXiv:1810.10546 [hep-th].

[40] V.-M. Enckell, K. Enqvist, S. Rasanen, and L.-P. Wahlman, "Higgs-R^2 inflation - full slow-roll study at tree-level," *JCAP* **01** (2020) 041, arXiv:1812.08754 [astro-ph.CO].

[41] M. He, R. Jinno, K. Kamada, S. C. Park, A. A. Starobinsky, and J. Yokoyama, "On the violent preheating in the mixed Higgs-R^2 inflationary model," *Phys. Lett. B* **791** (2019) 36–42, arXiv:1812.10099 [hep-ph].

[42] D. Gorbunov and A. Tokareva, "Scalaron the healer: removing the strong-coupling in the Higgs- and Higgs-dilaton inflations," *Phys. Lett. B* **788** (2019) 37–41, arXiv:1807.02392 [hep-ph].

[43] A. Salvio and A. Mazumdar, "Classical and Quantum Initial Conditions for Higgs Inflation," *Phys. Lett. B* **750** (2015) 194–200, arXiv:1506.07520 [hep-ph].

[44] T. d. P. Netto, A. M. Pelinson, I. L. Shapiro, and A. A. Starobinsky, "From stable to unstable anomaly-induced inflation," *Eur. Phys. J.* **C 76** no. 10, (2016) 544, arXiv:1509.08882 [hep-th].

[45] X. Calmet and I. Kuntz, "Higgs Starobinsky Inflation," *Eur. Phys. J. C* **76** no. 5, (2016) 289, arXiv:1605.02236 [hep-th].

[46] L.-H. Liu, T. Prokopec, and A. A. Starobinsky, "Inflation in an effective gravitational model and asymptotic safety," *Phys. Rev.* **D 98** no. 4, (2018) 043505, arXiv:1806.05407 [gr-qc].

[47] D. Ghilencea, "Two-loop corrections to Starobinsky-Higgs inflation," *Phys. Rev. D* **98** no. 10, (2018) 103524, arXiv:1807.06900 [hep-ph].

[48] Y. Ema, "Dynamical Emergence of Scalaron in Higgs Inflation," *JCAP* **09** (2019) 027, arXiv:1907.00993 [hep-ph].

[49] Y. Ema, K. Mukaida, and J. van de Vis, "Higgs Inflation as Nonlinear Sigma Model and Scalaron as its σ-meson," *JHEP* **11** (2020) 011, arXiv:2002.11739 [hep-ph].

[50] F. Bezrukov, D. Gorbunov, C. Shepherd, and A. Tokareva, "Some like it hot: R^2 heals Higgs inflation, but does not cool it," *Phys. Lett. B* **795** (2019) 657–665, arXiv:1904.04737 [hep-ph].

[51] M. He, R. Jinno, K. Kamada, A. A. Starobinsky, and J. Yokoyama, "Occurrence of Tachyonic Preheating in the Mixed Higgs-R^2 Model," *JCAP* **01** (2021) 066, arXiv:2007.10369 [hep-ph].

[52] F. Bezrukov and C. Shepherd, "A heatwave affair: mixed Higgs-R^2 preheating on the lattice," *JCAP* **12** (2020) 028, arXiv:2007.10978 [hep-ph].

[53] M. He, "Perturbative Reheating in the Mixed Higgs-R^2 Model," *JCAP* **05** (2021) 021, arXiv:2010.11717 [hep-ph].

[54] F. Bezrukov and D. Gorbunov, "Distinguishing between R^2-inflation and Higgs-inflation," *Phys. Lett. B* **713** (2012) 365–368, arXiv:1111.4397 [hep-ph].

[55] A. A. Starobinsky, "Spectrum of relict gravitational radiation and the early state of the universe," *JETP Lett.* **30** (1979) 682–685 (in Russian). [Pis'ma Zh. Eksp. Teor. Fiz. **30** (1979) 719–723].

[56] C. Armendariz-Picon, T. Damour, and V. F. Mukhanov, "k - inflation," *Phys. Lett.* **B458** (1999) 209–218, arXiv:hep-th/9904075 [hep-th].

[57] T. Kobayashi, M. Yamaguchi, and J. Yokoyama, "G-inflation: Inflation driven by the Galileon field," *Phys. Rev. Lett.* **105** (2010) 231302, arXiv:1008.0603 [hep-th].

[58] T. Kobayashi, M. Yamaguchi, and J. Yokoyama, "Generalized G-inflation: Inflation with the most general second-order field equations," *Prog. Theor. Phys.* **126** (2011) 511–529, arXiv:1105.5723 [hep-th].

[59] G. W. Horndeski, "Second-order scalar-tensor field equations in a four-dimensional space," *Int. J. Theor. Phys.* **10** (1974) 363–384.

[60] R. Kallosh and A. Linde, "Universality Class in Conformal Inflation," *JCAP* **07** (2013) 002, arXiv:1306.5220 [hep-th].

[61] R. Kallosh, A. Linde, and D. Roest, "Superconformal Inflationary α-Attractors," *JHEP* **11** (2013) 198, arXiv:1311.0472 [hep-th].

[62] K.-i. Maeda, "Inflation as a Transient Attractor in R**2 Cosmology," *Phys. Rev. D* **37** (1988) 858.

[63] K.-i. Maeda, "Towards the Einstein-Hilbert Action via Conformal Transformation," *Phys. Rev. D* **39** (1989) 3159.

[64] N. D. Birrell and P. C. W. Davies, *Quantum Fields in Curved Space*. Cambridge Monographs on Mathematical Physics. Cambridge Univ. Press, Cambridge, UK, 2, 1984.

[65] S. Renaux-Petel and K. Turzyński, "Geometrical Destabilization of Inflation," *Phys. Rev. Lett.* **117** no. 14, (2016) 141301, arXiv:1510.01281 [astro-ph.CO].

[66] H. Kodama and M. Sasaki, "Cosmological Perturbation Theory," *Prog. Theor. Phys. Suppl.* **78** (1984) 1–166.

[67] J. M. Maldacena, "Non-Gaussian features of primordial fluctuations in single field inflationary models," *JHEP* **05** (2003) 013, arXiv:astro-ph/0210603 [astro-ph].

[68] N. Bartolo, S. Matarrese, and A. Riotto, "Non-Gaussianity of Large-Scale Cosmic Microwave Background Anisotropies beyond Perturbation Theory," *JCAP* **0508** (2005) 010, arXiv:astro-ph/0506410 [astro-ph].

[69] X. Chen, M.-x. Huang, S. Kachru, and G. Shiu, "Observational signatures and non-Gaussianities of general single field inflation," *JCAP* **01** (2007) 002, arXiv:hep-th/0605045.

[70] X. Chen, "Primordial Non-Gaussianities from Inflation Models," *Adv. Astron.* **2010** (2010) 638979, arXiv:1002.1416 [astro-ph.CO].

[71] D. Baumann and D. Green, "Equilateral Non-Gaussianity and New Physics on the Horizon," *JCAP* **1109** (2011) 014, arXiv:1102.5343 [hep-th].

[72] A. A. Starobinsky, "Dynamics of Phase Transition in the New Inflationary Universe Scenario and Generation of Perturbations," *Phys. Lett. B* **117** (1982) 175–178.

[73] D. Polarski and A. A. Starobinsky, "Semiclassicality and decoherence of cosmological perturbations," *Class. Quant. Grav.* **13** (1996) 377–392, arXiv:gr-qc/9504030.

[74] D. Baumann, "Inflation," in *Physics of the large and the small, TASI 09, proceedings of the Theoretical Advanced Study Institute in Elementary Particle Physics, Boulder, Colorado, USA, 1-26 June 2009*, pp. 523–686. 2011. arXiv:0907.5424 [hep-th].

[75] R. L. Arnowitt, S. Deser, and C. W. Misner, "The Dynamics of general relativity," *Gen. Rel. Grav.* **40** (2008) 1997–2027, arXiv:gr-qc/0405109 [gr-qc].

[76] C. W. Misner, K. S. Thorne, and J. A. Wheeler, *Gravitation*. W. H. Freeman, San Francisco, 1973.

[77] R. M. Wald, *General Relativity*. Chicago Univ. Pr., Chicago, USA, 1984.

[78] E. Gourgoulhon, "3+1 formalism and bases of numerical relativity," arXiv:gr-qc/0703035.

[79] Y. Wang, "Inflation, Cosmic Perturbations and Non-Gaussianities," *Commun. Theor. Phys.* **62** (2014) 109–166, arXiv:1303.1523 [hep-th].

[80] J. M. Bardeen, "Gauge Invariant Cosmological Perturbations," *Phys. Rev.* **D22** (1980) 1882–1905.

[81] J. M. Bardeen, P. J. Steinhardt, and M. S. Turner, "Spontaneous Creation of Almost Scale - Free Density Perturbations in an Inflationary Universe," *Phys. Rev.* **D28** (1983) 679.

[82] M. Sasaki, "Large Scale Quantum Fluctuations in the Inflationary Universe," *Prog. Theor. Phys.* **76** (1986) 1036.

[83] V. F. Mukhanov, "Quantum Theory of Gauge Invariant Cosmological Perturbations," *Sov. Phys. JETP* **67** (1988) 1297–1302. [Zh. Eksp. Teor. Fiz.94N7,1(1988)].

[84] S. Weinberg, *Cosmology*. Oxford Univ. Press, 2008.

[85] D. H. Lyth and A. R. Liddle, *The primordial density perturbation: Cosmology, inflation and the origin of structure*. Cambridge Univ. Press, Cambridge, UK, 2009.

[86] C. Gordon, D. Wands, B. A. Bassett, and R. Maartens, "Adiabatic and entropy perturbations from inflation," *Phys. Rev. D* **63** (2000) 023506, arXiv:astro-ph/0009131.

[87] D. Polarski and A. A. Starobinsky, "Spectra of perturbations produced by double inflation with an intermediate matter dominated stage," *Nucl. Phys.* **B385** (1992) 623–650.

[88] D. Polarski and A. A. Starobinsky, "Isocurvature perturbations in multiple inflationary models," *Phys. Rev.* **D50** (1994) 6123–6129, arXiv:astro-ph/9404061 [astro-ph].

[89] S. Weinberg, "Can non-adiabatic perturbations arise after single-field inflation?," *Phys. Rev.* **D70** (2004) 043541, arXiv:astro-ph/0401313 [astro-ph].

[90] S. Weinberg, "Must cosmological perturbations remain non-adiabatic after multi-field inflation?," *Phys. Rev.* **D70** (2004) 083522, arXiv:astro-ph/0405397 [astro-ph].

[91] E. D. Stewart and D. H. Lyth, "A More accurate analytic calculation of the spectrum of cosmological perturbations produced during inflation," *Phys. Lett.* **B302** (1993) 171–175, arXiv:gr-qc/9302019 [gr-qc].

[92] T. S. Bunch and P. C. W. Davies, "Quantum Field Theory in de Sitter Space: Renormalization by Point Splitting," *Proc. Roy. Soc. Lond.* **A360** (1978) 117–134.

[93] A. R. Liddle and D. H. Lyth, "COBE, gravitational waves, inflation and extended inflation," *Phys. Lett. B* **291** (1992) 391–398, arXiv:astro-ph/9208007.

[94] V. A. Rubakov, M. V. Sazhin, and A. V. Veryaskin, "Graviton Creation in the Inflationary Universe and the Grand Unification Scale," *Phys. Lett. B* **115** (1982) 189–192.

[95] R. Fabbri and M. d. Pollock, "The Effect of Primordially Produced Gravitons upon the Anisotropy of the Cosmological Microwave Background Radiation," *Phys. Lett. B* **125** (1983) 445–448.

[96] L. F. Abbott and M. B. Wise, "Constraints on Generalized Inflationary Cosmologies," *Nucl. Phys. B* **244** (1984) 541–548.

[97] L. A. Boyle and P. J. Steinhardt, "Probing the early universe with inflationary gravitational waves," *Phys. Rev. D* **77** (2008) 063504, arXiv:astro-ph/0512014.

[98] A. De Felice and S. Tsujikawa, "f(R) theories," *Living Rev. Rel.* **13** (2010) 3, arXiv:1002.4928 [gr-qc].

[99] M. B. Mijic, M. S. Morris, and W.-M. Suen, "The R^2 Cosmology: Inflation Without a Phase Transition," *Phys. Rev.* **D34** (1986) 2934.

[100] R. Jinno, *Gravitational effects on inflaton decay at the onset of reheating*. PhD thesis, The University of Tokyo, 2016.

[101] A. Kehagias, A. Moradinezhad Dizgah, and A. Riotto, "Remarks on the Starobinsky model of inflation and its descendants," *Phys. Rev.* **D89** no. 4, (2014) 043527, arXiv:1312.1155 [hep-th].

[102] Y. Hamada, H. Kawai, K.-y. Oda, and S. C. Park, "Higgs Inflation is Still Alive after the Results from BICEP2," *Phys. Rev. Lett.* **112** no. 24, (2014) 241301, arXiv:1403.5043 [hep-ph].

[103] F. Bezrukov and M. Shaposhnikov, "Higgs inflation at the critical point," *Phys. Lett. B* **734** (2014) 249–254, arXiv:1403.6078 [hep-ph].

[104] Y. Hamada, H. Kawai, K.-y. Oda, and S. C. Park, "Higgs inflation from Standard Model criticality," *Phys. Rev. D* **91** (2015) 053008, arXiv:1408.4864 [hep-ph].

[105] C. Burgess, H. M. Lee, and M. Trott, "Power-counting and the Validity of the Classical Approximation During Inflation," *JHEP* **09** (2009) 103, arXiv:0902.4465 [hep-ph].

[106] J. Barbon and J. Espinosa, "On the Naturalness of Higgs Inflation," *Phys. Rev. D* **79** (2009) 081302, arXiv:0903.0355 [hep-ph].

[107] C. Burgess, H. M. Lee, and M. Trott, "Comment on Higgs Inflation and Naturalness," *JHEP* **07** (2010) 007, arXiv:1002.2730 [hep-ph].

[108] M. P. Hertzberg, "On Inflation with Non-minimal Coupling," *JHEP* **11** (2010) 023, arXiv:1002.2995 [hep-ph].

[109] A. Barvinsky, A. Kamenshchik, C. Kiefer, A. Starobinsky, and C. Steinwachs, "Higgs boson, renormalization group, and naturalness in cosmology," *Eur. Phys. J. C* **72** (2012) 2219, arXiv:0910.1041 [hep-ph].

[110] F. Bezrukov, A. Magnin, M. Shaposhnikov, and S. Sibiryakov, "Higgs inflation: consistency and generalisations," *JHEP* **01** (2011) 016, arXiv:1008.5157 [hep-ph].

[111] F. Bezrukov and M. Shaposhnikov, "Standard Model Higgs boson mass from inflation: Two loop analysis," *JHEP* **07** (2009) 089, arXiv:0904.1537 [hep-ph].

[112] F. Bezrukov, J. Rubio, and M. Shaposhnikov, "Living beyond the edge: Higgs inflation and vacuum metastability," *Phys. Rev. D* **92** no. 8, (2015) 083512, arXiv:1412.3811 [hep-ph].

[113] M. P. DeCross, D. I. Kaiser, A. Prabhu, C. Prescod-Weinstein, and E. I. Sfakianakis, "Preheating after Multifield Inflation with Nonminimal Couplings, I: Covariant Formalism and Attractor Behavior," *Phys. Rev. D* **97** no. 2, (2018) 023526, arXiv:1510.08553 [astro-ph.CO].

[114] Y. Hamada, K. Kawana, and A. Scherlis, "On Preheating in Higgs Inflation," *JCAP* **03** (2021) 062, arXiv:2007.04701 [hep-ph].

[115] D. H. Lyth and A. Riotto, "Particle physics models of inflation and the cosmological density perturbation," *Phys. Rept.* **314** (1999) 1–146, arXiv:hep-ph/9807278.

[116] D. Baumann and L. McAllister, *Inflation and String Theory*. Cambridge Monographs on Mathematical Physics. Cambridge University Press, 5, 2015. arXiv:1404.2601 [hep-th].

[117] A. A. Starobinsky and J. Yokoyama, "Density fluctuations in Brans-Dicke inflation," in *4th Workshop on General Relativity and Gravitation*. November, 1994. arXiv:gr-qc/9502002.

[118] X. Chen and Y. Wang, "Large non-Gaussianities with Intermediate Shapes from Quasi-Single Field Inflation," *Phys. Rev.* **D81** (2010) 063511, arXiv:0909.0496 [astro-ph.CO].

[119] A. D. Linde, "Hybrid inflation," *Phys. Rev.* **D49** (1994) 748–754, arXiv:astro-ph/9307002 [astro-ph].

[120] J. A. Adams, G. G. Ross, and S. Sarkar, "Multiple inflation," *Nucl. Phys.* **B503** (1997) 405–425, arXiv:hep-ph/9704286 [hep-ph].

[121] B. A. Bassett, S. Tsujikawa, and D. Wands, "Inflation dynamics and reheating," *Rev. Mod. Phys.* **78** (2006) 537–589, arXiv:astro-ph/0507632 [astro-ph].

[122] M. Sasaki and E. D. Stewart, "A General analytic formula for the spectral index of the density perturbations produced during inflation," *Prog. Theor. Phys.* **95** (1996) 71–78, arXiv:astro-ph/9507001 [astro-ph].

[123] A. Achucarro, J.-O. Gong, S. Hardeman, G. A. Palma, and S. P. Patil, "Features of heavy physics in the CMB power spectrum," *JCAP* **1101** (2011) 030, arXiv:1010.3693 [hep-ph].

[124] S. Cespedes, V. Atal, and G. A. Palma, "On the importance of heavy fields during inflation," *JCAP* **1205** (2012) 008, arXiv:1201.4848 [hep-th].

[125] A. Achucarro, V. Atal, S. Cespedes, J.-O. Gong, G. A. Palma, and S. P. Patil, "Heavy fields, reduced speeds of sound and decoupling during inflation," *Phys. Rev.* **D86** (2012) 121301, arXiv:1205.0710 [hep-th].

[126] V. F. Mukhanov and P. J. Steinhardt, "Density perturbations in multifield inflationary models," *Phys. Lett. B* **422** (1998) 52–60, arXiv:astro-ph/9710038.

[127] G. A. Palma, S. Sypsas, and C. Zenteno, "Seeding primordial black holes in multifield inflation," *Phys. Rev. Lett.* **125** no. 12, (2020) 121301, arXiv:2004.06106 [astro-ph.CO].

[128] J. Fumagalli, S. Renaux-Petel, J. W. Ronayne, and L. T. Witkowski, "Turning in the landscape: a new mechanism for generating Primordial Black Holes," arXiv:2004.08369 [hep-th].

[129] G. F. Giudice and H. M. Lee, "Unitarizing Higgs Inflation," *Phys. Lett. B* **694** (2011) 294–300, arXiv:1010.1417 [hep-ph].

[130] J. Barbon, J. Casas, J. Elias-Miro, and J. Espinosa, "Higgs Inflation as a Mirage," *JHEP* **09** (2015) 027, arXiv:1501.02231 [hep-ph].

[131] H. M. Lee, "Light inflaton completing Higgs inflation," *Phys. Rev. D* **98** no. 1, (2018) 015020, arXiv:1802.06174 [hep-ph].

[132] D. Y. Cheong, S. M. Lee, and S. C. Park, "Primordial black holes in Higgs-R^2 inflation as the whole of dark matter," *JCAP* **01** (2021) 032, arXiv:1912.12032 [hep-ph].

[133] V.-M. Enckell, K. Enqvist, S. Rasanen, and L.-P. Wahlman, "Inflation with R^2 term in the Palatini formalism," *JCAP* **02** (2019) 022, arXiv:1810.05536 [gr-qc].

[134] S. Pi, Y.-l. Zhang, Q.-G. Huang, and M. Sasaki, "Scalaron from R^2-gravity as a heavy field," *JCAP* **1805** no. 05, (2018) 042, arXiv:1712.09896 [astro-ph.CO].

[135] Y. Ema, K. Mukaida, and J. Van De Vis, "Renormalization group equations of Higgs-R^2 inflation," *JHEP* **02** (2021) 109, arXiv:2008.01096 [hep-ph].

[136] C. G. Callan Jr., S. Coleman, and R. Jackiw, "A new improved energy-momentum tensor," *Annals of Physics* **59** no. 1, (1970) 42–73.

[137] S. Coleman and R. Jackiw, "Why dilatation generators do not generate dilatations," *Annals of Physics* **67** no. 2, (1971) 552–598.

[138] G. 't Hooft and M. J. G. Veltman, "One loop divergencies in the theory of gravitation," *Ann. Inst. H. Poincare Phys. Theor. A* **20** (1974) 69–94.

[139] M. He, "Inflation in the Mixed Higgs-R^2 Model," Master's thesis, The University of Tokyo, 2018.

[140] L. A. Kofman, A. D. Linde, and A. A. Starobinsky, "Inflationary Universe Generated by the Combined Action of a Scalar Field and Gravitational Vacuum Polarization," *Phys. Lett. B* **157** (1985) 361–367.

[141] A. A. Starobinsky, "Multicomponent de Sitter (Inflationary) Stages and the Generation of Perturbations," *JETP Lett.* **42** (1985) 152–155.

[142] A. Berera, "Interpolating the stage of exponential expansion in the early universe: A Possible alternative with no reheating," *Phys. Rev.* **D55** (1997) 3346–3357, arXiv:hep-ph/9612239 [hep-ph].

[143] A. Berera and T. W. Kephart, "The Ubiquitous Inflaton in String-Inspired Models," *Phys. Rev. Lett.* **83** (1999) 1084–1087, arXiv:hep-ph/9904410 [hep-ph].

[144] J. Yokoyama and A. D. Linde, "Is warm inflation possible?," *Phys. Rev. D* **60** (1999) 083509, arXiv:hep-ph/9809409.

[145] J. Martin, C. Ringeval, and V. Vennin, "Observing Inflationary Reheating," *Phys. Rev. Lett.* **114** no. 8, (2015) 081303, arXiv:1410.7958 [astro-ph.CO].

[146] J.-O. Gong, S. Pi, and G. Leung, "Probing reheating with primordial spectrum," *JCAP* **05** (2015) 027, arXiv:1501.03604 [hep-ph].

[147] J. L. Cook, E. Dimastrogiovanni, D. A. Easson, and L. M. Krauss, "Reheating predictions in single field inflation," *JCAP* **1504** (2015) 047, arXiv:1502.04673 [astro-ph.CO].

[148] S. Y. Khlebnikov and I. I. Tkachev, "Relic gravitational waves produced after preheating," *Phys. Rev. D* **56** (1997) 653–660, arXiv:hep-ph/9701423.

[149] J. Garcia-Bellido and D. G. Figueroa, "A stochastic background of gravitational waves from hybrid preheating," *Phys. Rev. Lett.* **98** (2007) 061302, arXiv:astro-ph/0701014.

[150] J. Garcia-Bellido, D. G. Figueroa, and A. Sastre, "A Gravitational Wave Background from Reheating after Hybrid Inflation," *Phys. Rev. D* **77** (2008) 043517, arXiv:0707.0839 [hep-ph].

[151] R. Easther and E. A. Lim, "Stochastic gravitational wave production after inflation," *JCAP* **04** (2006) 010, arXiv:astro-ph/0601617.

[152] R. Easther, J. T. Giblin, Jr., and E. A. Lim, "Gravitational Wave Production At The End Of Inflation," *Phys. Rev. Lett.* **99** (2007) 221301, arXiv:astro-ph/0612294.

[153] J. F. Dufaux, A. Bergman, G. N. Felder, L. Kofman, and J.-P. Uzan, "Theory and Numerics of Gravitational Waves from Preheating after Inflation," *Phys. Rev. D* **76** (2007) 123517, arXiv:0707.0875 [astro-ph].

[154] M. Kawasaki, K. Kohri, and N. Sugiyama, "Cosmological constraints on late time entropy production," *Phys. Rev. Lett.* **82** (1999) 4168, arXiv:astro-ph/9811437.

[155] M. Kawasaki, K. Kohri, and N. Sugiyama, "MeV scale reheating temperature and thermalization of neutrino background," *Phys. Rev. D* **62** (2000) 023506, arXiv:astro-ph/0002127.

[156] G. N. Felder, L. Kofman, and A. D. Linde, "Instant preheating," *Phys. Rev. D* **59** (1999) 123523, arXiv:hep-ph/9812289.

[157] L. Parker, "Particle creation in expanding universes," *Phys. Rev. Lett.* **21** (1968) 562–564.

[158] L. Parker, "Quantized fields and particle creation in expanding universes. 1.," *Phys. Rev.* **183** (1969) 1057–1068.

[159] Y. B. Zeldovich and A. A. Starobinsky, "Particle production and vacuum polarization in an anisotropic gravitational field," *Zh. Eksp. Teor. Fiz.* **61** (1971) 2161–2175.

[160] L. H. Ford, "Gravitational Particle Creation and Inflation," *Phys. Rev.* **D35** (1987) 2955.

[161] P. J. E. Peebles and A. Vilenkin, "Quintessential inflation," *Phys. Rev. D* **59** (1999) 063505, arXiv:astro-ph/9810509.

[162] S. A. Fulling, "Nonuniqueness of canonical field quantization in Riemannian space-time," *Phys. Rev. D* **7** (1973) 2850–2862.

[163] P. C. W. Davies, "Scalar particle production in Schwarzschild and Rindler metrics," *J. Phys. A* **8** (1975) 609–616.

[164] W. G. Unruh, "Notes on black hole evaporation," *Phys. Rev. D* **14** (1976) 870.

[165] S. W. Hawking, "Black hole explosions," *Nature* **248** (1974) 30–31.

[166] S. W. Hawking, "Particle Creation by Black Holes," *Commun. Math. Phys.* **43** (1975) 199–220. [Erratum: Commun.Math.Phys. 46, 206 (1976)].

[167] J. S. Schwinger, "On gauge invariance and vacuum polarization," *Phys. Rev.* **82** (1951) 664–679.

[168] V. Mukhanov and S. Winitzki, *Introduction to quantum effects in gravity*. Cambridge University Press, Jun., 2007.

[169] L. Li, T. Nakama, C. M. Sou, Y. Wang, and S. Zhou, "Gravitational Production of Superheavy Dark Matter and Associated Cosmological Signatures," *JHEP* **07** (2019) 067, arXiv:1903.08842 [astro-ph.CO].

[170] S. Hashiba and Y. Yamada, "Stokes phenomenon and gravitational particle production – How to evaluate it in practice," *JCAP* **05** (2021) 022, arXiv:2101.07634 [hep-th].

[171] N. N. Bogolyubov, "A New method in the theory of superconductivity. I," *Sov. Phys. JETP* **7** (1958) 41–46.

[172] Y. B. Zel'dovich and A. A. Starobinsky, "Rate of particle production in gravitational fields," *JETP Lett.* **26** no. 5, (1977) 252.

[173] J. F. Dufaux, G. N. Felder, L. Kofman, M. Peloso, and D. Podolsky, "Preheating with trilinear interactions: Tachyonic resonance," *JCAP* **07** (2006) 006, arXiv:hep-ph/0602144.

[174] L. D. Landau and E. M. Lifshits, *Quantum Mechanics: Non-Relativistic Theory*, vol. 3 of *Course of Theoretical Physics*. Butterworth-Heinemann, Oxford, 1981.

[175] S. Kasuya and M. Kawasaki, "Restriction to parametric resonant decay after inflation," *Phys. Lett. B* **388** (1996) 686–691, arXiv:hep-ph/9603317.

[176] I. Kovacic, R. Rand, and S. Mohamed Sah, "Mathieu's Equation and Its Generalizations: Overview of Stability Charts and Their Features," *Applied Mechanics Reviews* **70** no. 2, (2018) 020802.

[177] D. Gorbunov and A. Tokareva, "R^2-inflation with conformal SM Higgs field," *JCAP* **12** (2013) 021, arXiv:1212.4466 [astro-ph.CO].

[178] A. Kamada, "On Scalaron Decay via the Trace of Energy-Momentum Tensor," *JHEP* **07** (2019) 172, arXiv:1902.05209 [hep-ph].

[179] D. S. Gorbunov and A. G. Panin, "Scalaron the mighty: producing dark matter and baryon asymmetry at reheating," *Phys. Lett.* **B700** (2011) 157–162, arXiv:1009.2448 [hep-ph].

[180] T. Futamase and K.-i. Maeda, "Chaotic inflationary scenario of the universe with a nonminimally coupled "inflaton" field," *Phys. Rev. D* **39** (1989) 399–404.

[181] S. Tsujikawa, K.-i. Maeda, and T. Torii, "Preheating of the nonminimally coupled inflaton field," *Phys. Rev. D* **61** (2000) 103501, arXiv:hep-ph/9910214.

[182] C. Fu, P. Wu, and H. Yu, "Nonlinear preheating with nonminimally coupled scalar fields in the Starobinsky model," *Phys. Rev. D* **99** no. 12, (2019) 123526, arXiv:1906.00557 [astro-ph.CO].

[183] M. A. Amin and D. Baumann, "From Wires to Cosmology," *JCAP* **02** (2016) 045, arXiv:1512.02637 [astro-ph.CO].

[184] D. I. Podolsky and A. A. Starobinsky, "Chaotic reheating," *Grav. Cosmol. Suppl.* **8N1** (2002) 13–18, arXiv:astro-ph/0204327.

[185] Y. Jin and S. Tsujikawa, "Chaotic dynamics in preheating after inflation," *Class. Quant. Grav.* **23** (2006) 353–372, arXiv:hep-ph/0411164.

[186] O. Iarygina, E. I. Sfakianakis, D.-G. Wang, and A. Achúcarro, "Multi-field inflation and preheating in asymmetric α-attractors," arXiv:2005.00528 [astro-ph.CO].

[187] J. Fan, M. Reece, and Y. Wang, "An Inflationary Probe of Cosmic Higgs Switching," *JHEP* **05** (2020) 042, arXiv:1905.05764 [hep-th].

[188] M. Toda, "Instability of trajectories of the lattice with cubic nonlinearity," *Physics Letters A* **48** no. 5, (1974) 335 – 336.

[189] P. Brumer, "Stability concepts in the numerical solution of classical atomic and molecular scattering problems," *Journal of Computational Physics* **14** no. 4, (1974) 391 – 419.

[190] Z. X. Wang and D. R. Guo, *Special Functions*. WORLD SCIENTIFIC, 1989. https://www.worldscientific.com/doi/abs/10.1142/0653.

[191] A. Stephenson, "On a New Type of Dynamical Stability," in *Memoirs and proceedings of the Manchester Literary and Philosophical Society*, vol. 52 (1907-1908), pp. 1–10. Manchester Literary and Philosophical Society, Manchester, UK, 1908.

[192] A. Stephenson, "XX. On induced stability," *The London, Edinburgh, and Dublin Philosophical Magazine and Journal of Science* **15** no. 86, (1908) 233–236.

[193] P. Kapitza, "Dynamic stability of the pendulum with vibrating suspension point," *Soviet Physics–JETP* **21** no. 5, (1951) 588–597.

[194] P. L. Kapitza, "A pendulum with oscillating suspension," *Uspekhi fizicheskikh nauk* **44** (1951) 7–20.

[195] L. Landau and E. Lifshitz, *Mechanics*, vol. 1 of *Course of Theoretical Physics*. Butterworth-Heinemann, Oxford, 1982.

[196] M. Abramowitz, *Handbook of Mathematical Functions, With Formulas, Graphs, and Mathematical Tables,*. Dover Publications, Inc., USA, 1974.

[197] D. Buttazzo, G. Degrassi, P. P. Giardino, G. F. Giudice, F. Sala, A. Salvio, and A. Strumia, "Investigating the near-criticality of the Higgs boson," *JHEP* **12** (2013) 089, arXiv:1307.3536 [hep-ph].